

**Processes controlling the isotopic composition of
CO₂ and O₂ in canopy air: A theoretical analysis with
some observations in a Sitka spruce plantation**

Dissertation
zur Erlangung des Doktorgrades
der Naturwissenschaften im Fachbereich
Geowissenschaften
der Universität Hamburg

vorgelegt von

Ulrike Seibt

aus Chemnitz

Hamburg

2003

Als Dissertation angenommen vom Fachbereich Geowissenschaften
der Universität Hamburg
auf Grund der Gutachten von Prof. Dr. H. von Storch
und Dr. J. Lloyd.

Hamburg, den 23. Juni 2003

Prof. Dr. H. Schleicher
Dekan
des Fachbereichs Geowissenschaften

Sollte alles denn gewußt sein ?

- Ach, ich glaube nein.

Paul Klee

Contents:

1. Introduction	1
-----------------	---

Part I: Process Studies

2. Methods	13
Field Site	13
Experimental Setup	13
Collection of air samples	15
Sampling protocol	17
Analysis of air samples	19
Collection of water and organic materials	20
Analysis of water and organic materials	21
Calculations of gas exchange and discrimination	22
Error sources and estimation of data uncertainties	25
3. $\delta^{13}\text{C}$ of CO_2	29
3.1 Discrimination against ^{13}C during photosynthesis	29
Introduction	29
Theory	30
Results	36
Field observations of $^{13}\Delta$ during photosynthesis	36
Parameters for predicting $^{13}\Delta$	36
C_i/C_a	36
Respiratory contributions to gas exchange	36
Isotopic composition of canopy CO_2	42
Effective fractionation during dark respiration in the light	42
Mesophyll conductance	44
Predictions of $^{13}\Delta$ during photosynthesis	45
$\delta^{13}\text{C}$ of plant material assimilated over the diurnal cycle	49
Discussion	53
3.2 $\delta^{13}\text{C}$ of CO_2 from foliage and soil respiration	57
Introduction	57
Results	58
$\delta^{13}\text{C}$ of foliage respiration during the night	58

$\delta^{13}\text{C}$ of soil respiration	60
$\delta^{13}\text{C}$ of ecosystem respiration	63
Discussion	64
4. $\delta^{18}\text{O}$ of CO_2	67
4.1 Discrimination against ^{18}O during photosynthesis	67
Introduction	67
Theory	68
Results	73
Field observations of $^{18}\Delta$ during photosynthesis	73
Parameters for predicting $^{18}\Delta$	76
C_i/C_a and C_c/C_a	76
Isotopic composition of canopy CO_2	76
Isotopic composition of needle water at evaporating sites	77
Isotopic composition of bulk needle water	80
Predictions of $^{18}\Delta$ during photosynthesis	82
Discussion	86
4.2 $\delta^{18}\text{O}$ of CO_2 from foliage and soil respiration	93
Introduction	93
Theory	94
Results	95
$\delta^{18}\text{O}$ of foliage respiration during the night	95
$\delta^{18}\text{O}$ of soil respiration	97
$\delta^{18}\text{O}$ of ecosystem respiration	101
Discussion	102
5. O_2 : CO_2 exchange of photosynthesis and respiration	107
Introduction	107
Theory	109
Results	110
Diurnal cycles of $\delta(\text{O}_2/\text{N}_2)$ ratios	110
Photosynthesis and foliage respiration	112
Soil respiration	116
Integrated canopy exchange	117
Discussion	119

6. $\delta^{18}\text{O}$ of O_2 in photosynthesis and respiration	123
Introduction	123
Theory	124
Results and Discussion	126

Part II : Canopy scale integration of processes

7. Canopy scale integration of CO_2 exchange	133
Introduction	133
Theory	134
Additional observations	135
7.1 Net ecosystem exchange of CO_2	136
7.2 $\delta^{13}\text{C}$ of canopy CO_2 exchange	142
7.3 $\delta^{18}\text{O}$ of canopy CO_2 exchange	146
Discussion	151
8. $\delta^{18}\text{O}$ of canopy O_2 exchange	153
Introduction	153
Theory	153
Ecosystem exchange of O_2	155
$\delta^{18}\text{O}$ of canopy O_2 exchange	157
Variations in isotopic signatures of CO_2 and O_2 in canopy air	161
9. Application of canopy scale integration:	
Partitioning net ecosystem exchange of CO_2	165
Introduction	165
Net isoflux approach	166
One-way isoflux approach	170
Dual discrimination approach	176
Comparison	180
10. Summary and Conclusions	185
11. References	191
Appendix	203

1. Introduction

Carbon dioxide absorbs thermal radiation in the atmosphere, affecting the surface temperature of our planet ("greenhouse" effect). The atmospheric concentration of carbon dioxide (CO₂) has been rising during the past century due to human activities such as fossil fuel combustion, land use changes and biomass burning. This is receiving increasing attention because it has been correlated to changes in global climatic patterns (IPCC 2001). Through photosynthesis and respiration, large amounts of carbon are exchanged annually between the ocean, the atmosphere and the terrestrial biosphere. If we want to analyse or predict implications and feedbacks of climate changes on a global scale, we have to gain detailed understanding of the natural cycling of carbon within the climate system. This dissertation will focus on isotopic methods applied to investigate the terrestrial component of the global carbon cycle.

The global terrestrial biosphere contains approximately 1500 GtC (1GtC = 10¹⁵g carbon) in soil organic matter and 500 GtC in plant biomass. The atmosphere contains about 730 GtC. About 38000 GtC is stored in the ocean. Although the carbon inventories of the terrestrial biosphere and the ocean differ by more than one order of magnitude, their gross rates of carbon exchange with the atmosphere are comparable: 90 GtC are exchanged with the ocean and 120 GtC with the terrestrial biosphere per year. Current anthropogenic carbon emissions have been estimated at about 7 GtC per year, with 5.3 GtC per year from fossil fuel combustion. About one third of that is removed from the atmosphere by the ocean and the terrestrial biosphere, with average annual net uptake rates of approximately 1.9 and 1.4 GtC through the 1990s. Accurately assessing these small (and interannually variable) net fluxes as residuals from large gross fluxes remains a challenge because extrapolations of carbon exchange to the global scale introduce considerable uncertainties into estimates of fluxes and pool sizes (IPCC 2001).

Photosynthesis and respiration dominate the exchange of carbon dioxide between the atmosphere and the global terrestrial biosphere. A schematic drawing of the cycling of carbon through terrestrial ecosystems is shown in Figure 1.1. Carbon is removed from the atmosphere by the biological process of photosynthesis taking place in chloroplasts, mostly located in foliage, and used in assembling new organic material. The organic carbon compounds are partly designated for growing and maintaining foliage and partly

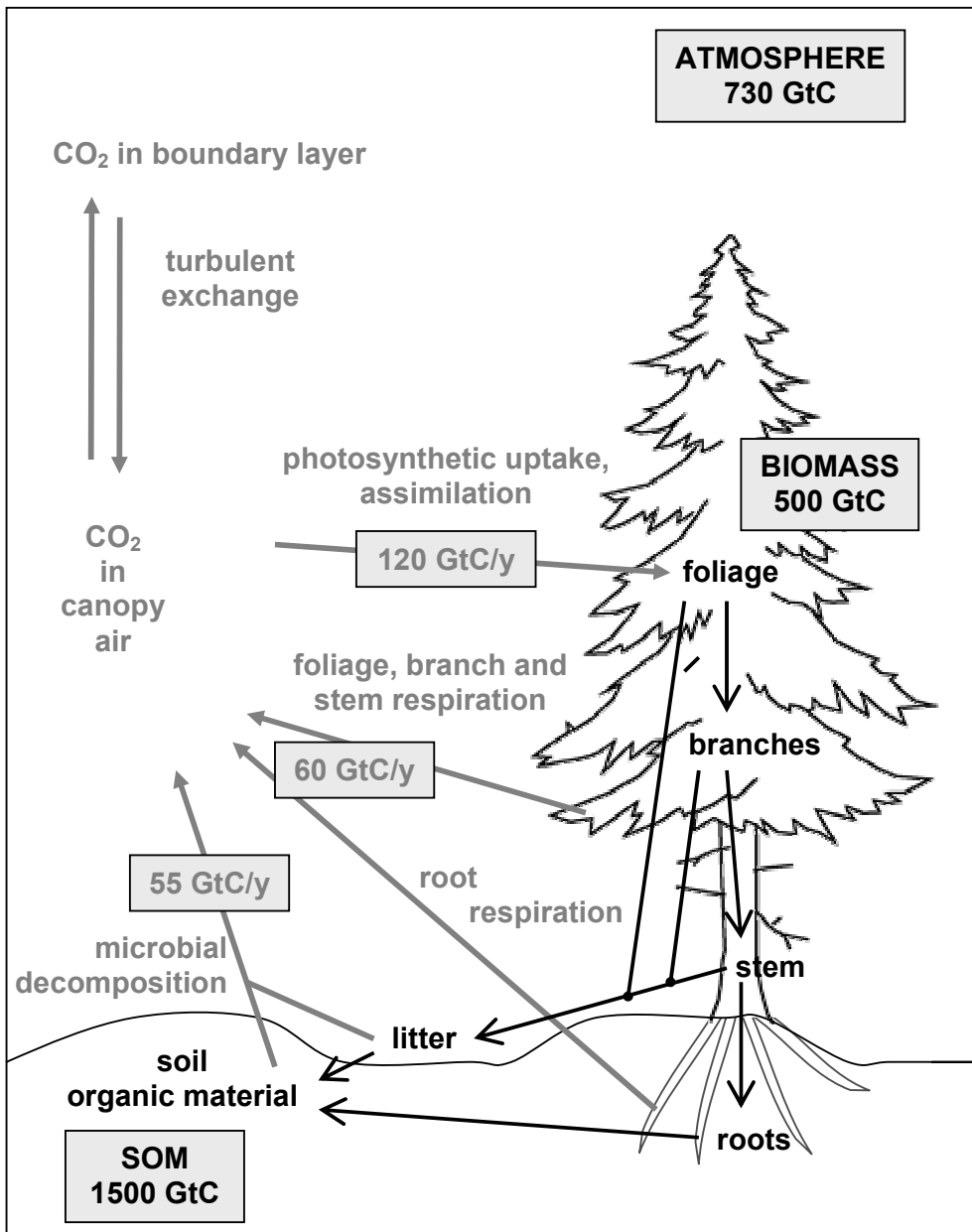


Figure 1.1: Schematic drawing of carbon cycling between the atmosphere and terrestrial ecosystems. CO₂ exchange processes are labelled in grey. Grey arrows indicate CO₂ fluxes, with total annual carbon exchanges between the atmosphere and the global terrestrial biosphere listed in grey boxes (4 GtC/y are returned to the atmosphere by combustion of organic material in natural and human-induced fires). Organic plant and soil components are labelled in black. Black arrows indicate transport of organic carbon. Global carbon pools are listed in black boxes. All numbers from IPCC (2001).

exported to grow and maintain branches, stems, roots and other parts of plants. Most dead plants and plant parts (litter) are deposited on top of or in the soil where they are decomposed by soil microbes. During growth and maintenance of plant parts and microbial decomposition, carbon is released from organic material in the biological processes of autotrophic (plant) and heterotrophic (microbial) respiration. Thus, carbon is cycled through terrestrial ecosystems from the uptake of atmospheric CO₂ during photosynthesis to the release of CO₂ into the atmosphere in respiration via assimilation into organic compounds. The storage times of these compounds are highly variable, ranging from days (soluble carbohydrates respired by foliage and roots) to years (litter, most soil carbon) and even centuries ("passive" soil carbon, Bird et al. 2001). Storage of carbon in terrestrial ecosystems depends on the amount of plant material assimilated in photosynthesis and the amount lost in plant respiration and microbial decomposition. Thus, rates of photosynthesis and respiration will determine whether an ecosystem is increasing or decreasing its carbon stocks.

An ecosystem that is increasing its carbon pool acts as a net sink of atmospheric CO₂, whereas an ecosystem with a decreasing carbon pool constitutes an atmospheric CO₂ source. One way to evaluate the source or sink strength of a specific ecosystem is to estimate its gross rates of photosynthesis and respiration. This requires the rate of uptake and release of CO₂ from and into the atmosphere to be determined separately. However, CO₂ concentrations (in the following expressed as mole fractions, i.e. μmole of CO₂ per mole of air, or in ppm) within or above the canopy will always be influenced by both processes simultaneously. Thus, measuring variations of CO₂ mole fractions in atmospheric or canopy air alone cannot reveal magnitudes or variability of the separate processes. Stable isotopes provide independent tracers of physical transport or biological activity during carbon exchange, and help to resolve this difficulty.

The stable isotope ratios of major interest for CO₂ and O₂ in the global climate system are ¹³C/¹²C and ¹⁸O/¹⁶O, expressed as relative abundances of the rarer with respect to the more abundant isotopes (see section 2 for notations and standards referred to in the following). The mean natural abundances of ¹²C and ¹³C are approximately 98.89 and 1.11 %, and 99.76 and 0.20 % for ¹⁶O and ¹⁸O. Because ¹³C and ¹⁸O also form CO₂, O₂ and organic material, they cycle through terrestrial ecosystems (and the rest of the global carbon cycle) like their more abundant counterparts, ¹²C and ¹⁶O. But because of their greater atomic mass, heavier isotopes often move and react slightly slower. The resulting separation effects during physical and biological processes are called isotope

fractionation, causing characteristic differences in isotopic composition between source and product material. For example, the organic material of plants (the product of photosynthesis) contains less ^{13}C than atmospheric CO_2 (the source material) due to photosynthetic fractionation against $^{13}\text{CO}_2$. Together, the isotopic exchanges constitute cycles of $^{13}\text{CO}_2$ and $\text{C}^{18}\text{O}^{16}\text{O}$ parallel to that of $^{12}\text{C}^{16}\text{O}_2$ ("normal" CO_2).

Examples of isotopic compositions of compartments and exchange fluxes of a forest ecosystem are presented in Figure 1.2. Photosynthetic carbon uptake discriminates against ^{13}C (Farquhar et al. 1982), leaving plant material depleted and atmospheric CO_2 enriched in ^{13}C . In the commonly used δ -notation (expressed with respect to a standard, see equation 2.1), isotopic enrichment corresponds to increasingly positive and depletion to increasingly negative $\delta^{13}\text{C}$ values (irrespective of the initial sign). The average carbon isotopic composition, $\delta^{13}\text{C}$, of atmospheric CO_2 is approximately -8 ‰ (Mook 1986). Globally, photosynthesis discriminates against ^{13}C by about 17 to 18 ‰ (for example, Keeling et al. 1989, Kaplan et al. 2001), resulting in a mean $\delta^{13}\text{C}$ of plant material of about -25 to -26 ‰. The extent of ^{13}C discrimination depends on the species, on metabolic pathways and on environmental factors such as humidity, temperature, nutrient supply and CO_2 mole fraction (Berry 1988). The $\delta^{13}\text{C}$ of plant material ranges from -35 to -9 ‰ (Smith and Turner 1975, O'Leary 1988). Respiration is thought to release CO_2 without significant fractionation of carbon isotopes (Lin and Ehleringer 1997), hence the global respiratory flux carries the mean $\delta^{13}\text{C}$ signature of plant or soil organic material.

The influence of photosynthesis on the oxygen isotopic composition of CO_2 is different from that on the $\delta^{13}\text{C}$ signature, because CO_2 exchanges isotopically with water. In foliage, this reaction is catalysed by the enzyme carbonic anhydrase. The average $\delta^{18}\text{O}$ value of atmospheric CO_2 is about 0 ‰ (Goodman and Francey 1988). Photosynthetic ^{18}O discrimination has a global average value of about 14 ‰ (Farquhar et al. 1993). The magnitude of oxygen isotope discrimination during photosynthesis does, however, vary widely depending on the $\delta^{18}\text{O}$ signature of water in chloroplasts, themselves located close to the sites of evaporation. The $\delta^{18}\text{O}$ value of foliage water at these evaporating sites becomes enriched during the day due to fractionation against ^{18}O during transpiration. The $\delta^{18}\text{O}$ signatures of foliage and soil respired CO_2 fluxes mostly reflect $\delta^{18}\text{O}$ compositions of foliage and soil water. $\delta^{18}\text{O}$ values of soil respired CO_2 range between -20 and -2 ‰, while those of foliage respiration range between -8 and +10 ‰,

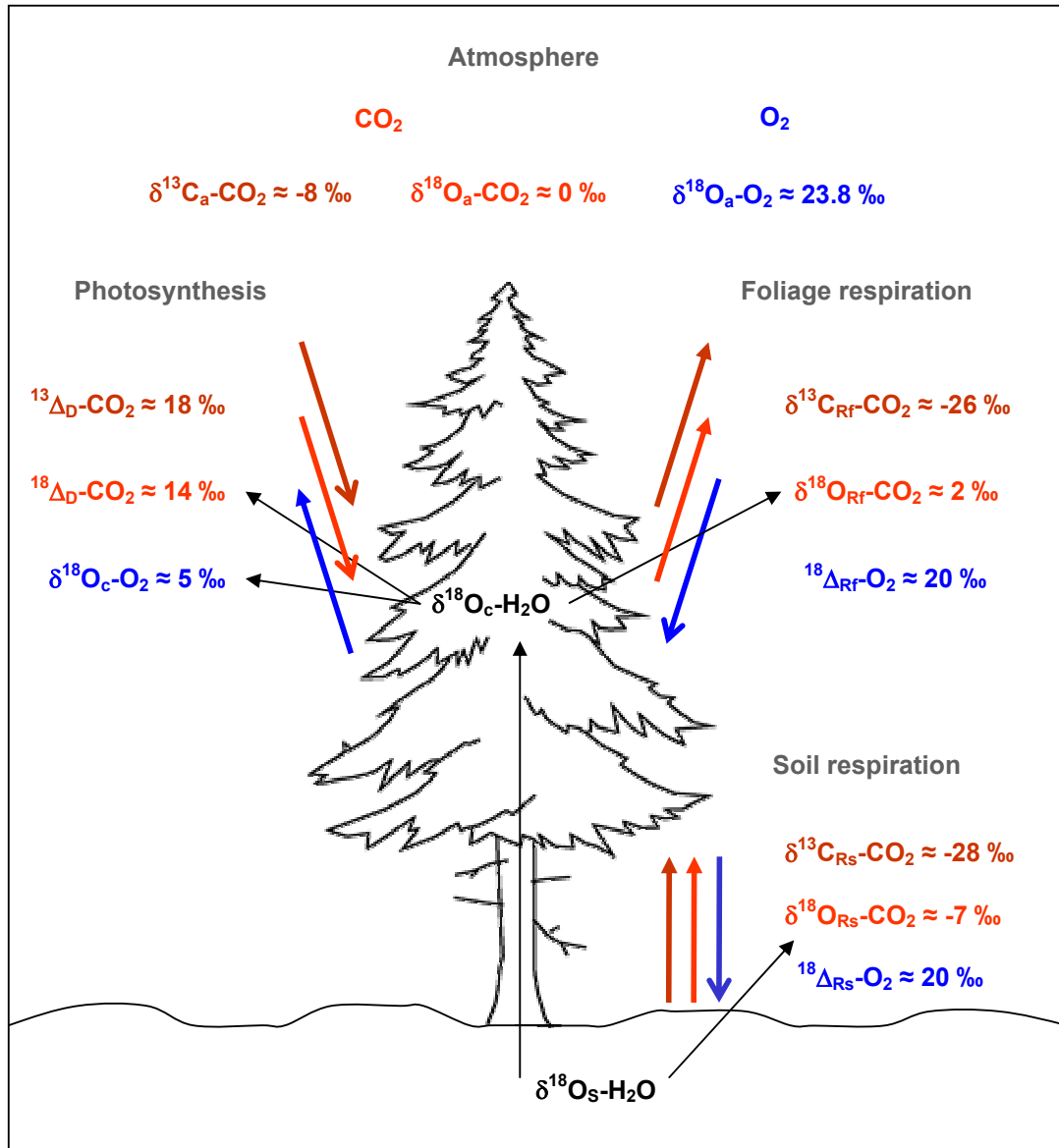


Figure 1.2: Overview over isotopic compositions of component fluxes of carbon exchange between the atmosphere and terrestrial ecosystems. Dark red labels indicate $\delta^{13}\text{C}$ signatures of CO_2 fluxes, light red labels $\delta^{18}\text{O}$ signatures of CO_2 fluxes, and blue labels $\delta^{18}\text{O}$ signatures of O_2 fluxes. Black arrows indicate isotopic signatures influenced by $\delta^{18}\text{O}$ values of water. Open arrow heads indicate discrimination processes, closed arrow heads fluxes carrying isotopic signatures of their source materials. All numbers are approximate values of global averages, see text.

with a global average $\delta^{18}\text{O}$ signature of respiratory CO_2 release of -14‰ (Farquhar et al. 1993).

The $\delta^{18}\text{O}$ signature of O_2 released in photosynthesis also depends on the $\delta^{18}\text{O}$ value of chloroplast water, surrounding the sites of O_2 production. The global mean $\delta^{18}\text{O}$ signature of photosynthetic O_2 is about 5‰ (Farquhar et al. 1993). O_2 uptake during respiration discriminates against ^{18}O in atmospheric O_2 by about 20‰ (Guy et al. 1993). Atmospheric O_2 has a global mean $\delta^{18}\text{O}$ value of 23.8‰ (Kroopnick and Craig 1972, Horibe et al. 1973). All isotopic signatures introduced here will be discussed in detail in the respective sections.

Some physical and biological fractionation processes are sensitive to parameters such as temperature, relative humidity and CO_2 mole fraction. Fluctuations in environmental conditions can thus create temporary isotopic disequilibria, where fluxes of photosynthesis affect the isotopic composition of atmospheric CO_2 in a way different from fluxes of respiration, providing a natural labelling of fluxes.

A simple example illustrates how this information can be used to constrain relative rates of component fluxes (see for instance Lloyd et al. 1996). Consider the mass balance of CO_2 within a closed system. Assimilation (A , $\mu\text{mol}/\text{m}^2/\text{s}$) and respiration (R , $\mu\text{mol}/\text{m}^2/\text{s}$) lead to opposite changes in the CO_2 mole fraction (C , $\mu\text{mol}/\text{mol}$) of canopy air in a column of arbitrary height (moles of air per unit ground area, M , mol/m^2):

$$M \frac{dC}{dt} = R - A$$

If assimilation and respiration occur simultaneously, then separate contributions of A and R cannot be inferred from observations of dC/dt . An equivalent mass balance can be constructed incorporating the isotopic composition of each of the components:

$$MC \frac{d\delta_a}{dt} = (\delta_R - \delta_a)R + \Delta A$$

where δ_a and δ_R (‰) are the isotopic compositions of atmospheric and respired CO_2 , respectively, and Δ (‰) is the discrimination against CO_2 containing the heavier isotopes, ^{13}C or ^{18}O , during photosynthetic CO_2 uptake (see section 2 for notations and

definitions). With the two equations, contributions of A and R can now be determined separately from observations of $d\delta_a/dt$ and dC/dt . This requires that isotopic signatures of the separate processes have been established and are detectably different. Combining knowledge about isotopic gradients and flux signatures will thus help in constraining the rates of component fluxes on the ecosystem scale. They will also be useful for studying the global carbon cycle. In principle, the same two equations presented above can be used to construct global mass balances for mole fraction and isotopic compositions of CO_2 , allowing to distinguish between contributions from different ecosystems if the isotopic signatures of their CO_2 exchange fluxes differ.

Such isotopic methods have a wide range of potential applications. Relative contributions from the ocean and land biospheres to the global carbon cycle as well as locations and strengths of terrestrial carbon sources and sinks have been estimated from observed global atmospheric patterns of CO_2 and its $^{13}\text{C}/^{12}\text{C}$ and $^{18}\text{O}/^{16}\text{O}$ ratios in combination with atmospheric transport models (for example, Keeling et al. 1989, Farquhar et al. 1993, Francey et al. 1995, Bousquet et al. 1999, Rayner et al. 1999). It is important to note in this context that changing the assumed carbon isotopic composition of the terrestrial biosphere by 10 % (equivalent to 1 - 2 ‰ in $\delta^{13}\text{C}$) will result in a change in the inferred terrestrial carbon sink equal to the entire magnitude of the sink (Fung et al. 1997). The carbon isotopic composition of foliage material has been used to estimate plant physiological parameters such as C_i/C_a , the ratio of substomatal to ambient CO_2 mole fraction (Flanagan et al. 1997, Katul et al. 2000), or water use efficiency (Farquhar and Richards 1984). In addition, spatial and temporal variations of environmental conditions such as temperature and humidity have been derived from analyses of carbon and oxygen isotope signatures of plant material (for example, Barbour et al. 2001, Beerling et al. 2002) or of air enclosed in ice cores (for example, Bender et al. 1994, Malaize et al. 1999). Important contributions towards a more detailed understanding of carbon exchange with terrestrial ecosystems have also been made with process based model simulations at global and ecosystem scales (for example, Riley et al. 2002, Scholze et al. 2003, Ogee et al. submitted).

The studies listed above rely on detailed and accurate descriptions of isotopic fractionations during photosynthesis and respiration. The theory of this has been developed (see Farquhar and Lloyd 1993) and tested in the laboratory (for example, Evans et al. 1986, Lloyd et al. 1992, Williams et al. 1996, Gillon and Yakir 2000). However, only the effects of these processes on the isotopic composition of air within

canopies have been studied extensively under natural conditions (for example, Francey et al. 1985, Lloyd et al. 1996, Flanagan et al. 1997, Harwood et al. 1999, Buchmann et al. 2002). Observations of isotopic signatures of separate fluxes under natural conditions are scarce. In particular, only one study on the isotope discrimination during photosynthesis under natural conditions has been published so far (Harwood et al. 1998). As a consequence, the natural variability of isotope discrimination is largely unknown. Clearly, more investigations of isotopic fractionation under natural conditions are needed to test the assumptions and approximations used in numerical models.

Ideally, contributions of component processes to canopy gas exchange should be investigated using all available tracers, i.e. mole fractions and $\delta^{13}\text{C}$ and $\delta^{18}\text{O}$ signatures of CO_2 and O_2 , in an integrated approach. Several of these signals are coupled through their co-dependencies on environmental parameters. This is illustrated in Figure 1.3 in a schematic drawing of a stoma, the opening where gases enter and leave the intercellular spaces of foliage. Both $\delta^{13}\text{C}$ and $\delta^{18}\text{O}$ of CO_2 depend on the gradient of CO_2 mole fraction from ambient air (C_a) to the photosynthetic sites in chloroplasts (C_c). At the same time, both $\delta^{18}\text{O}$ of CO_2 and of O_2 also depend on the enrichment of chloroplastic water ($\delta^{18}\text{O}_{\text{cw}}$). Concurrent changes in isotopic signatures of gases in canopy air can thus provide additional constraints for assessing gas exchange rates. In such multi-tracer studies, fluxes and isotopic compositions of canopy gas exchange need to be characterised separately, for example by using chamber methods such as the branch bags that constitute the main experimental tool in this study (see Figure 1.4 box 3). The two equations for mass balances of mole fractions and isotopic compositions of CO_2 presented above can be applied at the leaf (or branch) level as well as at ecosystem or global scales. The main difference between chamber measurements and observations at other scales is that the composition of air in chambers is altered by only one process at a time. Isotopic signatures or fractionations can then be inferred from resulting changes in the gas composition of chamber air.

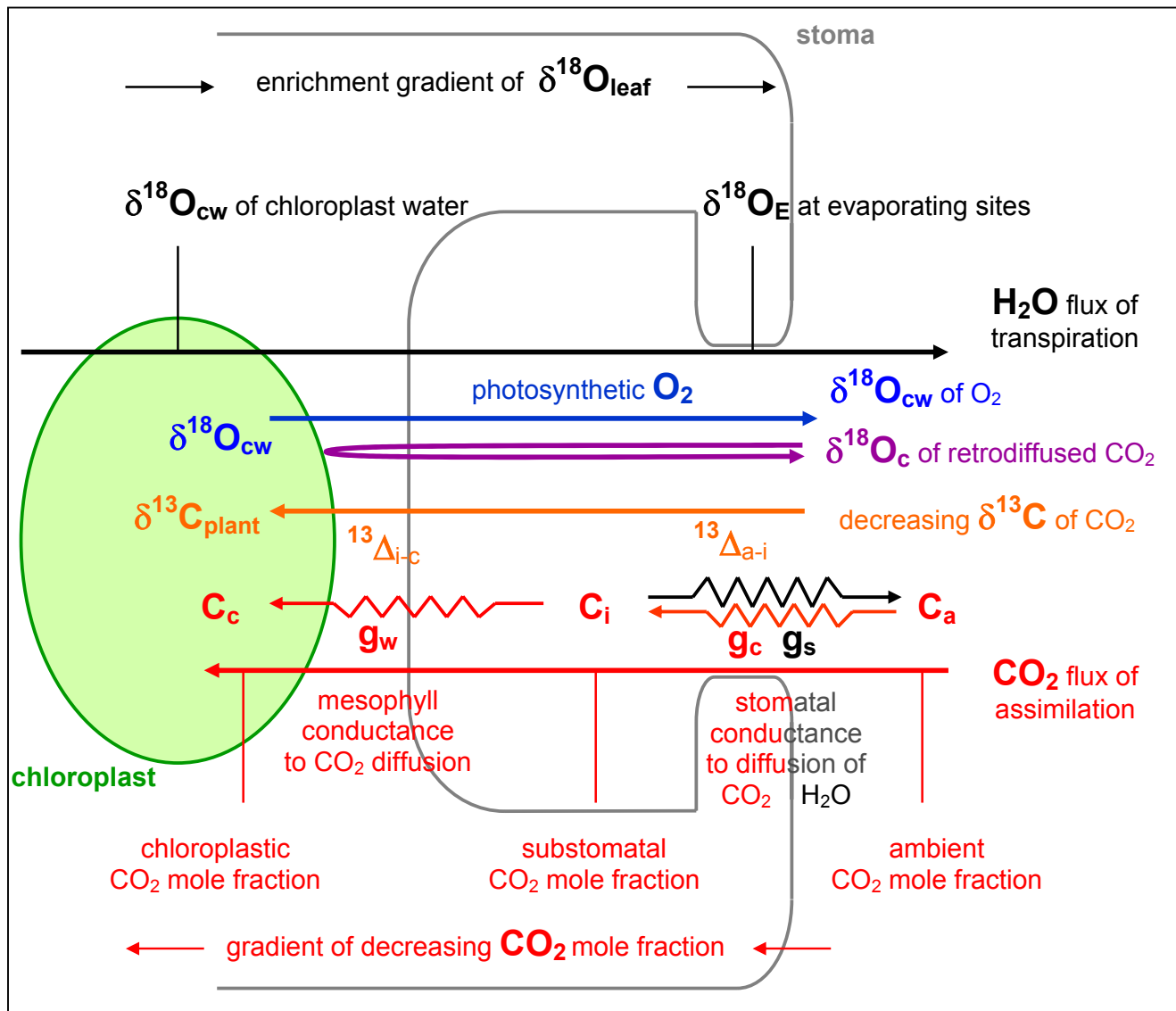


Figure 1.3: Schematic drawing of photosynthetic gas exchange through stomata, with fluxes, gradients, $\delta^{13}\text{C}$ and $\delta^{18}\text{O}$ of CO_2 (red), and fluxes and $\delta^{18}\text{O}$ of O_2 (blue) and of H_2O (black).

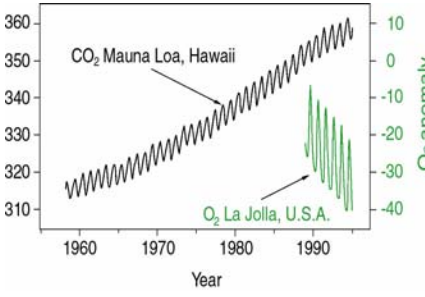
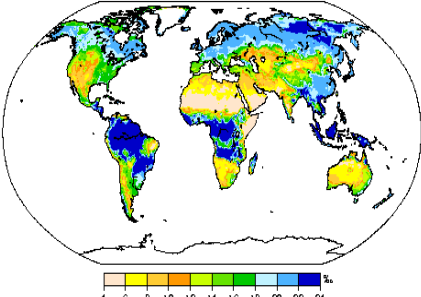
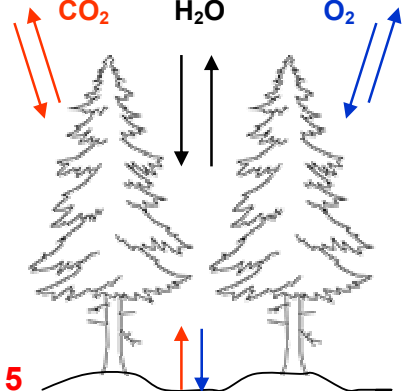
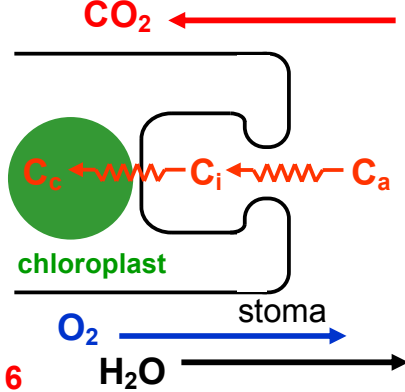
<u>Scales</u>	Measurements	Models
Global	 <p>1</p>	<p>Ecosystem ¹³C Discrimination</p>  <p>4</p> <p>Kaplan, 2001</p>
Eco-system	 <p>2</p>	 <p>5</p>
Leaf / Cell	 <p>3</p>	 <p>6</p>

Figure 1.4: Overview over the different scales involved in carbon cycle research. Left: Measurements of mole fraction and isotopic composition of atmospheric gases at the global, ecosystem and leaf/cell scales. Right: Theoretical descriptions (process based models) of rates and isotopic signatures of gas exchange at the global, ecosystem and leaf/cell scales.

The aim of this work is to improve our understanding of the mechanisms and the coupling of isotopic gas exchange in terrestrial ecosystems. To this end, a theoretical analysis of processes controlling the carbon and oxygen isotopic compositions of CO₂ and O₂ is combined with observations from a field study. Figure 1.4 gives an overview over the different spatial scales involved in carbon cycle research. Interpreting measurements of atmospheric gas compositions made at global (box 1) and ecosystem scales (box 2) requires process based models at these scales (boxes 4 and 5). Numerical models of isotopic gas exchange with the terrestrial biosphere at global (box 4) and ecosystem scales (box 5) rely on theoretical descriptions of isotopic gas exchange at the level of leaves or cells (box 6). Due to a scarcity of measurements at the leaf level under natural conditions (box 3), a gap exists between theory on the one hand (box 6) and models and data on the other hand (boxes 1, 2, 4, 5).

This dissertation attempts to evaluate the applicability of commonly used theoretical descriptions (box 6) to isotopic gas exchange under natural conditions, focussing on the leaf level (box 3) and scaling up to the canopy level (box 2). This is the first study so far where flux measurements are combined with concurrent observations of isotopic signatures for all separate biological fluxes of canopy carbon exchange. Furthermore, an example for constraining carbon exchange fluxes at the ecosystem scale using an integrated multi-tracer approach is demonstrated, taking advantage of the simultaneous availability of independent information from mole fractions and carbon and oxygen isotopic compositions of CO₂ and O₂ in canopy air.

Structure of this work:

This thesis is divided into 2 main parts, each consisting of several sections. All sections contain brief introductions outlining the relevant background and objectives, followed by introduction of variables and theory applicable to the section.

Part I of the thesis contains separate studies of biological processes of gas exchange occurring in terrestrial ecosystems, photosynthesis and respiration. It relates to a study of diurnal and seasonal patterns of canopy exchange of CO₂ and its stable isotopic signatures, $\delta^{13}\text{C}$ and $\delta^{18}\text{O}$, for a stand of Sitka spruce (*Picea sitchensis*) growing in Central Scotland. Measurements of environmental parameters were combined with analysis of the trace gas composition of air samples from branch bags and soil

chambers. These represented well-defined, enclosed subspaces within the forest canopy allowing to simultaneously investigate concurrent processes.

Within Part I, section 2 (Methods) describes materials and methods of field experiments relating to process studies, including experimental setup, sampling protocol, laboratory procedures, and basic calculations of gas exchange referred to in all subsequent sections. Error analyses are also presented.

Influences of photosynthesis and respiration on diurnal and seasonal variations in carbon and oxygen isotopic composition of CO₂ in canopy air are discussed in sections 3 and 4. Here, field observations have been used to evaluate theoretical predictions of isotopic signatures of CO₂ altered by photosynthesis and respiration. The main emphasis of the two sections is on theory and measurements of photosynthetic discrimination, as "canopy photosynthetic discrimination cannot presently be measured directly" (Dawson et al. 2002).

First results from measurements of O₂ : CO₂ exchange ratios and of the isotopic composition of O₂ exchanged during photosynthesis and respiration are then presented in sections 5 and 6.

Part II of the thesis contains canopy scale integrations of the separate processes described in Part I. In section 7.1, rates of photosynthesis and respiration are scaled up to the canopy level to obtain estimates of net ecosystem exchange of CO₂. Exchange fluxes are then combined with their carbon and oxygen isotopic signatures as described in the respective sections of Part I. Sections 7.2 and 7.3 then present the predicted carbon and oxygen isotopic exchange of CO₂, and in section 8 the oxygen isotopic exchange of O₂ is considered. Section 9 contains an analysis of potential applications of isotopic methods to studies of canopy exchange of CO₂, partitioning net ecosystem exchange into component fluxes of photosynthesis and respiration. It is also quantified how well rates of assimilation used as input parameters for ecosystem integrations of gas exchange (section 7.1) could be recovered from patterns of isotopic gas exchange (sections 7.2 and 7.3), with estimates of the turbulent CO₂ exchange provided from measurements at a nearby eddy flux tower. Three different partitioning approaches are compared, two from the literature (one-way and net isoflux method) and a new approach developed here (dual discrimination method).

Finally, section 10 provides a summary and presents the main conclusions arising from this study.

Part I :

Process Studies

2. Methods

Field site

The experimental canopy was located at the foot of the Scottish Highlands near Aberfeldy, Perthshire, UK (56°37' N, 3°48' W). The study site, Griffin Forest, is situated on a gentle north-facing slope at an elevation of 340 m. Mean annual temperature at the site is 8°C, mean annual precipitation is 1400 mm. Griffin Forest is part of the network of CarboEuroFlux sites (www.bgc.jena.mpg.de/public/carboeur/sites/index_s.html). It is a plantation of Sitka Spruce (*Picea sitchensis* (Bong.) Carr.) of Queen Charlotte Islands provenance that was planted on a pre-existing moorland in 1981. It stretches across a total area of 3862 ha and contains 2000 trees per ha on average. Mean stem diameter at breast height was 13 cm. The canopy reached a maximum height of approximately 14 m, with an average tree height of 10 m. Projected leaf surface area was $6 \pm 2 \text{ m}^2 / \text{m}^2$. Few live needles were found below a height of 4 m in the canopy profile. The understory was a mixture of ericaceous shrubs, grasses and mosses, except underneath the dense canopy itself where in most places the ground was covered by a layer of needle litter of about 3 cm thickness. The soil type was a peaty gley with seasonal water-logging a typical occurrence. The soil surface formed a pattern of furrows, flats and ridges parallel to the hillside with Sitka spruce trees planted on top of the ridges.

Experimental setup

Different canopy layers were accessed using a scaffolding tower of 15 m height. Branch bags were installed by suspending them from poles attached to the tower at different heights in the canopy. Two branch bags were situated near the top of the canopy, at 10.5 and 9.5 m height (“top bags”, see Figure 2.1). One branch bag was located at an intermediate level of 8 m (“mid bag”). The middle branch bag was left empty and used as a control bag in July 2001. Campaign dates, locations and IDs of bags, needle area and dry mass for each branch are presented in Table 2.1.

Branch bags were 30 x 60 cm wide with an oval cross section (acrylic side pieces) and had variable lengths (adjustable stainless steel rods). They enclosed air volumes of 120



Figure 2.1: Photograph of branch bag installed at 10.5 m (Griffin Forest, Aberfeldy, Scotland)

Campaign dates	Location (bag #)	Projected Leaf Area (cm ²)	SD (cm ²)	Dry Mass (g)
18 / 19 May 2001	top (1)	1309	8	115
	top (3)	1671	11	67
	mid (4)	920	19	81
20 / 21 July 2001	top (1)	2888	30	195
	top (3)	2100	34	104

Table 2.1: Location, projected leaf area, standard deviation of leaf area and dry mass for foliage in branch bags during May and July 2001.

to 130 liters. The branch bags were covered with sheets of transparent plastic (ICI Propafilm, Dumfries, UK), allowing light to enter. A branch with one or two lateral shoots, comprising a total length of 76 to 144 cm, was inserted into each of the bags through a small hole on the side of the bag facing the stem. The remaining gaps were sealed with silicone sealant. On the opposite side, the branch bags had a flap that could be moved with a small motor, thereby opening the bag and bringing the air inside in contact with outside air, or shutting the bag, isolating its air with the enclosed branch from the ambient canopy air. Electric fans were used to circulate the air inside branch bags when bags were closed and to mix it with outside air when bags were open.

Bags were instrumented to monitor environmental parameters experienced over the course of the samplings: photon flux density (PPFD) (SD101QV, Macam, Livingstone), relative humidity and air temperature (HMB 30A, Vaisala (UK) Ltd., Cambridge). Three 0.2 mm diameter Cu-Con thermocouples referenced to the air temperature sensor were used to determine leaf temperature. A schematic drawing of a branch bag including the instrumentation can be found in Rayment and Jarvis (1999). Further details of the equipment used are listed in Wingate (2003).

Two soil chambers were placed on the forest floor in the vicinity of the tower (approximately 15 m distance). Chambers enclosed a soil area of 0.64 m² and an air volume of 384 L. They consisted of side pieces and a manually operated lid of 5 mm thick transparent acrylic. Soil chambers contained a 12V fan (RS 250-1561, RS Components Ltd., Corby) mounted on a bracket attached to one of the walls to provide air mixing within the chambers and with outside air when chambers were open.

Collection of air samples

Pairs of air samples from branch bags and soil chambers were collected at intervals of approximately three hours over a 24 hour period for two days in spring (18/19 May) and summer (20/21 July) 2001. Sampling times were chosen so as to achieve as good a coverage of the diurnal cycle as was possible with a limited supply of flasks. Sampling lines were attached to branch bags and the tower. Potential contaminations with water or other substances were avoided by cleaning the tubing by flushing with pressurized N₂ from a gas cylinder prior to sampling periods. Air was circulated from branch bags through a line of 3 mm i.d. Bev-A-Line (Thermoplastic Processes INC, Stirling, NJ) to an

Infra Red Gas Analyser (LI-6262, LI-COR Inc., Lincoln, NE) and back into the chamber. The IRGA was operated in absolute mode. CO₂ and H₂O vapour mole fractions of the air stream passing the IRGA as well as temperature, relative humidity and photon irradiance data from sensors inside the branch bags were recorded every 5 seconds by a Campbell CR10 data logger (Campbell Scientific Ltd., Shepshed, Leicestershire). From branch bags and soil chambers, air was pumped through a line of 5 mm i.d. Dekabon (Dekabon, Furon, Gembloux, Belgium) into a flask sampling system with a 12V battery-operated pump (PM 14625-86, KNF Neuberger GmbH, Freiburg, Germany) built into the sampling system (see Figure 2.2). The air stream was kept constant with a mass flow controller set to a flow rate of 3 liters per minute. The calculated mean residence time of gas in the lines was 6 to 8 seconds depending on the canopy level reached by the tubing.

Within the flask sampling system, the air stream was first passed through a magnesium perchlorate cylinder to remove water vapour from the gas, after which the air was pumped through two flasks in series. We used 1 L glass flasks with a valve (Glass Expansion, Melbourne, Australia) on each end, sealed with Teflon[®] PFA O-rings. For analysis of O₂/N₂ and δ¹⁸O-O₂, we used 1.3 L flasks with two valves (Hapers-Louwert, Netherlands) on the same end.

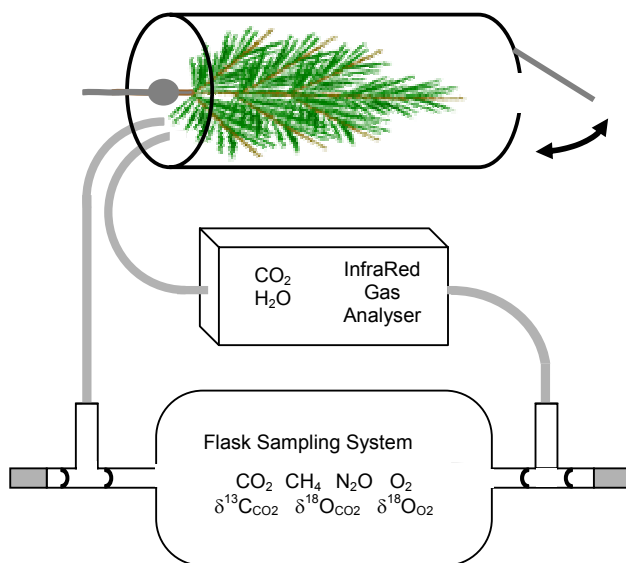


Figure 2.2: Schematic drawing of setup including branch bag, IRGA and flask sampling system.

Sampling protocol

The two flasks attached to the sampling system were open for 5 minutes during the day or 10 minutes at night, the air being circulated back through a parallel line into the same branch bag or soil chamber, creating a loop. The circulation of air through the flasks was stopped after 5 (10) minutes by interrupting the air flow at the exhaust pressure control. The flasks were then pressurized to 1 bar above ambient pressure over the course of one minute and closed with the stopcocks. Due to logistic restrictions, we did not take duplicate samples. For each sampling time, only one of the set of two flasks was taken off the sampling system and replaced by a new flask.

For each branch bag (or soil chamber), the combined setup of bag plus flask sampling system was switched between an open and a closed mode of operation by opening and closing the bag itself at regular intervals. For example, during daytime, foliage inside the bags usually assimilates carbon, lowering the CO₂ mole fraction (see Figure 2.3) and enriching (or depleting) CO₂ in the heavier isotopes. When the branch bag is open, the air inside is quickly mixed into the large pool of surrounding canopy air, thereby diluting the impact of photosynthesis on the trace gas composition of branch bag air. When the

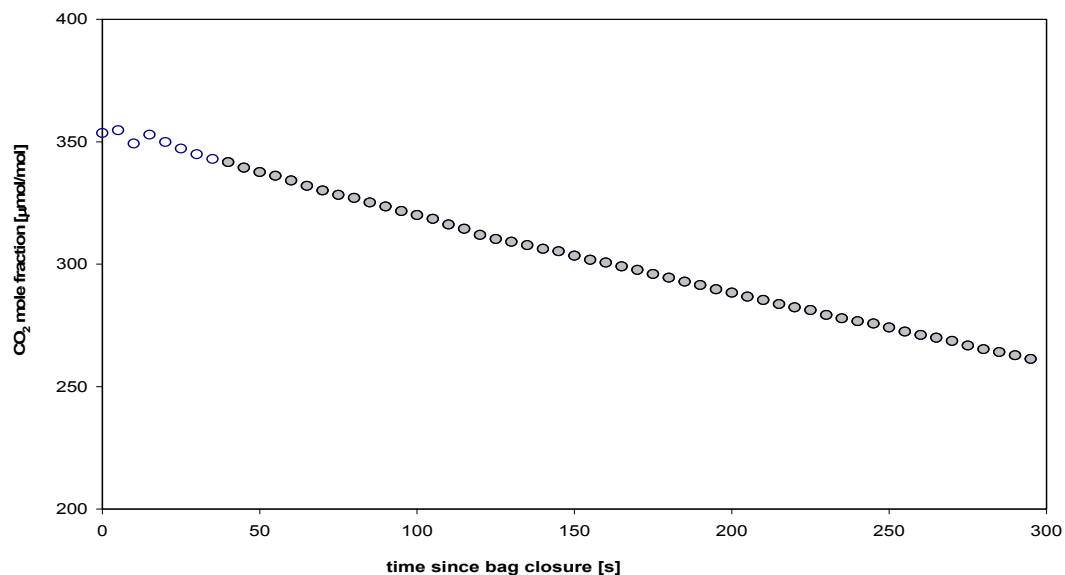


Figure 2.3: Example for the collection of CO₂ mole fraction data in bag 1 during the closure period from 15:00 to 15:05 on 20 July 2001. Data from the initial 40 seconds (open circles) were excluded from gas exchange calculations.

bag is closed, only the CO₂ pool of the much smaller bag air space is affected. Within the closed loop system, the air trace gas composition changes noticeably.

The automated system was switched between 4 branch bags. One bag was closed at a time. During the closure period, data was collected every 5 seconds for environmental variables from the sensors and for CO₂ mole fractions from the IRGA (in the following referred to as "continuous data"). The system was then switched to the next branch bag. With 5 minute closure periods at day-time, CO₂ mole fractions were found to reliably exhibit linear changes over time. At night, dusk and dawn, the branch bags were closed for 10 minutes because of low gas exchange rates at these times. Thus, each of the 4 bags was measured every 20 minutes during the day and every 40 minutes at night. Figure 2.3 gives an example of the decrease in CO₂ mole fraction due to photosynthetic carbon uptake over a day-time closure period. Data from the initial 40 seconds of each cycle were excluded from gas exchange calculations to ensure the separation of data from current and previous samples.

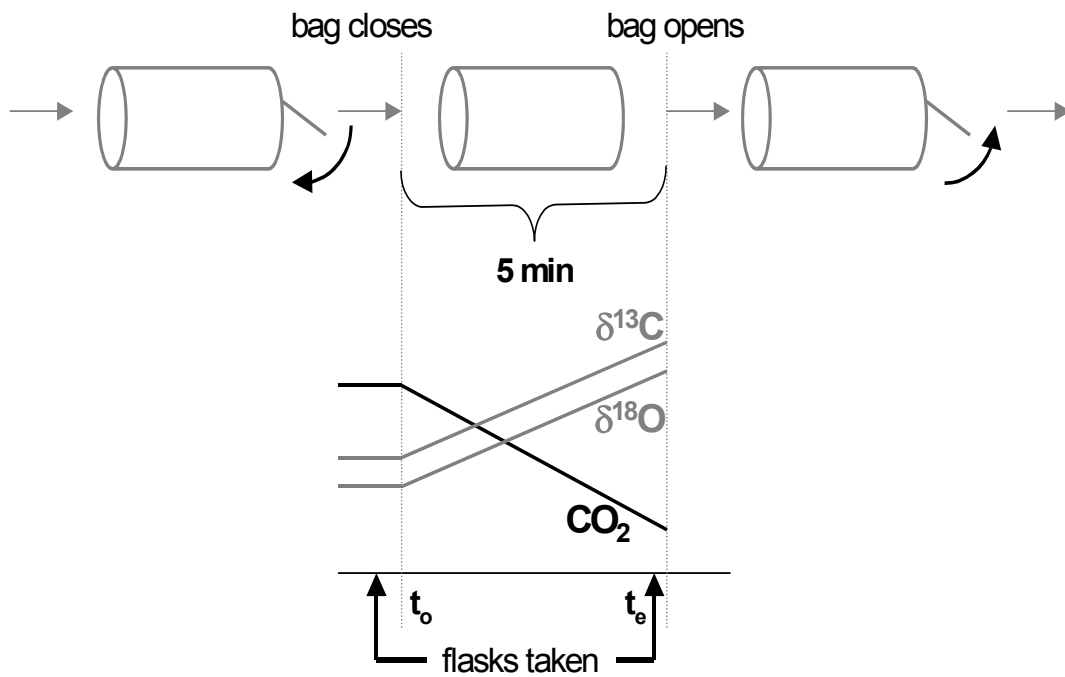


Figure 2.4: Schematic drawing of change in trace gas composition over branch bag sampling interval during photosynthesis. Shortly before closing of the branch bag (at time t_0) the open sample is taken. Shortly before reopening of the bag (at time t_e) the closed sample is collected.

Flask samples were taken at two points in the sequence of opening and closing of chambers. The first sample was taken from an open chamber, 3 to 4 minutes before closure. It was labelled "open sample", reflecting the CO₂ mole fraction and isotopic composition of ambient canopy air. It can also be considered the initial point (background) for the subsequent measuring period. After this, a second flask was attached to the sampling system and the flask and pressure control valves opened. With the start of flushing of the second set of flasks the preconditioning gas was released into the still open chamber for about 1 minute to remove as much of the pre-conditioning gas from the sampling air space as possible prior to closure. This also ensured a sufficient amount of time for air circulation through the second set of flasks. The second flask was then filled after the chamber had been closed for the appropriate time and labelled "closed sample". It was collected shortly before reopening of the chamber so that the full extent of changes in trace gas composition could be captured (see Figure 2.4).

Analysis of air samples

All flasks were analysed at the GasLab and IsoLab of the Max-Planck-Institut für Biogeochemie in Jena, Germany. The preconditioning of the flasks prior to field campaigns was also carried out here (M. Rothe). CO₂ mole fractions in the air samples were analysed by gas chromatography (A. Jordan). The GC system is based on a HP 6890 gas chromatograph (Hewlett Packard, USA) equipped with two sets of chromatographic columns linked to a flame ionization detector (FID, for CO₂ analysis) and an electron capture detector (ECD, for N₂O analysis). The two sample loops (FID-line: 2.2 ml; ECD-line: 5 mL) are linked in series and are kept at ± 0.1 °C in a tempering oven. For determination of trace gas mole fractions, 30 ml of the air sample was flushed through two sample loops. The gas in the loops was equilibrated with ambient pressure, then injected onto the precolumn (Hayesep Q, 6ft *1/8") and passed through the main GC column (Porapak Q, 12ft*1/8") held at 60 °C. After chromatographic separation, CO₂ was converted to CH₄ over a hot Nickel catalyst ("methanizer") using hydrogen before being detected by the FID. To increase precision injections were made alternately from samples and a reference gas resulting in a reproducibility of 0.08 ppm for CO₂.

The CO₂ in the dry air samples was extracted cryogenically with an automated sampling line ("BGC-AirTrap"). The ¹³C/¹²C and ¹⁸O/¹⁶O ratios of the separated CO₂ were determined on a Delta⁺XL dual inlet isotope ratio mass spectrometer (Finnigan MAT,

Bremen, Germany) (M. Rothe). The analytical precision was in the order of 0.01 ‰ for $\delta^{13}\text{C}$ and 0.02 ‰ for $\delta^{18}\text{O}$. Details of the analysis procedure can be found in Werner et al. (2001). For a review of referencing strategies and techniques in isotopic ratio mass spectrometry see Werner and Brand (2001).

Analyses of O_2 and $\delta^{18}\text{O}_{\text{O}_2}$ of air samples were performed with a mass spectrometric inlet system for measuring O_2/N_2 ratios (W. Brand, U. Seibt). The system includes a 16 connection multiport valve and an open split which is fed alternately from a sample and a reference gas, both switched on and off a common transfer point to a Delta⁺XL isotope ratio mass spectrometer (Finnigan MAT, Bremen, Germany). Referencing is made in a very similar fashion as for CO_2 in air by measuring versus an air reference and implementing a multiple referencing hierarchy system. There is currently no international scale for this kind of work. Thus, at the present time, consistency in the data is achieved by matching the scales of longer term records measured by different laboratories. O_2/N_2 and $\delta^{18}\text{O}-\text{O}_2$ data are reported in units of permeg. One permeg is 0.001 ‰ in δ -notation. A 1 permeg change in the O_2/N_2 ratio corresponds to a change of approximately 0.2 ppm in the mixing ratio of O_2 in air. At the time of sampling, the analytical precision of O_2/N_2 measurements was at the 10 permeg level and that of $\delta^{18}\text{O}$ of O_2 was approximately 12 permeg. For the interpretation of O_2/N_2 and $\delta^{18}\text{O}-\text{O}_2$ data and the derived results reported in this study, it should be kept in mind that the development of analytical facilities for O_2/N_2 and $\delta^{18}\text{O}-\text{O}_2$ measurements is very much an ongoing process. Furthermore, because these are the first such measurements, there are no comparisons with other data currently available.

Collection of water and organic materials

Needle and non-green twig samples were collected during branch bag measurement intervals from two Sitka spruce trees adjacent to the access tower. Samples were taken at the same heights and close to the locations of the branch bags, at 10 m (top), 8 m (middle), and 6 m (low) height. Soil samples were collected from two locations in the vicinity of the tower. The litter layer was removed and soil from the first 5 cm of the soil profile was extracted. All samples were filled in glass containers (exetainers). The sealed containers were stored in a cooler in the field and transferred to a freezer in the lab as soon as practical until further processing.

Analysis of water and organic material samples

Water was extracted from the needle, twig and soil samples cryogenically using vacuum lines. The extraction temperature never exceeded 75°C. The water was collected in small glass vials to which a known amount of CO₂ was added. The vials were then left for a minimum of three days to allow CO₂/H₂O equilibration to occur. Subsequently, the equilibrated CO₂ was purified and its δ¹⁸O was measured on a dual inlet isotope ratio mass spectrometer as detailed in Harwood et al. (1998). The external precision for water δ¹⁸O data was 0.4 ‰. Water extractions (U. Seibt), CO₂ purifications and mass spectrometric analyses (N. Betson) were undertaken at the laboratory of Physiological Ecology at the Department of Plant Sciences, University of Cambridge, England.

The cryogenically dried needle, twig and soil samples were ground with a ball mill to a fine homogeneous powder (U. Seibt). Small subsamples of the powdered substances were weighted and placed into tin cups (J. Schmerler, U. Seibt). The tin capsules were loaded in the auto-sampler tray of a NA 1110 CN elemental analyser (CE Instruments, Rodano, Italy), coupled via a ConFlo III open split interface to a Delta⁺XL mass spectrometer (Finnigan MAT, Bremen, Germany), and analysed for carbon content and δ¹³C at the Max-Planck-Institut für Biogeochemie, Jena, Germany (H. Geilmann). The standard deviation for δ¹³C of dry material was 0.05 ‰. For a description of the analytical setup see Werner et al. (1999).

All isotopic compositions are reported in δ-notation and units of permil (‰):

$$\delta_{sample} = \left(\frac{R_{sample}}{R_{std}} - 1 \right) \quad (2.1)$$

where R_{sample} is the ¹³C/¹²C or ¹⁸O/¹⁶O ratio of CO₂, O₂, water or plant material, and R_{std} is that of the respective standard: V-PDB for δ¹³C, V-PDB-CO₂ for δ¹⁸O of CO₂, and V-SMOW for δ¹⁸O of H₂O and O₂.

Calculations of gas exchange and discrimination

Net carbon fluxes F ($\mu\text{mol}/\text{m}^2/\text{s}$), standing for carbon uptake (assimilation rate A) and carbon release (respiration rate R), were calculated according to:

$$F = \frac{dC}{dt} \cdot \frac{v}{L_{\text{branch}}} \quad (2.2)$$

where dC/dt is the rate of change of CO_2 mole fraction, determined from a linear regression of CO_2 mole fraction against time, v is temperature dependent molar volume of branch bag air (mol) and L_{branch} is projected surface area of branch bag foliage (m^2).

Due to some problems with the IRGA water vapour channel, transpiration rates, E ($\text{mmol}/\text{m}^2/\text{s}$), were calculated from relative humidity data from the branch bag sensors:

$$E = \frac{d}{dt} \left(\frac{h \cdot P_{\text{sat}}}{P_{\text{atm}}} \right) \cdot \frac{v}{L_{\text{branch}}} \quad (2.3)$$

where P_{sat} and P_{atm} are saturated vapour pressure at air temperature and atmospheric pressure (hPa), assumed constant, and h is relative humidity. dh/dt was obtained from the derivative of a quadratic equation fit to relative humidity data ($R^2 > 0.99$ (July), > 0.9 (May)) at its initial phase of increase (corresponding to time zero) in the branch bags. For flask sampling periods, the amount of water vapour removed in the drying cylinder was estimated from the flow rates of air circulated through the flask sampling unit.

Stomatal conductance to water vapour, g_s ($\text{mol}/\text{m}^2/\text{s}$), was calculated according to:

$$g_s = \frac{E}{D_{\text{leaf}}} \quad (2.4)$$

where E is the transpiration rate and D_{leaf} is the needle to air vapour mole fraction deficit (mmol/mol). g_s was only calculated when both input variables were significantly different from zero ($E > 0.02 \text{ mmol}/\text{m}^2/\text{s}$, $D_{\text{leaf}} > 0.2 \text{ mmol}/\text{mol}$). Potential influences of the boundary layer on water fluxes were neglected because experiments were conducted under conditions of high boundary layer conductance (Rayment et al. 2002).

Stomatal conductance to CO₂, g_C , is proportional to that of H₂O, g_S , with a factor of 1.6 that reflects the ratio of diffusivities of CO₂ and H₂O:

$$g_C = \frac{g_S}{1.6} \quad (2.5)$$

The ratio of substomatal (intercellular) to ambient CO₂ mole fraction during photosynthesis, C_i/C_a , was derived from A ($\mu\text{mol}/\text{m}^2/\text{s}$), E (in $\text{mol}/\text{m}^2/\text{s}$) and g_C ($\text{mol}/\text{m}^2/\text{s}$) following von Caemmerer and Farquhar (1981):

$$\frac{C_i}{C_a} = \frac{\left(g_C - \frac{E}{2}\right)C_a - A}{\left(g_C + \frac{E}{2}\right)C_a} \quad (2.6)$$

The expression for stomatal conductance (modified by the transpiration flux) accounts for the interaction between CO₂ and water because the CO₂ flux into stomata is considerably smaller than the simultaneous water flux outwards.

The pair of flask samples represents the situation at the beginning (t_o) and end (t_e) of isolation periods (see Figure 2.4). By comparing the trace gas composition of sample pairs, fractionation processes during gas exchange of branch bag foliage could therefore be determined. For day time measurements, differences between sample pairs can be primarily attributed to photosynthesis. Calculation of photosynthetic discrimination against ¹³C or ¹⁸O has to reflect that the isotope ratio of source CO₂ changes simultaneously with that of the product. Isotope discrimination is defined as $\Delta = R_{\text{source}}/R_{\text{prod}} - 1$, where R_{source} and R_{prod} are the isotope ratios of the source (atmospheric CO₂) and the product (organic plant material) of photosynthesis. Alternatively, this can be expressed in δ -notation as $\Delta = \delta_{\text{plant}} - \delta_{\text{atm}}$ (Farquhar et al. 1982). Photosynthetic gas exchange enriches (or depletes) air in the heavier isotopes, ¹³C and ¹⁸O, and this air becomes the new source for assimilation. In analogy to a Rayleigh process, net observed discrimination Δ_{obs} (‰) can be obtained following Guy et al. (1989):

$$\Delta_{\text{obs}} = -\frac{\ln(R_e/R_o)}{\ln(C_e/C_o)} \left(1 + \frac{\ln(R_e/R_o)}{\ln(C_e/C_o)}\right)^{-1} \quad (2.7)$$

where C_o and C_e are CO_2 mole fractions ($\mu\text{mol}/\text{mol}$) and R_o and R_e their isotope ratios ($^{13}\text{C}/^{12}\text{C}$ or $^{18}\text{O}/^{16}\text{O}$) at the beginning and end of isolation periods (see Figure 2.4). In the following, $^{13}\Delta_{\text{obs}}$ and $^{18}\Delta_{\text{obs}}$ will be used to denote net observed ^{18}O and ^{13}C discrimination during carbon uptake, respectively.

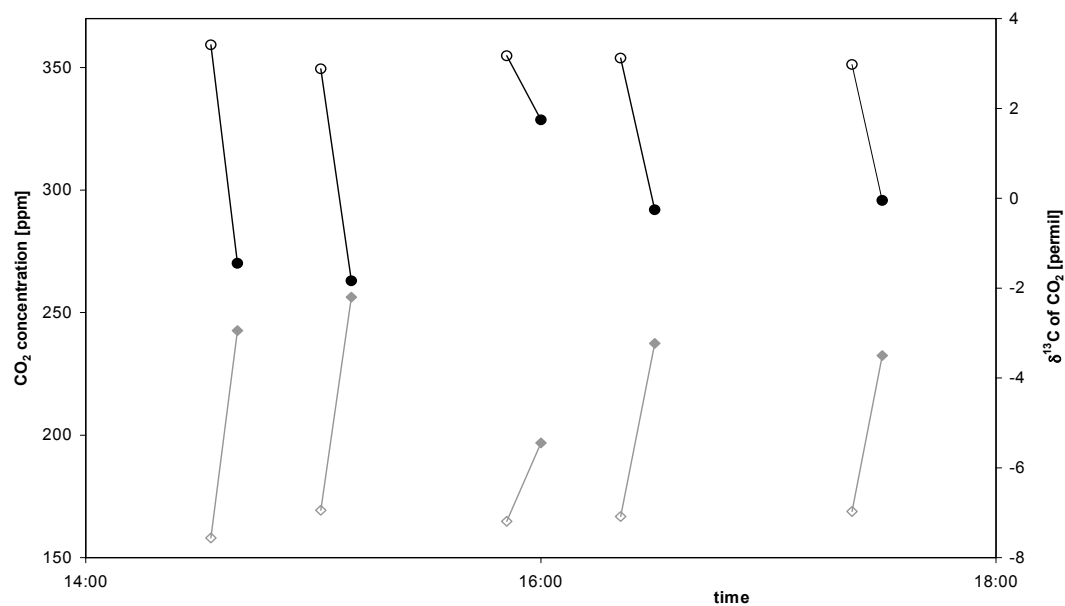


Figure 2.4: Some examples of simultaneous change in CO_2 mole fraction (black dots) and $\delta^{13}\text{C}$ (grey diamonds) from open (t_o , open) to closed samples (t_e , full symbols) due to photosynthetic carbon uptake by foliage, from 5 flask pairs collected in July 2001.

During respiration, CO₂ released from foliage and soils accumulates within soil chambers and branch bags. Isotopic signatures of respiratory CO₂ fluxes reflect diffusional and respiratory fractionation processes as well as δ¹³C values of respiratory substrates (organic material) and δ¹⁸O values of CO₂ in equilibrium with foliage or soil water. Carbon and oxygen isotopic composition of respiratory CO₂ sources, δ_{source}, were calculated from simple isotopic mass balance equations:

$$\delta_{source} = \frac{C_e \delta_e - C_o \delta_o}{C_e - C_o} \quad (2.8)$$

where δ_o and δ_e (δ¹³C or δ¹⁸O), and C_o and C_e are isotopic composition (‰) and mole fraction (μmol/mol) of CO₂ in start (open) and end (closed) air samples. In the following, δ¹³C_{source} and δ¹⁸O_{source} will be used to denote carbon and oxygen isotopic composition of CO₂ released during respiration (and before taking potential additional fractionation into account), respectively.

As an alternative method, regressions between isotopic composition and inverse of CO₂ mole fraction of air samples ("Keeling plots"), were constructed following the relationship:

$$\delta_e = C_o (\delta_o - \delta_{source}) \frac{1}{C_e} + \delta_{source} \quad (2.9)$$

with δ_{source} (δ¹³C_{source} or δ¹⁸O_{source}) as intercept of the regression, i.e. at infinite C_e. For two data points (specifically, sample pairs), both equations are numerically equivalent, but the principle can be applied to other combinations of samples as long as δ_{source} can be assumed constant at the temporal and spatial scale under study.

Error sources and estimation of data uncertainties

Errors in calculated CO₂ flux rates are directly proportional to errors in needle area measurements and to the span setting of the gas analyser. Errors of needle area measurements were small (see Table 2.1, relative errors less than 0.5 %). A (hypothetical) drift of 1 μmol/mol in the calibration span of the IRGA during the course of a five minute measurement would correspond to an error of less than 0.1 μmol/m²/s in

calculated gas exchange rates. This is small compared to usual day-time flux rates of 5 to 10 $\mu\text{mol}/\text{m}^2/\text{s}$, however, it can amount to large relative errors in the order of 10% for low dawn, dusk and night-time flux rates.

Transpiration measurements were subject to errors arising from adsorption or desorption of water vapour to or from the inside of the bags. The effect was reduced as far as possible by using Propafilm, having a low susceptibility to water adsorption and desorption, as the main material for the bags. However, IRGA water vapour measurements were found to be implausible and not in agreement with other data, possibly due to adsorption or desorption of water vapour inside the tubing. This was especially problematic during the day, when the water vapour content of bag air was rising rapidly because of branch transpiration. Compared to that, impacts of concurrent temperature changes on relative humidity measurements were negligible. Alternative methods of deriving transpiration fluxes had to be employed (detailed above).

In a study using the same kind of branch bags, Rayment and Jarvis (1999) found that during the daytime the temperature within each bag was slightly, but consistently higher than the ambient external temperature. This effect was linearly correlated to photon irradiance. The difference between bag and ambient air temperature may have affected CO_2 and water vapour exchange, both directly (i.e. by influencing biochemical activity) and indirectly (e.g. by increasing the humidity deficit of the air). However, temperature differences were small and, as in our study, there was no evidence of any systematic change in the temperature regime during the course of a measurement period. Further details on temperature anomalies can be found in Rayment and Jarvis (1999).

Likely sources of errors associated with isotopic composition measurements of flask samples include contaminations of branch bag air with conditioning gas or other previous flask fillings, interactions of sampling gas with tubing, pumps and branch bag materials, gas leakage from the experimental system, and the influence of changing conditions inside the branch bags on gas exchange and isotope fractionation characteristics during the period the bag was closed. The effect of changing gas concentrations and environmental parameters on plant gas exchange was reduced by short bag closure intervals and the large branch bag volumes. Contaminations with conditioning gas were small since flasks were replaced one at a time, with only 2 liters released compared to 120 liters of branch bag air. The second flask already contained

gas from the previous filling with canopy air. Furthermore, flushing always started while the bags were open so that contaminating gas was diluted by mixing with ambient air before bag closure. Compared with the magnitude of errors introduced through the flask sampling procedure, uncertainties of the laboratory analyses were negligible.

Combined estimates of uncertainties from the sampling procedure can be obtained with control measurements using an empty branch bag. Since it represents the standard sampling situation, it includes all sources of error except the response of branches to changed environmental conditions within the branch bag. Figure 2.5 shows the observed changes in CO₂ mole fraction and isotopic composition of an empty control bag (no branch present) during the period of bag closure. These changes were not correlated with CO₂ mole fraction, temperature or relative humidity, so the observed shifts probably reflect experimental uncertainties. Measurement uncertainties deduced from the control bag experiments were therefore taken as 1.3 ppm for CO₂, 0.1 ‰ for δ¹³C and 0.2 ‰ for δ¹⁸O values, applying to all closed bag measurements irrespective of the duration of closure periods.

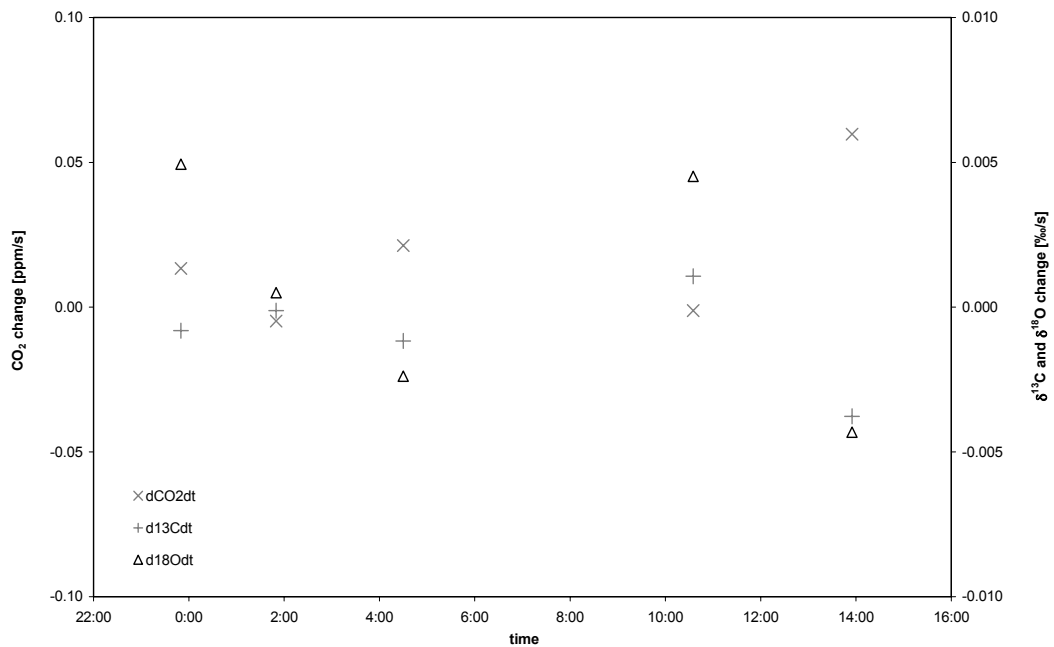


Figure 2.5: Changes in CO₂ mole fraction, dCO₂/dt (x), and isotopic composition, d¹³Δ/dt (+) and d¹⁸Δ/dt (triangles), during control bag measurements on 20 July 2001.

Open bag measurement uncertainties are more difficult to assess, so estimates are instead based on standard deviations of laboratory analyses of duplicate flasks (0.13 ppm for CO₂, 0.01 ‰ for δ¹³C and 0.03 ‰ for δ¹⁸O). Taking errors associated with leaf area measurements into account gives overall uncertainties of CO₂ fluxes between 0.1 and 0.3 μmol/m²s. Examples for standard deviations of CO₂ fluxes, isotope discriminations and other parameters are listed in Table 2.2. All standard deviations were calculated from the above described uncertainties using Gaussian error propagation. As can be seen from Table 2.2, standard deviations of inferred parameters are larger for smaller CO₂ fluxes, i.e. for smaller differences between start and end values. This complicates interpretation of field data obtained early in the morning or late in the evening, when irradiance and temperature are low and fluxes are small.

The slopes and intercepts of linear regressions were calculated by geometrical mean regression if both x and y variables were associated with an error, such as for δ¹³C vs. the inverse of the CO₂ mole fraction ("Keeling plot"). Different regressions were tested against each other by introducing indicator ("dummy") variables into a multiple regression model (Neter et al. 1985). The software package JMP (Version 4, SAS Institute Inc., Cary, N.C., USA) was used for statistical analyses. Correlations between observed and predicted values of photosynthetic isotope discrimination were weighted according to the standard deviations of the measurements.

typical flux rate:	high	SD	medium	SD	low	SD
CO ₂ flux [μmol/m ² /s]	9.0	0.2	4.7	0.15	1.7	0.1
¹³ Δ [‰]	14.8	0.7	17.3	1.2	31.5	5.8
¹⁸ Δ [‰]	8.5	1.2	11.0	2.2	98.3	8.8
C _i /C _a	0.41	0.03	0.51	0.05	1.06	0.20

Table 2.2: Examples for typical values and standard deviations of CO₂ fluxes, isotope discriminations (¹³Δ and ¹⁸Δ) and C_i/C_a for different CO₂ flux rates.

3. $\delta^{13}\text{C}$ of CO_2

3.1 Discrimination against ^{13}C during photosynthesis

Introduction

The carbon isotopic composition of CO_2 is a powerful tracer that has been used for studying global patterns of carbon exchange, including the role of different biomes in the terrestrial part of this exchange through their respective magnitudes of ecosystem ^{13}C discrimination (Rayner et al. 1999, Kaplan et al. 2001), and extending to the contributions of component fluxes to net ecosystem exchange partitioned with the $\delta^{13}\text{C}$ of gross fluxes (Bowling et al. 2001). Other studies made use of the isotopic composition of organic material to infer photosynthetic or plant physiological characteristics like stomatal conductance, the ratio of substomatal to ambient CO_2 mole fraction (C_i/C_a), or water use efficiency (for example, Flanagan et al. 1997, Katul et al. 2000).

$\delta^{13}\text{C}$ values of canopy CO_2 are influenced by photosynthetic discrimination, the isotopic signature of respiratory CO_2 , and turbulent mixing with air from the convective boundary layer (Lloyd et al. 1996). During photosynthesis, ambient CO_2 will be enriched in ^{13}C , because photosynthetic carbon uptake discriminates against ^{13}C . At the same time, photosynthesis leaves plant material depleted in ^{13}C , and this organic material becomes the source for respiration. If there is no pronounced isotopic fractionation during respiration, the isotopic signature of respiratory CO_2 will be mainly determined by the depleted isotopic composition of plant and soil organic carbon. During the day, turbulent mixing of canopy air with tropospheric background air in the convective boundary layer dampens short term fluctuations of the mole fraction and $\delta^{13}\text{C}$ value of canopy CO_2 . If the rates of photosynthesis or respiration are high relative to turbulent mixing, CO_2 mole fractions and isotope ratios inside the canopy can differ from those above the canopy. Changes in environmental conditions may also cause diurnal and seasonal variations of ^{13}C discrimination during photosynthesis. These in turn will also influence the isotopic composition of biomass and hence of integrated ecosystem exchange, or ecosystem discrimination, over time.

A commonly applied method to obtain ecosystem discrimination is to construct integrated mass balances ("Keeling plots", after Keeling 1961) from air samples collected in and above a plant canopy. Because a prerequisite of the method is that variable mixing occurs between only two isotopically distinct pools of CO₂, it is restricted to night times and can only reflect the isotopic signal of respiratory CO₂ sources. During the day, the approach is complicated by fluctuations in the extent of turbulent mixing so that information on the variability of photosynthetic discrimination has been limited. On the other hand, photosynthetic discrimination is a parameter that is either required or would be helpful in all of the above studies. Its magnitude has often been assumed constant, substituted by other proxies like δ¹³C of foliage material. So far, there has been only one attempt to measure directly variations of photosynthetic discrimination under natural conditions (Harwood et al. 1998). Clearly, many more measurements of discrimination under field conditions will help to refine our understanding of theoretically derived relationships for use in empirical predictions and models.

This section focuses on the influence of photosynthesis on the δ¹³C signature of canopy CO₂ and contributions of concurrent photorespiration and day-time dark respiration to the observed net photosynthetic ¹³C discrimination. Predictions and field observations of ¹³C discrimination during photosynthesis are described. Relationships between ¹³C discrimination, predicted from environmental parameters, and canopy gas exchange fluxes obtained for the Sitka spruce study site will be applied in Part II, section 7.2, to estimate diurnal patterns and integrated values of δ¹³C of ecosystem gas exchange for the days following measuring campaigns. In addition, the δ¹³C signatures of canopy fluxes will be employed in Part II, section 9, to evaluate different approaches for the partitioning of net ecosystem exchange into its component fluxes.

Theory

Photosynthetic carbon uptake discriminates against the heavy carbon isotope because ¹²C and ¹³C differ in their reaction kinetics and diffusion coefficients. Following the simplest (and most often used) formulation of ¹³C discrimination (Farquhar et al. 1982), ¹³Δ_S ("simple", ‰) is related to the ratio of intercellular (substomatal) to ambient CO₂ mole fraction, C_i/C_a, according to:

$$^{13}\Delta_S = a + (b - a) \frac{C_i}{C_a} \quad (3.1)$$

where a is the fractionation factor for the diffusion of CO₂ in air (≈ 4.4 ‰, Craig 1953) and b is the carboxylation fractionation associated with the activity of the enzyme Rubisco during CO₂ uptake inside the leaf. The magnitude of b can vary across species, and measurements have reported values from 27 to 38 ‰ (see review of O'Leary 1981). Because it has not been determined for Sitka spruce yet, a value of 30 ‰ has been assumed here. In the above version of the discrimination equation, all respiratory terms are neglected. Thus, the magnitude of ¹³C discrimination is governed solely by C_i/C_a , the ratio of intercellular to ambient CO₂ mole fractions ($\mu\text{mol/mol}$, or ppm) across stomata. Consequently, the range of predicted discrimination values must lie between 4.4 ‰ for diffusion limited carbon uptake, where stomata are closed and $C_i/C_a \rightarrow 0$, and 30 ‰ for the enzyme limited case, with open stomata and $C_i/C_a \rightarrow 1$.

Any respiratory CO₂ fluxes occurring concurrently during photosynthetic gas exchange can change net observed discrimination due to their distinct isotopic signatures. The more extensive formulation of the discrimination equation (Farquhar et al. 1982) thus includes contributions from photorespiration and from day-time dark respiration to predict discrimination. Including the respiratory terms (see also Farquhar 1983, Farquhar and Richards 1984), ¹³ Δ_C can be calculated from:

$$^{13}\Delta_C = a + (b - a) \frac{C_i}{C_a} - f \frac{\Gamma^*}{C_a} - e \frac{R_d}{kC_a} \quad (3.2)$$

where k is carboxylation efficiency ($\text{mol/m}^2/\text{s}$), Γ^* is the CO₂ compensation point in the absence of dark respiration ($\mu\text{mol/mol}$), R_d is the rate of dark respiration in the light ($\mu\text{mol/m}^2/\text{s}$), e and f (‰) are the fractionation factors associated with dark respiration and photorespiration, respectively. Following the definition of carboxylation efficiency used in its derivation (see Farquhar et al. 1982), the above equation is here written as:

$$^{13}\Delta_C = a + (b - a) \frac{C_i}{C_a} - f \frac{\Gamma^*}{C_a} - e \frac{R_d}{A + R_d} \frac{C_i - \Gamma^*}{C_a} \quad (3.3)$$

where net assimilation rate A ($\mu\text{mol/m}^2/\text{s}$) was obtained following equation 2.2.

The CO₂ photocompensation point, Γ^* , denotes the partial pressure of CO₂ where the rate of CO₂ uptake by photosynthesis is exactly equal to the rate of CO₂ release by photorespiration. Brooks and Farquhar (1985) and Atkin et al. (2000) reported that this point was comparable for a range of plant species and for each species only depended on leaf temperature (T in °C). The regression parameters reported in Brooks and Farquhar (1985) were used to calculate Γ^* :

$$\Gamma^* = 44.7 + 1.88 \cdot (T - 25) + 0.036 \cdot (T - 25)^2 \quad (3.4)$$

In photorespiration ("respiration", because CO₂ is released while O₂ is taken up), the enzyme Rubisco catalyzes the binding of O₂ (oxygenase) instead of CO₂ (carboxylase activity) to ribulose biphosphate. The rate of photorespiration increases with light and temperature. Photorespiration rate, R_p ($\mu\text{mol}/\text{m}^2/\text{s}$), can be calculated following the method of Farquhar and von Caemmerer (1982):

$$R_p = \frac{A + R_d}{\frac{C_i}{\Gamma^*} - 1} \quad (3.5)$$

With the isotopic composition of photorespired CO₂ equal or very close to newly assimilated carbon, the isotopic signal of the photorespiratory CO₂ flux differs from that of the photosynthetic flux into the leaf by the magnitude of the fractionation during photorespiration. Estimates of the photorespiratory fractionation factor, f , are +7 ‰ (Rooney 1988) and +8 ‰ (Gillon 1997, Griffiths et al. 1999). This positive fractionation factor means that photorespired CO₂ is depleted with respect to its source, newly assimilated carbon. Thus, taking photorespiration into account would decrease the predicted overall photosynthetic discrimination values.

For the study here, day-time dark respiration was assumed to be inhibited depending on irradiance and temperature (Atkin et al. 2000). Using a set of regression parameters from Atkin et al. (2000) determined for Snow gum (*Eucalyptus pauciflora*), the ratio of day-time relative to night-time dark respiration, $R_d/R_n(T, I)$, was obtained from concurrent measurements of needle temperature, T (°C), and incident solar irradiance, I ($\mu\text{mol}(\text{quanta})/\text{m}^2/\text{s}$). The rate of day-time dark respiration, R_d , was then calculated from temperature dependent R_n estimates as:

$$R_d = \frac{R_d}{R_n}(T, I) \cdot R_n \quad (3.6)$$

Night-time foliage respiration, R_n ($\mu\text{mol}/\text{m}^2/\text{s}$), was calculated using the Arrhenius function approach (Lloyd and Taylor 1994), with parameters fitted to branch night-time respiration data:

$$R_n = R_{20} \cdot \exp\left[\frac{E_0}{RT}\left(\frac{T}{T_{20}} - 1\right)\right] \quad (3.7)$$

where R_{20} is respiration rate at 20 °C, T is needle temperature in K, R is the gas constant (8.314 J/mol/K), and E_0 is the activation energy, taken here as 56734 J/mol (Rayment et al. 2002).

According to equation 3.3, dark respiration has an impact on the net observed $^{13}\Delta$ value only if there is intrinsic discrimination against ^{13}C during dark respiration, i.e. the CO_2 released in day-time dark respiration is enriched (negative fractionation factor) or depleted (positive factor) with respect to its source. Whether there is fractionation during dark respiration, and to what extent, is still under debate. Estimates of e range from zero (Lin and Ehleringer 1997) to -6 ‰ (Duranceau et al. 1999). In our study, we could not confirm a fractionation during respiration (as described in section 3.2). In this case, equation 3.3 cannot be applied, since for $e = 0$, the dark respiration term on the right hand side of the equation disappears. But CO_2 released in dark respiration originates from a pool of leaf assimilates, representing an integral of $^{13}\Delta$ over a preceding time interval (see equation 3.12) that is different from instantaneous $^{13}\Delta$ at most times. Therefore, even if there was no intrinsic fractionation during dark respiration, the isotopic signal of the dark respiratory flux would still differ from that of the photosynthetic flux into the leaf. To take this into account, an effective fractionation factor for day-time dark respiration, e^* (‰), was defined as:

$$e^* = \delta^{13}C_{plant} - \delta^{13}C_{atm} - ^{13}\Delta \quad (3.8)$$

where $\delta^{13}C_{plant}$ (‰) is the isotopic composition of the pool of recently assimilated needle carbohydrates as derived from nocturnal measurements of the isotopic signature of dark

respiration (assuming there is no intrinsic fractionation during dark respiration) and $\delta^{13}\text{C}_{\text{atm}}$ (‰) is the isotopic composition of ambient CO_2 in the canopy air space, varying around the background value of tropospheric CO_2 of ≈ -8 ‰ (Goodman and Francey 1988). A more detailed derivation of equation 3.8 is given in the Appendix.

Lastly, isotopic fractionations during diffusion of CO_2 through a laminar boundary layer or internal transfer through mesophyll cells to the chloroplasts also impact the magnitude of discrimination. Because experiments were conducted under conditions of high boundary layer conductance (equivalent to those used in the study of Rayment et al. 2002), the CO_2 mole fraction at the needle surface, C_s , was assumed to be equal to C_a , so that fractionation associated with diffusion through a laminar boundary layer ($a_b = 2.9$ ‰) could be neglected. Combining the different contributions, ^{13}C discrimination, $^{13}\Delta_F$ ("full"), was calculated using:

$$^{13}\Delta_F = a \frac{C_a - C_i}{C_a} + a_m \frac{C_i - C_c}{C_a} + b \frac{C_c}{C_a} - f \frac{\Gamma^*}{C_a} - (e^* + e) \frac{R_d}{A + R_d} \frac{C_i - \Gamma^*}{C_a} \quad (3.9)$$

where $a_m (= e_s + a_i)$ is the sum of fractionation factors during internal CO_2 transfer, combining equilibrium fractionation of CO_2 entering solution ($e_s = 1.1$ ‰ at 25°C , Mook et al. 1974) and fractionation during diffusion of dissolved CO_2 in water ($a_i = 0.7$ ‰, O'Leary et al. 1984). C_c is the chloroplast CO_2 mole fraction. C_i , the CO_2 mole fraction in the stomatal cavities, was taken as representative of that at the mesophyll cell wall surface (Farquhar and von Caemmerer 1982). C_i corresponds to C_{st} in equations 15 and 16 of Lloyd and Farquhar (1993).

The ^{13}C fractionation during internal CO_2 transfer is weighted by the drawdown in the CO_2 mole fraction between stomatal cavities and the chloroplasts. In analogy to stomatal conductance, the two CO_2 mole fractions, C_i and C_c , are related to net CO_2 uptake, A , and mesophyll conductance, g_w ($\text{mol}/\text{m}^2/\text{s}$), according to:

$$A = g_w \cdot (C_i - C_c) \quad (3.10)$$

Hence, mesophyll conductance can be derived from a regression of the difference between predicted discrimination (including concurrent respiratory contributions) and observed discrimination, $^{13}\Delta_C - ^{13}\Delta_{\text{obs}}$, versus A/C_a , assuming that $^{13}\Delta_{\text{obs}}$ corresponds to

the full derivation value of $^{13}\Delta_F$ as obtained from equation 3.9. Subtracting equation 3.9 from equation 3.3, and substituting $(C_i - C_c)$ from equation 3.10, allows to calculate mesophyll conductance, g_w , and thereby C_c , from the slope of the regression (see Evans and von Caemmerer 1996):

$$^{13}\Delta_C - ^{13}\Delta_{obs} = ^{13}\Delta_C - ^{13}\Delta_F = (b - a_m) \frac{C_i - C_c}{C_a} = \frac{(b - a_m) A}{g_w C_a} \quad (3.11)$$

The isotopic composition of newly assimilated material, $\delta^{13}C_D$, constitutes a time integrated signal of assimilation weighted ^{13}C discrimination:

$$\delta^{13}C_D = \frac{\int A \cdot (\delta^{13}C_{atm} - ^{13}\Delta) dt}{\int A dt} \quad (3.12)$$

where $^{13}\Delta$ is the discrimination against ^{13}C weighted by the assimilation rate A during the photosynthetic period over the day. The weighting also has to account for diurnal variations of $\delta^{13}C_{atm}$, the isotopic composition of canopy CO_2 . Calculated values of $\delta^{13}C_D$ also depend on the specific formulation used for ^{13}C discrimination ($^{13}\Delta_S$, $^{13}\Delta_C$, $^{13}\Delta_F$).

During photosynthesis, newly assimilated material is added to the carbohydrate pool of needles. Therefore, diurnal variations in the magnitude of discrimination will be reflected by changes in the isotopic composition of foliage carbohydrate pools, which in turn will influence discrimination values because of its feedback as isotopic signature of day-time dark respiration. Therefore, calculations of $\delta^{13}C_{plant}$ were performed fully coupled with discrimination predictions:

$$\delta^{13}C_{plant}(t) = \left(1 - \frac{\int A dt}{M_c}\right) \delta^{13}C_{plant}(t-1) + \frac{\int A dt}{M_c} (\delta^{13}C_{atm}(t) - ^{13}\Delta(t)) \quad (3.13)$$

where M_c ($\mu molC/m^2$) is total carbon content per surface area of branch bag foliage. Here, the assimilation rate A was integrated over one sampling interval, usually 20 minutes, assuming that the values for discrimination and $\delta^{13}C_{atm}$ were constant over that time period. The isotopic composition of the needle carbohydrate pools from the previous time step, $\delta^{13}C_{plant}(t-1)$, was then used as isotopic signature of day-time dark

respiration to calculate instantaneous values of discrimination in the next time step:
 $^{13}\Delta(t) = f(\delta^{13}\text{C}_{\text{plant}(t-1)})$.

When the initial value of $\delta^{13}\text{C}_{\text{plant}}$ was prescribed from the isotopic signature of nocturnal dark respiration, $\delta^{13}\text{C}_{\text{plant}}$ showed strong drifts over short time periods because diurnal discrimination integrals were substantially different from initial $\delta^{13}\text{C}_{\text{plant}}$. Instead, an initial value was chosen such that drifts of $\delta^{13}\text{C}_{\text{plant}}$ over time were minimised, i.e. the system was assumed to be in dynamic steady state.

Results

Field observations of $^{13}\Delta$ during photosynthesis

From flask sample pairs, estimates of photosynthetic ^{13}C discrimination ($^{13}\Delta_{\text{obs}}$) were obtained following equation 2.7 for two sampling campaigns, 18/19 May (6:55 – 18:40, dawn samples taken on next day at 5:00 and 5:20) and 20 July 2001 (3:40 – 17:30, complete diurnal cycle). All values are reported with respect to V-PDB. Figure 3.1 shows net observed discrimination values for the different branch bags (top1 and top3, 10 m (both months) and mid, 8 m (May only)). On all days, $^{13}\Delta_{\text{obs}}$ for the top bags had maximum values of $> 30 \text{ ‰}$ at dawn and dusk. During the rest of the day, $^{13}\Delta_{\text{obs}}$ was consistently lower, 15 – 18 ‰ in the morning and $\approx 20 \text{ ‰}$ in the afternoon. $^{13}\Delta_{\text{obs}}$ in the middle bag was slightly higher (20 – 26 ‰) at most times. At noon, the highest $^{13}\Delta_{\text{obs}}$ value of both campaigns (41 ‰) was measured in the middle bag. In July, $^{13}\Delta_{\text{obs}}$ was overall slightly smaller than in May. Estimated uncertainties were largest at dawn, dusk and (mid bag) noon, when the highest values of $^{13}\Delta_{\text{obs}}$ were observed.

Surprisingly high values for net observed discrimination were found in both months at dawn and dusk and in May at noon, mid bag. Following the simple relationship of equation 3.1, this would imply that C_i is higher than C_a . From equation 2.1 can be concluded that C_i cannot exceed C_a at times of net CO_2 uptake. There are three potential explanations for this discrepancy: firstly, the fractionation factor (b) for Sitka spruce during carboxylation could be higher than generally thought, secondly, C_i could be indeed higher than C_a if photosynthetic rates were lower than those of concurrent respiration, thirdly, there could be influences of distinct isotopic signatures of respiratory

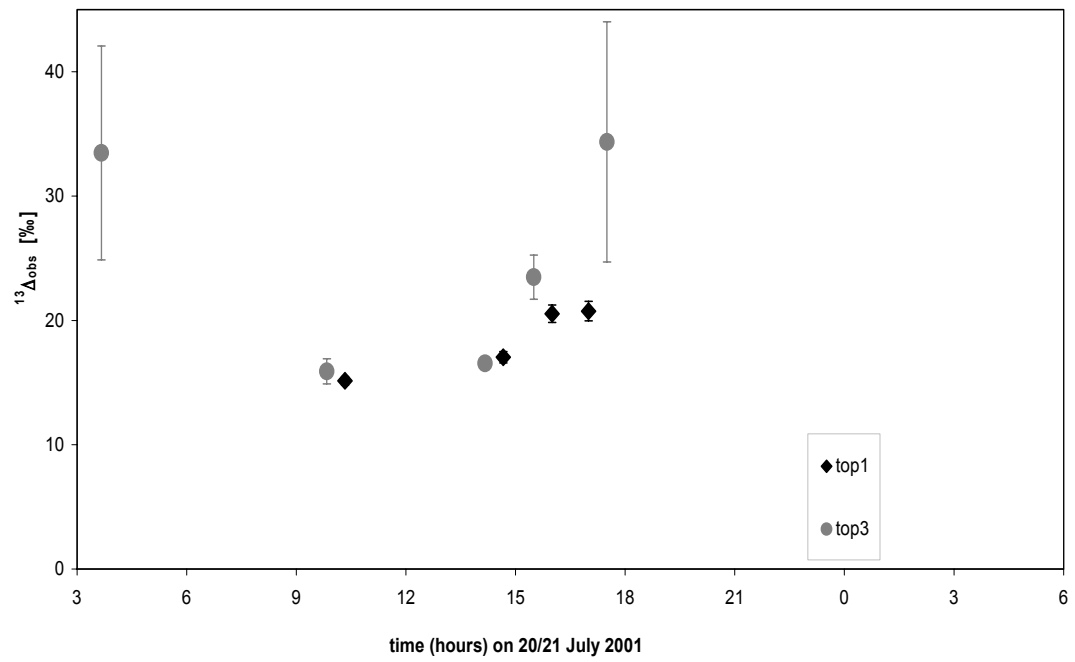
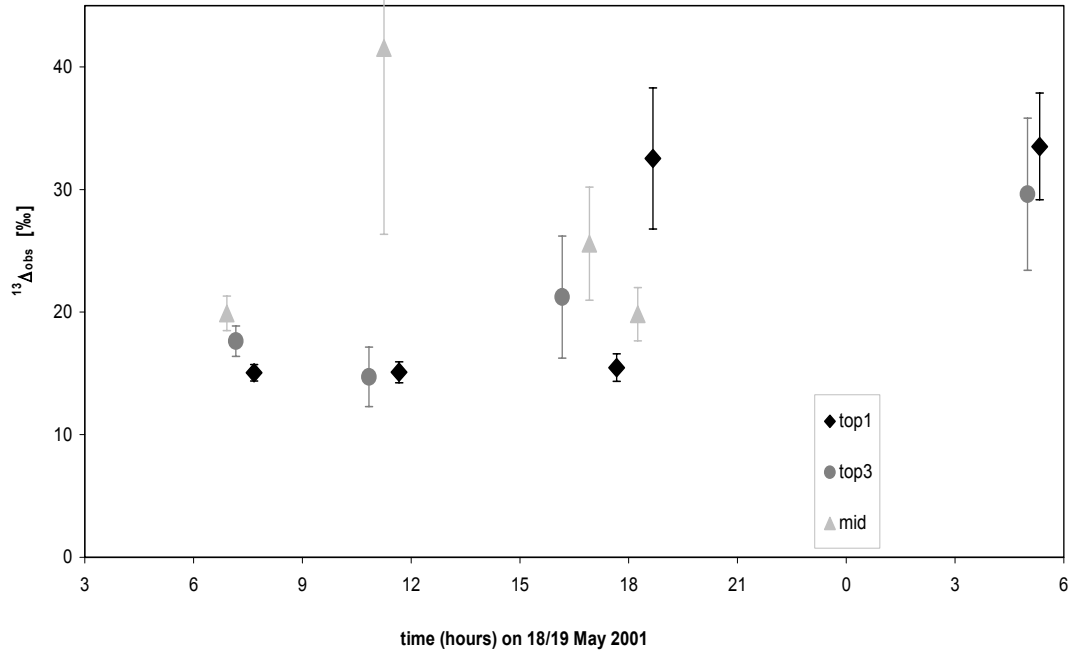


Figure 3.1: Net observed photosynthetic discrimination ($^{13}\Delta_{\text{obs}}$) of branch bag foliage.

contributions on net observed discrimination. However, for the first explanation to apply, a value of 41 ‰ would be needed for carboxylation fractionation. This is outside the range of previously reported values (Roeske and O'Leary 1984). Regarding the second option, a net assimilatory flux is a prerequisite for the calculation of isotopic discrimination. That there was net CO₂ uptake at the respective times can also be seen in Figure 3.4. Therefore, the high ¹³Δ_{obs} values found in our study can only be satisfied by the third explanation of additional processes contributing to isotopic gas exchange, i.e. to net observed discrimination, in the branch bags. Hence, the more extensive formulation (equation 3.9) needs to be applied to relate ¹³C discrimination to C_i/C_a.

Parameters for predicting ¹³Δ

C_i/C_a

C_i/C_a was calculated from CO₂ mole fraction and flux measurements obtained from the IRGA and relative humidity sensors for each time step (interval 20 min per bag, see section 2). Figure 3.2 shows that diurnal variations of C_i/C_a were generally similar to those of ¹³Δ_{obs}. Included in Figure 3.2 is stomatal conductance data for both months. Diurnal patterns were clearest in July. In general, C_i/C_a was higher at dawn and dusk than during the rest of the day. At dawn, low assimilation rates coincided with high stomatal conductance in conditions of low light and high humidity. At dusk, C_i/C_a was again approaching higher values although stomatal conductance had not increased back to morning values, indicating that low assimilation values (see Figure 3.4) were responsible for evening increases in C_i/C_a (see equation 2.6). Day-time values were lower during the July campaign. In May, C_i/C_a values were generally noisier due to more pronounced variability of environmental conditions, and not continuous for the top bags on the first half day when instrumental problems occurred. C_i/C_a values were more stable in July, when diurnal variations in environmental conditions were more gradual.

Respiratory contributions to gas exchange

Rates of temperature dependent dark respiration, R_n (from equation 3.7), and rates of temperature and light inhibited day-time dark respiration, R_d , obtained via equation 3.6 using nocturnal dark respiration rates, are presented in Figure 3.3. The environmental parameters determining the degree of respiration inhibition, solar irradiance (PPFD) and

needle temperature obtained from branch bag sensors, are also shown. Irradiance was highly variable due to rapid changes in cloud cover during the May sampling campaign, but values were lower and with less variability in July due to a relatively uniform cloud cover. Changes in temperature followed irradiance patterns with slightly damped short-term fluctuations. Because of its temperature dependence (see equation 3.7), diurnal patterns of R_n also showed a high degree of variability. However, R_d variability was less pronounced because at higher temperature and light levels higher R_n rates coincided with stronger inhibition of R_d rates, whereas at conditions of lower light and temperatures, R_d rates were less inhibited while R_n rates were lower, leading to overall more uniform, smoothed diurnal patterns of R_d (see equations 3.6 and 3.7).

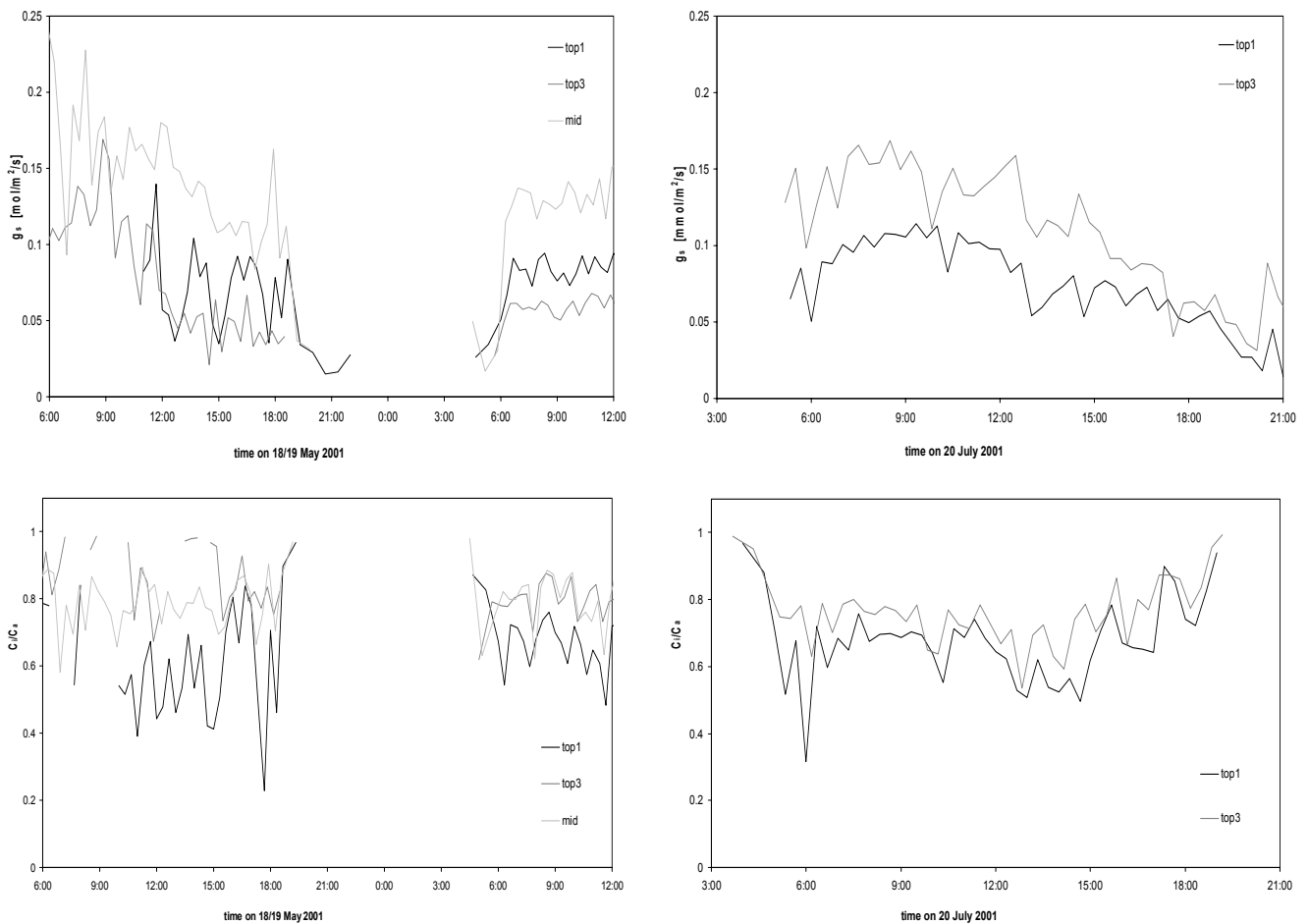


Figure 3.2: Top: Stomatal conductance to water vapour, g_s . Bottom: C_i/C_a , calculated following equations 2.4 and 2.6 for May (left) and July (right) 2001.

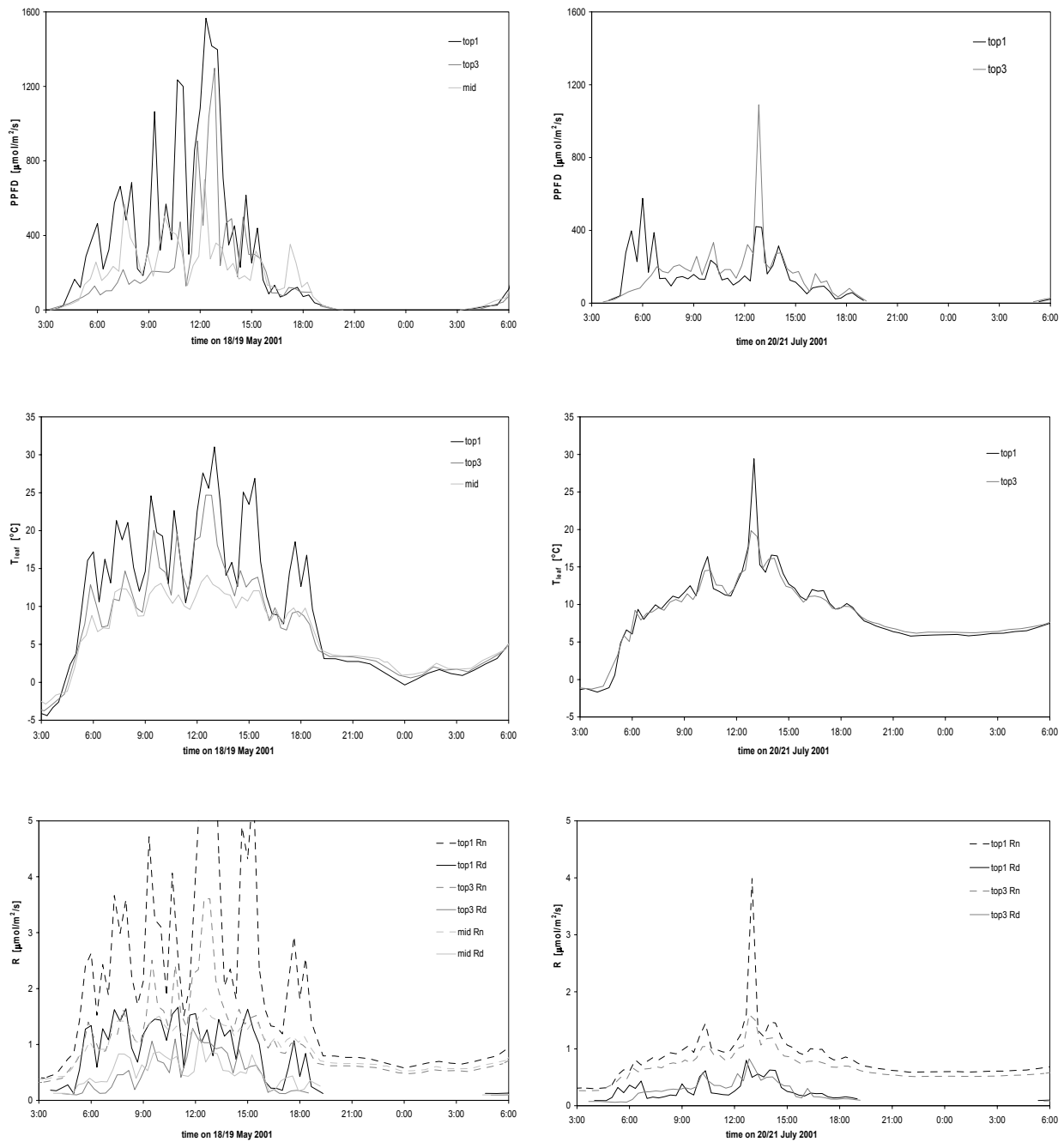


Figure 3.3: Top: Irradiance (PPFD), Middle: Leaf temperature (T_{leaf}) from branch bag sensors, Bottom: Rates of day-time dark respiration (R_d) and nocturnal dark respiration (R_n).

The gross photosynthetic CO₂ flux is always larger than the net CO₂ assimilation rate by an amount equivalent to the sum of the rates of CO₂ release during photorespiration and day-time dark respiration. Figure 3.4 shows how much net assimilation (A), photorespiration (R_p) and dark respiration (R_d) were estimated to have contributed to the gross photosynthesis rate ($V_c = A + R_p + R_d$) during the two sampling campaigns, 18/19 May and 20 July 2001, both as absolute flux rates and as relative contributions to gross photosynthesis in %. Dark respiration had a significant influence at dawn and dusk, with high proportions (30 - 50 %) of gross photosynthesis respired. R_d fluxes in May were generally higher than in July as light inhibition was stronger in July. On the other hand, rates of photorespiration were almost negligible at dawn and dusk, when temperatures were low (1°C at dawn). At all other times, around 15 % of photosynthetic uptake was lost in photorespiration.

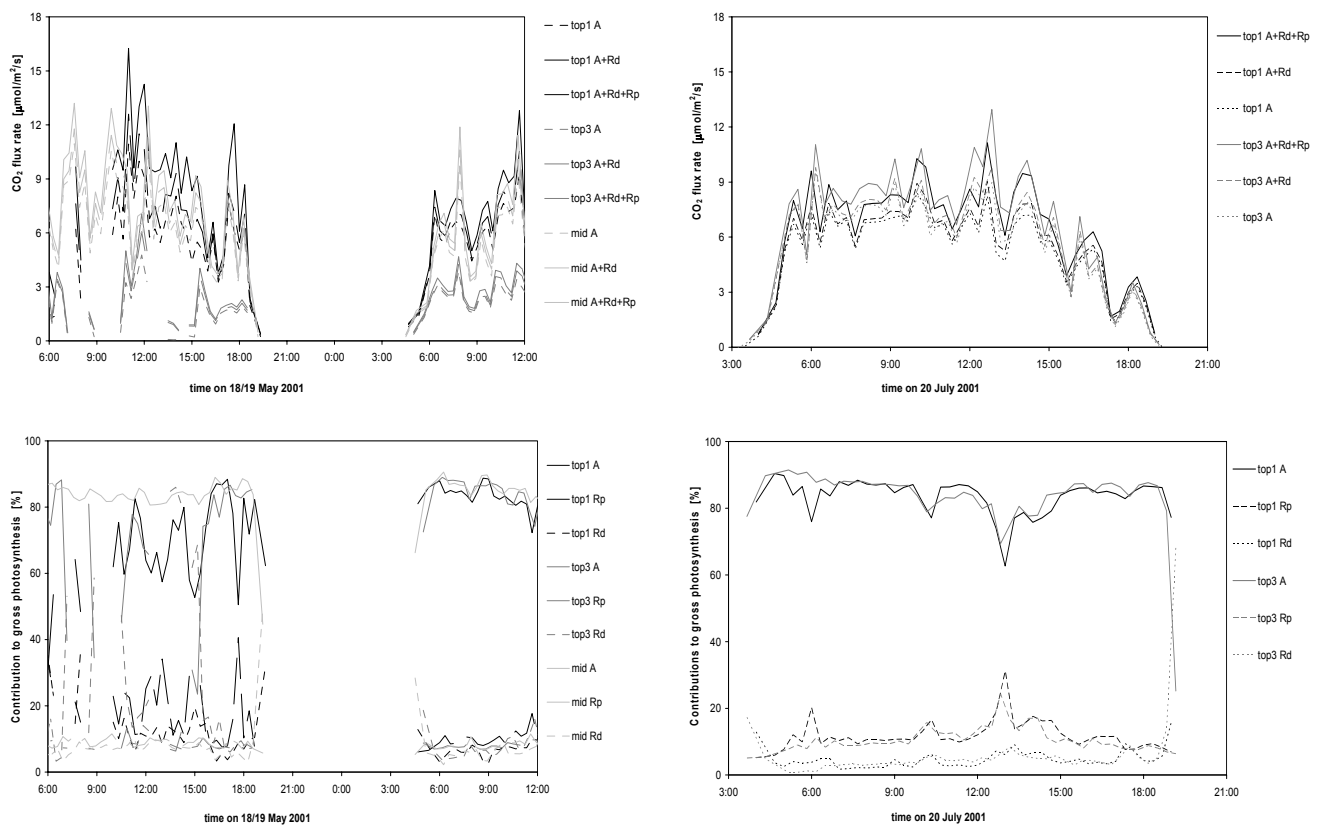


Figure 3.4: Top: Summing up of net assimilation (A), dark respiration (R_d) and photorespiration (R_p) to gross photosynthesis ($A + R_d + R_p$), Bottom: Contributions of these fluxes to gross photosynthesis in %, both for May (left) and July (right) 2001.

Isotopic composition of canopy CO₂

$\delta^{13}\text{C}_{\text{atm}}$, the carbon isotopic composition of canopy CO₂, obtained from measurements on open branch bags, is shown in the top panel of Figure 3.5. Complete diurnal cycles of $\delta^{13}\text{C}_{\text{atm}}$ were derived from a regression of $\delta^{13}\text{C}_{\text{atm}}$ against the inverse of canopy CO₂ mole fraction, assuming mixing of two sources of different isotopic composition into a pool of canopy air (Keeling 1961). Even though this assumption might not be strictly fulfilled during the day, it can also be valid for more than two sources with distinct isotopic signatures provided the relative contributions from these sources do not change over time. Regressions had R² values of > 0.95 in both months, with intercepts of $-25.5 \pm 1.1 \text{ ‰}$ (May) and $-27.5 \pm 0.6 \text{ ‰}$ (July). No significant difference was found between the two regressions. Differences between regressed and measured $\delta^{13}\text{C}_{\text{atm}}$ are probably caused by (random) offsets in CO₂ mole fraction data between IRGA and flask samples.

Effective fractionation during dark respiration in the light

The middle panels of Figure 3.5 shows the calculated isotopic signature of day-time dark respiration with respect to canopy air, $\delta^{13}\text{C}_{\text{R}} = \delta^{13}\text{C}_{\text{atm}} - \delta^{13}\text{C}_{\text{plant}}$, and $^{13}\Delta_{\text{obs}}$ from branch bag measurements. The isotopic composition of the respiration substrate (soluble needle carbohydrates), $\delta^{13}\text{C}_{\text{plant}}$, was assumed to be in a dynamic steady state with discrimination as described above (equation 3.13). Initial $\delta^{13}\text{C}$ values were -26 ‰ (top1), -31.5 ‰ (top3) and -29.5 ‰ (mid) in May, -25 ‰ (top1) and -28 ‰ (top3) in July. Overall, the average isotopic signal of dark respiration was 22 ‰ . Variations in $\delta^{13}\text{C}_{\text{R}}$ over the photosynthetic period were around 1 ‰ , similar to those of $\delta^{13}\text{C}_{\text{plant}}$ but smaller than those of $\delta^{13}\text{C}_{\text{atm}}$ ($\approx 2 \text{ ‰}$). Of course, any fractionation would additionally change the respiratory signal.

Presented in the bottom panel of Figure 3.5, the effective fractionation factor of day-time dark respiration, e^* , was calculated by subtracting the two curves shown in the middle panel ($\delta^{13}\text{C}_{\text{R}} - ^{13}\Delta$, see equation 3.8). It illustrates how the difference between the curves, or effective fractionation factor, changes its sign where the isotopic signature of the respiratory contribution is equal to the value of photosynthetic discrimination. Accordingly, dark respiration in the light effectively expresses a negative fractionation mostly early and late in the photosynthetic period and a positive fractionation during the rest of the day. As with fractionation during photorespiration, a positive factor means

that respired CO_2 is isotopically depleted with respect to its source material, whereas a negative factor indicates isotopic enrichment of respired CO_2 . Hence, taking the influence of concurrent dark respiration during photosynthetic gas exchange into account increases predictions of ^{13}C discrimination at dawn and dusk and decreases predicted discrimination for most other times.

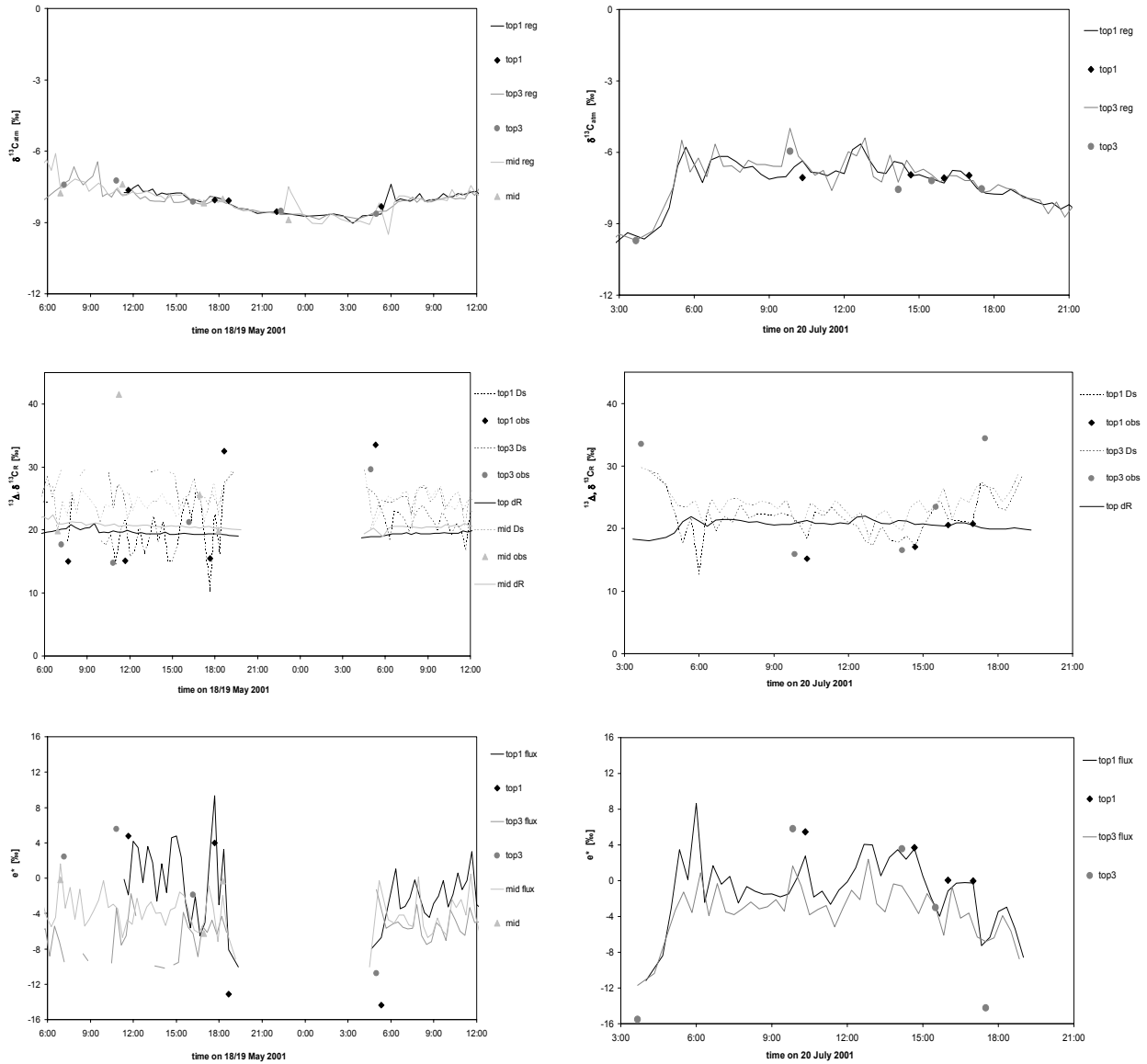


Figure 3.5: Top: observed and regressed (lines) $\delta^{13}\text{C}_{\text{atm}}$ of canopy CO_2 , middle: $^{13}\Delta_{\text{obs}}$, simple flux derived $^{13}\Delta$ (dashed lines) and $\delta^{13}\text{C}$ signature ($\delta^{13}\text{C}_{\text{R}}$, solid lines) of day-time dark respiration with respect to $\delta^{13}\text{C}_{\text{atm}}$ of canopy CO_2 , bottom: effective fractionation factor, e^* , from $^{13}\Delta_{\text{obs}}$ and simple flux derived $^{13}\Delta$ (solid lines).

Mesophyll conductance

Mesophyll conductance, g_w , was obtained from a regression of the difference between predicted and observed discrimination, ($^{13}\Delta_C - ^{13}\Delta_{obs}$), versus A/C_a . Predictions included contributions of concurrent respiration on isotopic gas exchange so that differences between the two values can be attributed predominantly to the influence of fractionation during internal CO_2 transfer on the overall discrimination value. The regression was based on combined data from all branch bags and for both months because mesophyll resistance to CO_2 diffusion should not change substantially over such (relatively short) time periods (Evans et al. 1986, Evans and von Caemmerer 1996).

Regression data is shown in Figure 3.6, excluding data where A/C_a was not significantly different from zero ($< 0.001 \text{ mol/m}^2/\text{s}$). Mesophyll conductance for needles in the branch bags was $0.29 \text{ mol/m}^2/\text{s}$, only slightly higher than the maximum values obtained for stomatal conductance ($\approx 0.24 \text{ mol/m}^2/\text{s}$) over the sampling periods. From this constant value for mesophyll conductance, C_c was calculated using equation 3.10. The offset between C_c and C_i , expressed as $(C_i - C_c)/C_a$, was in the order of 0.1 at times of high assimilation rates, in good agreement with values reported for leaves of other woody species (Syvertsen et al. 1995).

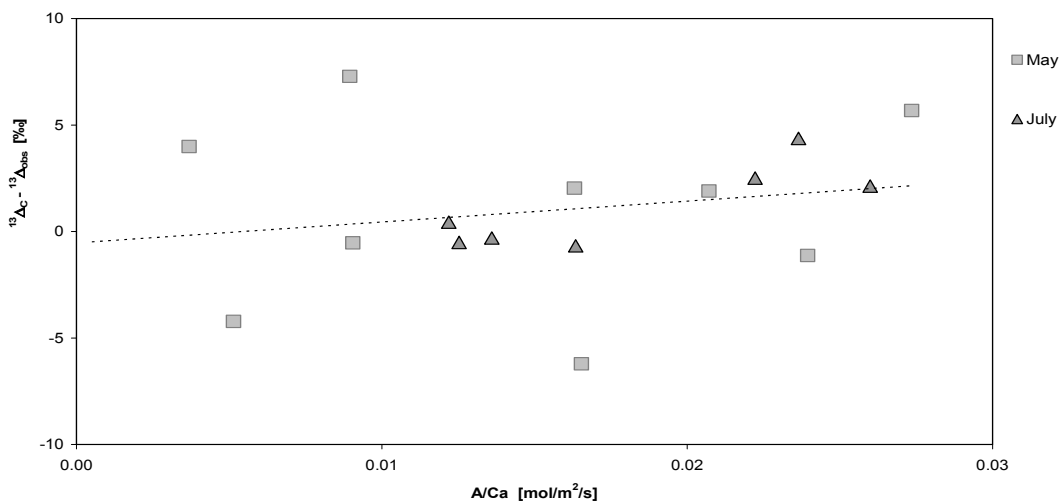


Figure 3.6: Difference between respiration corrected predicted and net observed discrimination ($^{13}\Delta_C - ^{13}\Delta_{obs}$) versus A/C_a , as regression to derive mesophyll conductance, g_w , with data from both months where A/C_a was above $0.001 \text{ mol/m}^2/\text{s}$.

Predictions of $^{13}\Delta$ during photosynthesis

From C_i/C_a and the parameters described above, $^{13}\Delta$ values were predicted using simple uncorrected (equation 3.1), respiration corrected, mesophyll conductance corrected, and full formulations (equation 3.9), yielding 5 sets of predictions for each branch bag and sampling campaign. Results are presented in Figure 3.7, together with net observed discrimination, $^{13}\Delta_{\text{obs}}$, for 18/19 May and 20 June 2001. Calculations were done separately to examine the impact of each of these contributions on the predicted discrimination. In the three panels of Figure 3.7 are highlighted the offsets from simple uncorrected discrimination values due to, top: photorespiration and day-time dark respiration, middle: mesophyll conductance, bottom: a combination of all corrections.

Contributions of dark respiration in the light did not change predicted discrimination values significantly during most of the day, when both relative rates of dark respiration and effective fractionation, e^* , were small. Relative rates at dawn and dusk were, however, much larger, and together with concurrent high negative effective fractionation factors, corrected discrimination values were up to 10 ‰ higher than without correction. In May, this was also the case for several mid-day sampling intervals. However, this might have been caused or amplified by technical problems with the experimental equipment in the morning of the first May measuring day. Data obtained during that time period from the top branch bags was excluded from quantitative analyses. Correcting for concurrent day-time dark respiration did not fully account for the high values of discrimination that were observed at dawn and dusk. The discrepancy was even higher for the May mid bag sampling at 11:15, where predicted discrimination was only increased by 1 to 28 ‰, much lower than the observed value of 41 ‰, again probably due to a technical problem with that measurement.

Taking contributions of photorespiration to isotopic gas exchange in the branch bags into account decreased predicted discrimination values by around 0.5 ‰. The effect of this correction was slightly higher at mid-day with gradual morning increases and afternoon decreases as a consequence of temperature changes. The influence of fractionation during internal CO_2 transfer ("mesophyll conductance") is similar to that of photorespiration, leading to a decrease in predicted discrimination compared to simple uncorrected values. The decrease was more pronounced at 1 to 2 ‰ and not as uniform over the diurnal cycle because it is scaled by assimilation rate instead of temperature.

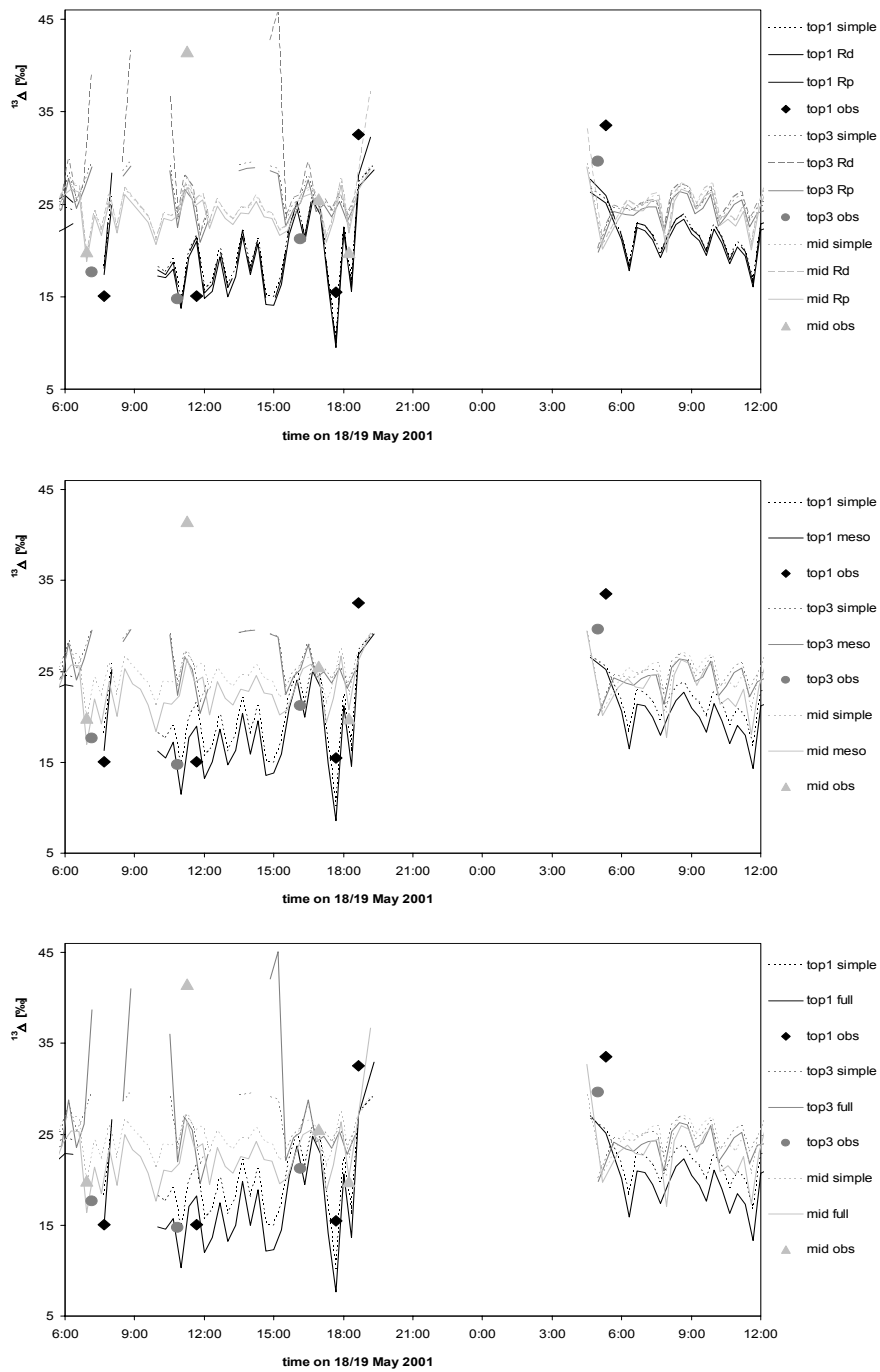


Figure 3.7a: Photosynthetic discrimination against ^{13}C predicted from flux derived C_i/C_a using the uncorrected ("simple") version and the different corrected formulations for May 2001. Corrections include: top: photorespiration ("Rd") or day-time dark respiration ("Rd"), middle: mesophyll conductance ("meso"), bottom: all of the above ("full").

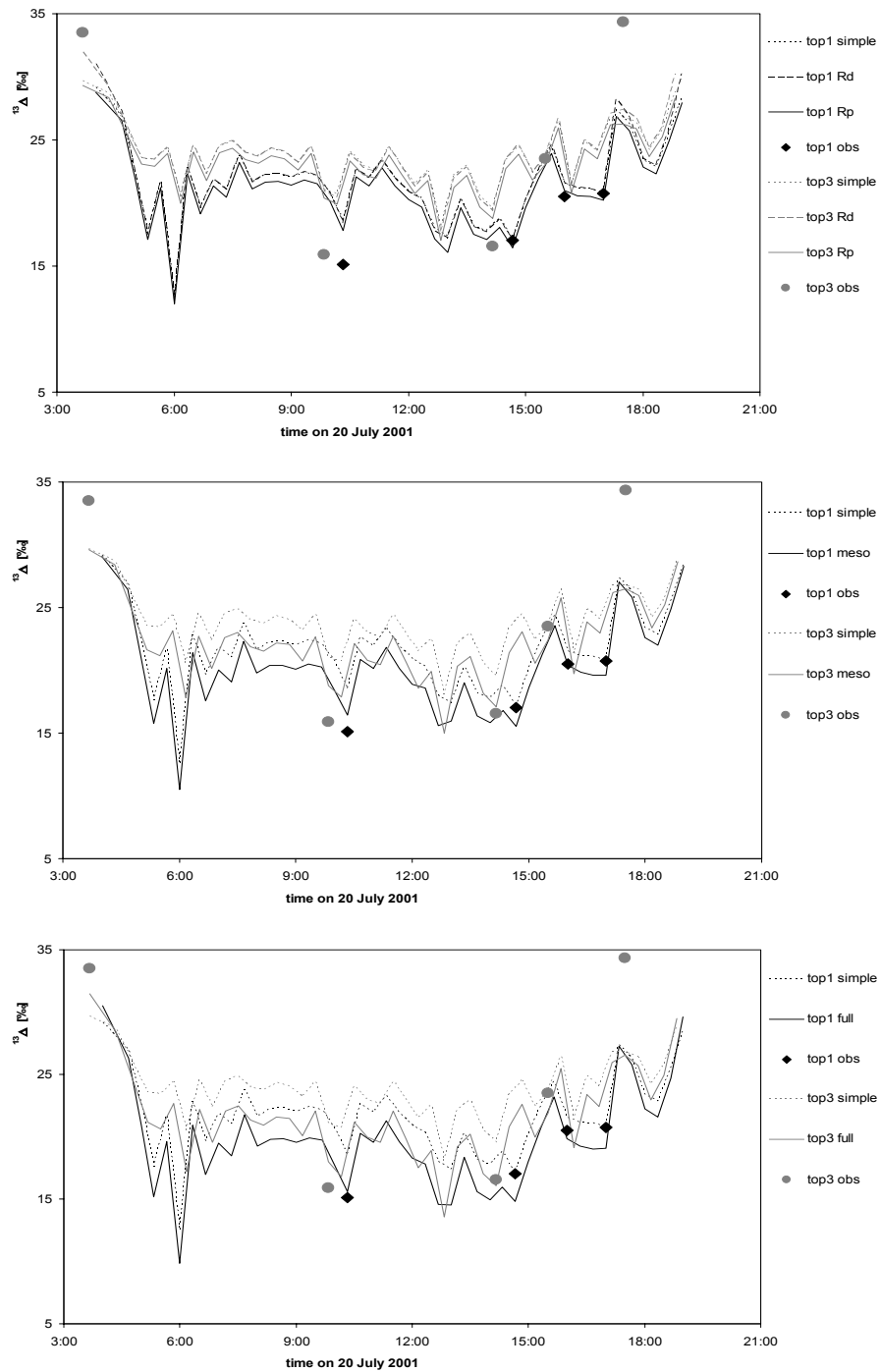


Figure 3.7b: Photosynthetic discrimination against ^{13}C predicted from flux derived C_i/C_a using the uncorrected ("simple") version and the different corrected formulations for July 2001. Corrections include: top: photorespiration ("Rd") or day-time dark respiration ("Rd"), middle: mesophyll conductance ("meso"), bottom: all of the above ("full").

This also resulted in the disappearance of corrections at dawn and dusk, when assimilation fluxes were low.

In Figure 3.8, predicted discrimination values from the fully corrected formulation are shown versus observations. Regression parameters obtained for all different combinations are listed in Table 3.1. The regressions were weighted according to the standard deviations of the measurements. The $^{13}\Delta_{\text{obs}}$ value at 7:10 on 18 May was excluded from the regressions because technical problems occurred in one of the top bags (#3). Clearly, including the isotopic signature of respiratory contributions on discrimination improves the agreement of predictions with data. Photorespiration has the smallest impact on predicted discrimination. Including contributions from dark respiration in the light enhances general predictions, but its effect is limited to times of low assimilation, when simple predictions underestimate discrimination. Mesophyll conductance, on the other hand, mainly influences discrimination at times of high assimilation, when simple predictions overestimate discrimination. Combining these two therefore helps to improve predictions for times of high and of low assimilation, so that the best agreement between predicted and observed discrimination is achieved by a combination of all contributions, using the full formulation of equation 3.11. Taking contributions of concurrent respiration and internal CO₂ transfer on net isotopic gas exchange into account also improves the correlation between predicted and observed discrimination. However, at times of low net uptake, uncertainties in discrimination measurements are too large to allow comparison so that reliable estimates of discrimination under such conditions could not be established in our study.

Prediction	simple	R _p	R _d	meso	full
Slope	0.44 (0.14)	0.46 (0.14)	0.48 (0.14)	0.54 (0.14)	0.60 (0.14)
Intercept	11.9 (2.6)	11.9 (2.6)	11.2 (2.6)	8.3 (2.6)	6.6 (2.6)
R ²	0.51	0.53	0.53	0.58	0.62

Table 3.1: Parameters for regressions of discrimination from simple, photo-, dark respiration and mesophyll conductance corrected and full formulations vs. net observed discrimination (weighted according to the standard deviations, standard errors in parentheses). All regressions were significant ($P < 0.01$).

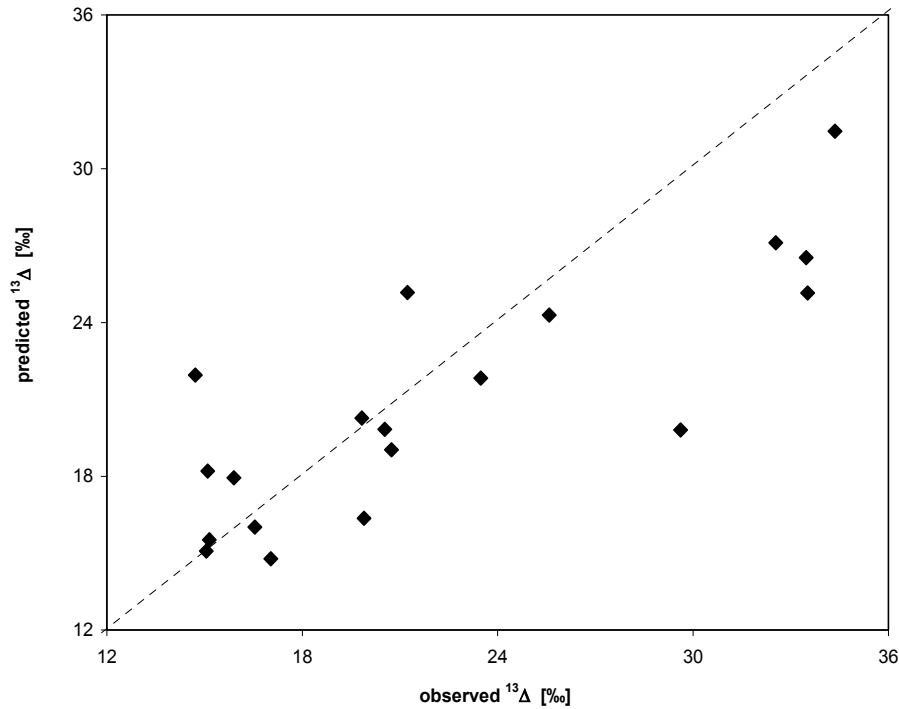


Figure 3.8: Quantitative comparison of discrimination predicted from C_i/C_a using fully corrected formulation versus observed discrimination for data combined from May and July 2001.

$\delta^{13}\text{C}$ of plant material assimilated over the diurnal cycle

The above described discrimination values were integrated over the full diurnal cycle to yield average isotopic compositions of plant material assimilated during that time (equation 3.12). The purpose of these simulations is to derive estimates for the isotopic signature of concurrent day-time dark respiration, i.e. the $\delta^{13}\text{C}$ value of plant material used as a substrate for dark respiration. Table 3.2 lists the isotopic composition of bulk needle and twig material, $\delta^{13}\text{C}_B$, the isotopic signature of CO_2 released in nocturnal dark respiration, $\delta^{13}\text{C}_{\text{plant}}$, obtained from night-time branch bag measurements, and diurnal integrals of assimilation weighted discrimination following the different formulations, $\delta^{13}\text{C}_D$. May discrimination integrals are reported only for 19 May because of technical difficulties on the morning of 18 May. The $\delta^{13}\text{C}$ signature of dark respiration in the mid bag had a large uncertainty (12 ‰) because of the low rate of respiration. For July, bulk material was assumed to have the same isotopic composition as in May, because its main component, structural carbon, is unlikely to change over such short time periods.

The $\delta^{13}\text{C}$ values of bulk needle material collected in May 2001 exhibited a gradient of 0.5 ‰ per m height in the canopy profile (significant at $P < 0.001$). The $\delta^{13}\text{C}$ enrichment of bulk twig material of ≈ 1 ‰ compared to the respective needle samples (same as in September, data not shown) was not significant ($P = 0.077$). Most bulk needle $\delta^{13}\text{C}$ values were isotopically lighter than $\delta^{13}\text{C}$ values of nocturnal dark respiration as well as of diurnal discrimination integrals. Discrimination integrals were in better agreement with isotopic signatures of dark respiration than with bulk $\delta^{13}\text{C}$ data. Since carbohydrates assimilated during the day are the source material for dark respiration, in the absence of respiratory fractionation, $\delta^{13}\text{C}_{\text{plant}}$ obtained from night-time mass balance calculations should indeed be close to discrimination integrals. Corrections for day-time dark respiration (not shown) did not affect diurnally integrated discrimination values because they were calculated in, or close to, dynamic equilibrium with the diurnal cycle of discrimination (equation 3.13 with $\int e^*dt = 0$, see also Appendix). Applying corrections for

$\delta^{13}\text{C}$ (‰)	bulk needle	bulk twig	dark resp.	$^{13}\Delta_{\text{D}}$ simple	$^{13}\Delta_{\text{D}}$ R_p	$^{13}\Delta_{\text{D}}$ g_w	$^{13}\Delta_{\text{D}}$ full
May top 1	-29.0	-27.7	-27.7 (4.4)	-29.0	-28.4	-27.3	-26.9
May top 3	(0.2)	(0.3)	-27.4 (5.5)	-32.9	-32.3	-32.2	-31.7
May mid	-30.1 (0.4)	-	-26.1 ^a (12.3)	-32.3	-31.7	-30.7	-30.2
May low	-31.1 (0.1)	-30.4 (n.a.)	-	-	-	-	-
July top 1	-29.0 *	-27.7 *	-25.7 (7.2)	-27.7	-27.1	-26.0	-25.4
July top 3			-	-28.4	-27.7	-26.3	-25.6

Table 3.2: $\delta^{13}\text{C}$ of bulk needle and twig samples, of nocturnal dark respiration, and of simple uncorrected, photorespiration (" R_p "), mesophyll conductance (" g_w ") and fully corrected diurnal discrimination integrals (* assumed equal to May data, ^a very low flux rate). Standard deviations of measurements in parentheses.

photorespiration and fractionation during internal CO₂ transfer ("g_w") increased discrimination integrals by around 0.5 and 1.5 ‰, respectively. Fully corrected diurnal discrimination integrals were thus about 2 ‰ more enriched than simple uncorrected values, and thereby closer to isotopic signatures of dark respiration. It should be noted, however, that measurements of the δ¹³C of dark respiration had large uncertainties because of the low nocturnal flux rates.

Time lags between assimilation of organic carbon and its use in respiration were estimated from daily average turnover times of leaf carbohydrate pools. Leaf carbohydrate turnover depends on rates of assimilation, respiration and export of organic material to stems and roots relative to total carbohydrate pool of needles. Daily integrated values of assimilation, constituting the influx into the foliage carbohydrate pool, were used to calculate turnover times. Carbohydrates constitute only a small part of total needle mass, usually around 7 % of dry weight, depending on needle age (Barton 1997). Measurements of specific needle area ranged from 30 to 50 cm²/g, yielding carbohydrate pools of around 0.5 and 0.6 molC/m² for top and mid bag foliage, respectively. With total assimilation rates of 0.2 to 0.3 molC/m² per day, mean turnover times were thus in the order of 2 days. In this case, δ¹³C of dark respiration would correspond to discrimination integrated over more than one full diurnal cycle, and knowledge about the conditions on previous days would be required to link the isotopic composition of dark respiration to diurnal discrimination integrals.

Changes in δ¹³C of soluble needle carbohydrates, obtained using equation 3.13, over time periods of three days are shown in Figure 3.9. To illustrate the impact of carbohydrate pool sizes, they were assigned values of half or double that (0.25 and 1 molC/m²), corresponding to average needle carbohydrate turnover times of 1 and 4 days, respectively. In the legend of Figure 3.9, pool sizes are indicated by their corresponding average turnover times of 1, 2, or 4 days. Amplitudes of variations depend on the size of the carbohydrate pool, being smaller with larger pool size and, therefore, slower turnover. Night to night changes in the resulting isotopic composition of carbohydrates were up to 0.6 ‰ for the assumed average turnover time of 2 days, 1.1 ‰ for 1 day and 0.3 ‰ for 4 days. Potential impacts of fractionation during dark respiration on the time development of needle carbohydrate δ¹³C were, however, not explored because of the uncertainties connected with both discrimination and nocturnal respiration data.

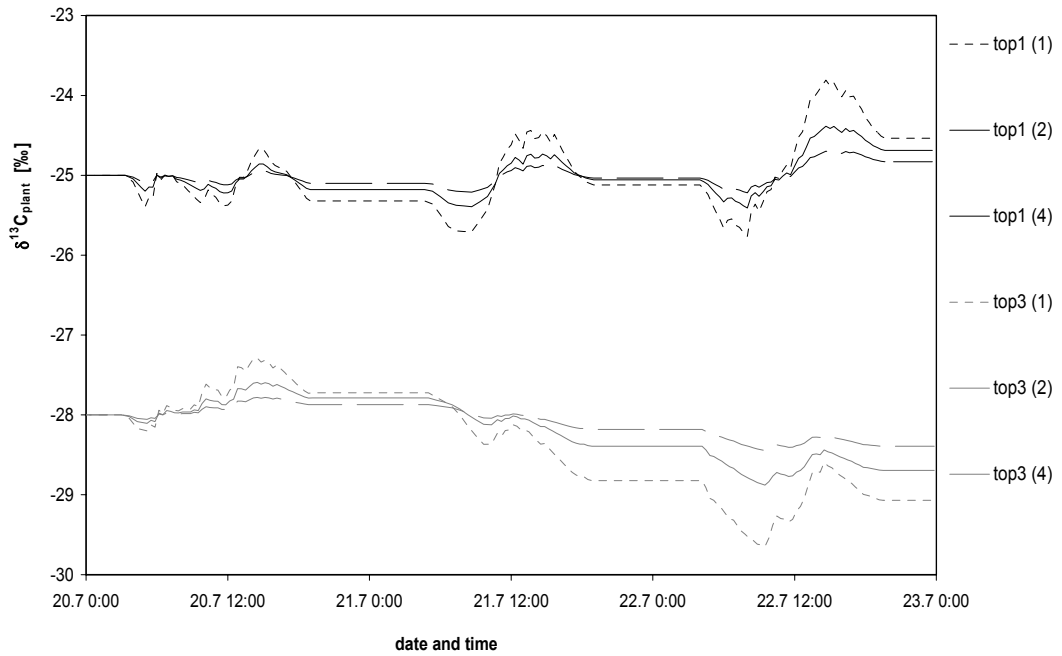
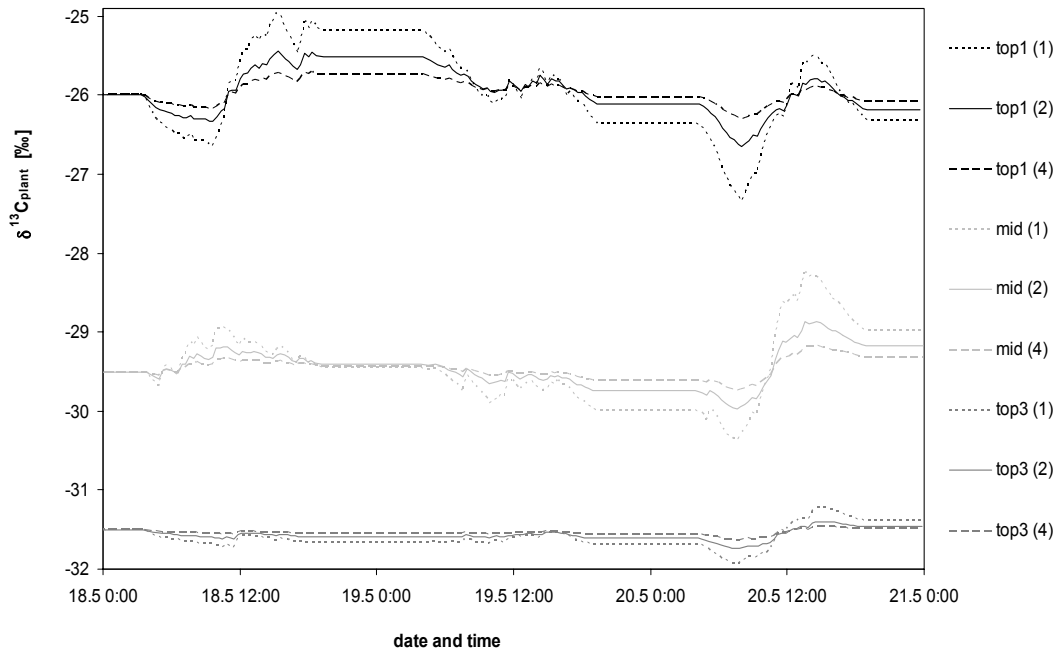


Figure 3.9: Temporal changes of $\delta^{13}\text{C}$ of soluble needle carbohydrates, with discrimination and $\delta^{13}\text{C}$ of dark respiration in steady state, assuming 1, 2, or 4 days of average turnover time of the carbohydrate pool, for May (top) and July (bottom) 2001.

Discussion

The magnitude and diurnal variations of $^{13}\Delta$ observed over the diurnal cycle in the top bags were similar for the two sampling days in May and July 2001, although the environmental conditions were different. Overall, photon irradiance, air temperature and water vapour mole fraction deficit were higher during the May compared to the July sampling period. The May sampling day was characterised by sunny conditions with some intermittent clouds, whereas the sky was mostly overcast with more diffuse light on the July sampling day. The similarity of $^{13}\Delta$ values on both days probably reflects the fact that both assimilation rates and stomatal conductance were somewhat lower on the July day (see Figures 3.2 and 3.4). Such differences would have opposing influences on C_i/C_a (see equation 2.6) and thus on $^{13}\Delta$ values. The similarity of C_i/C_a values on both days indicates that these concurrent differences might have balanced each other to some degree (see Figure 3.2). At dawn and dusk, high humidity and low irradiance lead to open stomata accompanied by low assimilation rates, resulting in high $^{13}\Delta$ values. During the day, rising irradiances and temperatures were followed by declining relative humidity. As a result, stomatal conductance decreased, limiting the CO_2 flux through stomatal openings. At the same time, assimilation rates were rising along with irradiances, leading to overall lower C_i/C_a and therefore $^{13}\Delta$.

The conspicuously high dawn and dusk values of ^{13}C discrimination found in our study could not be fully explained by contributions of concurrent day-time dark respiration. However, assumptions regarding the rate of dark respiration in the light were taken from the literature (Atkin et al 2000), obtained for a different plant species (*Eucalyptus pauciflora*) grown under controlled conditions (20 °C). It is unlikely that these assumptions are valid for our field observations. To account for discrepancies between predicted and observed dawn and dusk values while leaving C_i/C_a unchanged would require the rate of concurrent day-time dark respiration to be approximately the same as that of assimilation, corresponding to more than 50 % of gross photosynthesis. The rate would have to be 10 to 20 times that of R_d from equation 3.6, higher than R_n from equation 3.7 or from observations. On the other hand, C_i/C_a could be higher than calculated from gas exchange at these times. With the respective C_i/C_a values changed to 0.95, the rate of dark respiration in the light would only have to be twice that obtained using the temperature and light inhibited formulation, well within the range of observed nocturnal dark respiration rates. These rates would correspond to 30 % of gross

photosynthesis, plausible relative contributions similar to those obtained for several other times. This indicates that C_i/C_a values inferred from gas exchange data may not have been reliable at dawn and dusk. Of course, all relative errors are larger for smaller fluxes. At the same time, accurate estimation of the impact of dark respiratory corrections depends on correct determination of C_i/C_a . Therefore, discrimination could not be reliably predicted at dawn and dusk. Fortunately, predicted ^{13}C discrimination values are not sensitive to rates of day-time dark respiration when e^* is small, (see top panel of Figure 3.7), so that the corresponding $^{13}\Delta$ uncertainties are small during most of the day.

We found a gradient of foliage material $\delta^{13}\text{C}$, with more depleted values towards the forest floor, similar to that reported in previous studies (Francey et al. 1985, Buchmann et al. 1997). The gradient may be explained predominantly by consistently lower vapour pressure deficits leading to higher C_i/C_a and hence discrimination values lower in the canopy profile, rather than by partial re-assimilation of respired CO_2 that is already depleted in ^{13}C . Evidence for this came from higher stomatal conductance values in the mid than in top bags (see Figure 3.2) and from the lack of canopy $\delta^{13}\text{C}_{\text{atm}}$ gradients between mid and top bag levels (see Figure 3.5).

The difference between $\delta^{13}\text{C}$ of twig and needle material agrees with the results of Francey et al. (1985), obtained in a study on Huon pine. According to their hypothesis, twig material is exported from mature needles that tend to have lower C_i so that average discrimination is lower and hence resulting organic substrate not as depleted, i.e. isotopically heavier. This is supported by the finding that diurnal discrimination integrals were generally closer to the isotopic composition of twig than to that of needle material. Bulk material mainly consists of structural carbon ($\approx 90\%$ cellulose), largely unavailable to autotrophic respiration. It should reflect the average magnitude of discrimination during the growing season where the majority of needle structural carbon was laid down, taking additional fractionation during synthesis of organic compounds into account. If there was no fractionation during respiration or other plant metabolic processes, a less depleted $\delta^{13}\text{C}$ caused by lower discrimination implies relatively more influence of diffusive and less of biochemical fractionation due to more pronounced stomatal closure. Stronger stomatal opening, i.e. higher average C_i/C_a , has been observed during needle growth (see Francey et al. 1985, or Evans et al. 1986 and references therein).

Using variations in the $\delta^{13}\text{C}$ signature of ecosystem respiration, Ekblad and Högberg (2001) examined the speed of carbon cycling through plants from its uptake during foliage photosynthesis to its release in root respiration. They measured the speed of this link by relating changes in $\delta^{13}\text{C}$ of ecosystem respiration to the variability of environmental conditions that are translated into magnitude of photosynthetic ^{13}C discrimination and imprinted in the isotopic composition of newly assimilated organic carbon. Assuming that the carbon isotope ratio of microbial respiration has very little variations on short time scales (days), they attributed changes in $\delta^{13}\text{C}$ of soil respiration to those of root respiration, reflecting the isotopic composition of plant assimilates. Here, the first estimates of night to night variability in $\delta^{13}\text{C}$ of needle carbohydrates are presented. These estimates were obtained from field observations and linked to diurnal patterns of photosynthetic ^{13}C discrimination. Even over short time periods of a few days, the variability of $\delta^{13}\text{C}$ of assimilates was surprisingly high, and night to night changes might be big enough to enable estimation of the speed of assimilate transfer to the roots. Furthermore, these results emphasizes the importance of determining carbohydrate pool sizes and hence turnover times influencing amplitudes of temporal variations that are used to link uptake and release of organic carbon in ecosystems.

Compared to the only other study of ^{13}C discrimination during photosynthesis under field conditions so far (Harwood et al. 1998), the observations reported here show a more pronounced diurnal variability, in discrimination as well as in C_i/C_a values determined from gas exchange. The data presented here also allowed the derivation of an estimate for mesophyll conductance. The rate of transpiration, subsequently used in determination of C_i/C_a , was identified as one potentially problematic parameter that needs to be accurately determined. The value obtained for mesophyll conductance will be different if predicted discrimination used in the regression is corrected for concurrent respiration, rather than taken from the simple uncorrected formulation. In the original equation (see for example Evans and Von Caemmerer 1996), respiratory contributions are reflected in the intercept of the regression. This is only the case if respiratory contributions are constant over the full range of A/C_a values, as can be assumed for photorespiration. On the other hand, the results obtained in this study show that it is probably not valid for day-time dark respiration. However, differences in regression parameters between simple uncorrected and respiration corrected versions should be (and were) only minor because corrections had most impact on values where A/C_a was not significantly different from zero, excluded from the regression for numerical stability.

Pronounced differences were found between the isotopic composition of nocturnal dark respiration and bulk needle material, and also between both of these two signatures and instantaneous values of discrimination. This is important because the isotopic composition of bulk foliage material is often used to obtain estimates for average C_i/C_a values of plants under natural conditions. For example, in the study of Flanagan et al. (1997), an average C_i/C_a value was estimated from bulk needle isotopic composition, and used as constant parameter to predict photosynthetic ^{18}O discrimination over the diurnal cycle. As shown here, not only is C_i/C_a not constant over the day, but needle isotopic composition is also probably not a good estimate for discrimination, or C_i/C_a , at a time other than that of needle development. The influence of changes in C_i/C_a on diurnal patterns of ^{18}O discrimination is examined in detail in section 4.

3.2 $\delta^{13}\text{C}$ of CO_2 from foliage and soil respiration

Introduction

At night, changes in $\delta^{13}\text{C}$ values of canopy CO_2 reflect the isotopic composition of organic material constituting the substrate of autotrophic respiration from foliage and roots and heterotrophic respiration from soil microorganisms. In the absence of turbulent mixing with air from outside the canopy, pronounced concurrent gradients often develop in the mole fraction and $\delta^{13}\text{C}$ of CO_2 , with stronger depleted $\delta^{13}\text{C}$ values at higher CO_2 mole fractions, i.e. towards the forest floor. As described in the previous section, ^{13}C discrimination during photosynthesis results in plant material depleted in ^{13}C . Thus, if there is no fractionation during respiration, $\delta^{13}\text{C}$ of canopy CO_2 will be simply determined by relative rates and isotopic composition of foliage, root and soil respiration. However, separating component respiratory sources using their $\delta^{13}\text{C}$ signatures in a "Keeling plot" approach might be difficult because different sources often have similar isotopic compositions. For example, foliage and root respiration are both supplied from soluble carbohydrates so that they may be isotopically indistinguishable (Ekblad and Höglberg 2001).

In this study, $\delta^{13}\text{C}$ of foliage and soil respired CO_2 were estimated from measurements of isotopic gas exchange during September 2000, May and July 2001. In the steady state (with respect to diffusion), the isotopic composition of CO_2 leaving the soil or foliage must be equal to the CO_2 produced in soil or foliage. Although CO_2 within the soil is enriched through diffusional fractionation (≈ 4.4 ‰, Craig 1953), the flux of CO_2 leaving would only have an isotopic composition different from its substrate if it was affected by fractionation during respiration itself. Thus, under natural conditions, existence or magnitude of respiratory fractionation can be estimated by comparing $\delta^{13}\text{C}$ of respired CO_2 with $\delta^{13}\text{C}$ of its substrate. Here, diurnal and seasonal changes in $\delta^{13}\text{C}$ of foliage, soil and ecosystem respiration are presented and compared to $\delta^{13}\text{C}$ of bulk organic material from concurrently collected foliage and soil samples as estimates of the $\delta^{13}\text{C}$ of substrates of respiratory CO_2 fluxes.

Results

$\delta^{13}\text{C}$ of foliage respiration during the night

Figure 3.10 shows Keeling plots (equation 2.9) constructed from combined open and closed air samples collected in the top branch bags at night, during May and July 2001. Data from September 2000 is shown for comparison and to highlight possible seasonal variations. The isotopic signature of foliage respiration was obtained from intercepts of linear regressions (geometric mean regression), yielding $\delta^{13}\text{C}$ values of $-26.9 \pm 0.2 \text{ ‰}$ for September, $-27.5 \pm 0.7 \text{ ‰}$ for May and $-27.9 \pm 1.4 \text{ ‰}$ for July (all $R^2 > 0.95$). No significant differences were found between the seasons ($P > 0.32$ for all combinations).

Figure 3.11 illustrates that respiratory $\delta^{13}\text{C}$ values did not significantly covary with respiration rates ($R^2 = 0.13$, $P = 0.37$). Correlation might indicate occurrence of feedback processes of the changing trace gas composition within the branch bags on the isotopic composition of CO_2 released in foliage respiration. Only very few mass balances (equation 2.8) could be calculated from observations of dark respiration in branch bags, because pair measurements consisting of open and closed air samples at night were sparse. This was due to difficult sampling conditions at night, as well as low nocturnal respiration rates of branch bag foliage resulting in small gradients of CO_2 mole fractions with large uncertainties over the closure period (see error bars in Figure 3.11).

Table 3.3 lists $\delta^{13}\text{C}$ values for averages of the isotopic signature of CO_2 released in nocturnal dark respiration calculated using isotopic mass balances, intercepts of regressions ("Keeling plots") combined from all (open and closed) air samples collected at night during each field campaign (see Figure 3.10), and for bulk needle and twig material. All values refer to top bags, as measurements of rate and $\delta^{13}\text{C}$ of respiration in mid or low bags were difficult to obtain due to very low fluxes. All $\delta^{13}\text{C}$ values were more depleted in May 2001 than in September 2000. Keeling plot intercepts in July were even more depleted than in May, but mass balance average was less depleted than in May. However, most values had large uncertainties, so that existence or direction of seasonal changes cannot be established. Bulk needle and twig samples as well as Keeling plot intercepts showed a decrease in $\delta^{13}\text{C}$ of a comparable magnitude between September and May (0.6 ‰). It was, however, based on only one bulk sample each for September.

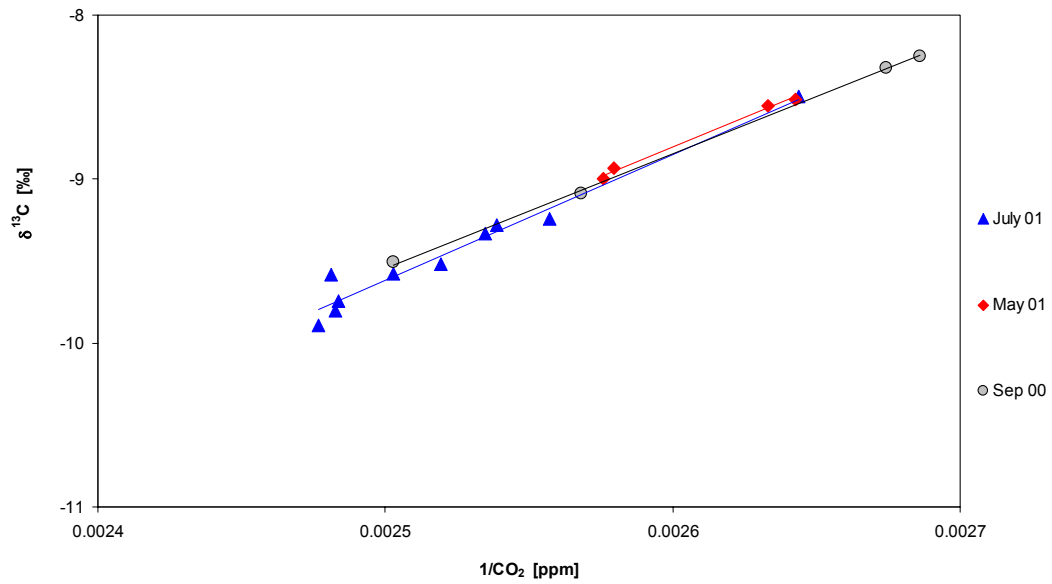


Figure 3.10: Keeling plot of all air samples (open and closed) collected during nocturnal respiration from the top branch bag in September 2000 and May and July 2001.

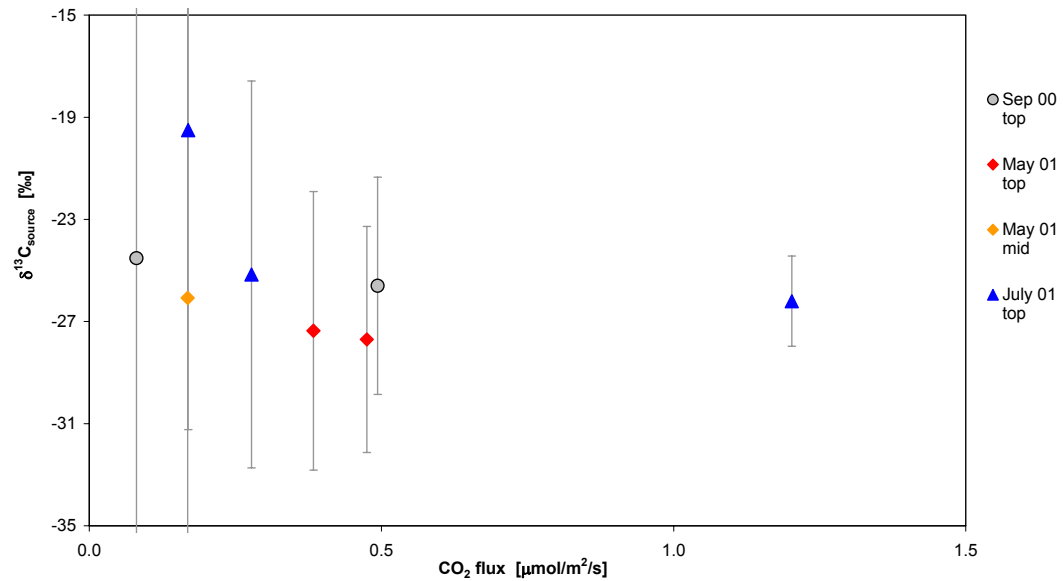


Figure 3.11: Isotopic composition of foliage respiration versus respiration rate, obtained from sample pairs of top and mid branch bag air in September 2000 and May and July 2001. Error bars indicate standard deviations of measurements.

field campaign	mass balance averages (‰)	Keeling plot intercepts (‰)	bulk needle samples (‰)	bulk twig samples (‰)
Sep 2000	-25.1 (14.4)	-26.9 (0.2)	-28.4 (0.3)	-27.0 (0.3)
May 2001	-27.5 (5.2)	-27.5 (0.7)	-29.0 (0.2)	-27.7 (0.3)
July 2001	-25.7 (7.2)	-27.9 (1.4)	-	-

Table 3.3: Isotopic composition of foliage respiration at night from mass balance averages and combined Keeling plot intercepts, and bulk needle and twig $\delta^{13}\text{C}$ values for September 2000 and May and July 2001 (standard deviations in parentheses, for September bulk samples from average precision of analyses).

$\delta^{13}\text{C}$ of soil respiration

In analogy to foliage respiration, Keeling plots were constructed from the CO_2 mole fraction and isotopic composition of air samples of open and closed soil chambers. Keeling plots for two soil chambers, soil 1 and soil 2, are presented in Figure 3.12. The $\delta^{13}\text{C}$ values of soil respired CO_2 were obtained from intercepts of regressions as described above, yielding -27.6 ± 0.5 (soil 1) and -28.7 ± 0.5 ‰ (soil 2) in September ($R^2 > 0.95$), -29.3 ± 2.1 (soil 1) and -29.1 ± 1.5 ‰ (soil 2) in May ($R^2 > 0.9$) and -28.6 ± 0.3 (soil 1) and -29.6 ± 0.3 ‰ (soil 2) in July ($R^2 > 0.95$). Seasonal differences in the $\delta^{13}\text{C}$ of soil respired CO_2 were not significant for either soil 1 ($P > 0.06$) or soil 2 ($P > 0.24$). The $\delta^{13}\text{C}$ signature of soil 2 was depleted by about 1 ‰ with respect to that of soil 1 in September and July and enriched by 0.2 ‰ in May. However, the differences between the two chambers were only significant for July ($P = 0.01$) but not for September ($P = 0.16$) or May ($P = 0.72$). Keeling intercepts and mass balance averages were similar, with differences (< 1 ‰) mostly smaller than uncertainties.

Figure 3.13 presents $\delta^{13}\text{C}$ of soil respiration versus respiration rate. Again, the absence of a significant correlation between the two variables confirms that experimental conditions did not create feedbacks on isotopic gas exchange. At lower respiration rates of 0.5 to 2 $\mu\text{mol}/\text{m}^2/\text{s}$, several $\delta^{13}\text{C}$ values were more strongly depleted, between -30 and -32 ‰. At respiration rates higher than 2 $\mu\text{mol}/\text{m}^2/\text{s}$, $\delta^{13}\text{C}$ values converged at a stable level of -28.3 ± 0.6 ‰ for soil 1 and -29.3 ± 1.0 ‰ for soil 2. This difference of

approximately 1 ‰ in the mean $\delta^{13}\text{C}$ signature of soil respiration between the two soil chambers was significant ($P < 0.01$). At lower respiration rates, there was more scatter of $\delta^{13}\text{C}$ values (with higher measurement uncertainties, see error bars in Figure 3.13).

Figure 3.14 shows $\delta^{13}\text{C}$ values of soil respiration obtained from mass balance calculations over the course of the sampling days in September 2000, May and July 2001. In May, $\delta^{13}\text{C}$ values of respiration in both soil chambers seemed to increase by 5 ‰, i.e. towards less depleted values, during the day. It is difficult to imagine possible explanations for such a large diurnal cycle of $\delta^{13}\text{C}$ of soil respiration, even taking any temporal variability of $\delta^{13}\text{C}$ of plant assimilates (as discussed in previous section) into account. Accordingly, the $\delta^{13}\text{C}$ value of around -29 ‰ obtained at 6:00 on the following morning did not confirm this pattern. In addition, the isotopic signatures of respired soil CO_2 in September and July were also more stable, not displaying any clear diurnal patterns and less overall variability.

Table 3.4 gives an overview over results of different analyses of $\delta^{13}\text{C}$ of soil respiration and bulk soil material from the September, May and July sampling campaigns. Similar $\delta^{13}\text{C}$ values of soil respired CO_2 were obtained from both mass balance averages and

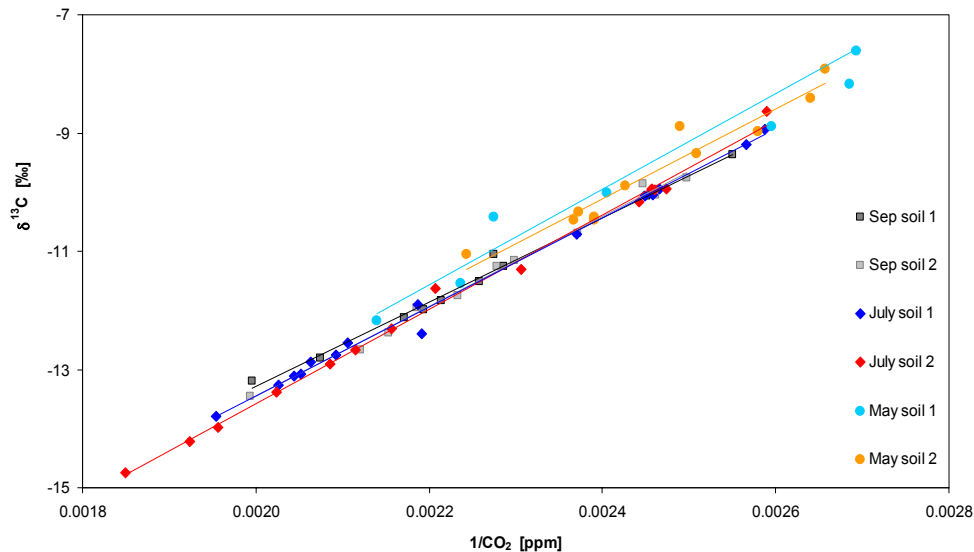


Figure 3.12: Keeling plot of isotopic composition against the inverse of CO_2 mole fraction from open and closed soil air samples collected in September 2000 and May and July 2001.

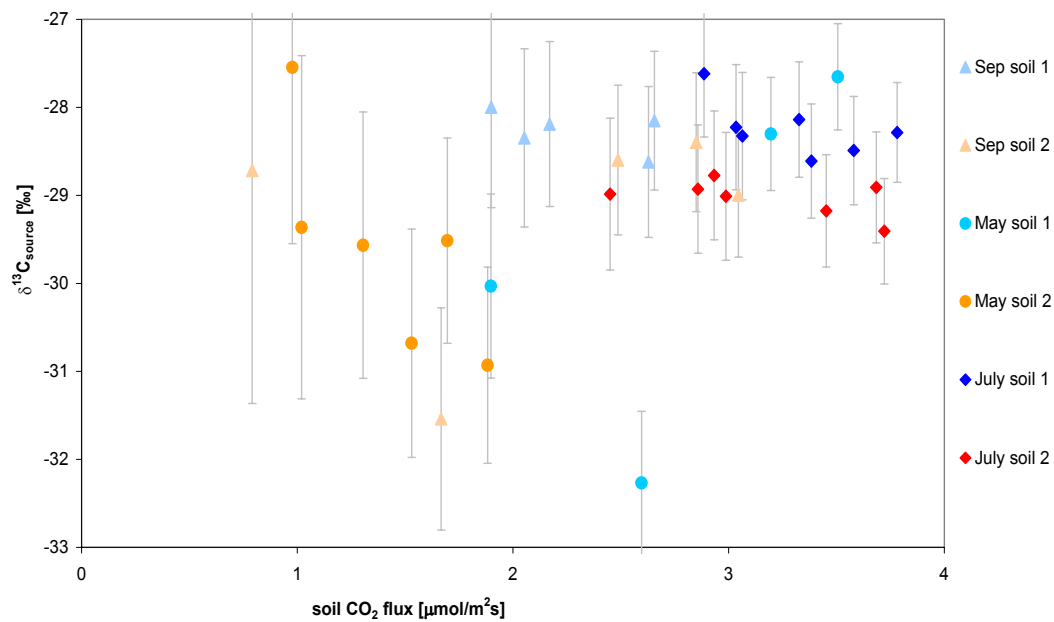


Figure 3.13: Isotopic composition of soil respiration source versus soil respiration rate. Error bars indicate standard deviations of measurements.

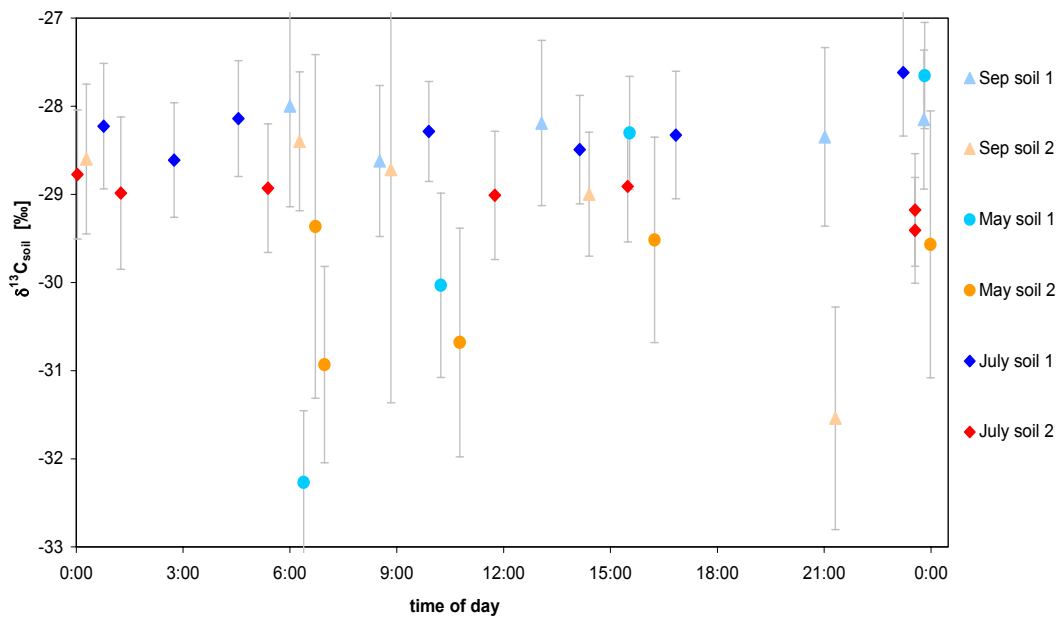


Figure 3.14: Diurnal cycle of isotopic composition of soil respiration source for September 2000, and May and July 2001. Error bars indicate standard deviations of measurements.

Keeling intercepts (within ± 0.7 ‰ of each other). The $\delta^{13}\text{C}$ values of respired CO_2 calculated from mass balance averages were depleted with respect to $\delta^{13}\text{C}$ of bulk soil samples by 0.7 to 1.5 ‰. $\delta^{13}\text{C}$ values of respired CO_2 from Keeling plot intercepts were equal or slightly depleted (by up to 0.9 ‰) with respect to bulk $\delta^{13}\text{C}$ values. These differences were, however, mostly small compared to the standard deviations (see table) and not significant.

	soil 1 – $\delta^{13}\text{C}$ (‰)			soil 2 – $\delta^{13}\text{C}$ (‰)		
	mass balance	Keeling intercept	bulk soil	mass balance	Keeling intercept	bulk soil
Sep 00	-28.3 (0.2)	-27.6 (0.5)	-27.6 (0.3)	-29.3 (1.3)	-28.7 (0.5)	-27.8 (0.3)
May 01	-29.6 (2.1)	-29.3 (2.1)	-28.8 (0.3)	-29.6 (1.2)	-29.1 (1.5)	-28.5 (0.3)
July 01	-28.2 (0.3)	-28.6 (0.3)	-	-28.9 (0.1)	-29.6 (0.3)	-

Table 3.4: Isotopic composition of foliage respiration at night from mass balance averages and combined Keeling plot intercepts, and bulk needle and twig $\delta^{13}\text{C}$ values for September 2000 and May and July 2001 (standard deviations in parentheses). Standard deviations of September bulk samples (only one sample per month) indicate average analytical uncertainties from repeated analyses of laboratory standards.

$\delta^{13}\text{C}$ of ecosystem respiration

Figure 3.15 shows Keeling plots for September, May and July, combining all air samples collected from open branch bags and open soil chambers at night, i.e. samples of unperturbed canopy air. The $\delta^{13}\text{C}$ signatures of ecosystem respiration integrated throughout the canopy obtained from regression intercepts were: -28.8 ± 0.5 ‰ in September, -29.3 ± 1.0 ‰ in May and -28.8 ± 0.2 ‰ in July (all $R > 0.9$). Thus, seasonal variations in the carbon isotopic signature of ecosystem respiration were not significant ($P > 0.78$). Note that in May, only 5 data points were available to construct the regression.

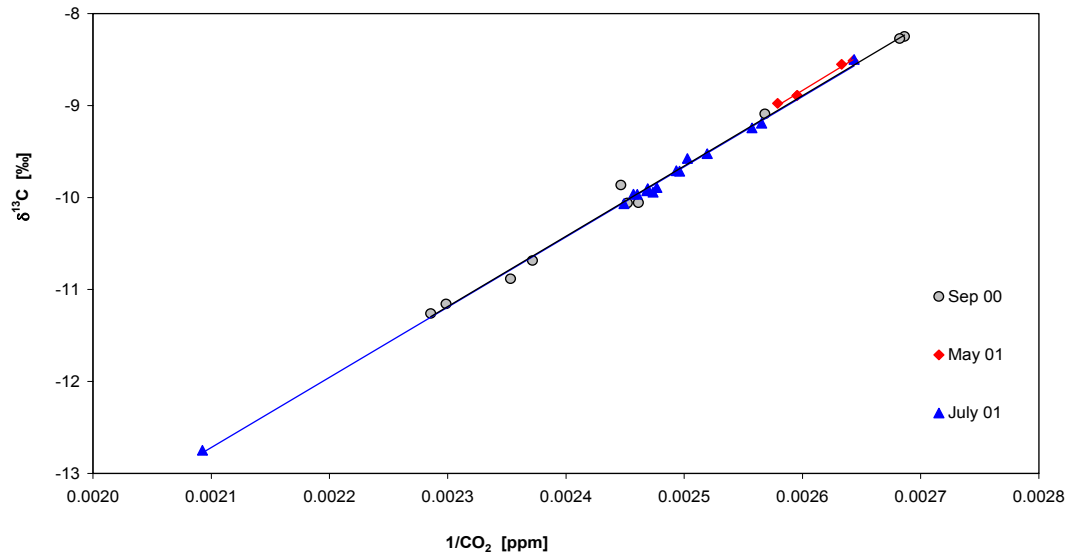


Figure 3.15: Keeling plot from nocturnal samples of open branch bag and soil chamber air collected in September 2000, and May and July 2001.

Discussion

Differences between $\delta^{13}\text{C}$ of respired CO_2 from plants and that of its substrate were used in a number of studies examining direction and magnitude of fractionation during autotrophic respiration. Lin and Ehleringer (1997) found no such fractionation with respect to soluble carbohydrates used as substrates by isolated protoplasts from leaves of C_3 and C_4 species. Smith (1971) reported a depletion by 1 ‰ in respired CO_2 with respect to whole plant material of wheat, radish and pea. Park and Epstein (1961) reported 2 to 5 ‰ enrichment with respect to whole tomato plant. Duranceau et al. (1999) reported ≈ 6 ‰ enrichment with respect to sucrose in leaves of bean plants. Duranceau et al. (2001) and Ghashghaie et al. (2001) found respired CO_2 isotopically enriched by 2 to 6 ‰ with respect to soluble carbohydrates and whole leaves of tobacco and sunflower, and argued that direction and magnitude of respiratory fractionation of CO_2 may vary depending on environmental conditions and species.

In this study, $\delta^{13}\text{C}$ of soluble carbohydrates, assumed to form the substrate for foliage respiration, was not analysed directly. Although fractionation between respired CO_2 and carbohydrates could thus not be derived, preliminary estimates of fractionation between respired CO_2 and bulk foliage material were obtained. Respired CO_2 , inferred from Keeling plot intercepts and mass balance averages, was found to be isotopically

enriched by 1.5 to 3.3 ‰ compared to bulk needle material, less pronounced but in general agreement with the results of Park and Epstein (1961), Duranceau et al. (1999, 2001) and Ghashghaie et al. (2001).

The scatter in soil respiration $\delta^{13}\text{C}$ values at low respiration rates seem to have affected predominantly May data. At the same time, average respiration rates were somewhat lower in May ($2.4 \mu\text{mol}/\text{m}^2/\text{s}$ in September, $2.0 \mu\text{mol}/\text{m}^2/\text{s}$ in May, $3.2 \mu\text{mol}/\text{m}^2/\text{s}$ in July). This could have at least contributed to noisy May data as lower respiration rates translate to higher measurement uncertainties, increasing the relative errors of inferred soil respiration $\delta^{13}\text{C}$ values. However, the reason for lower May soil respiration rates is unclear. Average soil temperatures in May were not lower than in the other two months (10°C in September and May, 7°C in July). In addition, occurrence of more strongly depleted values (that can be interpreted as scatter) was confined to two sampling times (at around 7:00 and 10:00), pointing to unidentified technical problems during soil chamber measurements at the respective sampling periods in May as a potential cause.

In soils, there are two simultaneous sources of respired CO_2 , root (autotrophic) and microbial (heterotrophic) respiration. If their respective $\delta^{13}\text{C}$ values differ significantly, then their relative contributions can be inferred. Accordingly, Ekblad and Högberg (2001) estimated that root respiration contributed at least 65 % to total soil respiration in a boreal mixed coniferous forest. They reported seasonal variations in $\delta^{13}\text{C}$ of soil respiration of almost 5 ‰. Flanagan et al. (1996, 1999) also found seasonal changes of up to 2 ‰ in $\delta^{13}\text{C}$ of soil respiration in boreal forest ecosystems. Assuming that the isotopic composition of microbial soil respiration does not have pronounced variations over short time periods, they attributed the day to day variability mainly to changes in $\delta^{13}\text{C}$ of root respiration, mirroring environmental conditions via photosynthetic discrimination (see section 3.1).

In this study, $\delta^{13}\text{C}$ values of bulk soil samples were not as depleted as expected from the $\delta^{13}\text{C}$ values of the collected samples of plant biomass such as needles and twigs (see Table 3.3). Soil microbial respiration has been found to release CO_2 with an isotopic signature close to that of soil organic matter (Santruckova et al. 2000). Soil organic matter consists of a mixture of plant and microbial biomass. Because of selective utilisation of the different available biomolecules by soil microbes and isotope discrimination during the microbial metabolism, soil material usually contains less ^{13}C

than the average aboveground (plant) material as well as less ^{13}C with increasing depth in the soil profile (see Santruckova et al. 2000 and references therein). Although the soil samples were collected from the soil surface layer (top 5 cm after litter removal), the data presented here confirm to the pattern of enriched soil with respect to plant material reported in these other studies. However, bulk soil samples were analysed instead of soil organic carbon, limiting the interpretation of the observed patterns.

The second source of respired CO_2 from soil are roots. Source material for root respiration consists of soluble carbohydrates assimilated during the day. Its $\delta^{13}\text{C}$ value should therefore be similar to that of foliage respiration at night. By comparing $\delta^{13}\text{C}$ values listed in Tables 3.2 and 3.3 it is evident that the isotopic signature of root respiration is likely to be similar or somewhat enriched compared to the isotopic signature of the microbial source of respiratory CO_2 (from bulk soil material). However, the $\delta^{13}\text{C}$ signature of combined soil respiration (-28.2 to -29.6 ‰) was found to be more negative than either the soil (-27.6 to -28.8 ‰) or the root respiration source material (-25.1 to -27.9 ‰). This could have been caused by fractionation during respiration, or it could reflect the fact that analyses were performed on whole soil bulk samples instead of separated organic soil components.

$\delta^{13}\text{C}$ values of integrated ecosystem respiration were remarkably constant over the seasons. They were also all close to the isotopic signature of soil respiration in the respective months. Relative rates of foliage or root versus microbial respiration could not be quantified from our data. Temporal variability of $\delta^{13}\text{C}$ of microbial respiration was small, as indicated by $\delta^{13}\text{C}$ values of bulk soil organic material. Assuming that roots contribute 65 % to total soil respiration with $\delta^{13}\text{C}$ of recently assimilated carbohydrates (Ekblad and Högberg 2001), stability of $\delta^{13}\text{C}$ values of ecosystem respiration would imply that $\delta^{13}\text{C}$ of photoassimilates did not change greatly over time, in contrast to results in the discrimination section, where surprisingly variable $\delta^{13}\text{C}$ of assimilates over short time periods of a few days were inferred. Otherwise, similar environmental conditions during sampling campaigns could also explain why $\delta^{13}\text{C}$ values would appear stable over time. This would require comparable magnitudes of photosynthetic discrimination in the days immediately before sampling campaigns, as well, because of time lags between assimilation of carbohydrates and their consumption in root respiration. Ultimately, these questions can be only answered through more extensive, long term sampling.

4. $\delta^{18}\text{O}$ of CO_2

4.1 Discrimination against ^{18}O during photosynthesis

Introduction

The oxygen isotopic composition of atmospheric CO_2 exhibits a strong meridional gradient (Francey and Tans 1987) and varies seasonally. During transpiration from the leaves of plants, the heavy oxygen isotope, ^{18}O , accumulates in the leaf water. Because CO_2 exchanges isotopically with water, the oxygen isotope signal of leaf water is transferred to atmospheric CO_2 during leaf gas exchange (Farquhar et al. 1993). In summer, leaf water is mostly enriched in ^{18}O and photosynthetic activity thus increases the $^{18}\text{O}/^{16}\text{O}$ ratio of CO_2 in the atmosphere. In winter, the respiratory fluxes from plants and the soil mostly release isotopically depleted CO_2 , decreasing the isotopic ratio of atmospheric CO_2 . This seasonality is most pronounced in the northern hemisphere due to the contribution from the vegetation covers of the large continents (see Ciais et al. 1997b, Peylin et al. 1999). Changing environmental conditions alter the magnitude of fractionation by leaves, thereby determining the isotopic signal of the CO_2 that enters the atmosphere from the canopy.

The intercept derived from the relationship of the isotopic composition against the inverse of the CO_2 mole fraction (Keeling 1961) can give estimates of the isotopic signal of the respiratory pool at night, but it cannot be used to constrain photosynthetic isotope fractionation over a diurnal cycle, when gradients in trace gas composition caused by plant gas exchange are diluted by turbulent mixing with air from above the canopy to varying degrees. There has been only one study so far to examine the magnitude and diurnal variability of photosynthetic oxygen isotope discrimination under natural conditions (Harwood et al. 1998).

The steady state enrichment model of Craig and Gordon (1965) is widely used to predict the isotopic composition of water at the evaporating leaf surface (e.g. Farquhar et al. 1993, Ciais et al. 1997a). Isotopic steady state conditions, the basic assumption of this model, are not necessarily fulfilled at all times under natural conditions. Dongman et al.

(1974) developed a non steady state version of the enrichment equation, taking leaf water turnover rates into account. Because of its influence on the $\delta^{18}\text{O}$ signature of photosynthetic CO_2 , it is important to test how well these models predict the isotopic signature of water at the evaporating sites. However, comparison with measurements is difficult – one would have to carefully separate the surface areas from the rest of the foliage material during collection of water samples. Here, this problem was avoided by comparing photosynthetic ^{18}O discrimination predicted by the two models from leaf water isotopic composition at the evaporating sites to field data. This provides an evaluation of the applicability of theoretical relationships between canopy environmental parameters, isotope enrichment of evaporating site water and ^{18}O discrimination to Sitka spruce under field conditions. Furthermore, two different assumptions regarding the location of the catalysed isotopic exchange between CO_2 and water along the gradient of decreasing CO_2 mole fraction (C_i to C_c) are assessed by comparing predictions to field observations of photosynthetic ^{18}O discrimination.

This section describes predictions and field observations of ^{18}O discrimination during photosynthesis, i.e. the influence of photosynthesis on the $\delta^{18}\text{O}$ signature of canopy CO_2 and the role of leaf water isotopic enrichment and leaf internal CO_2 gradients in determining this signature. The relationships between $\delta^{18}\text{O}$ signals and environmental parameters described in this section are used subsequently in Part II, section 7.3, to estimate diurnal patterns and integrated values of $\delta^{18}\text{O}$ of ecosystem gas exchange for the days following measuring campaigns. Furthermore, in Part II, section 9, the $\delta^{18}\text{O}$ signatures of canopy fluxes are then used along with the $\delta^{13}\text{C}$ signatures (see sections 3.1 and 3.2) to evaluate a newly developed approach for partitioning of net ecosystem exchange into component fluxes.

Theory

The enrichment (or depletion) of ^{18}O in ambient CO_2 during photosynthesis differs from that in ^{13}C , because CO_2 exchanges isotopically with H_2O in a reaction catalysed by the enzyme carbonic anhydrase. This has two important implications: firstly, the oxygen isotopic composition of CO_2 will be predominantly influenced by the (mostly enriched) isotopic signature of the foliage water that it comes in contact with even if it only enters and diffuses back out of the stomatal cavity without being assimilated. Secondly, and because of this, photosynthetic ^{18}O enrichment is scaled by the backflux of CO_2 that can

far exceed net assimilation, therefore absolute values and diurnal amplitudes can be much higher than for ^{13}C .

Assuming full isotopic equilibrium with chloroplastic water, fractionation against ^{18}O during photosynthesis (" ^{18}O discrimination"), $^{18}\Delta$, can be written to reasonable approximation following Farquhar and Lloyd (1993) as:

$$^{18}\Delta = \bar{a} + \left(\delta^{18}\text{O}_c - \delta^{18}\text{O}_{\text{atm}} \right) \frac{C_c}{C_a - C_c} \quad (4.1)$$

where C_c and C_a are CO_2 mole fractions inside the chloroplasts and in ambient canopy air, respectively, \bar{a} is the average fractionation during diffusion of CO_2 in air (7.4 ‰), $\delta^{18}\text{O}_{\text{atm}}$ is the isotopic signal of ambient CO_2 , and $\delta^{18}\text{O}_c$ is the isotopic composition of CO_2 in equilibrium with the pool of foliage water that it exchanges with. This exchange is assumed to take place at the surface of the chloroplasts (Farquhar and Lloyd 1993), hence instead of C_c the CO_2 mole fraction at the chloroplast surface, C_{cs} , should be used in the above equation. However, Gillon and Yakir (2000) suggested that C_{cs} was close to C_i , the intercellular CO_2 mole fraction. As C_{cs} might be intermediate between C_c and C_i , both were obtained in our study from simultaneous measurements of ^{13}C discrimination (see Figure 1.3 for diagram of C_a , C_i and C_c).

Flux derived C_i/C_a and C_c/C_a were calculated using equations 2.6 and 3.10. C_i/C_a and C_c/C_a were also estimated from net observed ^{13}C discrimination, $^{13}\Delta_{\text{obs}}$, corrected for contributions from respiratory fluxes and internal CO_2 transfer (see section 3.1):

$$\frac{C_i}{C_a} = \frac{^{13}\Delta_{\text{obs}} - a + (b - a_m) \frac{A}{g_w C_a} + \left(f - (e + e^*) \frac{R_d}{A + R_d} \right) \frac{\Gamma^*}{C_a}}{b - a - (e + e^*) \frac{R_d}{A + R_d}} \quad (4.2)$$

$$\frac{C_c}{C_a} = \frac{^{13}\Delta_{\text{obs}} - a + (a - a_m) \frac{A}{g_w C_a} + \left(f - (e + e^*) \frac{R_d}{A + R_d} \right) \frac{\Gamma^*}{C_a}}{b - a - (e + e^*) \frac{R_d}{A + R_d}} \quad (4.3)$$

The derivation of equation 4.2 (4.3 derived analogously) is given in the Appendix.

The isotopic composition of CO₂, $\delta^{18}\text{O}_C$, is in equilibrium with that of water at the chloroplast surface, $\delta^{18}\text{O}_{CW}$. The equilibrium coefficient of the exchange reaction between CO₂ and water, $\varepsilon_{\text{CO}_2\text{-H}_2\text{O}}(T)$, can be calculated from leaf temperature T (K) using the formulation of Brenninkmeier et al. (1983):

$$\varepsilon_{\text{CO}_2\text{-H}_2\text{O}}(T) = \frac{17604}{T} - 17.93 \quad (4.4)$$

The isotopic composition of water at the chloroplast surface, $\delta^{18}\text{O}_{CW}$, is assumed to be close to that at the leaf evaporating sites. The latter is usually calculated using the steady state enrichment model of Craig and Gordon (1965). It describes evaporation from a water surface influenced by two source pools: ground or soil water on one hand, and atmospheric water vapour on the other hand, and two fractionating processes: a temperature dependent fractionation between the liquid and the vapour phase of water, and a kinetic fractionation where the lighter isotope is transpired faster and the heavier isotope stays behind, thereby enriching the isotopic composition of the leaf evaporating site water pool. The actual $\delta^{18}\text{O}$ value of evaporating site leaf water is controlled by the rate of transpiration from the leaf surface and thus proportional to relative humidity in the air surrounding the foliage. The isotopic composition of water in isotopic steady state (ISS) at the evaporating sites, $\delta^{18}\text{O}_{ISS}$, can thus be determined using the δ -notation of the Craig and Gordon model from Farquhar et al. (1993):

$$\delta^{18}\text{O}_{CW-ISS} = \delta^{18}\text{O}_{ISS} = \delta^{18}\text{O}_S + \varepsilon_k + \varepsilon_{eq} + \left(\delta^{18}\text{O}_V - \delta^{18}\text{O}_S - \varepsilon_k \right) \frac{e_a}{e_i} \quad (4.5)$$

where $\delta^{18}\text{O}_S$ and $\delta^{18}\text{O}_V$ are isotopic compositions of source water and canopy water vapour, respectively. ε_k is the kinetic fractionation factor during diffusion of water vapour in air, ε_{eq} is the equilibrium fractionation factor during water evaporation, and e_a/e_i is the ratio of ambient to leaf intercellular water vapour mole fraction. The latter corresponds to h^* , the relative humidity of ambient air corrected with respect to leaf temperature.

Buhay et al. (1996) concluded that kinetic fractionation factors can be reliably estimated based on leaf size and morphology. The diffusional fractionation factor, ε_k , was calculated from their equation (C6) for dissected needles:

$$\varepsilon_k = 28.5 \frac{\ln \left(\frac{V_k \cdot d_k}{\left(\frac{4.42 \cdot 10^{-4} \cdot d_k \cdot 698 \cdot 0.95 \cdot V_k^{0.97}}{0.044} \right)^{1.03} \cdot 0.63} \right)}{\ln 0.242} \cdot 10^{-3} \quad (4.6)$$

where V_k is airflow velocity and d_k is needle diameter. Airflow around the branches had a controlled speed of 25 cm/s for both open bags and when the bags were closed during measurement periods. With a mean diameter for Sitka spruce needles sampled from the branches of 1.5 ± 0.5 mm (depending on canopy level and needle age class distribution), this yields an estimate of 27.7 ± 0.2 ‰ for ε_k .

The equilibrium fractionation coefficient for the phase transition of water from liquid to vapour, $\varepsilon_{eq}(T)$, was determined using the regression parameters of Majoube (1971):

$$\varepsilon_{eq}(T) = \exp \left(\frac{1137}{T^2} - \frac{0.4156}{T} - 0.0020667 \right) \quad (4.7)$$

where T is leaf temperature (K). At the typical day-time temperatures of 9 to 14 °C of ambient canopy air, ε_{eq} was generally around 11 to 10 ‰.

The average isotopic composition of twig water was used to define the isotopic composition of source water, $\delta^{18}\text{O}_S$. Since water vapour within the canopy originates mainly from needle transpiration, $\delta^{18}\text{O}_V$ was assigned a value in temperature dependent isotopic equilibrium with water delivered through twigs. ε_{eq} values were calculated on the basis of day-time leaf temperatures weighted by measured leaf transpiration rates over the course of the diurnal cycle from all branch bags (10.4 to 10.8 ‰). This yielded a mean $\delta^{18}\text{O}_V$ of -18.6 ‰. A (hypothetical) contribution of 30 % soil evaporation ($\delta^{18}\text{O}_{soil} \approx -7$ ‰) to canopy water vapour would have increased $\delta^{18}\text{O}_V$ by only 0.3 ‰ on average.

In contrast to controlled laboratory experiments, plant foliage under fluctuating environmental conditions may rarely be in the isotopic steady state (ISS) with respect to leaf water enrichment, as represented by the Craig and Gordon model. Harwood et al. (1998) found that leaf water was at ISS only during a few hours after mid-day. The amount of time necessary for foliage water to attain an isotopic steady state will depend on transpiration rates. A decrease in transpiration rate will cause a decrease in the rate

of foliage water turnover, hence the isotopic steady state will be reached more slowly than at a higher transpiration rate. The rate of approach of leaf water isotopic composition towards an isotopic steady state can be incorporated into the Craig and Gordon model to obtain an expression for the non steady state (NSS) isotopic composition of evaporating site water, $\delta^{18}\text{O}_{\text{NSS}}$, following Dongmann et al. (1974):

$$\delta^{18}\text{O}_{\text{CW-NSS}}^t = \delta^{18}\text{O}_{\text{NSS}}^t = \delta^{18}\text{O}_{\text{ISS}} - (\delta^{18}\text{O}_{\text{ISS}} - \delta^{18}\text{O}_{\text{NSS}}^{t-1}) \cdot e^{-\frac{t-t_0}{\tau}} \quad (4.8)$$

where $\delta^{18}\text{O}_{\text{ISS}}$ is leaf water enrichment at time t in isotopic steady state with environmental conditions as calculated from equation 4, $\delta^{18}\text{O}_{\text{NSS}}^{t-1}$ is leaf water enrichment at the previous time step, and $t - t_0$ is the interval between time steps (usually 20 mins). The leaf water turnover time τ can be calculated from the ratio of leaf water volume V (mol/m^2) to transpiration rate E ($\text{mol}/\text{m}^2/\text{s}$) according to:

$$\tau = \frac{V}{E \cdot h^* \cdot (1 - \varepsilon_k)(1 - \varepsilon_{eq})} \quad (4.9)$$

where h^* is the relative humidity of ambient air corrected with respect to leaf temperature (as in equation 4.5). E has been obtained as described in the Methods section (equation 2.3).

Both versions (ISS and NSS) of the enrichment equation describe needle water isotopic composition at the evaporating sites. To obtain the isotopic signature of bulk needle water, less enriched components of the needle water volume have to be taken into account. Pine needles have centrally located vascular bundles (“leaf veins”) carrying unenriched source water that moves radially out through mesophyll tissue towards the needle surface. Opposed to that, enriched water from the evaporating surface diffuses back towards the vein, constituting a Péclet effect. The strength of the effect varies depending on relative rates of diffusive and convective water fluxes, creating a variable enrichment gradient along the path of water movement. The gradient is controlled by the transpiration flux - it is stronger for higher transpiration rates, when backdiffusion becomes relatively less important. Farquhar and Lloyd (1993) incorporated the Péclet effect to give an expression for average bulk leaf water enrichment, $\delta^{18}\text{O}_B$:

$$\delta^{18}O_B = \delta^{18}O_S + (\delta^{18}O_E - \delta^{18}O_S) \frac{1 - e^{-\rho}}{\rho} \quad (4.10)$$

This formulation applies to both $\delta^{18}O_{B-ISS}$ and $\delta^{18}O_{B-NSS}$, with evaporating site enrichment $\delta^{18}O_E$ substituted with $\delta^{18}O_{ISS}$ or $\delta^{18}O_{NSS}$, respectively. The Péclet number is defined as:

$$\rho = \frac{EL}{C_m D_{18}} \quad (4.11)$$

where E is transpiration rate, L is scaled effective mixing length, C_m is molar concentration of water ($5.56 \cdot 10^4 \text{ mol/m}^3$) and D_{18} is diffusivity of $H_2^{18}O$ in $H_2^{16}O$ ($2.66 \cdot 10^{-9} \text{ m}^2/\text{s}$). The Péclet number, ρ , is an expression for the gradient described above. The balance between convective and diffusive transport is influenced by the average transport velocity (E/C_m). The smaller the Péclet number the weaker the gradient, and so the greater the extent to which bulk leaf water $\delta^{18}O$ will be influenced by diffusion rather than convection. Wang et al. (1998) characterised conifers as having smaller Péclet numbers. With more emphasis on diffusion, bulk water $\delta^{18}O$ in conifer foliage should therefore be closer to evaporating site enrichment. The resulting predicted bulk needle water isotopic composition, $\delta^{18}O_B$, can then be compared to measurements of water extracted from bulk needle samples.

Results

Field observations of $^{18}\Delta$ during photosynthesis

In May 2001, flask sampling started after sunrise, with dawn samples taken on the next day. In July 2001, flask sampling started at dawn and a complete diurnal cycle was obtained. Figure 4.1 shows $^{18}\Delta_{obs}$ values for the different branch bags (top1 and top3, 10 m, and mid, 8 m) determined from sample pairs following equation 2.7. Noticeable are the extremely high dawn and dusk $^{18}\Delta_{obs}$ values of around 100 ‰, in sharp contrast to mid-morning values in the order of 10 ‰. Afternoon values were between 20 and 60 ‰. Mid bag values (only May data) were similar to those of top bags, except at noon, when the highest $^{18}\Delta_{obs}$ value of both campaigns was measured (126 ‰). $^{18}\Delta_{obs}$ was slightly smaller in July compared to May.

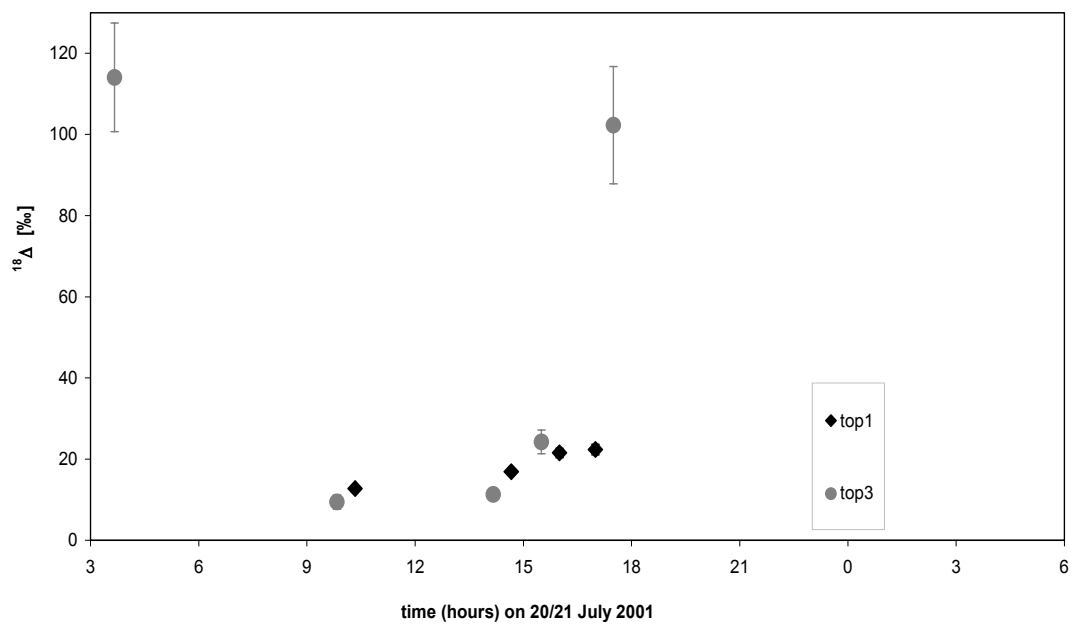
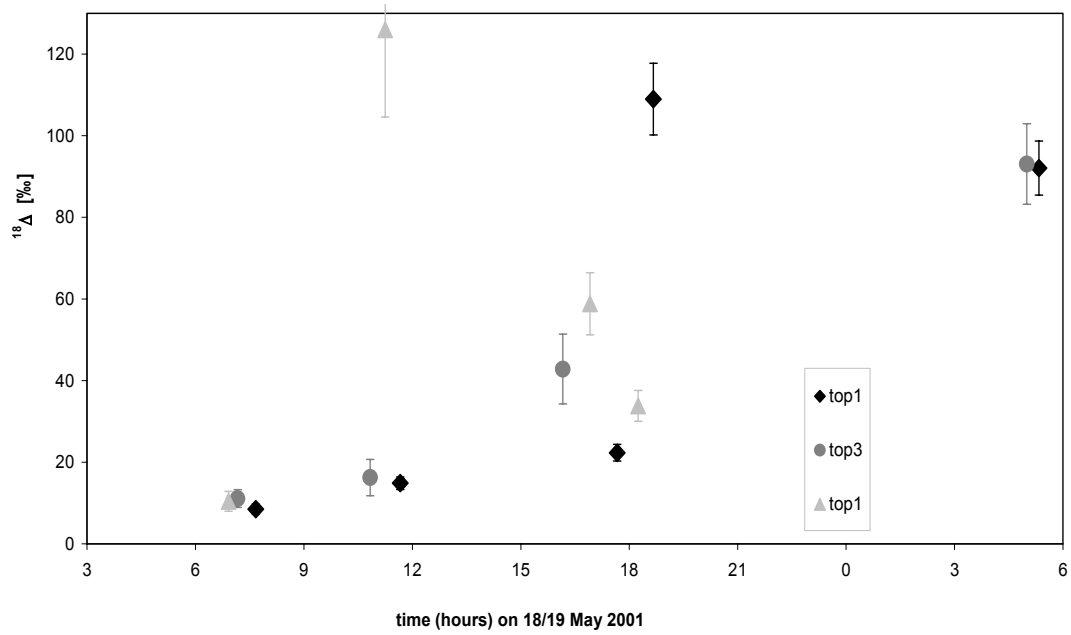


Figure 4.1: Observed ^{18}O discrimination, $^{18}\Delta_{\text{obs}}$, of branch bag foliage during photosynthesis obtained from top and mid bags in May 2001 and top bags in July 2001.

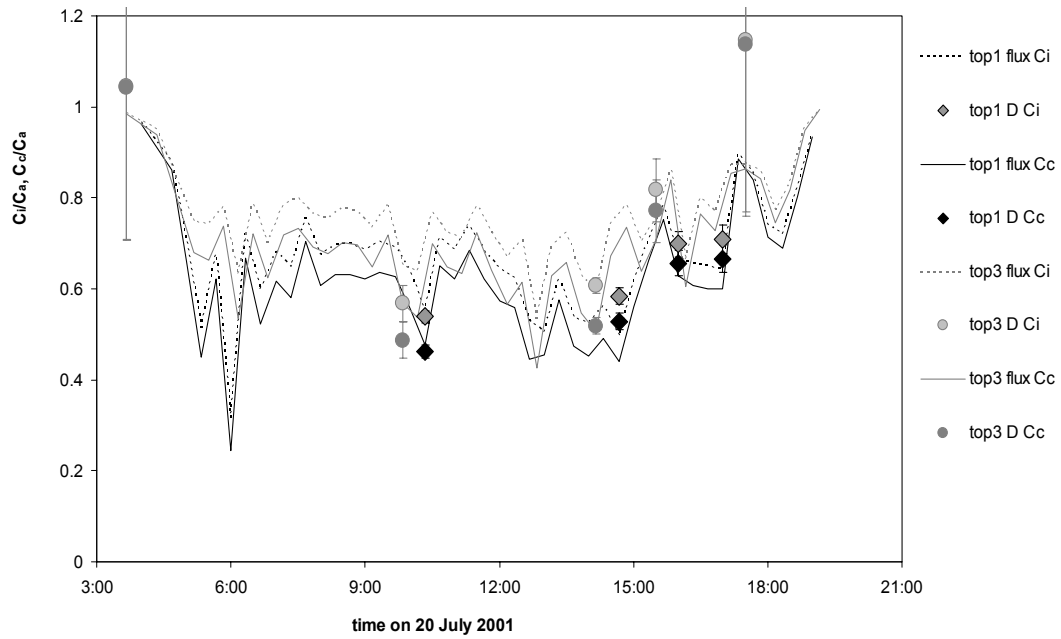
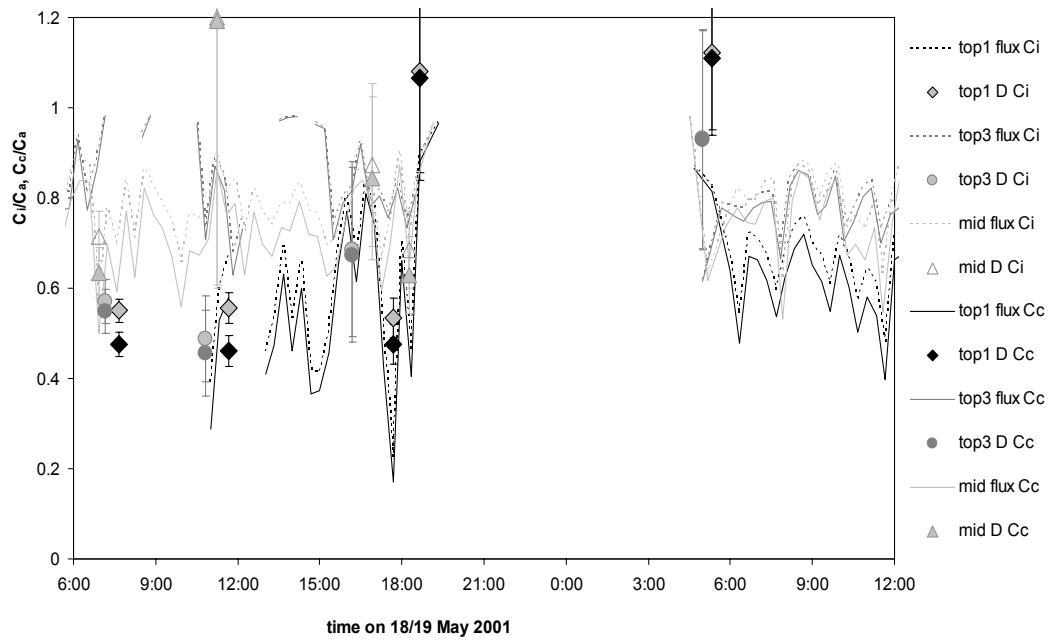


Figure 4.2: C_i/C_a and C_c/C_a calculated from fluxes and from ^{13}C discrimination (D), $^{13}\Delta_{\text{obs}}$, for top and mid branch bags in May and July 2001.

Parameters for predicting $^{18}\Delta$

C_i/C_a and C_c/C_a

C_i/C_a was calculated from CO_2 and H_2O mole fraction and flux measurements obtained from the IRGA and relative humidity sensors for each time step (interval 20 min per bag at day-time) as detailed in section 2 (Methods). To calculate C_c , mesophyll conductance, g_w , was obtained as described in section 3.1. Mesophyll conductance for branch bag foliage was estimated at $0.29 \text{ mol/m}^2/\text{s}$, only slightly greater than the upper range obtained for stomatal conductance ($\approx 0.24 \text{ mol/m}^2/\text{s}$). Flux based C_c/C_a was then calculated using equation 3.10. Estimates of C_i/C_a and C_c/C_a from net observed ^{13}C discrimination were obtained following equations 4.2 and 4.3. Figure 4.2 shows C_i/C_a and C_c/C_a from flux data and from ^{13}C discrimination. Flux based values for the top bags are not continuous on the first half day of the May campaign when some instrumental errors occurred. At most times, flux and discrimination based estimates agreed well. In contrast, when $^{13}\Delta_{\text{obs}}$ was above 30 ‰, respiratory corrections were not large enough to account for discrepancies between predicted and observed $^{13}\Delta$, and hence between flux and discrimination based estimates of C_i/C_a and C_c/C_a . For a more detailed discussion see section 3.1.

Isotopic composition of canopy CO_2

Figure 4.3 shows $\delta^{18}\text{O}_{\text{atm}}$, the oxygen isotopic composition of canopy CO_2 , obtained from open samples, i.e. measurements from open branch bags. These values are reported

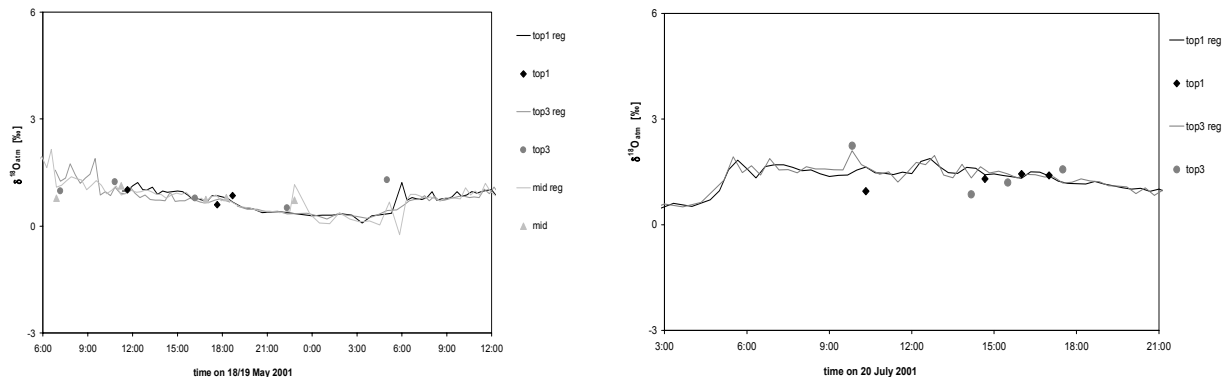


Figure 4.3: $\delta^{18}\text{O}_{\text{atm}}$ of canopy CO_2 : observations and regressions of open sample $\delta^{18}\text{O}$ vs. $1/[\text{CO}_2]$.

with respect to V-PDB-CO₂. The time course of $\delta^{18}\text{O}_{\text{atm}}$ was derived from a regression of $\delta^{18}\text{O}_{\text{atm}}$ against the inverse of the canopy CO₂ mole fraction. The prerequisite for application of this method, contributions from two pools of CO₂ with different isotopic signatures, is not likely to be strictly fulfilled inside the canopy during the day, as turbulent mixing with air from above the canopy, plant photosynthesis and soil respiration each carry their own distinct isotopic signatures. However, regression yielded R² values of > 0.9 for the May day-time data, with intercepts of -6.9 ‰ (May) and -5.9 ‰ (July). This might indicate that during the day, contributions from the soil (intercept at -14 ‰, May and July) can be largely neglected and the simple model of mixing between two pools can be applied. Apparent discrepancies between regressed and measured $\delta^{18}\text{O}_{\text{atm}}$ can be explained mostly by differences between IRGA and flask CO₂ mole fraction data, with flask samples collected from open branch bags 3 to 4 minutes before IRGA measurements started immediately after bag closure.

Isotopic composition of needle water at the evaporating sites

Micro-climate and transpiration data obtained from branch bag sensors were used for each time step and bag to calculate $\delta^{18}\text{O}_{\text{CW}}$ of needles according to equations 4.3 and 4.6. All water $\delta^{18}\text{O}$ values are reported with respect to V-SMOW. The isotopic composition of source water was obtained from average $\delta^{18}\text{O}_{\text{twig}}$, the isotopic composition of twig water (-8 ‰). Twig water was found to be depleted with respect to soil water from the top 5 cm of the soil profile by 0.3 to 5 ‰ at most times. Without fractionation during water uptake or transport through the xylem cells of tree stems, $\delta^{18}\text{O}_{\text{twig}}$ should represent an uptake weighted average isotopic composition of water from different soil layers, potentially also including ground water. Twig water should not experience the same degree of evaporative enrichment as soil water. Soil and twig water $\delta^{18}\text{O}$ values are discussed in more detail in section 4.2. The isotopic composition of canopy water vapour, $\delta^{18}\text{O}_{\text{V}}$, was calculated in temperature dependent equilibrium with source water. The leaf water volume (V) was assigned a value of 7.85 mol/m² for both months. It was determined from the difference between fresh and dry weight of 18 needle samples divided by the projected leaf area of the respective samples. The calculations of $\delta^{18}\text{O}_{\text{NSS}}$ values were initialised with the corresponding $\delta^{18}\text{O}_{\text{ISS}}$ values at 16:00 on the previous day (tests confirmed that this allowed enough turnover time to attain the dynamic steady state usually reached after about one day).

Predictions of evaporating site water enrichment obtained with ISS and NSS model versions, $\delta^{18}\text{O}_{\text{ISS}}$ and $\delta^{18}\text{O}_{\text{NSS}}$, are presented in Figure 4.4. Shortly after dawn, $\delta^{18}\text{O}_{\text{ISS}}$ values started rising rapidly by 5 to 10 ‰ within 1 to 2 hours whereas the increase in $\delta^{18}\text{O}_{\text{NSS}}$ values was slower. Only later during mid-morning did $\delta^{18}\text{O}_{\text{NSS}}$ values reach the same level of enrichment as the $\delta^{18}\text{O}_{\text{ISS}}$ values. This difference in timing was due to the low transpiration rates usually found in the morning. On the other hand, such low transpiration rates were also found in the evenings and sometimes even throughout the night. For this reason, $\delta^{18}\text{O}_{\text{NSS}}$ values were often not as depleted as $\delta^{18}\text{O}_{\text{ISS}}$ values during the night, when $\delta^{18}\text{O}_{\text{ISS}}$ values decreased to source water $\delta^{18}\text{O}$ values in the absence of evaporative enrichment (see equation 4.5). Thus, $\delta^{18}\text{O}_{\text{NSS}}$ values were often higher than $\delta^{18}\text{O}_{\text{ISS}}$ values at dawn and then started rising from already higher levels.

Typical maximum $\delta^{18}\text{O}_{\text{NSS}}$ values were around 5 ‰ lower than those of $\delta^{18}\text{O}_{\text{ISS}}$. Maxima of $\delta^{18}\text{O}_{\text{NSS}}$ were shifted towards the afternoon compared to those of $\delta^{18}\text{O}_{\text{ISS}}$. For both ISS and NSS versions, average $\delta^{18}\text{O}$ values were higher in top bags than in the mid bag, and higher in the afternoon than in the morning. Diurnal trends of $\delta^{18}\text{O}_{\text{ISS}}$ were superimposed by fluctuations on time scales of around one hour. These were not found in $\delta^{18}\text{O}_{\text{NSS}}$ because the transpiration rate dependent adjustment to changing environmental conditions effectively dampens short-term fluctuations and smoothes diurnal patterns.

Errors in calculated $\delta^{18}\text{O}$ caused by a hypothetical shift of 1 ‰ in $\delta^{18}\text{O}_v$ (for example from an underestimation of soil evaporation or tropospheric water vapour contributions) would be in the order of 1 ‰ at dawn, 0.8 ‰ at dusk and 0.4 ‰ (top bags) and 0.6 ‰ (middle bag) during the rest of the day. Such errors would be mostly negligible compared to differences between ISS and NSS values. Any impact on flux weighted values would also be small. This is because uncertainties due to variable $\delta^{18}\text{O}_v$ are scaled by relative humidity and are thus generally smaller at the times of high evaporation rates.

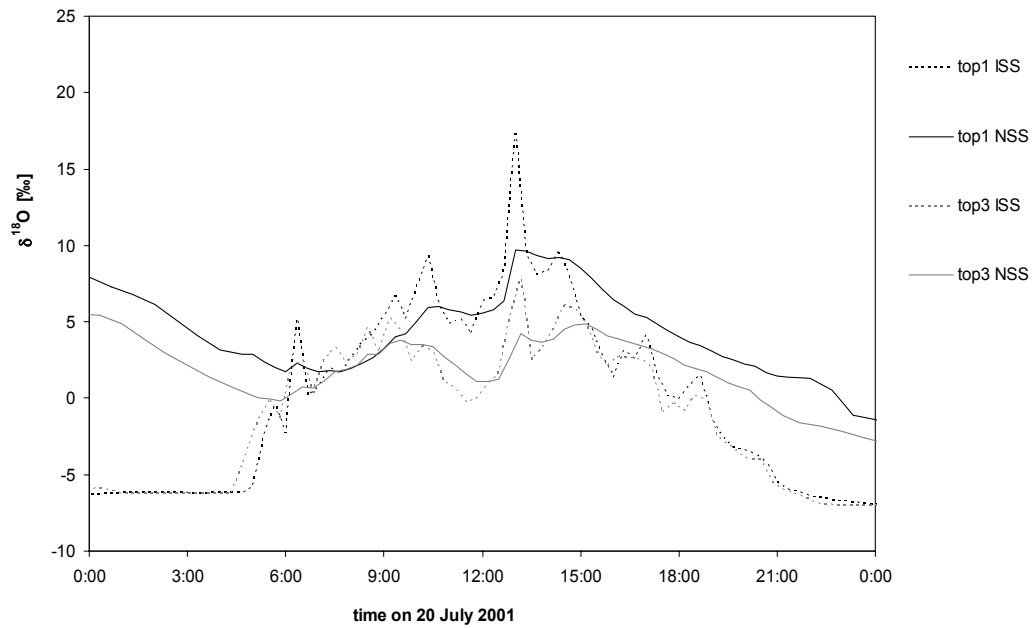
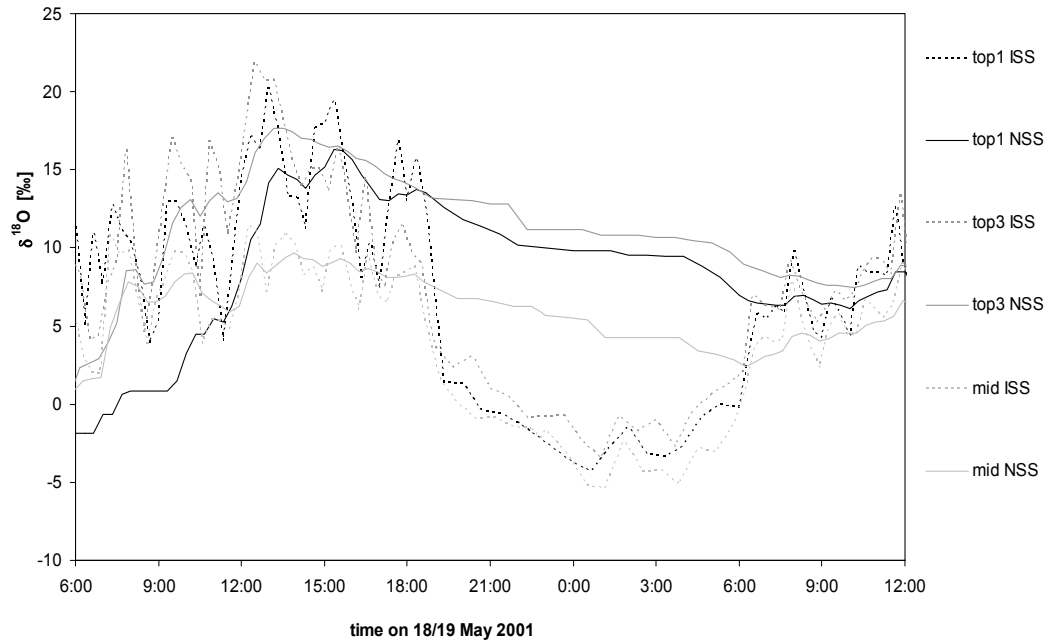


Figure 4.4: Needle water $\delta^{18}\text{O}$ and the effect of taking turnover rates into account: enrichment at evaporating sites of branch bag foliage assuming ISS (dashed lines) and NSS (solid lines).

Isotopic composition of bulk needle water

One test of needle water ^{18}O enrichment predictions is to simply compare them to bulk needle water $\delta^{18}\text{O}$ measurements. To do this, predictions were adjusted following equation 4.9 to take the Péclet effect on the average isotopic composition of bulk water into account. A scaled effective mixing length (L) of 100 mm was assumed (see equation 4.11). This value was chosen to achieve a reasonable qualitative agreement between predicted and measured $\delta^{18}\text{O}$ of bulk foliage water. Figure 4.5 shows the calculated isotopic compositions of bulk foliage ($\delta^{18}\text{O}_{\text{B-NSS}}$) and evaporating site ($\delta^{18}\text{O}_{\text{NSS}}$) water, illustrating the influence of transpiration rate on the leaf water gradient due to the Péclet effect. In both versions (ISS not shown), the respective bulk needle water isotopic composition was 3 to 4 ‰ depleted compared to evaporating site values.

Measured and predicted values for bulk foliage water isotopic composition are shown in Figure 4.6 for 18 May 2001 (July data not available). The isotopic composition of bulk needle water, $\delta^{18}\text{O}_{\text{N}}$, followed the same general trend as that predicted by the non steady state version of the bulk water enrichment equation, $\delta^{18}\text{O}_{\text{B-NSS}}$. It had only small average diurnal amplitudes of 5 to 8 ‰. Predicted and observed values were around 5 ‰ higher in the afternoon than in the morning, and 5 to 10 ‰ higher in the top than in the mid bag, although at several times, bulk needle water sampled from the top of the canopy was less enriched than bulk needle water samples from further down in the canopy profile. In the afternoon, predicted values in top bags were higher than those of the mid bag. In the mornings and evenings, bulk data measurements had a better agreement with $\delta^{18}\text{O}_{\text{B-NSS}}$ than with $\delta^{18}\text{O}_{\text{B-ISS}}$ values.

An unanticipated result of needle water analysis was that $\delta^{18}\text{O}_{\text{N}}$ did not decrease significantly during the night. At midnight, the largest difference between bulk needle and twig water $\delta^{18}\text{O}$ of 18 ‰ was observed, whereas it was 12 to 15 ‰ at all other times. These gradients were established even over small distances as twig and needle samples were usually sampled together, i.e. the attached needles were separated from the respective twigs. Results of the NSS bulk version agreed very well with enriched night time values found in bulk samples.

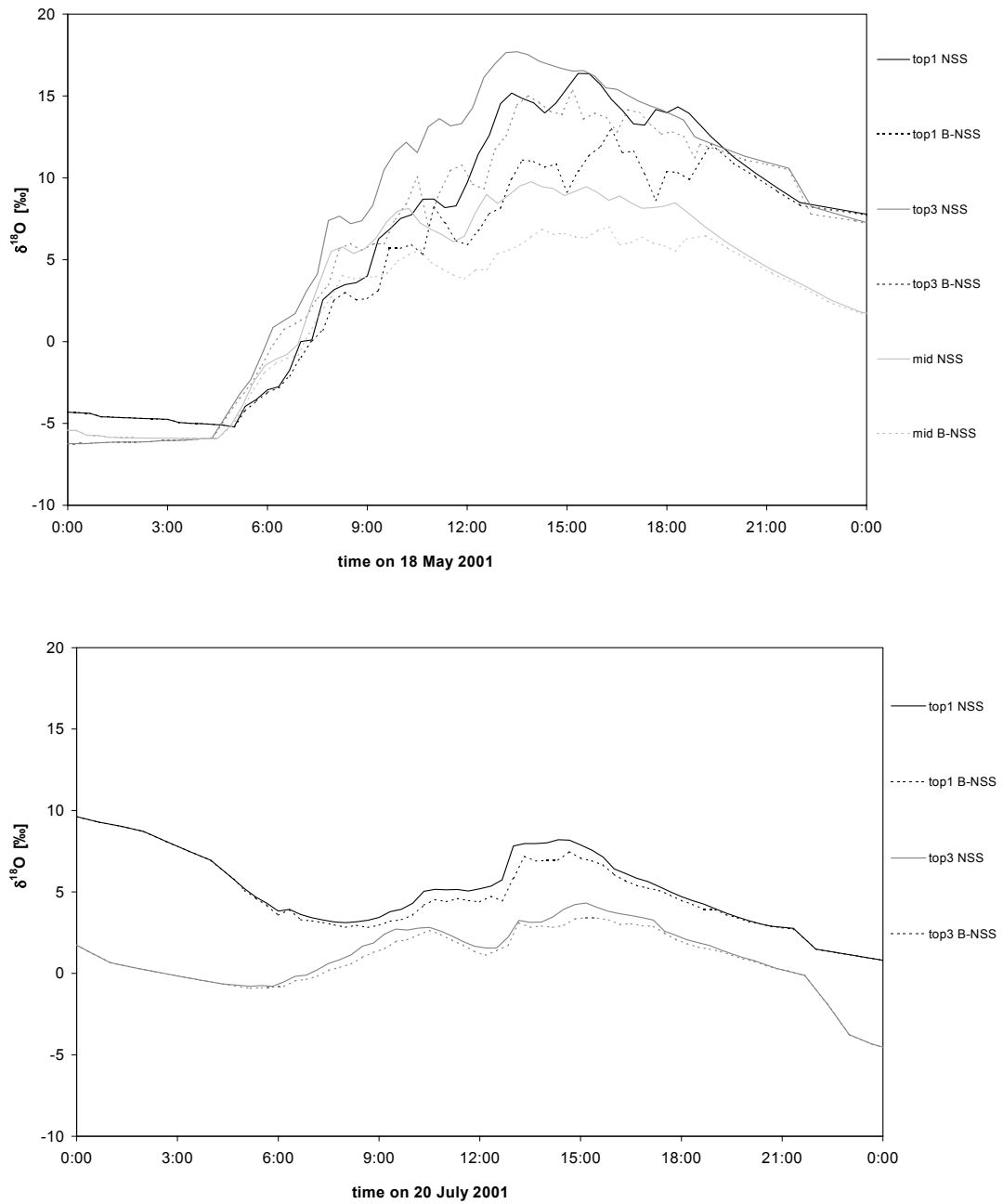


Figure 4.5: Bulk leaf water isotopic composition ($\delta^{18}\text{O}_{\text{B-NSS}}$, dashed lines) taking the Péclet effect into account and leaf water enrichment at the evaporating sites ($\delta^{18}\text{O}_{\text{NSS}}$, solid lines).

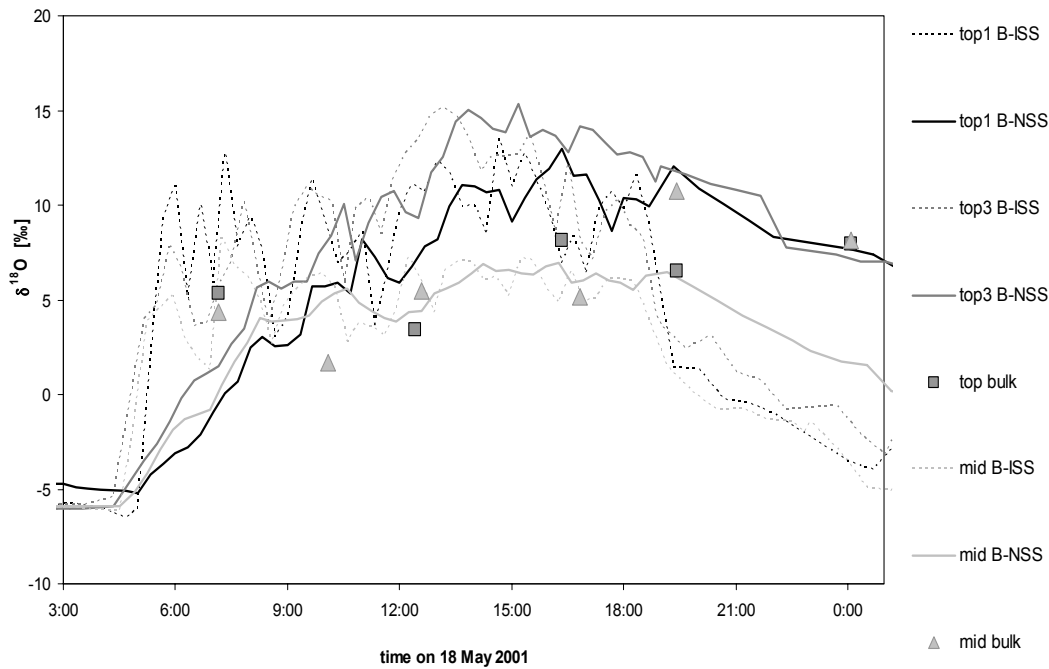


Figure 4.6: Predictions of bulk needle water isotopic composition assuming ISS ($\delta^{18}\text{O}_{\text{B-ISS}}$) or NSS ($\delta^{18}\text{O}_{\text{B-NSS}}$) conditions and measurements of bulk needle water enrichment.

Predictions of $^{18}\Delta$ during photosynthesis

$^{18}\Delta$ was predicted following equation 4.1 with the above described input variables C_i or C_c , $\delta^{18}\text{O}_{\text{atm}}$ and $\delta^{18}\text{O}_{\text{CW}}$ ($\delta^{18}\text{O}_{\text{ISS}}$ or $\delta^{18}\text{O}_{\text{NSS}}$) for each time step and bag. This yielded four sets of $^{18}\Delta$ predictions: $^{18}\Delta_{\text{ISS-C}_i}$, $^{18}\Delta_{\text{ISS-C}_c}$, $^{18}\Delta_{\text{NSS-C}_i}$ and $^{18}\Delta_{\text{NSS-C}_c}$. Three of these (without $^{18}\Delta_{\text{ISS-C}_i}$) are presented in Figure 4.7, together with the observed values. Predicted values were more variable in May than in July. NSS predicted values at dawn and dusk were highly enriched by up to 500 ‰ (or depleted in the ISS version, respectively) in both months, and also around noon in May. These values coincided with C_i/C_a or C_c/C_a close to 1, when stomata are open, hence at conditions of large CO_2 backfluxes that also amplified differences between $^{18}\Delta_{\text{ISS}}$ and $^{18}\Delta_{\text{NSS}}$ so that these reached up to 600 ‰. For most of the July campaign, environmental conditions were more stable resulting in more gradual changes in discrimination values over the course of the day. Variations and differences of $^{18}\Delta_{\text{ISS}}$ and $^{18}\Delta_{\text{NSS}}$ were small and mostly correlated with those of

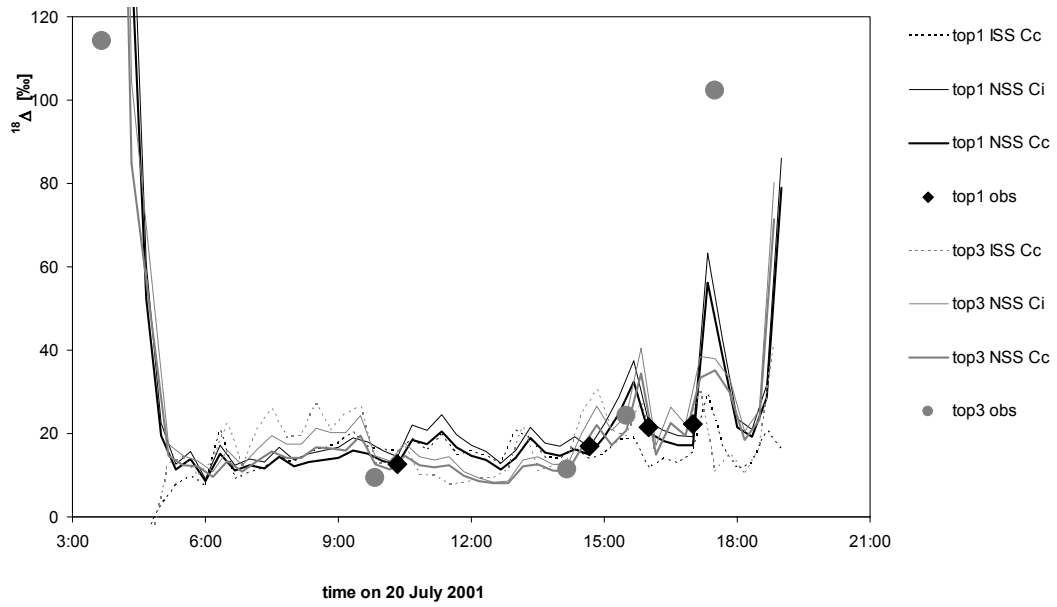
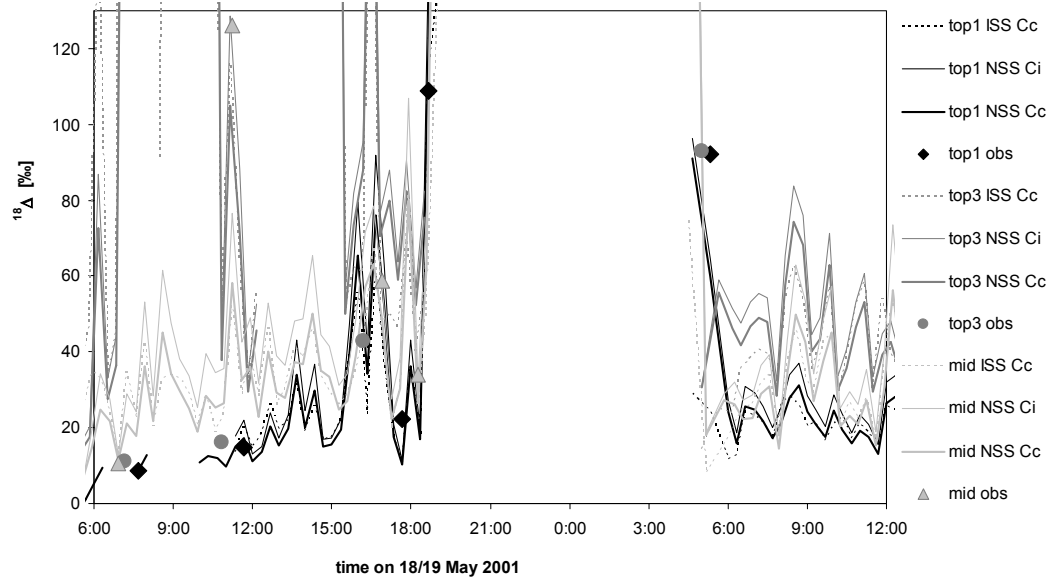


Figure 4.7: Observed and predicted $^{18}\Delta$ using flux derived C_i/C_a or C_o/C_a assuming ISS (dashed lines, not shown for C_i/C_a) or NSS (solid lines).

$\delta^{18}\text{O}_{\text{ISS}}$ and $\delta^{18}\text{O}_{\text{NSS}}$ because C_i/C_a (and hence $C_c/(C_a-C_c)$) values were low and not varying greatly. In contrast, variations and differences were again amplified by high rates of CO_2 backflux early and late in the day.

Predicted $^{18}\Delta$ values using $\delta^{18}\text{O}_{\text{NSS}}$ or C_c were generally in better agreement with $^{18}\Delta_{\text{obs}}$ than those using $\delta^{18}\text{O}_{\text{ISS}}$ or C_i . $^{18}\Delta_{\text{obs}}$ was clearly lower than $\delta^{18}\text{O}_{\text{ISS}}$ in the morning and higher towards the evening. For some of the afternoon sampling times (roughly between 12:00 and 15:00), there was little difference between ISS and NSS predictions. At these times, leaf water was close to isotopic steady state. In addition, there were only small differences between predicted $^{18}\Delta$ values using either C_i or C_c , so that at these times, predictions appear not to be very sensitive to exact formulations of their input variables, with differences between predictions based on $\delta^{18}\text{O}_{\text{ISS}}$ or $\delta^{18}\text{O}_{\text{NSS}}$, and C_i or C_c , smaller than measurement uncertainties of 1 to 2 ‰. In contrast, prediction differences were substantially larger than $^{18}\Delta_{\text{obs}}$ uncertainties of 9 ‰ at dawn and dusk (20 ‰ for May noon, mid-bag). On the other hand, even small changes in C_c/C_a have huge impacts on $^{18}\Delta$, while at the same time amplifying the impact of $\delta^{18}\text{O}_{\text{CW}}$ variations, causing predicted values to be extremely sensitive to correct determination of both C_c/C_a and $\delta^{18}\text{O}_{\text{CW}}$. Therefore, it is difficult to predict $^{18}\Delta$ with confidence at these times.

Measured $^{18}\Delta_{\text{obs}}$ values versus predictions of $^{18}\Delta$ using $\delta^{18}\text{O}_{\text{NSS}}$ and C_c/C_a combined from both sampling days are presented in Figure 4.8. Regression analyses were performed on all combinations of measured versus predicted data sets. The regressions were weighted according to the standard deviation of the observed discrimination values (see error bars of Figure 4.1). Regression parameters are listed in Table 4.1. The dawn and dusk $^{18}\Delta_{\text{obs}}$ values of 92 to 126 ‰ were excluded from the regressions, otherwise they would be overrepresented and bias the regressions. That is because the dawn and dusk samples are representative for only about 10 % of the photosynthetic period, whereas they constituted almost 30 % of all samples because of the chosen sampling strategy. The method of determination of leaf water enrichment (ISS or NSS) had more impact on regression parameters than the site of isotopic exchange (C_c or C_i), except for times when leaf water was at isotopic steady state. The correlations between predicted and measured values were better using NSS than using ISS versions (ISS regressions were not significant). Predictions using the NSS versions, i.e. taking into account non steady state effects on the enrichment of foliage water at the evaporating sites, were in significantly better agreement with observations than their corresponding ISS versions

($P < 0.05$). NSS predictions in combination with C_i , the substomatal CO_2 mole fraction, were slightly higher than observations, whereas in combination with C_c , the CO_2 mole fraction in the chloroplasts, NSS predictions were slightly lower than observations. No significant differences were found between these two combinations ($P = 0.61$).

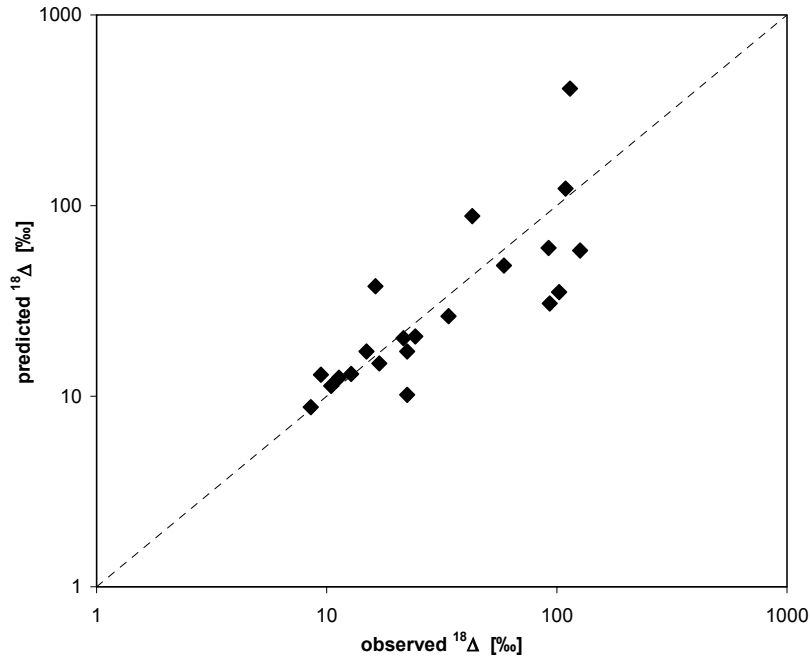


Figure 4.8: Comparison of $^{18}\Delta_{\text{obs}}$ with predicted $^{18}\Delta$, using $\delta^{18}\text{O}_{\text{NSS}}$ and C_c/C_a for data from May and July 2001. Note that both axes are on a logarithmic scale.

Prediction set	$^{18}\Delta_{\text{ISS-Ci}}$	$^{18}\Delta_{\text{ISS-Cc}}$	$^{18}\Delta_{\text{NSS-Ci}}$	$^{18}\Delta_{\text{NSS-Cc}}$
Slope	0.56 (0.29)	0.52 (0.24)	1.04 (0.26)	0.91 (0.24)
Intercept	10.2 (5.3)	8.1 (4.5)	1.6 (4.9)	1.3 (4.4)
correlation (R^2)	0.23	0.26	0.54	0.52
P	0.071	0.052	0.002	0.002

Table 4.1: Regression parameters of predicted $^{18}\Delta$, using $\delta^{18}\text{O}_{\text{ISS/NSS}}$ and C_i/C_a or C_c/C_a , versus $^{18}\Delta_{\text{obs}}$, for data from both months weighted according to the standard deviations of the respective measurements (standard errors of slopes and intercepts in parentheses).

Discussion

The discrimination against ^{18}O during photosynthesis, $^{18}\Delta_{\text{obs}}$, was sensitive to changes in environmental conditions in a way similar to ^{13}C discrimination, $^{13}\Delta_{\text{obs}}$. At dawn and dusk, high humidity lead to open stomata, enabling a high backflux coincident with low assimilation rates. This resulted in high C_i/C_a and $C_c/(C_a-C_c)$ values. During the day, humidity declined with rising irradiances and temperatures. Following humidity decrease, stomata closure reduced the gross CO_2 fluxes into and out of the substomatal cavities. Decreasing stomatal conductances were resulting in lower rates of CO_2 back diffusion, expressed in overall lower levels of C_i/C_a and $C_c/(C_a-C_c)$ (for discussion of $^{13}\Delta$ and C_i/C_a see section 3.1). While diurnal patterns of $^{18}\Delta_{\text{obs}}$ and $^{13}\Delta_{\text{obs}}$ were similar, changes in $^{18}\Delta_{\text{obs}}$ were much greater, since $^{13}\Delta$ is proportional to the ratio of intercellular to ambient CO_2 mole fraction, C_i/C_a . On the other hand, $^{18}\Delta$ also depends on the CO_2 flux diffusing back out of stomata and thus on $C_i/(C_a-C_i)$ (or $C_c/(C_a-C_c)$). This term rises exponentially with C_i/C_a . Besides its effect on $^{18}\Delta$ through scaling of fluxes, stomatal conductance also influences the isotopic composition of chloroplast water, $\delta^{18}\text{O}_{\text{CW}}$, the second main variable affecting $^{18}\Delta$, through regulation of evaporation rates.

The effects of $\delta^{18}\text{O}_{\text{CW}}$ changes on $^{18}\Delta$ were mostly counterbalanced by concurrent changes in C_c/C_a . At evening times, they reinforced each other, although the influence of $\delta^{18}\text{O}_{\text{CW}}$ was generally small compared to that of C_c/C_a . In addition, these changes might involve different time scales, with stomata potentially adapting more rapidly while $\delta^{18}\text{O}_{\text{CW}}$ responding more slowly to variations in natural conditions. In the morning, high relative humidity inhibited transpiration, resulting in less isotopic enrichment of leaf water. At the same time, open stomata enabled high rates of CO_2 backdiffusion while CO_2 assimilation rates were still low, outweighing the influence of low $\delta^{18}\text{O}_{\text{CW}}$ and leading to overall high $^{18}\Delta_{\text{obs}}$ values. With rising temperature and decreasing humidity, transpiration rates and $\delta^{18}\text{O}_{\text{CW}}$ increased. But stomatal closure to limit transpiration and rising CO_2 assimilation rates reduced CO_2 backdiffusion, and therefore overall $^{18}\Delta_{\text{obs}}$ values were low despite high $\delta^{18}\text{O}_{\text{CW}}$. When relative humidity again rose in the evening, stomatal opening and decreasing CO_2 assimilation enhanced CO_2 backdiffusion again. Because there was no large transpiration flux, $\delta^{18}\text{O}_{\text{CW}}$ retained its preceding enriched level, further increasing already high $^{18}\Delta_{\text{obs}}$ values.

The depletion of bulk needle water caused by the Péclet effect, or the gradient between evaporating sites and average bulk values, was stronger during the day because transpiration rates and hence the ratio of advective to diffusive fluxes were higher. At dawn, there was virtually no transpiration because canopy air was close to water vapour saturation. In the time period following dawn (1 to 2 hours), transpiration rates were still low despite already decreased relative humidity (or vapour mole fraction deficit, MFD). This indicates that transpiration was limited by closing of stomata. Supporting this, stomatal conductances had a brief local minimum at around 6:00. On the May sampling day, temperature and relative humidity were highly variable due to rapid changes in cloud cover. This was more pronounced within the top levels of the canopy, because irradiance fluctuations are damped by shading further down in the profile. In July, environmental conditions were more stable and temporal changes more gradual, with a clear maximum of steady state enrichment of evaporating site foliage water at noon.

Diurnal amplitudes of bulk needle water isotopic composition (5 - 8 ‰) were less than those observed in other studies (> 20 ‰, Cernusak et al. 2002). The increase in predicted and observed values over the day and towards the canopy top followed gradients in environmental parameters like temperature and humidity. However, transpiration rates were in fact not higher towards the top of the canopy, thus bulk needle water was sometimes less enriched there than lower in the canopy profile. With the slowing down of leaf water turnover in the evening the high levels of bulk needle water enrichment were retained over long periods (see Figure 4.6). The still enriched midnight values strongly support the interpretation that in the absence of an appreciable transpiration flux the approach to isotopic steady state can be slow enough to cause bulk needle water $\delta^{18}\text{O}$ values to stay enriched until morning.

Good agreement of calculated with measured bulk water isotopic composition was achieved when taking non steady state effects into account. The scaled effective mixing length (L) of 100 mm seems large for average needle dimensions of 1.5 x 20 mm, however, it is well within estimates of the scaling factor of 10^2 to 10^3 . The scaling reflects that water does not move through a body of water but through leaf tissue. The average Péclet number over the light period was 0.35 in May, within the range cited for conifers (0.15 to 0.5, Wang et al. 1998), and 0.1 in July, towards the lower end of that range. In general, when comparing measured and predicted bulk needle water enrichment values it should be kept in mind that these values represent different places within the canopy, as needles for bulk water analysis had been collected from the vicinity of the branch

bags, at the same heights but not from the exact same locations. Differences could have been caused or amplified by small-scale variability in canopy environmental conditions due to air movements and patchiness of sunlight. In addition, relative contributions from sun and shade foliage to needle samples might vary for each sampling time. Therefore, comparisons of predictions to measurements cannot be interpreted quantitatively. Nevertheless, they can be useful with respect to interpretation of general patterns.

During the day and under stable environmental conditions, the different predictions of photosynthetic ^{18}O discrimination did not differ greatly. Therefore, it could be argued that isotopic steady state for leaf water enrichment can be safely assumed for model predictions. Indeed, if assimilation was maximal at mid-day, observed diurnal discrimination integrals would reflect the steady state discrimination characteristic for these times. In such a case, taking NSS effects into account would not increase the accuracy of predicted diurnal discrimination integrals. However, if assimilation maxima were shifted in time (as observed for instance by Harwood et al. 1998, and references therein), the observed discrimination integrals would differ from those predicted assuming ISS conditions. This could be caused by systematic over- or underestimation of discrimination values due to the assumption of isotopic steady state at all times. In addition, the absolute differences in leaf water enrichment between ISS and NSS versions might be not exactly symmetrical with respect to noon values (i.e. afternoon NSS values are not higher than afternoon ISS values by the exact same amount as morning NSS values are lower than morning ISS values). This seems especially likely considering the already higher morning levels of evaporating site leaf water enrichment predicted under non steady state conditions.

This was emphasized by the differences between ISS and NSS diurnal integrals of discrimination calculated for the sampling days in our study: In May, taking NSS effects into account resulted in diurnally integrated discrimination of separate branches for the second sampling day that were 2 to 7 ‰ higher than those of the ISS version, although fluxes were rather uniform over the course of the day (on the first sampling day, pre-noon data was intermittent so that diurnal integrals would mainly reflect afternoon conditions). Overall discrimination weighted for all branches under study weighted by their respective assimilation rates was 30.3 ‰ in NSS version, 3 ‰ higher than in ISS version (27.1 ‰). In July, slightly higher fluxes were observed in the morning, and diurnal discrimination integrals in the NSS version were 0.5 and 3 ‰ higher than for the ISS version. Overall assimilation weighted discrimination was 15.5 ‰ in NSS version,

1.4 ‰ higher than in ISS version (14.1 ‰). Such differences might be less pronounced for species with higher transpiration rates that are closer to isotopic steady state conditions over longer periods of the day or experience morning and afternoon leaf water enrichment shifts of equal magnitude. They are, however, likely to be even greater when assimilation maxima are more strongly shifted in time. It is interesting to note the large difference between May and July diurnally integrated discrimination, with May integrals about twice as large as July integrated values. This was caused by overall lower fluxes in July due to lower temperature and humidity compared to May, with the effect of less enriched leaf water outweighing the effect of lower internal CO₂ gradients.

For diurnal integrals of ¹⁸O discrimination, the extreme dawn and dusk values found in our study are not the main determinants for the overall value as they are weighted by correspondingly low assimilation values. However, they suggest that the non steady state approach is required to predict evaporating site enrichment. Firstly, high evening values point to leaf water δ¹⁸O that is more enriched than at steady state. This cannot be explained by mixing with unenriched leaf water fractions, only by slowing down of leaf water turnover as incorporated into the NSS formulation. Secondly, high morning values also require leaf water δ¹⁸O to be more enriched than at steady state. This is because even slightly negative values of δ¹⁸O, as would be predicted assuming ISS, would lead to strongly depleted morning discrimination values that were not observed in this study.

The above arguments indicate that the magnitude of ¹⁸O discrimination at dawn and dusk helps to distinguish between ISS and NSS versions of evaporating site enrichment predictions, that might in turn control the magnitude of diurnal integrals. Therefore, reliable determination of these values is important for examining the validity of isotopic steady state or non steady state assumptions. Unfortunately, the accuracy of ¹⁸Δ predictions at dawn and dusk is limited by their extreme sensitivity to changes in C_l/C_a. A hypothetical change in C_l/C_a by 0.01 from 0.93 to 0.94 (only ≈ 4 ppm) would result in an increase of the predicted ¹⁸Δ value by 20 ‰ (for typical NSS evening leaf water δ¹⁸O of ≈ 5 ‰). If the same change of 0.01 would be from 0.96 to 0.97 instead, the increase of ¹⁸Δ would be even larger at 70 ‰. Such small changes in C_l/C_a could be caused by over- or underestimations of assimilation or transpiration rates of only 10 to 20 %, not unrealistic at times characterised by small gradients of branch bag CO₂ and H₂O mole fractions. In addition, ¹⁸Δ predictions are also more sensitive to changes in the evaporating site leaf water δ¹⁸O at high C_l/C_a. Increasing or decreasing the δ¹⁸O value

of leaf water at the evaporating sites by 5 ‰ would result in a corresponding increase or decrease of predicted $^{18}\Delta$ of 70 or 120 ‰ at C_c/C_a of 0.93 or 0.96. Therefore, $^{18}\Delta$ predictions have to be well constrained at dawn and dusk, and $^{18}\Delta$ measurements at these times contain valuable information even though they have large uncertainties.

Highly enriched morning discrimination values also indicate that needle water $\delta^{18}\text{O}$ does not decline to the depleted levels of source (twig) water during the night. Otherwise, even NSS predicted evaporating site $\delta^{18}\text{O}$ enrichment would start at negative values in the mornings. Support for that also comes from night-time bulk needle water $\delta^{18}\text{O}$ that were consistently at ≈ 8 ‰ (see Figure 4.6) and thus substantially enriched compared to twig water at -8 ‰. It is unclear whether stomata are open or closed during the night – studying leaf diffusive resistances, Grace et al. (1975) concluded that the stomata of Sitka spruce needles are open in the dark at high relative humidity. In our study, there was no detectable water flux from the needles at night (except after dusk in May), and ambient air was water vapour saturated at most times. In the absence of transpiration there should be no further enrichment of evaporating site leaf water. Thus, the $\delta^{18}\text{O}$ values of leaf water at the evaporating sites are assumed to decrease over time as water in needles mixes with water in twigs. This has been documented in previous studies (Cernusak et al. 2002). Depending on mixing time, the isotopic composition of foliage water might even reach that of the (depleted) water source. The exceptionally high night-time bulk water $\delta^{18}\text{O}$ values found in our study suggest a barrier to diffusional mixing between needle and twig water that might be characteristic for coniferous species. Taking the large water holding capacity of coniferous trees into account, and in the absence of water mixing, needle water therefore remained enriched during the night. This also agrees with evaporating site enrichment starting at already higher levels at dawn, as derived with the NSS version, and in discrepancy to depleted values of leaf water $\delta^{18}\text{O}$ at isotopic steady state. Because leaf water turnover depends on transpiration, deviations from steady state enrichment predictions are likely to be more pronounced in species with low transpiration rates such as conifers. For reliable estimation of non steady state enrichment effects, gradients of water $\delta^{18}\text{O}$ values within leaves, and of C_c/C_a it is important to accurately determine transpiration rates.

Photosynthetic ^{18}O discrimination might be overestimated due to incomplete isotopic exchange between CO_2 and leaf water (for equation applying in this case see Farquhar and Lloyd 1993). The exchange reaction is catalysed by the enzyme carbonic

anhydrase, abundant in chloroplasts. Since typical diffusion times of the CO₂ backflux that determines $^{18}\Delta$ are longer than the isotopic equilibration catalysed by carbonic anhydrase, the exchange results in almost instantaneous isotopic equilibrium between CO₂ and the pool of leaf water it exchanges with. The abundance level of carbonic anhydrase determines the degree to which this isotopic exchange is completed (Yakir and Wang 1996). For coniferous trees, the exchange can be assumed to be nearly complete so that equation 4.1 is a good approximation of the full formulation of Farquhar and Lloyd (1993). However, the location of carbonic anhydrase abundance will also determine the site of the isotopic equilibration between CO₂ and leaf water. Farquhar and Lloyd (1993) argued that carbonic anhydrase is limited to the chloroplasts. In this case, the site of isotopic equilibration would be at chloroplast surfaces, and the appropriate parameter for calculation of $^{18}\Delta$ would be $\delta^{18}\text{O}_{\text{CS}}$, isotopic composition of water at the chloroplast surface. $\delta^{18}\text{O}_{\text{CS}}$ could be less enriched than $\delta^{18}\text{O}_{\text{E}}$ of evaporating site water, because it reflects an intermediate point on the variable gradient between depleted source and enriched evaporating site water. In support of this, Yakir et al. (1994) reported chloroplast water 10 ‰ depleted compared to evaporating site water. Harwood et al. (1998) also found indications that chloroplast water was less enriched than evaporating site water. In contrast, Farquhar et al. (1993) found the isotopic signature of chloroplast water to be close to that of evaporating site water.

In this study, $\delta^{18}\text{O}_{\text{CS}}$ was approximated by $\delta^{18}\text{O}_{\text{E}}$, the isotopic composition of evaporating site water. In addition, a few estimates of $\delta^{18}\text{O}_{\text{CS}}$ could be derived from $^{18}\Delta_{\text{obs}}$ and C_c/C_a inferred from $^{13}\Delta_{\text{obs}}$ using equation 4.3. Because the Péclet effect is stronger when transpiration is higher, it should have made most impact at times of high transpiration rates. Although $\delta^{18}\text{O}_{\text{CS}}$ was less enriched than $\delta^{18}\text{O}_{\text{E}}$ (from $\delta^{18}\text{O}_{\text{NSS}}$) at most times, as illustrated in the top panel of Figure 4.9, the offset between the two values did not increase with transpiration rates, shown in the bottom panel of Figure 4.9, as would be expected from theory. Therefore, quantitative correlation between $\delta^{18}\text{O}$ of water at evaporating sites and in chloroplasts cannot be obtained from our data. However, times when the discrepancy caused by using $\delta^{18}\text{O}_{\text{E}}$ instead of $\delta^{18}\text{O}_{\text{CS}}$ would be greatest, corresponding to times with high transpiration rates with leaf water close to isotopic steady state, would mostly coincide with those characterised by low C_c/C_a , i.e. CO₂ backfluxes would be smaller and $^{18}\Delta$ lower as well as relatively less sensitive to changes in leaf water isotopic composition, as discussed above. Clearly, further measurements are needed to establish correlations between the isotopic composition of evaporating

site and chloroplast water under field conditions. This is important with respect to numerical simulations describing processes in natural environments, especially on smaller spatial resolution and shorter time scales.

Flanagan et al. (1997) analysed influences of photosynthesis and respiration on $\delta^{18}\text{O}$ of canopy CO_2 in boreal forest ecosystems. However, $^{18}\Delta$ values were not measured. Instead, $^{18}\Delta$ values were predicted based on the assumption of constant C_c/C_a . As a result of this, their $^{18}\Delta$ predictions exhibited diurnal changes of the opposite pattern to those found in this study. Observations of this study thus strongly emphasize the importance of taking into account diurnal variations in C_c/C_a for accurate predictions of photosynthetic ^{18}O discrimination.

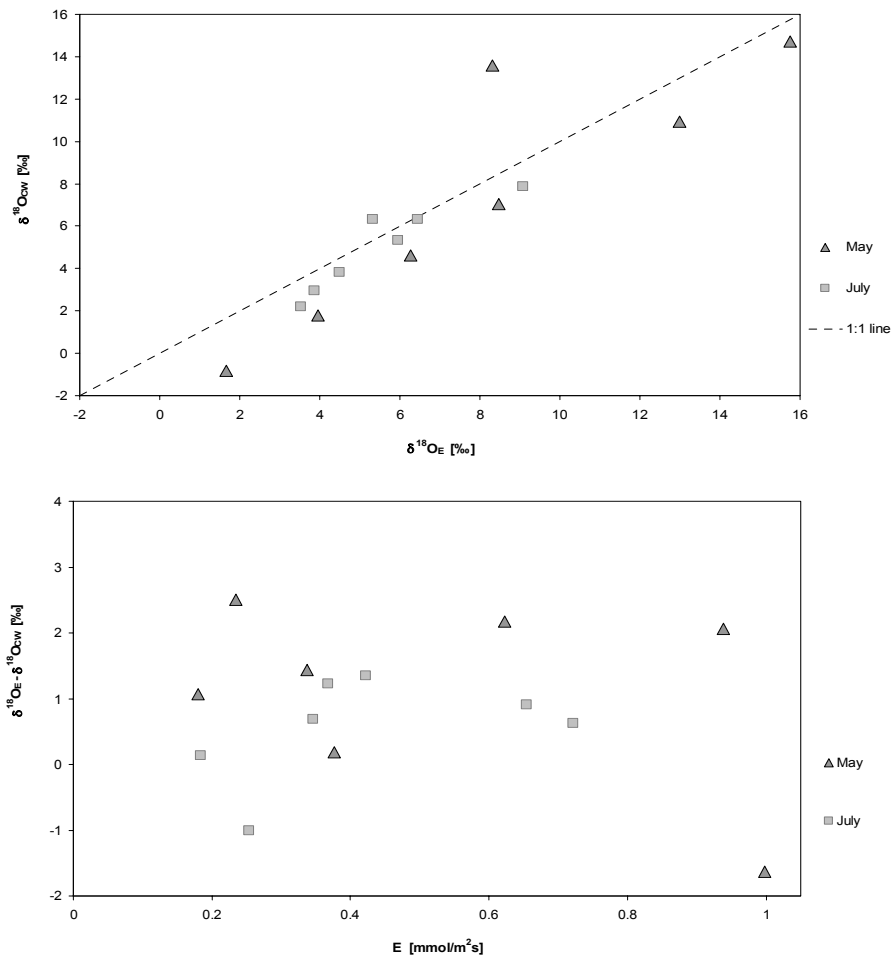


Figure 4.9: Comparison of isotopic composition of water at the evaporating sites, $\delta^{18}\text{O}_E$, and in chloroplasts, $\delta^{18}\text{O}_{CW}$ (top), and difference between the two versus transpiration rate, E (bottom).

4.2 $\delta^{18}\text{O}$ of CO_2 from foliage and soil respiration

Introduction

This section focuses on the role of respiration in determining the $\delta^{18}\text{O}$ signature of canopy CO_2 . To a large degree, $\delta^{18}\text{O}$ of CO_2 released in soil or nocturnal foliage respiration should reflect that of liquid water present at locations of its origin because of ^{18}O exchange between CO_2 and water (Hesterberg and Siegenthaler 1991). Analogous to isotope discrimination during photosynthesis, this is again the most important difference between carbon and oxygen isotopic signatures of CO_2 in canopy gas exchange. While respiratory CO_2 fluxes in most ecosystems have similar carbon isotope ratios, making it difficult to separate their contributions based on $\delta^{13}\text{C}$ signatures (see section 3.2), the same fluxes can have very distinct oxygen isotope ratios. Usually, soil CO_2 fluxes are strongly depleted in ^{18}O with respect to canopy CO_2 , resulting in depleted $\delta^{18}\text{O}$ values at higher CO_2 mole fractions similar to $\delta^{13}\text{C}$, especially towards the forest floor.

At night, generally there is little turbulent mixing, and the $\delta^{18}\text{O}$ signature of CO_2 in the canopy will be mainly determined by rates of foliage, root and soil respiration, $\delta^{18}\text{O}$ of water pools that CO_2 equilibrates with, and relative impacts of diffusional fractionation versus equilibration of soil CO_2 fluxes. Therefore, measurements of $\delta^{18}\text{O}$ of canopy CO_2 can in principle constrain component fluxes at the ecosystem scale. Several recent studies have used the oxygen isotope ratio of CO_2 in canopy air to distinguish between respiratory contributions from foliage and soil respiration (Wang and Yakir 2000, Flanagan et al. 1997, Mortazavi and Chanton 2002). In this study, the $\delta^{18}\text{O}$ signatures of foliage and soil respired CO_2 were estimated from measurements of isotopic gas exchange during September 2000, May and July 2001. In the following, diurnal and seasonal variations of $\delta^{18}\text{O}$ of foliage, soil and ecosystem respiration are presented and compared to $\delta^{18}\text{O}$ of bulk water extracted from concurrently collected foliage and soil samples, thought to represent the main determinant of $\delta^{18}\text{O}$ of CO_2 fluxes. Briefly, the problems encountered when trying to directly measure the $\delta^{18}\text{O}$ signal of CO_2 released by Sitka spruce foliage during the night are described.

Theory

The most important factor determining the oxygen isotopic composition of soil CO₂ fluxes is the δ¹⁸O of soil water that it equilibrates with (Stern et al. 1999). Soil water carries mostly depleted average δ¹⁸O signatures of local precipitation. Evaporation of water from the soil surface can lead to ¹⁸O enrichment of water in shallow compared to deeper layers of soils, potentially also diminishing offsets between δ¹⁸O of soil fluxes and those of canopy CO₂. In full isotopic equilibrium, the δ¹⁸O of CO₂ fluxes from soils will be depleted by ≈ 8.8 ‰ (Hesterberg and Siegenthaler 1991) compared to the δ¹⁸O of soil CO₂ due to slower diffusion of molecules containing the heavier oxygen isotope. Fractionation during diffusion in soils also increases δ¹³C of soil CO₂, but in steady state, CO₂ leaving soil has the same δ¹³C as CO₂ produced in soil (see section 3.2). For oxygen, the situation is different because δ¹⁸O of soil CO₂ is constantly re-equilibrated with soil water. Therefore, δ¹⁸O of CO₂ leaving the soil can be very different from that of CO₂ produced in soil.

Another feature unique to the δ¹⁸O signature of soil CO₂ exchange is that there can be a change in δ¹⁸O of the soil CO₂ flux without associated net CO₂ flux, caused by invasion of atmospheric CO₂ into the soil where it equilibrates with soil water, followed by backdiffusion into the atmosphere above (Tans 1998). As a consequence, δ¹⁸O values and the (inverse of) the CO₂ mole fraction are no longer linearly correlated. Instead, they will follow a relationship with increasing curvature for increasing rate of invasion (exchange) to respiration flux. Therefore, neglecting atmospheric invasion in mass balance approaches (and Keeling plots) will lead to errors in the derived isotopic signature of the source. Following Tans (1998), the apparent source signature including this error can be expressed as:

$$\delta^{18}O_A = \delta^{18}O_{source} + \beta(\delta^{18}O_{eq} - \delta^{18}O_{atm}) \quad (4.12)$$

where δ¹⁸O_A and δ¹⁸O_{source} are apparent and true source signatures of CO₂ flux from soil, δ¹⁸O_{eq} is soil water isotopic composition that CO₂ flux (δ¹⁸O_{source}) is in equilibrium with and δ¹⁸O_{atm} is isotopic composition of atmospheric CO₂, and β is the ratio of exchange to respiration flux of CO₂. With diffusional fractionation factor d (δ¹⁸O_{source} = δ¹⁸O_{eq} - d), the above equation can be modified to estimate δ¹⁸O_{eq}:

$$\delta^{18}O_{eq} = \frac{\delta^{18}O_A + d + \beta\delta^{18}O_{atm}}{1 + \beta} \quad (4.13)$$

The ratio of exchange to respiration, β , can be calculated from P and R_s ($\mu\text{mol}/\text{m}^2/\text{s}$), the invasion flux and soil respiration rates ($\beta = P / R_s$). The flux rate of atmospheric invasion, P , can be expressed as (Tans 1998):

$$P = \sqrt{\varepsilon_a B \varepsilon_w k_H \kappa D_{18-air} M C} \quad (4.14)$$

where the square root corresponds to a piston velocity (cm/s or m/day) of soil-air exchange, and ε_a (0.2) and ε_w (0.3) are fractions of total soil volume occupied by air and water filled pores, respectively. D_{18-air} (0.14 cm^2/s) is molecular diffusivity of $\text{C}^{18}\text{O}^{16}\text{O}$ in free air, while κ , the tortuosity factor (2/3), accounts for the fact that the path in soil air is often blocked by soil particles. The Bunsen solubility coefficient, B , can be calculated from: $B = 1.739 \exp(-0.039 T + 0.000236 T^2)$, and k_H , the rate of hydration of CO_2 , from: $k_H = 0.037 \exp(0.118(T - 25))$, where T is soil temperature in $^{\circ}\text{C}$ (all values and temperature regressions from Tans 1998 and references therein). M (mol/m^3) is air pressure and temperature dependent volumetric air density and C ($\mu\text{mol}/\text{mol}$) is the CO_2 mole fraction of ambient air.

Results

$\delta^{18}\text{O}$ of foliage respiration during the night

Figure 4.10 shows $\delta^{18}\text{O}_{\text{CO}_2}$ of CO_2 against the inverse of CO_2 mole fractions ("Keeling plot", equation 2.9) from open and closed air samples collected in the top branch bags at night, during September 2000 and May and July 2001. The apparent isotopic signature of foliage respiration was obtained from intercepts of geometric mean regressions, yielding $\delta^{18}\text{O}$ values of 9.5 ± 4.7 ‰ (Sep), 148 ± 33 ‰ (May) and 106 ± 29 ‰ (July). The September value, translated into $\delta^{18}\text{O}_{\text{H}_2\text{O}}$ of water (6.9 ± 2.1 ‰) was in reasonable agreement with that of water extracted from bulk foliage samples at night (4.3 ± 0.7 ‰). However, May and July $\delta^{18}\text{O}$ values were much higher than could be explained by a source of respired CO_2 with $\delta^{18}\text{O}$ of foliage water (7.9 ± 0.3 ‰ in May).

Figure 4.11 illustrates that these apparently extremely high values for $\delta^{18}\text{O}$ signature of the respiratory source were not confined to the Keeling plot approach. The few mass balances (equation 2.8) of foliage dark respiration that could be calculated also yielded highly elevated $\delta^{18}\text{O}$ values of respiration sources, 89 and 191 ‰ in May, and 44, 323, and 350 ‰ in July. In September, one value was also high, 29 ‰. In contrast, the other value was depleted, -18 ‰. Except for this depleted value, $\delta^{18}\text{O}$ sources from mass balances sharply decreased between respiration rates of 0.17 and 0.5 $\mu\text{mol}/\text{m}^2/\text{s}$.

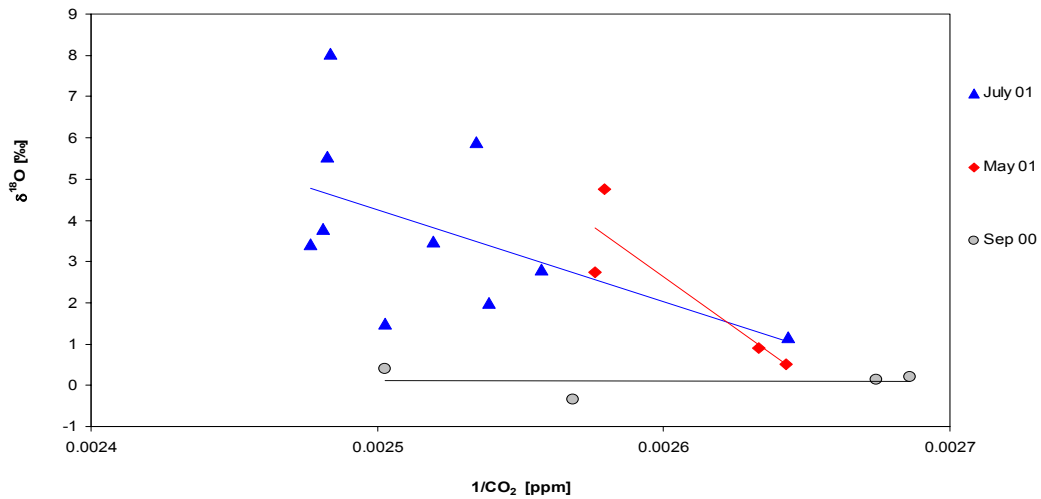


Figure 4.10: $\delta^{18}\text{O}_{\text{CO}_2}$ against inverse of CO_2 mole fractions ("Keeling plot") of all air samples collected at night from top branch bag in September 2000 and May and July 2001.

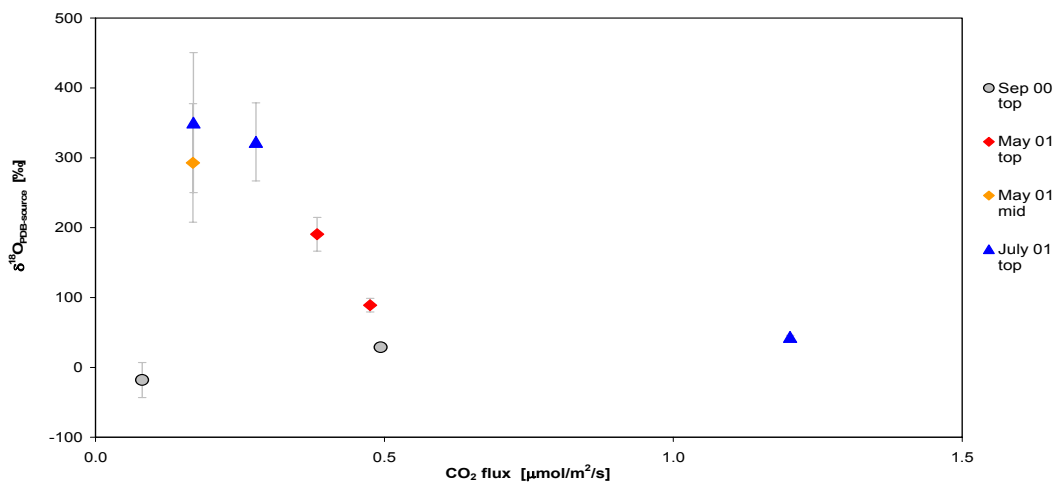


Figure 4.11: $\delta^{18}\text{O}_{\text{CO}_2}$ of source versus rate of foliage respiration, obtained from sample pairs of top and mid branch bag air in September 2000 and May and July 2001. Error bars indicate standard deviations of data.

$\delta^{18}\text{O}$ of soil respiration

Analogous to $\delta^{13}\text{C}$, Keeling plots were constructed from CO_2 mole fractions and oxygen isotopic composition of air samples of open and closed soil chambers. Figure 4.12 shows Keeling plots for two soil chambers, soil 1 and soil 2. $\delta^{18}\text{O}_{\text{CO}_2}$ signatures of soil respired CO_2 were obtained from regression intercepts (independent x and y axes). $\delta^{18}\text{O}_{\text{H}_2\text{O}}$ of soil water was estimated from $\delta^{18}\text{O}_{\text{CO}_2}$ assuming a fractionation of 8.8 ‰ during diffusion and CO_2 in full isotopic equilibrium with water. This yielded $\delta^{18}\text{O}_{\text{H}_2\text{O}}$ values of -14.5 ± 5.8 ‰ (soil 1) and -14.6 ± 5.2 ‰ (soil 2) in September, -9.9 ± 2.0 ‰ (soil 1) and -11.2 ± 2.7 ‰ (soil 2) in May, -20.4 ± 5.0 ‰ (soil 1) and -23.1 ± 4.1 ‰ (soil 2) in July. Correlation coefficients (R) were > 0.8 in May and > 0.6 in July, but only 0.14 and 0.4 in September.

$\delta^{18}\text{O}_{\text{CO}_2}$ of soil respiration versus soil respiration rate are shown in Figure 4.13. The top panel shows data derived assuming no atmospheric invasion ($\beta = 0$), the bottom panel shows data where atmospheric invasion was calculated from soil temperature, CO_2 mole fractions and respiration rates (variable β). For the $\beta = 0$ version, there was a positive correlation between respiration rate and $\delta^{18}\text{O}_{\text{CO}_2}$ of soil respiration in September and May, with less depleted $\delta^{18}\text{O}_{\text{CO}_2}$ at higher respiration rates. September and May

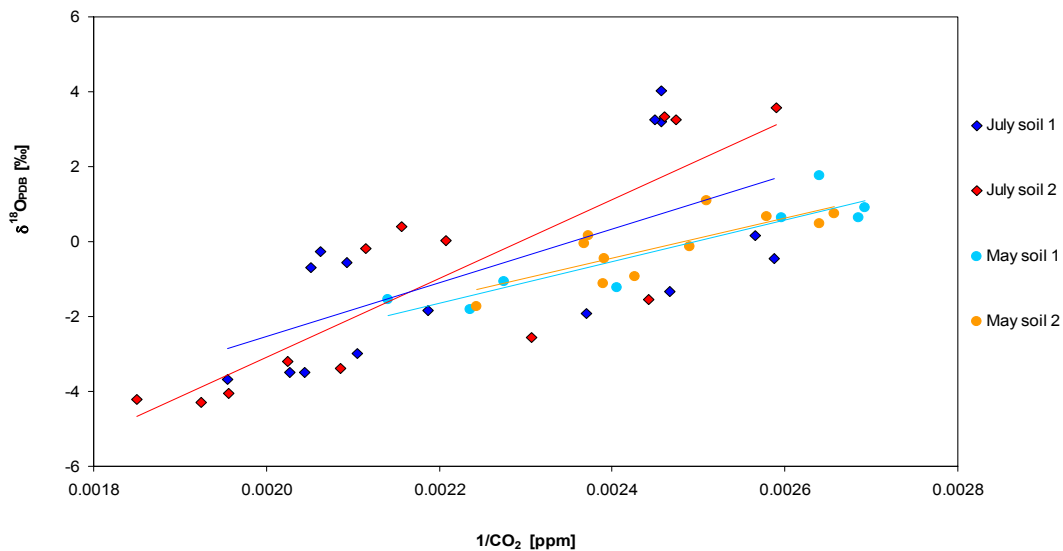


Figure 4.12: $\delta^{18}\text{O}_{\text{CO}_2}$ against the inverse of CO_2 mole fractions ("Keeling plot") from open and closed soil air samples collected in Sep 2000, May and July 2001.

$\delta^{18}\text{O}_{\text{CO}_2}$ values were about 5 ‰ higher at respiration rates above 2.5 $\mu\text{mol}/\text{m}^2/\text{s}$ (-13 ‰) than at respiration rates between 1 and 2 $\mu\text{mol}/\text{m}^2/\text{s}$ (-18 ‰). There was no clear trend of $\delta^{18}\text{O}_{\text{CO}_2}$ with respiration rate for July data. Some values at higher respiration rates between 3 and 4 $\mu\text{mol}/\text{m}^2/\text{s}$ were in the same range as September and May data (-13 ‰), whereas more strongly depleted $\delta^{18}\text{O}_{\text{CO}_2}$ values (-22 ‰) were found at only slightly lower respiration rates between 2.5 and 3.5 $\mu\text{mol}/\text{m}^2/\text{s}$.

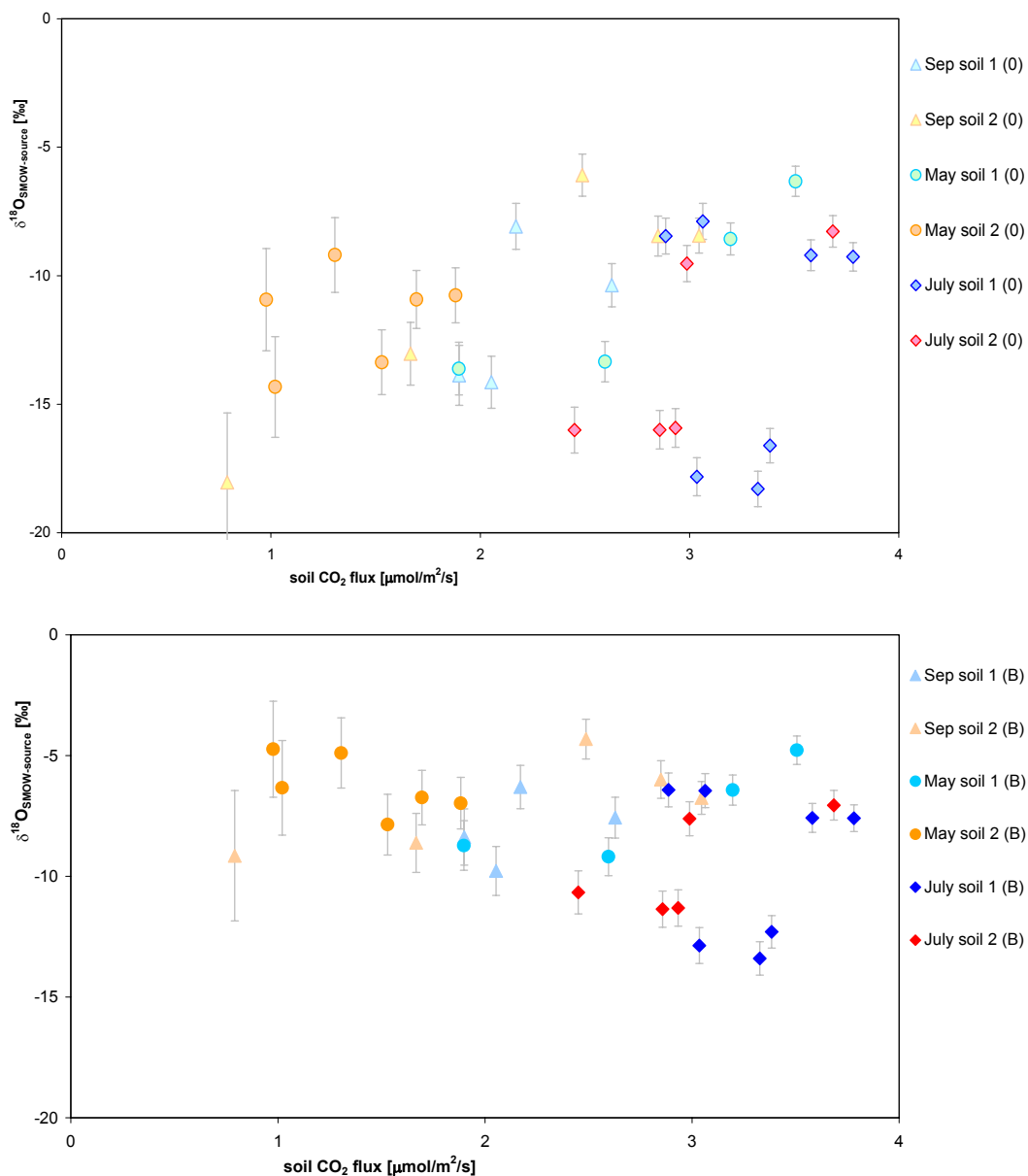


Figure 4.13: $\delta^{18}\text{O}_{\text{H}_2\text{O}}$ of source versus rate of soil respiration for Sep 2000, May and July 2001, top panel: for $\beta = 0$, bottom panel: for variable β .

The piston velocity was between 5.0 and 5.6 m/day. Diffusion was assumed to have a fractionation factor of 8.8 ‰. The temperature and CO₂ mole fraction dependent invasion exchange flux was in the order of $1.0 \pm 0.1 \mu\text{mol}/\text{m}^2/\text{s}$. With constant invasion flux, the ratio of invasion to respiration flux, β , was inversely correlated to respiration rate. β ranged from 0.3 at high rates to 1.4 at low rates of respiration. Thus, correlation of $\delta^{18}\text{O}_{\text{CO}_2}$ data with respiration rate effectively disappeared in the variable β version. Most $\delta^{18}\text{O}_{\text{CO}_2}$ values were within a range of -5 to -10 ‰ across all respiration rates, although a few July values were more depleted than that (-13 ‰). Generally, $\delta^{18}\text{O}_{\text{CO}_2}$ values with variable invasion flux rates were 3 to 4 ‰ higher than those assuming no atmospheric invasion.

Figure 4.14 shows diurnal cycles of soil water $\delta^{18}\text{O}_{\text{H}_2\text{O}}$ values estimated from isotopic mass balances of soil respiration, for $\beta = 0$ and for variable β , in September 2000, May and July 2001. There were no pronounced seasonal differences in $\delta^{18}\text{O}_{\text{H}_2\text{O}}$ values inferred from soil respiration. For the $\beta = 0$ version, soil water $\delta^{18}\text{O}_{\text{H}_2\text{O}}$ values increased in both chambers by about 10 ‰ over the day, from ≈ -17 ‰ in early morning to ≈ -7 ‰ in the afternoon. Taking atmospheric invasion into account almost completely removed diurnal changes, because night times were characterised by high β (0.8 to 1.4), whereas β was smaller during the day (0.3 to 0.5) at higher respiration rates. More depleted values (-13 ‰) at night were found in July. Day-time values were about -8 ‰ in all months. Average soil $\delta^{18}\text{O}_{\text{H}_2\text{O}}$ values taking atmospheric invasion into account were -7.4 ± 1.7 ‰ in September, -6.7 ± 1.6 ‰ in May and -9.5 ± 3.2 ‰ in July.

Variable β data is presented again in Figure 4.15, with the addition of $\delta^{18}\text{O}_{\text{H}_2\text{O}}$ of water extracted from bulk soil and twig samples collected in September and May. Diurnal changes in bulk soil $\delta^{18}\text{O}_{\text{H}_2\text{O}}$ values (3 to 6 ‰) were in the same order as those inferred from isotopic mass balance of soil respiration (5 ‰), with maximal values of ≈ -2 ‰ between 9:00 and 12:00 and minimum values of around -8 ‰ at 19:00. $\delta^{18}\text{O}_{\text{H}_2\text{O}}$ of twig water samples increased gradually by 4.5 ‰ over the course of the day. Twig water $\delta^{18}\text{O}_{\text{H}_2\text{O}}$ was more depleted than that of soil water until noon, reaching values in the range of soil water $\delta^{18}\text{O}_{\text{H}_2\text{O}}$ at around 16:00. Between 6:00 and 18:00, $\delta^{18}\text{O}_{\text{H}_2\text{O}}$ inferred from soil respiration was in good agreement with twig water values, and between 15:00 and 18:00 with soil water values, as well. Until around 6:00, values inferred from soil respiration were about 5 ‰ depleted with respect to soil water $\delta^{18}\text{O}_{\text{H}_2\text{O}}$.

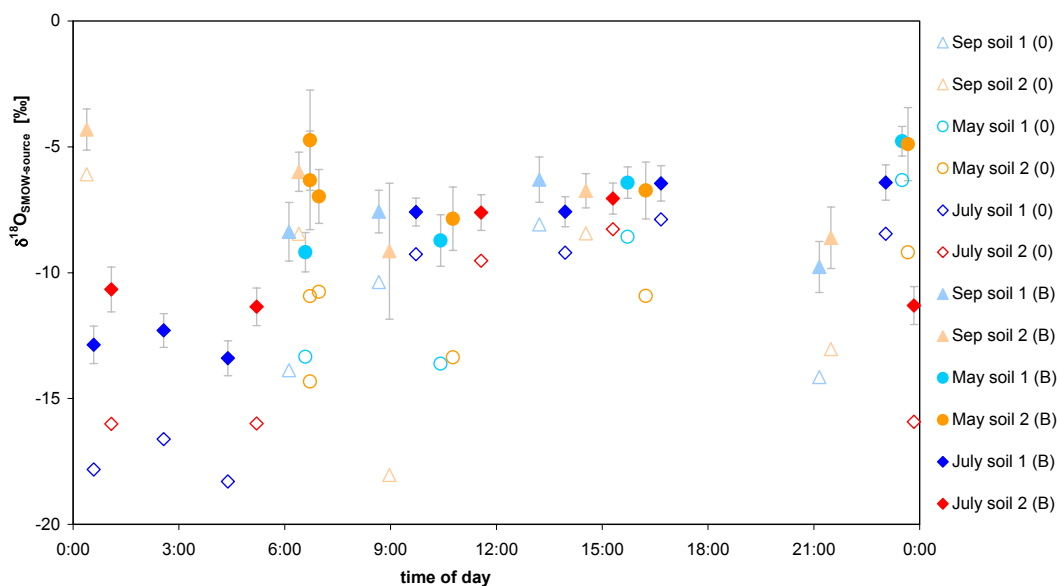


Figure 4.14: Diurnal cycle of $\delta^{18}\text{O}_{\text{H}_2\text{O}}$ of soil water inferred from $\delta^{18}\text{O}_{\text{CO}_2}$ of soil respiration source for Sep 2000, May and July 2001, for $\beta = 0$ and variable β , assuming diffusional fractionation of 8.8 ‰.

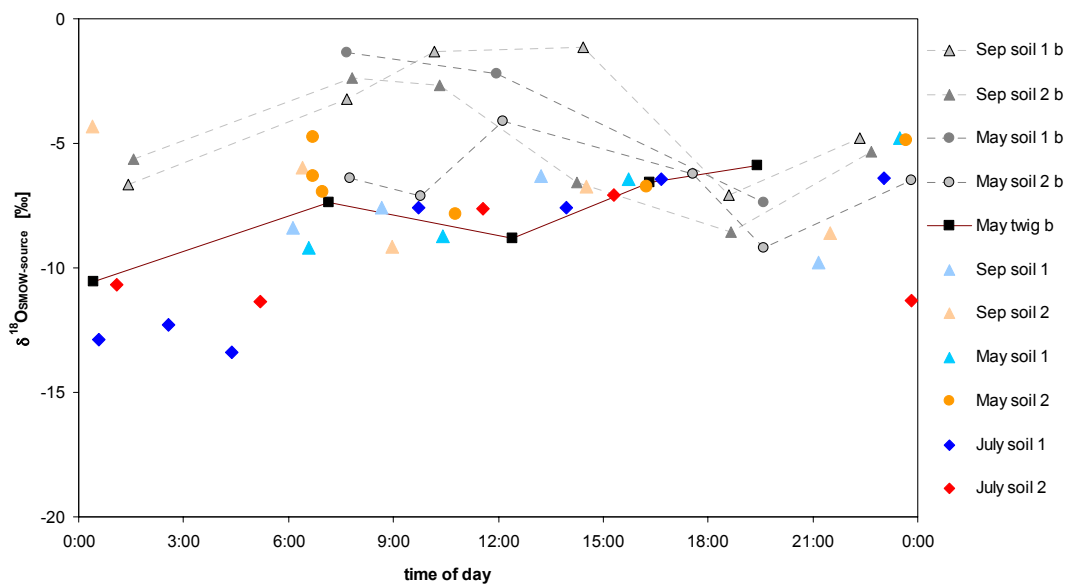


Figure 4.15: Diurnal cycle of $\delta^{18}\text{O}_{\text{H}_2\text{O}}$ from soil chamber gas exchange and of bulk water $\delta^{18}\text{O}_{\text{H}_2\text{O}}$ from soil and twig samples in Sep 2000, May and July 2001 (variable β).

$\delta^{18}\text{O}$ of ecosystem respiration

Figure 4.16 shows $\delta^{18}\text{O}_{\text{CO}_2}$ against the inverse of CO_2 mole fractions ("Keeling plot") for September, May and July, combining all air samples collected from open branch bags and soil chambers at night. Average $\delta^{18}\text{O}_{\text{CO}_2}$ values for each month increased from September to May to July. On average, September data was within the range expected for canopy $\delta^{18}\text{O}_{\text{CO}_2}$ values ($< 0\text{‰}$), May values were slightly elevated compared to that, but most July values were substantially higher, between 3 and 4 ‰. Obviously, $\delta^{18}\text{O}_{\text{CO}_2}$ and CO_2 mole fractions were not correlated. Hence, regressions ("Keeling plots") could not be used to estimate isotopic signatures of ecosystem respiration integrated throughout the canopy.

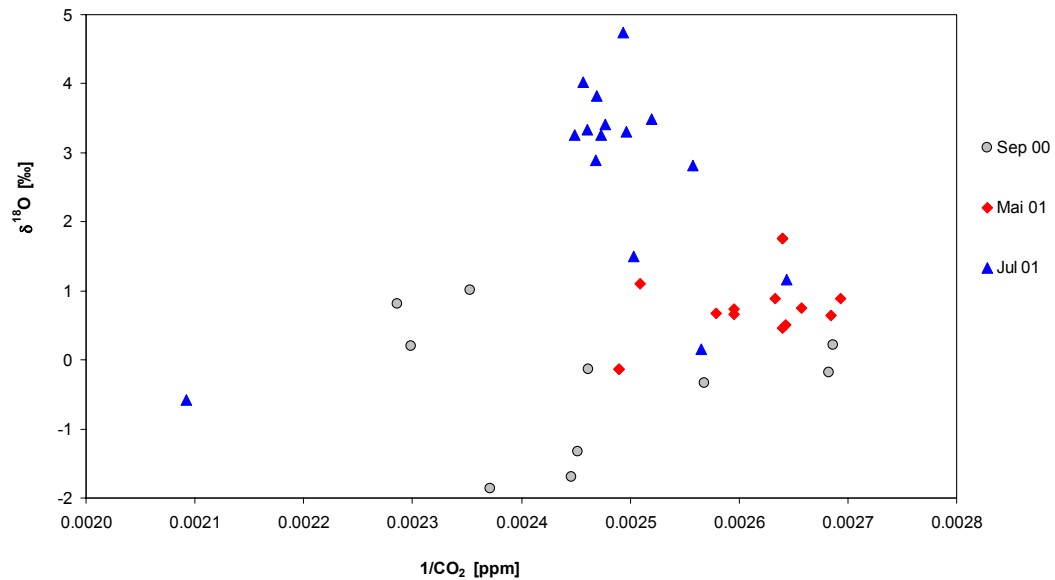


Figure 4.16: Isotopic composition versus $1/\text{CO}_2$ ("Keeling plot") from nocturnal samples of open branch bag and soil chamber air collected in September 2000, and May and July 2001.

Discussion

It is very unlikely that the extremely high source $\delta^{18}\text{O}$ values inferred from branch bag measurements at night were caused by simple equilibration of CO_2 with foliage water. This would have required unrealistic magnitudes of enrichment (30 to 350 ‰). Note that a similar phenomenon was observed for tobacco leaves at night in a laboratory gas exchange system (J. Lloyd, personal communication).

Subsequently, different hypotheses for explanation of these values were formulated: CO_2 could have equilibrated with foliage water by diffusing into and back out of stomata without an associated net flux, resulting in overestimation of source $\delta^{18}\text{O}$, analogous to atmospheric invasion in soils. Such an effect would ultimately depend on the abundance level of carbonic anhydrase, the enzyme that is catalysing the isotopic exchange, in water at the stomatal surfaces. Spatial limits of carbonic anhydrase have not been determined directly yet, but experiments indicated that activity of this enzyme is limited to chloroplasts (Gillon and Yakir 2000). In this case, diffusion probably would not have brought enough CO_2 in contact with water at chloroplast surfaces within the given time, especially against CO_2 gradients from respiratory CO_2 release. CO_2 could also have equilibrated with condensed water on insides of branch bag surfaces. This might lead to an apparent source $\delta^{18}\text{O}$ signature that would be intermediate of foliage and condensed water as CO_2 added by respiration would undergo this additional isotopic exchange. But it would not explain the effect in question, because CO_2 in branch bag air would be in equilibrium with condensed water, not causing differences between open and closed samples. In addition, the isotopic signature of condensed water would probably be depleted compared to that of foliage water, resulting in apparently lower source $\delta^{18}\text{O}$ signatures.

On the other hand, it could have also been some molecule other than $^{12}\text{C}^{18}\text{O}^{16}\text{O}$. It is well documented that plants produce and emit a huge variety of molecules such as biogenic volatile organic compounds (BVOC's) (for example, Kesselmeier 2001, Geron et al. 2000, Helmig et al. 1999). One of these studies specifically examined BVOC emissions from Sitka spruce trees (Street et al. 1996). Search for candidate molecules was constrained by several requirements Suspected compounds should have mass 46 or produce fragments of mass 46 when split in the ion source of the mass spectrometer. The latter is complicated by the fact that sensitivity of detection cups can be compound

specific, so the same voltage does not necessarily translate to the same number of molecules (W. Brand, personal communication). Compounds should not produce fragments of mass 45 (or 44) at substantial amounts as this would also affect $\delta^{13}\text{C}$ values. Compounds would also have to be emitted from foliage but not from soil, because this phenomenon did not occur in soil measurements. Compounds should be present at night, but not during the day, as would have been evident in measurements of photosynthetic ^{18}O discrimination. This might indicate that the responsible compounds would be removed by photochemical reactions in the light (and also applies to emissions from bag material). Compounds should not react with magnesium perchlorate (used as desiccant for air samples) and should not be water soluble. Compounds or fragments should have a freezing point range of -70 to -196 °C, otherwise they would be separated from the sample gas in the laboratory procedure (Werner et al. 2001).

For known BVOC's emitted by plants, no fragment of mass 46 has been identified (Lamb et al. 1999). In addition, BVOC emissions are usually very low at night (Pio et al. 2001, Apel et al. 2002). Several compounds with mass 46, NO_2 (Hargreaves et al. 2000, Sparks et al. 2001), formic acid (Sauer et al. 2001, Glasius et al. 2000, Glasius et al. 2001), dimethylether, wood ester and ethanol, could be excluded for one or several of the above reasons. Most of them, and compounds containing fragments of mass 46 were found to also produce equal or higher amounts of mass 45 fragments.

In contrast, many sulphur compounds produce fragments of mass 46 but not of mass 45. A data base search listed more than 7000 different sulphur compounds with this specification. However, presence or absence of specific compounds could not be verified without analysis of affected air samples. Unfortunately, flasks containing original air samples were not available after completion of laboratory analyses. Thus, the hypotheses listed above could not be tested and the mysterious nocturnal flux could not be identified.

Generally stronger depleted twig than soil water $\delta^{18}\text{O}_{\text{H}_2\text{O}}$ could indicate that twig water originated from deeper layers below the soil surface. In this case, twig water $\delta^{18}\text{O}_{\text{H}_2\text{O}}$ should be approximately constant over time, and not be affected by evaporative enrichment like water in surface soil layers. Twig water $\delta^{18}\text{O}_{\text{H}_2\text{O}}$ values were less variable than those of soil water, but increased slightly over the course of the day. This could have been caused by gradual enrichment of water in twigs, for example due to mixing with enriched foliage water fractions. It could also reflect gradients in $\delta^{18}\text{O}_{\text{H}_2\text{O}}$

values between the soil layers due to the natural variability of the $\delta^{18}\text{O}$ composition of water from different precipitation events. On the other hand, differences within and between soil and twig water $\delta^{18}\text{O}_{\text{H}_2\text{O}}$ values and those inferred from soil respiration measurements could have originated from the fact that soil and twig samples were collected from different and varying locations and not from those of gas exchange measurements (soil chambers).

Because soil (and ground) water pools are supplied by precipitation, seasonality in $\delta^{18}\text{O}_{\text{H}_2\text{O}}$ of precipitation can cause seasonal variations of soil water $\delta^{18}\text{O}_{\text{H}_2\text{O}}$, damped by mixing with larger soil water pools. Thus, absence of strong seasonal changes of $\delta^{18}\text{O}_{\text{H}_2\text{O}}$ in soil respiration and bulk water data indicates that $\delta^{18}\text{O}_{\text{H}_2\text{O}}$ of precipitation was largely constant during the respective months. In support of this, modelled $\delta^{18}\text{O}_{\text{H}_2\text{O}}$ values in the surface layer of the corresponding grid cell (57.5°N , 3.75°W , $3.75^\circ \times 3.75^\circ$) of the ECHAM4 general circulation model did not vary greatly over respective time periods (M. Werner, personal communication). $\delta^{18}\text{O}_{\text{H}_2\text{O}}$ of precipitation decreased from -6.0‰ in September to -7.0‰ in May and increased to -6.3‰ in July. Modelled $\delta^{18}\text{O}_{\text{H}_2\text{O}}$ of soil water increased from -7.5‰ in September to -7.2‰ in May to -6.7‰ in July. Both parameters had minimum values of -8.8‰ in winter. Precipitation had maximum $\delta^{18}\text{O}_{\text{H}_2\text{O}}$ values in August (-5.9‰), whereas soil maximum $\delta^{18}\text{O}_{\text{H}_2\text{O}}$ was lower (-6.5‰) and occurred later in the year (October), indicating that mixing of new precipitation with the soil water pool will not only dampen the seasonal cycle of soil water $\delta^{18}\text{O}_{\text{H}_2\text{O}}$ but also shift its phase.

The seasonal trend found in bulk soil water $\delta^{18}\text{O}_{\text{H}_2\text{O}}$ data (1.3‰ average decrease from Sep to May) presented here is in reasonably good agreement with model predictions (0.8‰ Sep to May decrease). The average $\delta^{18}\text{O}_{\text{H}_2\text{O}}$ values calculated from mass balances corrected for the atmospheric invasion flux were in good agreement with the soil $\delta^{18}\text{O}_{\text{H}_2\text{O}}$ values from the model. They also had a similar seasonal change (2‰ decrease from September to July). Regressions ("Keeling plots") not taking atmospheric invasion into account yielded more negative $\delta^{18}\text{O}_{\text{H}_2\text{O}}$ values, about 8‰ depleted with respect to modelled soil $\delta^{18}\text{O}_{\text{H}_2\text{O}}$, and stronger seasonal changes (7‰ decrease from September to July). However, the pronounced diurnal variations of $\delta^{18}\text{O}_{\text{H}_2\text{O}}$ found in soil flux measurements due to variable impacts of invasion fluxes with respect to soil respiration fluxes, as well as in bulk source water values, indicate that the "Keeling plot" approach cannot be applied to estimate $\delta^{18}\text{O}$ of soil respired CO_2 , because the

prerequisite of a constant isotopic composition of the source is not fulfilled. Furthermore, the full isotopic equilibrium between CO₂ and soil water might not be established. In this case, the fractionation factor of 8.8 ‰ would not be applicable for CO₂ diffusion out of the soil. However, such an effect could not be examined here because the necessary direct comparison between the δ¹⁸O signatures of the soil water and the equilibrated CO₂ flux was not available.

The data presented here underlines the importance of taking variable ratios of amount of exchanged CO₂ to amount of respired CO₂ into account, when studying impacts of soil respiration on δ¹⁸O_{CO₂} of atmospheric CO₂ (Tans 1998). This is supported by finding no correlation between rate and δ¹⁸O_{CO₂} of soil respiration data when corrected for impact of atmospheric invasion (in contrast to positive correlation with uncorrected data), because analytical analysis by Stern et al. (1999) established that respiration rate has only a minor effect on δ¹⁸O_{CO₂} of soil CO₂. Therefore, correcting the apparent source signature of δ¹⁸O_{CO₂} for influence of atmospheric invasion was necessary in order to compare respiration inferred δ¹⁸O_{H₂O} values of soil water to those of bulk soil water samples. Furthermore, variable impacts of atmospheric invasion fluxes are required to estimate the appropriate δ¹⁸O_{CO₂} signatures of soil CO₂ exchange fluxes. The ratios of invasion to respiration fluxes (β) are higher at night (≈ 0.9) because of smaller respiration rates at lower nocturnal temperatures, while ratios are lower during the day (≈ 0.4). Thus, diurnally variable apparent source δ¹⁸O_{CO₂} signatures, scaled by net soil respiration rates, can be used to describe the isotopic signature of total soil CO₂ exchange in ecosystem scale studies. This procedure will be followed in section 7.3 to estimate the diurnal variations in the δ¹⁸O_{CO₂} signature of CO₂ released from the soil for the integration of canopy exchange fluxes.

δ¹⁸O_{CO₂} values of integrated nocturnal ecosystem respiration did not decrease with CO₂ mole fractions (increase with 1/CO₂) as would be expected from addition of isotopically depleted CO₂ by, at least, soil respiration (foliage respiration might release CO₂ enriched in ¹⁸O, but usually at lower flux rates). Instead, δ¹⁸O_{CO₂} showed an average increase from September to May to July, with slightly elevated May and highly elevated July values (3 to 4 ‰). Such high night-time canopy δ¹⁸O_{CO₂} values are not plausible, even allowing for enriched foliage respiration. They must have been caused by the same effect responsible for high apparent foliage respiration δ¹⁸O_{H₂O} signatures. As argued for foliage respiration, it is likely that these enriched values do not represent

actual $\delta^{18}\text{O}$ signatures but instead some other, yet unidentified, molecule with mass 46. Therefore, $\delta^{18}\text{O}_{\text{CO}_2}$ values of overall ecosystem respiration could not be estimated in this study.

5. Stoichiometric ratio of O₂ : CO₂ exchange

Introduction

Both O₂ and CO₂ are exchanged during photosynthesis and respiration in the terrestrial biosphere. Thus, the biological productivity of terrestrial ecosystems influences the distribution of atmospheric O₂ as well as that of CO₂. On short time scales, variations in atmospheric O₂ concentrations result from terrestrial and oceanic photosynthesis and respiration, thermal ingassing and outgassing of O₂ in ocean water and combustion of fossil fuels and biomass. For most of these processes, O₂ exchange is anticorrelated with CO₂ exchange. The stoichiometric ratios of inverse O₂ and CO₂ exchange depend on the elemental composition and the reduction state of organic material. Fossil fuel combustion consumes O₂ and produces CO₂ with an O₂ : CO₂ exchange ratio varying from about 1.1 for coal to 2.0 for methane, with an utilisation weighted global average ratio of 1.38 (Keeling 1988a). Photosynthetic and respiratory fluxes from the terrestrial biosphere are assumed to have an O₂ : CO₂ exchange ratio of about 1.1 (Severinghaus 1995). Sources and sinks of CO₂ are thus stoichiometrically coupled to sources and sinks of O₂. The exception to this is the exchange with the ocean, proceeding through reaction of dissolved CO₂ with bicarbonate and carbonate, which does not affect O₂. Therefore, combined measurements of atmospheric CO₂ and O₂ mixing ratios give information on carbon fluxes that cannot be obtained from CO₂ measurements alone.

The distribution of O₂ in the atmosphere thus can be used as a tracer for studying the natural carbon cycle and its anthropogenic disturbances (Keeling 1988b). The magnitude and spatial distribution of net carbon storage in terrestrial ecosystems can be determined from measurements of the interhemispheric concentration gradient and the depletion rates of atmospheric O₂ in the atmosphere (Keeling et al. 1993). For example, the decrease in the mean atmospheric O₂ concentration averaged over 1990 – 1997 (15.6 ± 0.9 permeg/y in $\delta(\text{O}_2/\text{N}_2)$ ratio) was less than would be expected from fossil fuel combustion. This implies that the terrestrial biosphere has taken up about 1.5 ± 0.8 GtC/y over that time period (Heimann 2001).

The value for the stoichiometric ratio of O₂ and CO₂ exchange with the terrestrial biosphere needs to be well established to take advantage of measurements of the

distribution of atmospheric O₂ on the global scale. Furthermore, measuring the stoichiometric ratio of O₂ : CO₂ exchange allows to calculate O₂ fluxes from CO₂ fluxes on the ecosystem scale. In this study, stoichiometric ratios were obtained for O₂ : CO₂ exchange during photosynthesis in branch bags and during respiration in soil chambers. The observed CO₂ fluxes were then translated into O₂ flux rates at the canopy scale using the stoichiometric O₂ : CO₂ ratios of the separate processes. Subsequently, the O₂ fluxes were used in section 8 to determine the integrated exchange of δ¹⁸O of O₂ in canopy air.

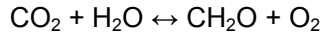
Data collected during two other field campaigns were included in the analysis presented here to increase the number of samples. Table 5.1 gives an overview over the field sites where O₂ samples were collected.

Date	3 - 6 August 1999	19 - 20 July 2001	6 - 11 August 2002
Field site	Harvard Forest (HF)	Griffin Forest (GF)	Nationalpark Hainich (NH)
Site location and elevation	near Petersham, Massachusetts, USA 42°32' N, 72°11' W 340 m	near Aberfeldy, Scotland, UK 56°37' N, 3°48' W 340 m	near Craula, Thüringen, Germany 51°05' N, 10°28' E 445 m
Dominant species	Red Oak and Red Maple	Sitka Spruce (plantation)	European Beech
Site description	Goulden et al. 1996	Section 2 (Methods)	www.bgc.jena.mpg.de/ public/carboeur/ sites/index_s.html
Samples collected	canopy air	branch bags, soil chambers	branch bags

Table 5.1: Field sites and campaigns where samples for O₂ analysis were collected. δ(O₂/N₂) ratios of the Harvard Forest samples were determined in the laboratory of J. Severinghaus at the Scripps Institution of Oceanography, La Jolla, CA, USA. All other analyses were carried out as described in section 2 (Methods).

Theory

Photosynthesis and respiration are represented by the forward and reverse directions of the following reaction:



where O_2 is released to the atmosphere during photosynthesis and taken up in respiration while CO_2 is taken up during photosynthesis and released to the atmosphere during respiration. The reaction equation implies a molar exchange ratio of 1 : 1 between rates of O_2 and CO_2 uptake and release. However, this is not exactly true, because organic material (approximated here as CH_2O) also contains small amounts of other elements such as nitrogen and sulphur. The elemental composition of organic matter thus controls the stoichiometric ratio of O_2 : CO_2 exchange over long time periods and large spatial scales. At shorter temporal and smaller spatial scales, O_2 : CO_2 ratios are additionally influenced by the reduction state of the organic material and by the separate processes contributing to gas exchange, photosynthesis, respiration, and biochemical reactions during higher plant metabolism, i.e. synthesis of organic compounds. Soil respiration could have even more variable ratios, depending on the nitrogen content and the different coefficients of gas diffusion from the soil.

Following the convention originally proposed by Keeling and Shertz (1992), changes in the atmospheric O_2 mixing ratio are reported as changes in the O_2/N_2 ratio. Assuming that variations in the atmospheric N_2 mixing ratio (expected to be on the order of 10^{-8} or less (Heimann 2001)) are substantially smaller than those of O_2 , changes in the O_2/N_2 ratio should predominantly reflect changes in the O_2 mixing ratio (Keeling 1988b). O_2/N_2 ratios are reported as deviations, $\delta(\text{O}_2/\text{N}_2)$, from an (arbitrary) reference:

$$\delta(\text{O}_2/\text{N}_2) = \frac{(\text{O}_2/\text{N}_2)_{\text{sample}}}{(\text{O}_2/\text{N}_2)_{\text{ref}}} - 1 \quad (5.1)$$

where the result is multiplied by 10^6 and expressed in units of permeg. Because O_2 comprises 20.95 % of air by volume, 4.8 permeg (= $1/0.2095$) is equivalent to 1 ppm ("ppm equivalent"). Thus, when 1 ppm of CO_2 is converted into O_2 , the $\delta(\text{O}_2/\text{N}_2)$ ratio of air increases by 4.8 permeg.

For calculating the stoichiometric ratio of O₂ : CO₂, it is necessary to report both mixing ratios on the ppm scale (equivalent to μmol/mol for CO₂), so that magnitudes of fluxes can be compared on a mol to mol basis. For branch bag measurements, the stoichiometric ratio, *S*, of exchange processes was calculated according to:

$$S = \frac{\Delta[\text{O}_2]}{\Delta[\text{CO}_2]} = \frac{0.2095 \cdot (\delta(\text{O}_2/\text{N}_2)_e - \delta(\text{O}_2/\text{N}_2)_o)}{C_e - C_o} \quad (5.2)$$

where *C* is the CO₂ mixing ratio (mole fraction), and the subscripts *o* and *e* refer to open and closed branch bag samples, respectively, indicating the start and end points of bag closure periods.

Results

Diurnal cycles of δ(O₂/N₂) ratios

Figure 5.1 shows δ(O₂/N₂) ratios of air samples collected from canopy air, open branch bags and open soil chambers during the different field campaigns. As explained above, all δ(O₂/N₂) ratios are reported with respect to an arbitrary standard. The common feature apparent in the δ(O₂/N₂) measurements from all campaigns is that δ(O₂/N₂) ratios were higher during the day and lower at night. The top panel presents δ(O₂/N₂) ratios of canopy air obtained in Harvard Forest in August 1999. The diurnal cycle of δ(O₂/N₂) ratios showed a minimum of -20 permeg at 5:00, followed by a rapid increase until 9:00. Throughout the day, δ(O₂/N₂) values were around 190 permeg with a gradual increase towards the afternoon. The maximum of 220 permeg at 18:00 was followed by a decrease of δ(O₂/N₂) values during the night. The value of 230 permeg at 16:00 was omitted from quantitative comparisons because the sample was lost after completion of the first analysis.

The middle panel presents δ(O₂/N₂) data obtained from open branch bags and soil chambers in Griffin Forest in July 2001. The δ(O₂/N₂) ratios of the open branch bag samples collected at 16:00 were higher (≈ 300 permeg) than those collected at 0:30 (≈ 80 permeg). The bottom panel presents δ(O₂/N₂) data from open branch bags in the Hainich in August 2002. In this campaign, air samples for δ(O₂/N₂) analysis were only

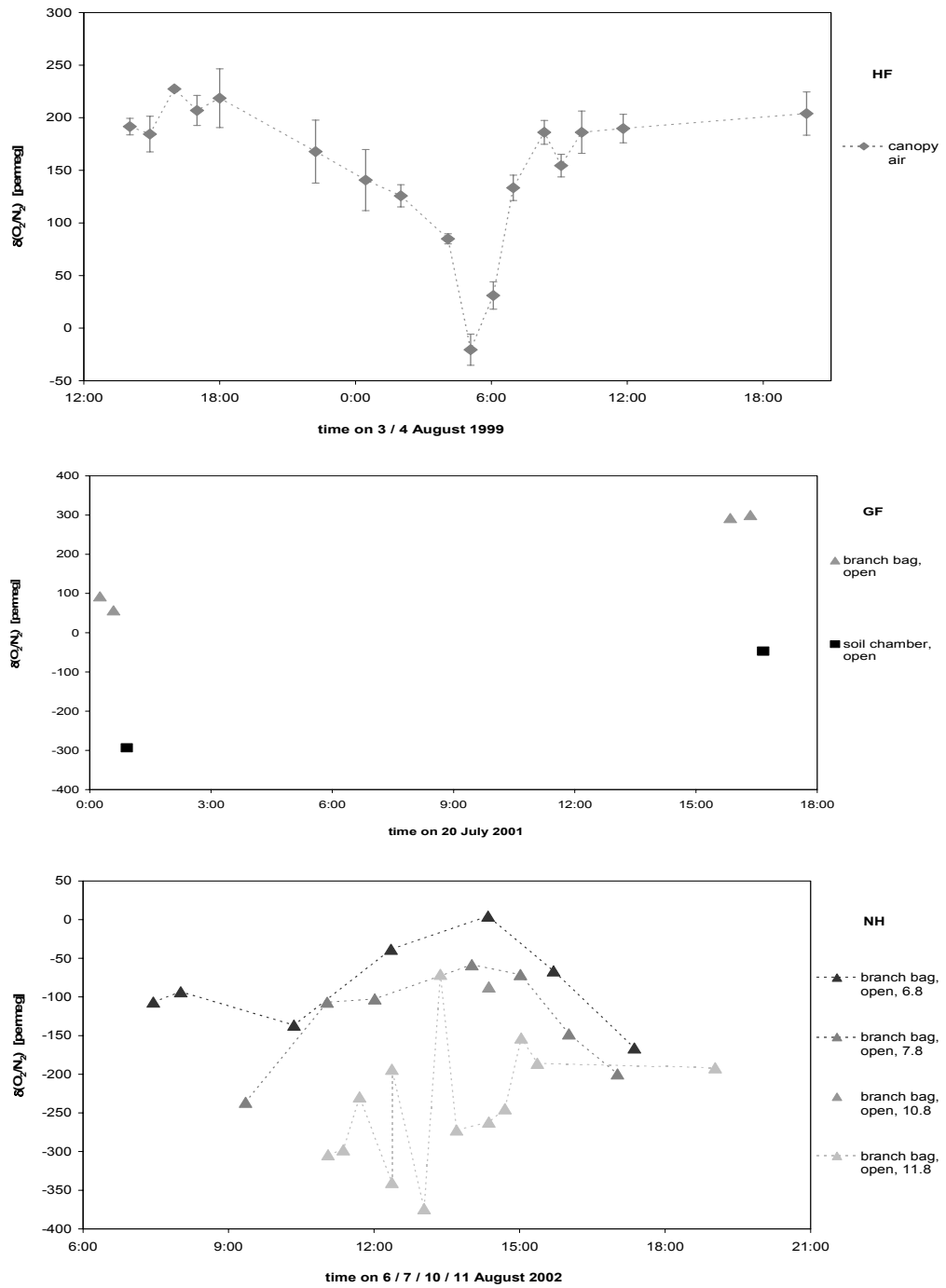


Figure 5.1: $\delta(O_2/N_2)$ ratios of air samples. Top: canopy air, Harvard Forest, 1999. Middle: open branch bags and soil chambers, Griffin Forest, 2001. Bottom: open branch bags, Hainich, 2002.

collected during the photosynthetic period of the sampling days. On 6 and 7 August, $\delta(\text{O}_2/\text{N}_2)$ ratios increased in the morning and decreased again in the afternoon. Maximum $\delta(\text{O}_2/\text{N}_2)$ values at around 14:00 were approximately 150 permeg higher than the respective morning and evening minimum values. There was no clear diurnal signal discernible on 11 August. Instead, $\delta(\text{O}_2/\text{N}_2)$ ratios showed several large fluctuations of up to 300 permeg over short time periods of 20 minutes. Overall, $\delta(\text{O}_2/\text{N}_2)$ ratios on 6 August were higher than on 7 August by about 50 permeg and higher than on 11 August by 100 to 200 permeg.

The Griffin Forest data shown in the middle panel of Figure 5.1 display higher $\delta(\text{O}_2/\text{N}_2)$ ratios at the top of the canopy than close to the ground at both sampling times. $\delta(\text{O}_2/\text{N}_2)$ ratios of air samples from open branch bags were about 350 permeg higher than from open soil chambers, establishing a vertical gradient of increasing ambient O_2 mixing ratios with height in the canopy profile. This gradient, equivalent to about 70 ppm in the O_2 mixing ratio, was also found (inversely) in CO_2 mixing ratios at day-times. During the day, the gradient was caused by the influence of photosynthesis, adding O_2 to ambient air at predominantly higher levels in the canopy. The existence of such a canopy gradient for both O_2 and CO_2 mixing ratios indicates that turbulent mixing of air from above into the canopy did not extend down to the forest floor during the day. Stronger turbulent mixing would have removed pronounced gradients in canopy air composition.

Photosynthesis and foliage respiration

O_2 mixing ratios of air samples obtained from branch bag measurements in Griffin Forest versus their respective CO_2 mixing ratio are presented in Figure 5.2. Standard deviations (similar size as symbols) were 10 permeg for $\delta(\text{O}_2/\text{N}_2)$ ratios (2.1 ppm equivalent) of open and closed samples, 0.13 ppm for the CO_2 mixing ratio of open samples, and 1.3 ppm for the CO_2 mixing ratio of closed samples (see section 2). Both mixing ratios are plotted as offsets from an arbitrary zero point defined by the sample with maximum O_2 and minimum CO_2 mixing ratio. Values are in ppm units (ppm equivalent for O_2) to highlight related changes in O_2 and CO_2 mixing ratios. In Griffin Forest, one sample pair was obtained from the control bag to rule out the possibility that any systematic drift affected the $\delta(\text{O}_2/\text{N}_2)$ ratios of air in branch bags. During the closure period in the control bag, the $\delta(\text{O}_2/\text{N}_2)$ ratio increased by 11 permeg. This is close to the 10 permeg standard deviation of the laboratory analyses. At the same time, the CO_2

mixing ratio increased by 1.4 ppm. Control bag CO₂ and O₂ changes were not inversely correlated, and both very likely reflect the experimental uncertainty. These observations were subsequently used to estimate uncertainties for stoichiometric ratios of O₂ : CO₂ exchange determined from sample pairs.

At approximately the same time as control bag samples were obtained in Griffin Forest (midnight), one branch bag sample pair was also collected to examine concurrent changes in O₂ and CO₂ mixing ratios due to foliage respiration. The $\delta(O_2/N_2)$ ratio decreased by 23 permeg (4.8 ppm equivalent in O₂ mixing ratio) over the closure period. However, the expected corresponding increase in the CO₂ mixing ratio was not found. In fact, CO₂ mixing ratios actually also decreased. Such a decrease would normally indicate photosynthetic CO₂ uptake, but the change was only 1 ppm, within limits of uncertainties of closed branch bag measurements. Therefore, the O₂ : CO₂ exchange ratio for foliage respiration could not be obtained from the observed changes.

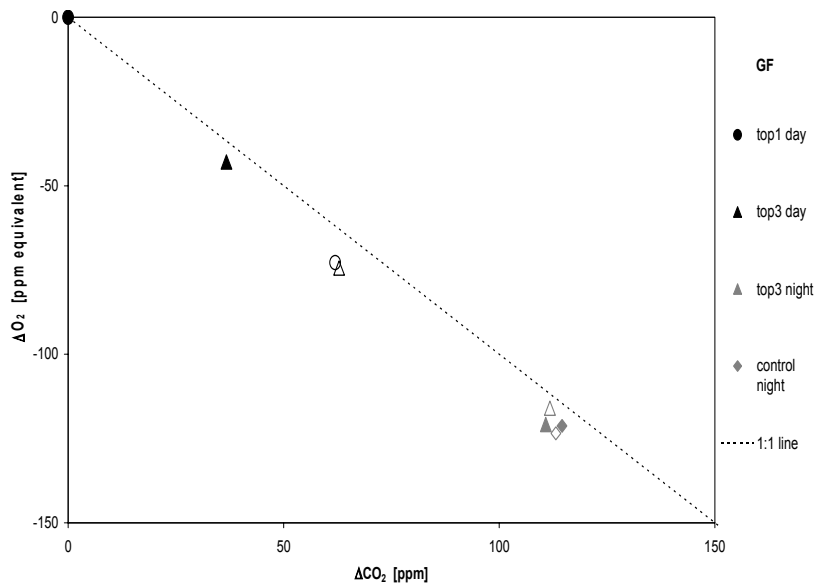


Figure 5.2: O₂ versus CO₂ mixing ratios of air samples from open (open symbols) and closed (full symbols) top and control branch bags, Griffin Forest, July 2001. Axes are scaled to zero point from sample with maximum O₂ and minimum CO₂ mixing ratio.

The impact of photosynthesis was evidenced by differences in $\delta(\text{O}_2/\text{N}_2)$ ratios between open and closed branch bag air samples during the day, with pronounced inverse changes in O_2 and CO_2 mixing ratios during the 5 minute closure periods. One of the branch bags (top 1) was receiving more solar radiation than the other (top 3). Accordingly, the rate of photosynthesis was higher, with a more rapid increase in O_2 and decrease in CO_2 mixing ratios in the top 1 bag. During closure periods, mixing ratios increased by 73 ppm (350 permeg) for O_2 and decreased by 62 ppm for CO_2 . Changes in the top 3 bag were smaller in magnitude, with 32 ppm (151 permeg) increase in O_2 and 26 ppm decrease in CO_2 mixing ratios. Stoichiometric $\text{O}_2 : \text{CO}_2$ exchange ratios of photosynthesis calculated using equation 5.2 were 1.18 ± 0.05 for the top 1 bag, and 1.20 ± 0.12 for the top 3 bag.

Figure 5.3 presents stoichiometric ratios of photosynthetic $\text{O}_2 : \text{CO}_2$ exchange of branch bag foliage obtained from sample pairs collected during the Hainich field campaign. The stoichiometric ratios are shown versus the time of day for the different sampling days in the top panel of Figure 5.3, and versus the flux of photosynthetic CO_2 assimilation in the bottom panel. The mean assimilation weighted stoichiometric ratio for the 26 data points from all days was 1.08 ± 0.16 (or 1.10 excluding data from 6.8, $n = 19$). The stoichiometric ratios inferred for the first sampling day (6.8) showed a high level of variability, ranging from 0.7 to 1.6 with three values below 1. At the same time, assimilation fluxes for several of these samples (4 of 7) were also on the lower end of the observed range of flux rates, at $2 \mu\text{mol}/\text{m}^2/\text{s}$ or lower. The maximum ratio of 1.25 on the other days was observed at a similarly low flux rate, $1.7 \mu\text{mol}/\text{m}^2/\text{s}$. All other samples from the following days had stoichiometric ratios between 1.0 and 1.2. For flux rates between 2 and $5 \mu\text{mol}/\text{m}^2/\text{s}$, and on all sampling days except the first (6.8), stoichiometric ratios of O_2 and CO_2 exchanges were between 1.04 and 1.20 and centred around a value of 1.10.

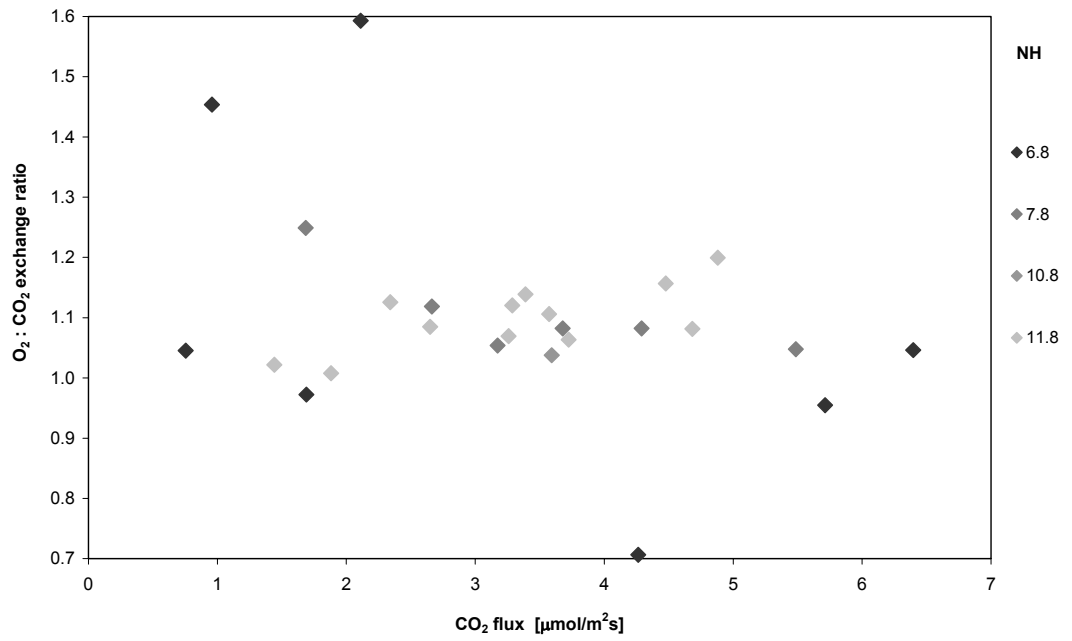
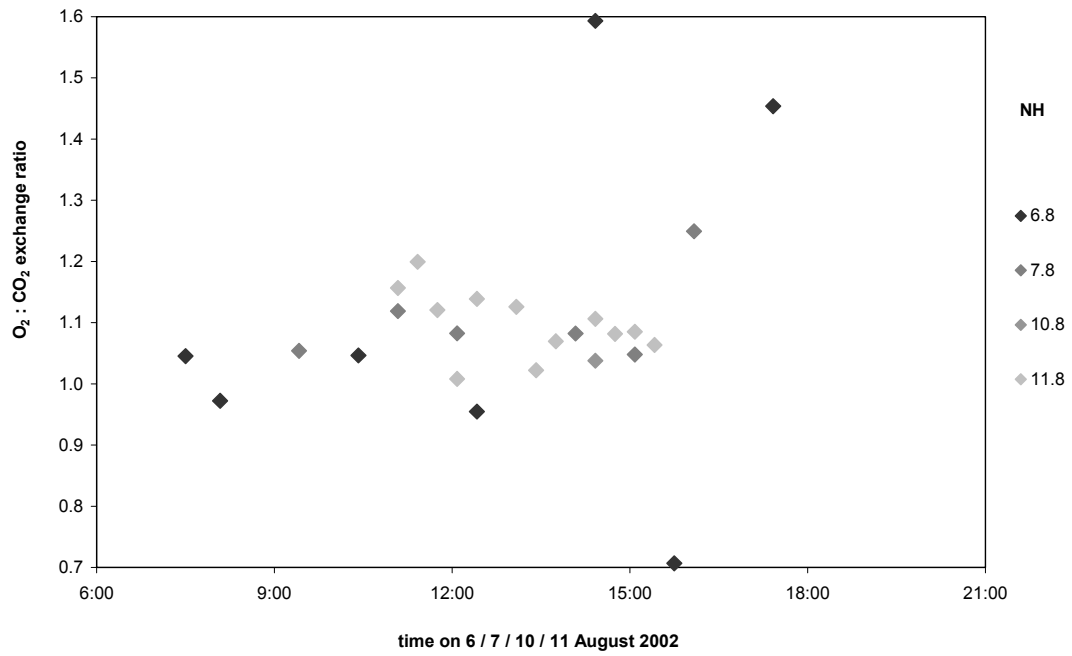


Figure 5.3: Stoichiometric ratios of photosynthetic $O_2 : CO_2$ exchange from pairs of air samples collected in branch bags, Nationalpark Hainich, August 2002. Top: versus time of day on 6, 7, 10 and 11 August. Bottom: versus CO_2 flux rates.

Soil respiration

Figure 5.4 presents data of sample pair O_2 and CO_2 mixing ratios taken from soil chamber measurements from Griffin Forest in July 2001. Measurement uncertainties indicated by error bars are smaller than symbols. The O_2 mixing ratios of open samples were 50 ppm (250 permeg) higher during the day than at night. On the other hand, open sample CO_2 mixing ratios were also 15 ppm higher during the day. This is in contrast to lower day-time CO_2 mixing ratios expected from a potential invasion of photosynthetically influenced air into lower canopy layers due to turbulent mixing. As a result of this discrepancy, data from day and night samples did not fall on the same line in the $O_2 : CO_2$ plot of Figure 5.4.

Furthermore, while changes in CO_2 mixing ratios over the closure periods of soil chambers were almost equal in magnitude, with increases of 72 and 71 ppm, they were accompanied by different changes in O_2 mixing ratios, decreases of 68 ppm (323 permeg) at day-time and 46 ppm (220 permeg) at night. Stoichiometric $O_2 : CO_2$ ratios inferred for respiration in the soil chambers were 0.94 ± 0.04 for the day, and 0.65 ± 0.04 for the night time measurement.

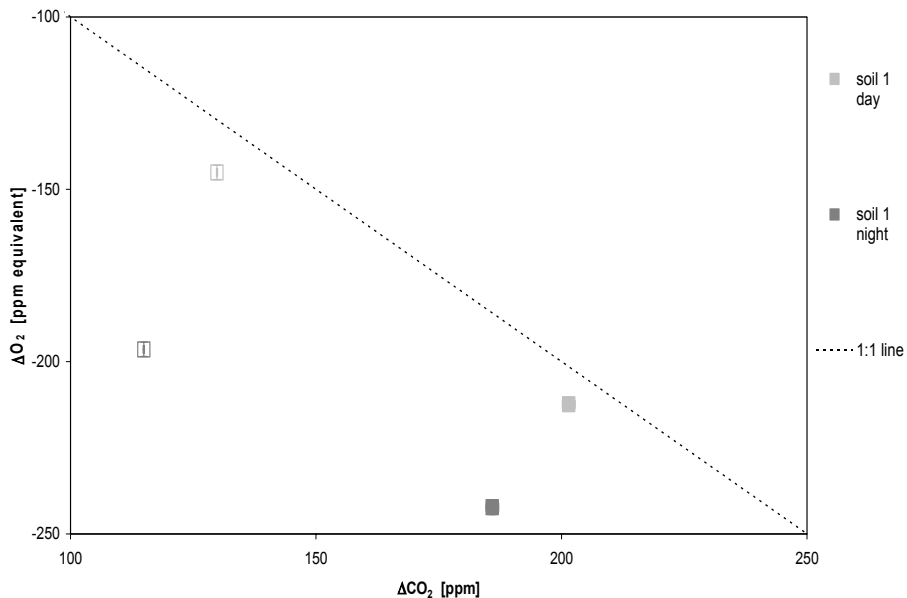


Figure 5.4: O_2 versus CO_2 mixing ratios of Griffin Forest air samples from open (open) and closed (full symbols) soil chambers on 20 July 2001. Axes same as for branch data (Fig 5.2).

Integrated canopy exchange

Figure 5.5 presents O₂ versus CO₂ mixing ratios of all open data points obtained during the field campaigns from samples of canopy air or from open branch bag and soil chamber measurements. Data points were combined to obtain the stoichiometric ratio of integrated canopy gas exchange from a regression of O₂ versus CO₂ mixing ratios. In the regressions, O₂ and CO₂ mixing ratios were treated as independent variables. The top panel of Figure 5.5 shows data collected during the Harvard Forest sampling campaign. The stoichiometric ratios of canopy O₂ : CO₂ exchange were 1.14 ± 0.19 during the light period on both days, 1.16 ± 0.02 during the night, and 1.03 ± 0.05 over the full diurnal cycle, with correlation coefficients of > 0.85 .

The middle panel of Figure 5.5 shows Griffin Forest data. The night-time open soil chamber data point did not follow the same relationship as the other data points. Canopy air close to the ground will be predominantly influenced by soil respiration at night, whereas its impact will be partly removed by turbulent mixing during the day. If the stoichiometric ratios of soil respiration are as variable as indicated by the two measurements reported above, soil air might not conform to any stable relationship between O₂ and CO₂ exchange, especially at night. Therefore, this data point was excluded from further analysis. Regression of mixing ratio data yielded a stoichiometric ratio of canopy O₂ : CO₂ exchange of 1.01 ± 0.06 for day and night samples, with a correlation coefficient of 0.99.

The bottom panel of Figure 5.5 shows data from air samples collected in open branch bags in the Hainich. Stoichiometric ratios of canopy O₂ : CO₂ exchange were calculated for three days separately. The ratios were 1.12 ± 0.08 on 6 August and 1.19 ± 0.03 on 11 August 2002. On 7 August, the first sample collected after the onset of measurable photosynthesis in the branch bag (indicated by an open symbol) had a CO₂ mixing ratio of 30 ppm higher than the other samples from that day, and might have been influenced by respiration. Regression excluding this sample yielded a stoichiometric ratio of 1.14 ± 0.04 , whereas the ratio including the first sample was 0.98 ± 0.03 . All correlation coefficients of regressions from Hainich data were > 0.98 .

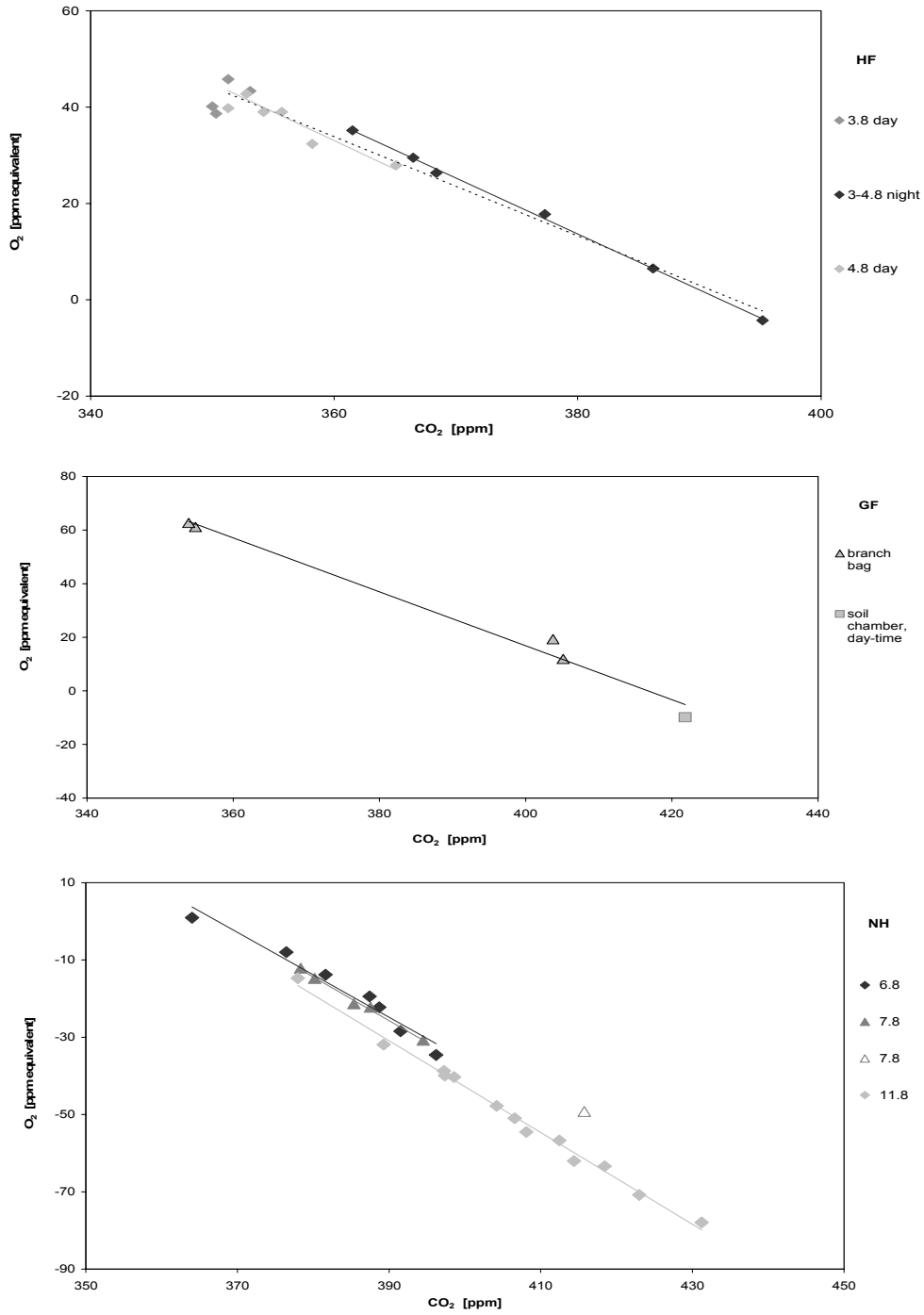


Figure 5.5: O₂ versus CO₂ mixing ratios of air samples used to construct stoichiometric ratios of integrated canopy gas exchange. Top: Harvard Forest, August 1999. Middle: Griffin Forest, July 2001 (the soil chamber night time data point was excluded). Bottom: Hainich, August 2002.

Discussion

During the day, $\delta(\text{O}_2/\text{N}_2)$ ratios of canopy air increased because of release of photosynthetically produced O_2 from foliage, whereas nocturnal canopy $\delta(\text{O}_2/\text{N}_2)$ ratios were lower due to O_2 uptake in foliage and soil respiration (samples were not collected at night in the Hainich). Similar night to day differences in $\delta(\text{O}_2/\text{N}_2)$ ratios of around 230 permeg were found for data from Harvard Forest (canopy air samples) and from Griffin Forest (open branch bags). For both campaigns, the maximum value of the diurnal amplitude in $\delta(\text{O}_2/\text{N}_2)$ ratios was observed at approximately the same time in the afternoon. The minimum value in Harvard Forest was observed at 5:00, shortly after dawn. On the other hand, the corresponding night-time values reported for Griffin Forest were obtained at 0:30. The latter do not necessarily reflect the minimal values of $\delta(\text{O}_2/\text{N}_2)$ ratios potentially reached during the night, especially if the timing of $\delta(\text{O}_2/\text{N}_2)$ minima seen in Harvard Forest was typical for diurnal patterns in the canopy gas composition. In this case, the earlier nocturnal sampling times in the Griffin Forest compared to the Harvard Forest campaign might have resulted in an underestimation of the diurnal amplitudes of $\delta(\text{O}_2/\text{N}_2)$ ratios in Griffin Forest. The steep decrease in $\delta(\text{O}_2/\text{N}_2)$ ratios between 4:00 and 5:00 in Harvard Forest could have been caused by the onset of vertical mixing at dawn. As a result of this, canopy air at 18 m height would have been influenced by air parcels from the forest floor depleted in O_2 due to soil respiration.

It is obvious that the exchange patterns found in the Griffin Forest sampling campaign cannot be valid in general. Stoichiometric ratios were found to be higher than 1 for photosynthetic O_2 release and lower than 1 for O_2 uptake in soil respiration. Thus, both processes would favour the accumulation of atmospheric O_2 , increase ambient O_2 mixing ratios without affecting CO_2 mixing ratios at an equal magnitude. If this was the case, O_2 and CO_2 exchanges would not be in balance, and atmospheric O_2 mixing ratios would continue to rise.

The data set presented here was derived from measurements aimed to determine O_2 : CO_2 ratios of canopy gas exchange under field conditions. The ratios obtained are thus not necessarily equivalent to those reported in other studies as they do not relate to elemental abundances but instead to gas fluxes that can be influenced by other processes such as turbulent mixing of canopy air and diffusion in soils. For example, Keeling (1988a) derived oxidative ratios of 1.05 ± 0.02 and 1.07 ± 0.05 from elemental

abundance data for wood and soil organic material, respectively. The ratio of soil organic matter (more specifically, humic acids and humins) was later arithmetically corrected to 1.12 ± 0.06 (Severinghaus 1995).

Based on elemental abundances, Severinghaus (1995) calculated an oxidative ratio of 1.25 for oxidation of a hypothetical mix of 35 % protein (C_4H_5ON), 50 % cellulose ($C_6H_{10}O_5$) and 15 % lignin ($C_6H_{12}O_2$), where for example protein alone would have an oxidative ratio of 1.5. The ratios depend on whether oxidation includes nitrification. In the absence of nitrification, the resulting oxidative ratio would be close to 1. These considerations indicate that $O_2 : CO_2$ ratios during gas exchange, like oxidative ratios, might depend on the nitrogen content of organic matter. For example, Sitka spruce needles were found to contain 41 ± 5 % cellulose and 22 ± 4 % lignin, with a total nitrogen concentration of 1.7 ± 0.4 % (Wainhouse et al. 1998, O'Neill et al. 2002). The content of soluble carbohydrates was estimated at 7 ± 2 % (Barton 1997), with protein comprising the majority of the rest (≈ 30 %). Such a composition would yield an oxidative ratio of 1.23, close to the stoichiometric ratio of approximately 1.2 found in the Griffin Forest campaign. However, complete agreement between the stoichiometric ratio of instantaneous photosynthetic gas exchange and the oxidative ratio of needle organic material would require all plant metabolic processes involved in the synthesis of the various needle organic compounds to proceed at equal, constant rates, a condition unlikely to be fulfilled at most times.

Severinghaus (1995) also calculated stoichiometric ratios of soil gas exchange by measuring concurrent O_2 and CO_2 changes in flow-through chambers under laboratory conditions. Results were between 1.06 and 1.22, and nitrification was suspected to determine where in this range values for separate soils would fall. Although it was concluded that soil gas exchange will have highly variable oxidative ratios from place to place, values below 1 were not found in any of these experiments. It is difficult to explain the stoichiometric ratios of 0.9 and 0.65 for soil gas exchange found in this study. Oxidation of other elements like nitrogen or hydrogen would require the removal of more O_2 from ambient air. Dissolution of evolving CO_2 in soil water would also cause stoichiometric ratios to be even higher. The decomposition of oxidised compounds such as citric acid (with an oxidative ratio of ≈ 0.8) could explain ratios below 1, but contributions from specific compounds are unlikely to dominate total rates of soil respiration. Another potential explanation is horizontal movements of gases in the soil,

with O_2 diffusing more easily into the soil in places where roots enhance soil air circulation. Any O_2 transferred horizontally to the places of oxidation would escape the measurements in the chamber spaces above. This is a possible scenario because soil chambers were not installed where large roots were visible at the soil surface. However, it would also mean that the overall stoichiometric ratio of soil gas exchange should be closer to the oxidative ratio of soil organic matter, because integration over larger areas should remove small scale anomalies. In light of this, the vertical gradient in the $\delta(O_2/N_2)$ ratio of canopy air at night probably was an artefact, caused by the locally highly variable O_2 distribution of soil air.

Stoichiometric ratios of $O_2 : CO_2$ exchange for photosynthesis or integrated canopy gas exchange that can be compared directly to the results of this study have only been reported in a limited number of studies so far. Bloom et al. (1989) reported stoichiometric ratios for photosynthesis of barley shoots from experiments in flow-through growth chambers. $O_2 : CO_2$ exchange ratios during photosynthetic gas exchange were found to depend on the source of nitrogen: 1.26 with nitrate, but 1.0 with ammonium. Thus, differences in nitrogen sources can cause $O_2 : CO_2$ exchange ratios to vary by more than 25 %. A stoichiometric ratio of 1.08 was obtained for locally integrated $O_2 : CO_2$ exchange at Baring Head, New Zealand (A. Manning, personal communication). This ratio was determined from analysing atmospheric data when air masses influenced by the land were encountered, so that concurrent changes in atmospheric $\delta(O_2/N_2)$ ratios and CO_2 mixing ratios could be attributed to terrestrial activity alone.

Agreeing with these results, the stoichiometric ratios of photosynthetic gas exchange were found to be approximately 1.1 in this study, from averages over branch bag measurements as well as from regressions of data from canopy air samples collected during the photosynthetic period. The average value of stoichiometric ratios of 1.1 during photosynthesis could reflect the elemental composition of foliage material, while fluctuations of mostly 0.1 around this average could reflect short-term variations of the complex interplay of reactions involved in photosynthesis (see for example Pessarakli 1997). In contrast, the stoichiometric ratios of integrated canopy $O_2 : CO_2$ exchange were indistinguishable from a 1 : 1 relationship for data over the full diurnal cycle from Harvard Forest and for the night and day samples from Griffin Forest. Although stoichiometric ratios of photosynthesis can vary substantially, those of plant respiration

ratios are determined solely by the elemental composition and the level of reduction or oxidation of the organic material. The stoichiometric ratios of soil respiration averaged over larger areas (to remove small scale anomalies such as found in this study) can additionally be influenced by anaerobic metabolism, for example in water logged soils.

The ratio of integrated canopy O_2 : CO_2 exchange (from variations in mixing ratios of O_2 and CO_2 in canopy air, see Figure 5.5) of approximately 1.0 was consistently different from stoichiometric ratios found for photosynthetic and respiratory gas exchange separately (1.1 to 1.2). This implies that the processes contributing to canopy gas exchange did not confirm to the same relationship of O_2 : CO_2 exchange. However, data on the stoichiometric ratios of soil respiration or turbulent exchange were not obtained in this study. A potential explanation is that the stoichiometric ratios from separate day or night time samples refer to gross exchange, whereas integrated stoichiometric ratios from combined day and night time samples refer to the daily net exchange. Thus, the integrated ratio could reflect the average composition of newly assimilated plant material during that day. Another scenario is that the variations of O_2 : CO_2 mixing ratios over a full diurnal cycle form a hysteresis curve (as illustrated in Figure 8.2). The shape of such a curve would be determined by differences in the stoichiometric ratios of separate gas exchange processes as well as by phase shifts of these processes with respect to each other (see for example the discussion of seasonal variations in $\delta^{13}C$ versus CO_2 mixing ratio in Heimann et al. (1989)). It is conceivable that the choice of sampling times results in stoichiometric ratios combined from these samples that are not representative for the total integrated canopy exchange (i.e. the full hysteresis curve). However, it is unclear whether the differences in O_2 : CO_2 exchange ratios between separate and integrated gas exchange constitute a typical pattern or a sampling artefact. This can only be answered through more extensive sampling.

Measurements of gas exchange during separate processes under field conditions will help to better constrain the stoichiometric ratio of O_2 and CO_2 exchange for use in global or ecosystem models of the carbon cycle. As discussed above, the magnitude and variability of this ratio might depend on the relative importance of gross and net fluxes contributing to gas exchange, and therefore on the scale examined. Clearly, further studies under field conditions as well as in the laboratory are needed to estimate the natural variability of stoichiometric ratios on different spatial and temporal scales.

6. $\delta^{18}\text{O}$ of O_2 in photosynthesis and respiration

Introduction

The $^{18}\text{O}/^{16}\text{O}$ composition of atmospheric O_2 is a potentially important tracer of the global oxygen cycle and hence of the carbon cycle coupled to it (see section 5), because it is sensitive to gross gas exchange between the atmosphere and the terrestrial and marine biospheres (Berry 1992). The isotopic composition of O_2 in air (23.8 ‰) is heavier (i.e. contains more ^{18}O) than expected from oxygen in equilibrium with ocean water (6 ‰). This isotopic enrichment, originally called the Dole-Morita effect, was discovered independently by Dole (1935) and Morita (1935). After a series of studies (Ruben et al. 1941, Dole and Jenks 1944, Dole et al. 1947, Roake and Dole 1950, Rakestraw et al. 1951, Dole et al. 1954), the primary cause of the Dole-Morita effect was established: terrestrial and marine organisms process ^{16}O faster than ^{18}O in respiration so that the remaining air is enriched in the heavy oxygen isotope (Lane and Dole 1956). Later, additional processes that contribute to the Dole-Morita effect were identified, requiring integration of the global oxygen and water cycles for quantitative estimations of its value (see Berry 1992, Bender et al. 1994, Seibt 1997).

The Dole-Morita effect can be calculated from an isotopic mass balance that includes all relevant O_2 exchange processes, analogous to calculations for ^{13}C in CO_2 (Tans 1980). The biological component of the mass balance consists of two major processes: photosynthetic release of O_2 carrying the isotopic composition of water at the site of O_2 production in chloroplasts, and fractionation during respiratory O_2 uptake. Both processes occur in the terrestrial as well as in the marine biosphere. An important difference between the two is that O_2 released in terrestrial photosynthesis is enriched compared to that released in marine photosynthesis because the water surrounding the sites of O_2 production in the foliage becomes enriched through transpiration (see section 4.1), whereas the oxygen produced by marine organisms carries an isotopic signature that is close to that of average ocean water. The isotopic signatures of the O_2 released from the terrestrial and marine biospheres have been estimated to differ by ≈ 5 ‰ (Farquhar et al. 1993, Seibt 1997), making the magnitude of the Dole-Morita effect sensitive to relative rates of terrestrial and marine gas exchange. The value of the Dole-Morita effect cited most often is 23.5 ‰ (Kroopnick and Craig 1972). However,

correcting this value by using the fractionation factor of 1.0412 for oxygen isotopes between water and CO₂ as recommended by Friedman and O'Neil (1977) yields a value of 23.8 ± 0.1 ‰. Horibe et al. (1973) also reported a value of 23.8 ± 0.06 ‰.

A promising application of the Dole-Morita effect arises from the fact that δ¹⁸O of O₂ is preserved in air bubbles in ice cores. Whereas temporal information on δ¹⁸O of CO₂ is not available because CO₂ equilibrates isotopically with water (see section 4), O₂ does not undergo isotopic exchange with water. If the precise age of the air is established, then the ¹⁸O record of past atmospheric O₂ can be linked to ¹⁸O records of ocean water (inferred from marine sediments) to yield information on temporal variations in the magnitude of the Dole-Morita effect, a measure of relative biological productivity of the marine and terrestrial biospheres because of its sensitivity to gross oxygen exchange fluxes (Bender et al. 1994, Malaize et al. 1999).

Theory

In this study, δ¹⁸O values of O₂ were not determined on an absolute scale but with respect to air from high pressure cylinders used as reference gases for mass spectrometric measurements. Therefore, δ¹⁸O values are reported here as offsets from an (arbitrary) standard that was assumed to correspond to the average δ¹⁸O of atmospheric O₂ of 23.8 ‰. Values can be expressed in ‰, but because they are usually very small, units of permeg are introduced by multiplying values by 10⁶ (instead of 10³, as for ‰).

During the light period, the mixing ratio and isotopic composition of O₂ in branch bag air will be changed by the addition of photosynthetically produced O₂. Photosynthesis has been found to release O₂ with an isotopic composition identical to that of water surrounding the sites of O₂ production (Stevens et al. 1975, Guy et al. 1993, Yakir et al. 1994). Thus, for the (extremely simplified) case where photosynthesis is the only process affecting the isotopic composition of O₂, the expected temporal change in δ¹⁸O of O₂ in a branch bag can be calculated from:

$$\frac{d}{dt}(\delta^{18}O_{atm}) = \frac{(\delta^{18}O_C - \delta^{18}O_{atm})}{O} \cdot \frac{d}{dt}O \quad (6.1)$$

where $\delta^{18}\text{O}_c$ and $\delta^{18}\text{O}_{\text{atm}}$ (‰) are the isotopic compositions of chloroplast water and of ambient O_2 , and O is the O_2 mixing ratio (in ppm equivalent) of branch bag air. Temporal changes of $\delta^{18}\text{O}_{\text{atm}}$ and O were estimated from pairs of samples collected at the beginning (open) and end (closed sample) of isolation periods (analogous to CO_2 , see Figures 2.3 and 2.4).

In principle, equation 6.1 allows to estimate the isotopic composition of chloroplast water from observed changes in $\delta^{18}\text{O}_{\text{atm}}$ and O_2 mixing ratio. Difficulties and limitations of this approach will be discussed below. Note that O is $\approx 21\%$, whereas changes (dO/dt) were of the order of 30 to 70 ppm O_2 over the bag closure period. Because of this, photosynthetically induced changes of $\delta^{18}\text{O}_{\text{atm}}$ in branch bag air were so small (> 20 permeg) that the $\delta^{18}\text{O}_{\text{atm}}$ value on the right hand side of equation 6.1 could be assumed constant.

The isotopic composition of chloroplast water, $\delta^{18}\text{O}_c$, that is transferred to O_2 during its photosynthetic production, was estimated from $\delta^{18}\text{O}$ of CO_2 as detailed in section 4. In the above formulation, impacts of concurrent respiratory fluxes on gas exchange in the branch bags have been neglected. Photorespiration and day-time dark respiration were estimated to take up 10 to 30 % and 5 to 10 % of gross photosynthetic O_2 production, respectively (see Figure 3.4). Thus, the flux rate appropriate for scaling of $\delta^{18}\text{O}_c$, gross photosynthetic O_2 production, was 10 to 50 % higher than estimated by the net rate of O_2 increase in branch bag air (dO/dt). Discrimination during respiratory oxygen uptake causes enrichment of $\delta^{18}\text{O}$ in ambient O_2 , whereas oxygen released in photosynthesis is mostly depleted in $\delta^{18}\text{O}$ with respect to ambient O_2 . Often, the resulting changes in $\delta^{18}\text{O}_{\text{atm}}$ are small, because these contrasting effects partly balance each other. Such additional influences will be neglected in the present case as they are not important for the general picture presented here. This also applies to the exact value of $\delta^{18}\text{O}_c$, as will be seen later.

Discrimination against $^{18}\text{O}_{\text{atm}}$ in atmospheric O_2 during respiration is in principle equivalent to that against CO_2 isotopes during photosynthesis (Rayleigh process), causing simultaneous changes in isotopic composition of source and product (see equation 2.7). However, changes in $\delta^{18}\text{O}_{\text{atm}}$ over chamber closure periods were so small that this feedback could be neglected (as above). Hence, for simplicity, the same approach as for photosynthesis (equation 6.1) is used:

$$\frac{d}{dt}(\delta^{18}O_{atm}) = \frac{\Delta_R}{O} \cdot \frac{d}{dt}O \quad (6.2)$$

where Δ_R (‰) is the ^{18}O discrimination during respiratory O_2 uptake. As in equation 6.1, Δ_R can be estimated in principle from observed changes in $\delta^{18}O_{atm}$ and the O_2 mixing ratio. However, both equations also allow to calculate expected $\delta^{18}O_{atm}$ changes from observed changes in the O_2 mixing ratio and assumed $\delta^{18}O$ values of fluxes. Here, -20 ‰ was used for soil respiration discrimination. Again, the exact value is not important for the following considerations.

Results and Discussion

Figure 6.1 shows $\delta^{18}O_{atm}$ (as offset from 23.8 ‰) and O_2 mixing ratios (as $\delta(O_2/N_2)$ ratios) of air samples obtained from open and closed branch bags and soil chambers during the sampling campaign on 20 July 2001. $\delta^{18}O_{atm}$ values displayed the changes expected from influences of the dominant biological processes during the chamber closure periods. In branch bags during the day, $\delta^{18}O_{atm}$ decreased by about 20 permeg

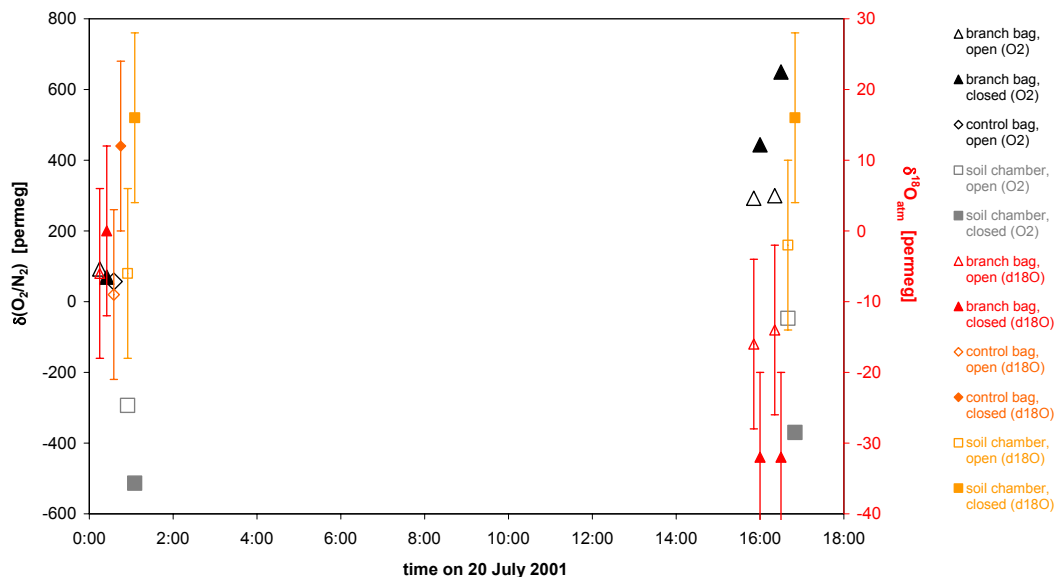


Figure 6.1: $\delta(O_2/N_2)$ ratio and isotopic composition of O_2 in air samples obtained from open and closed branch bags and soil chambers in July 2001.

due to release of depleted O_2 during photosynthesis. In soil chambers, $\delta^{18}O_{atm}$ increased by about 20 permeg due to discrimination against ^{18}O during respiratory O_2 uptake. In the control bag, an apparent change of comparable magnitude, 21 permeg, was observed in $\delta^{18}O_{atm}$ of O_2 while $\delta(O_2/N_2)$ only changed by 10 permeg (≈ 2 ppm). Error bars of $\delta(O_2/N_2)$ ratios are smaller than symbols (10 permeg). Obviously, uncertainties in measurements of $\delta^{18}O_{atm}$ are large compared to signals, i.e. differences between open and closed samples. All error bars for $\delta^{18}O_{atm}$ of sample pairs are overlapping. Analytical precision of laboratory measurements was used for error bars of $\delta^{18}O_{atm}$ (12 permeg). Uncertainties of closed samples might be even larger, but this cannot be estimated because error bars of the sample pair obtained from the control bag overlap as well.

Figure 6.2 presents the observed changes of $\delta^{18}O_{atm}$ in branch bag and soil chamber air versus the expected changes in $\delta^{18}O_{atm}$ over closure periods based on observed changes in the O_2 mixing ratio, calculated from equations 6.1 and 6.2. Error bars of observed changes in $\delta^{18}O_{atm}$ represent combined uncertainty for sample pair data, 17 permeg. Although error bars overlap the 1:1 line, it is evident that no conclusions can be derived from data that has such large levels of uncertainty. The calculations illustrated in Figure 6.2 were based on the assumption that only one process is affecting the isotopic

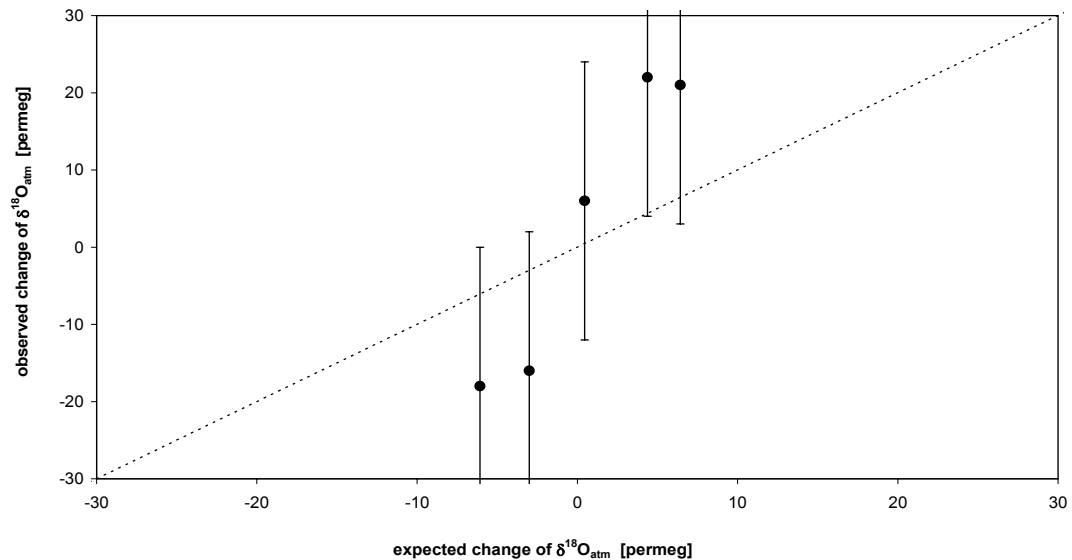


Figure 6.2: Expected and measured change in $\delta^{18}O$ of O_2 in air samples during closure periods of branch bags (three, left) and soil chambers (two, right) in July 2001.

composition of O₂, photosynthesis in branch bags (during the day) and respiration in soil chambers. For branch bag air, contributions of concurrent respiration to gas exchange were neglected (see above). For soil chamber air, influences of possible diffusional fractionation were neglected. Of course these assumptions are unrealistic. Calculations taking into account such additional processes would reflect more accurately the situation encountered under natural conditions. However, expected changes of $\delta^{18}\text{O}_{\text{atm}}$ under more plausible scenarios would be even smaller, so that estimates reported here can be viewed as representing their upper limits.

Clearly, data from this study cannot be analysed on a sample pair basis, but might yield a correlation for canopy air composition similar to "Keeling plot" type relationships. Figure 6.3 illustrates the existence of such a correlation between $\delta^{18}\text{O}_{\text{atm}}$ and O₂ mixing ratio, with higher O₂ mixing ratios accompanied by lower $\delta^{18}\text{O}_{\text{atm}}$ values. Even though changes in isotopic composition of O₂ cannot be analysed quantitatively due to large uncertainties of $\delta^{18}\text{O}$ data, a general trend is evident Figure 6.3 from all data, and also from open sample data alone. Qualitatively, the trend follows theoretical predictions, where O₂ released during photosynthesis carries an isotopic signature (of chloroplast water, 3 to 15 ‰) that is depleted with respect to ambient O₂ (23.8 ‰), thereby leading

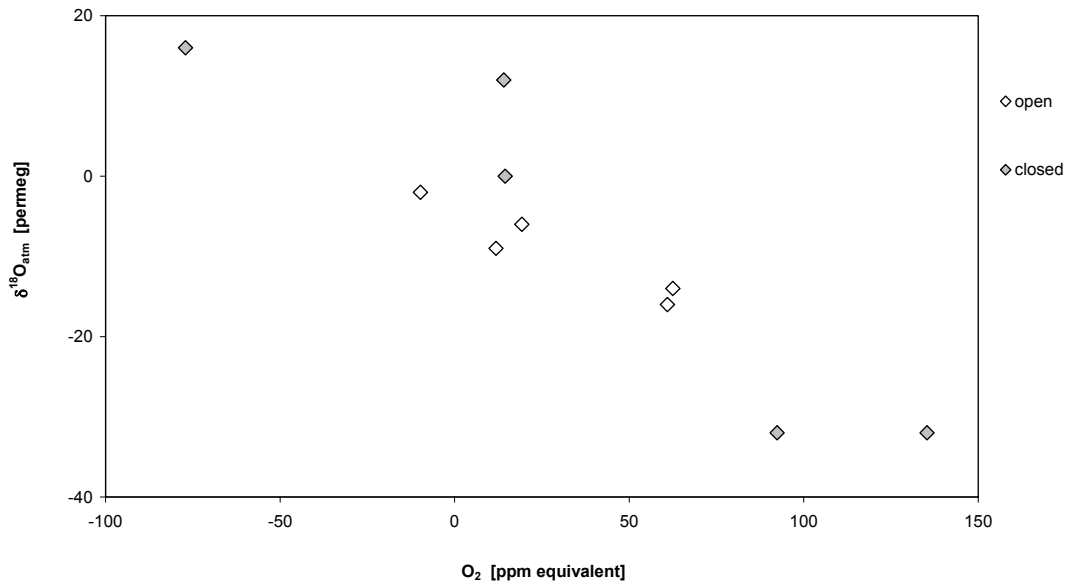


Figure 6.3: Isotopic composition versus mixing ratio of O₂ in air samples obtained from open and closed branch bags and soil chambers in July 2001 (as offsets from mean, arbitrary axis).

to lower $\delta^{18}\text{O}_{\text{atm}}$ at higher O_2 mixing ratios, and discrimination during foliage or soil respiration enriches the remaining air in ^{18}O , thereby leading to higher $\delta^{18}\text{O}_{\text{atm}}$ at lower O_2 mixing ratios. Regression of $\delta^{18}\text{O}_{\text{atm}}$ versus $1/[\text{O}_2]$ from open branch bag air samples, analogous to "Keeling plots", yielded -8 ‰ for $\delta^{18}\text{O}$ of chloroplast water that is transferred to photosynthetically added O_2 . However, disturbances from turbulent mixing and respiratory fluxes violate the two pool mixing assumption for canopy O_2 during the day, and $\delta^{18}\text{O}$ of leaf (and chloroplast) water varies diurnally. Also, measured values are extremely far from intercepts of inverse mixing ratios, amplifying uncertainties in source isotopic compositions derived from Keeling plots.

The $\delta^{18}\text{O}_{\text{atm}}$ measurements presented here were made at the highest level of precision currently available. Thus, the question arising is: with this precision, how large would changes in O_2 mixing ratios have to be to cause concurrent changes in $\delta^{18}\text{O}_{\text{atm}}$ large enough to be reliably detected? The top panel of Figure 6.4 shows expected changes in $\delta^{18}\text{O}_{\text{atm}}$ depending on O_2 mixing ratio changes, calculated for different $\delta^{18}\text{O}$ values of leaf (chloroplast) water following equation 6.1. For example, a $\delta^{18}\text{O}_{\text{atm}}$ difference of 18 permeg between start and end samples would require the $\delta(\text{O}_2/\text{N}_2)$ ratio to change by about 1000 permeg. The concurrent decrease in the CO_2 mixing ratio of about 200 ppm would be very large, more than half of the CO_2 usually present in branch bag air at the beginning of closure periods during the photosynthetic period ($< 380 \text{ ppm}$).

The bottom panel of Figure 6.4 shows the change in O_2 mixing ratio ($\delta(\text{O}_2/\text{N}_2)$ ratio on the right axis) required to change $\delta^{18}\text{O}_{\text{atm}}$ by 12 permeg, the current laboratory precision of single $\delta^{18}\text{O}_{\text{atm}}$ measurements, versus leaf water isotopic composition. For example, with water in the chloroplasts having a $\delta^{18}\text{O}_c$ of 12 ‰, a change of 1000 permeg would be required in the $\delta(\text{O}_2/\text{N}_2)$ ratio to achieve the 12 permeg change in $\delta^{18}\text{O}_{\text{atm}}$. As the top panel of Figure 6.4 illustrates, required O_2 changes rise with increasing $\delta^{18}\text{O}_c$ values. Higher $\delta^{18}\text{O}_c$ result in smaller differences between the isotopic signature of photosynthetically released O_2 and the isotopic composition of O_2 already present in the air. The closer $\delta^{18}\text{O}_c$ is to 23.8 ‰, the larger the changes in O_2 mixing ratios would need to be to cause measurable changes in $\delta^{18}\text{O}_{\text{atm}}$.

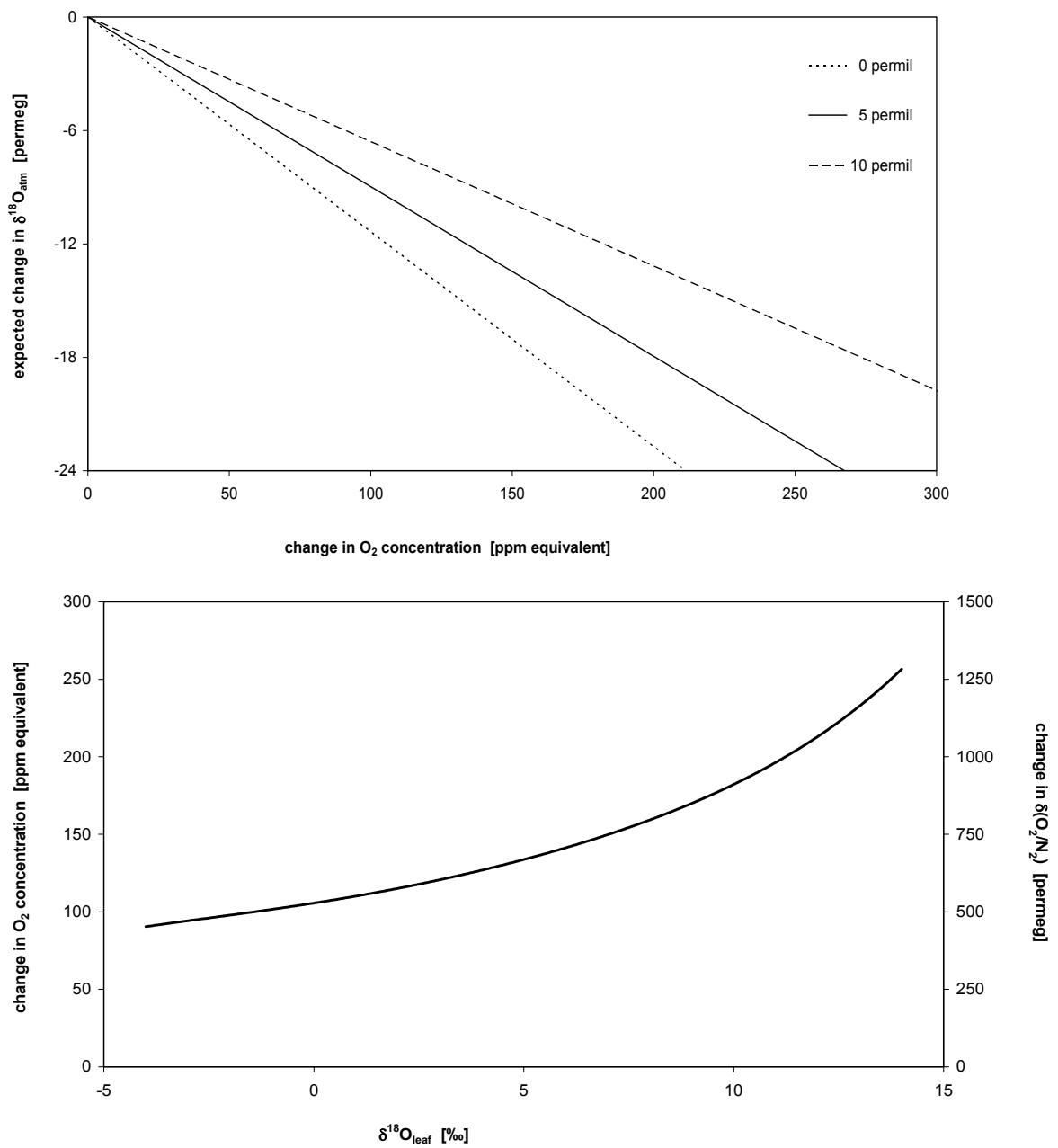


Figure 6.4: Top panel: Differences in isotopic composition of branch bag air expected from changes in the O_2 mixing ratio for different $\delta^{18}\text{O}_\text{C}$ of leaf water (0, 5 and 10 ‰), corresponding to the isotopic signature of photosynthetically added O_2 . Bottom panel: Change in the O_2 mixing ratio required to change the isotopic composition by 12 permeg, the current level of single sample analytical precision, versus $\delta^{18}\text{O}$ of leaf water.

Changes of this magnitude might be achieved either by choosing species and conditions with high rates of photosynthesis or by extending the time span of closure periods. Both possible solutions however have serious problems. High photosynthetic rates, i.e. high CO₂ and O₂ fluxes, are usually coupled with high rates of transpiration through stomatal openings. High transpiration fluxes lead to isotopic enrichment of leaf water, requiring larger changes in O₂ mixing ratios as argued above. In addition, photorespiration fluxes are likely to be substantial when high photosynthetic rates cause decrease of internal CO₂ mixing ratios (see section 3.1). Extended closure periods circumvent the problems of high flux rates, but photorespiration will probably start to disturb the system when CO₂ mixing ratios fall to very low levels. Other feedbacks between carbon and water exchange rates and micro-environment of the plants under study will also increase over time, making exact determinations of experimental parameters difficult. On the other hand, at times of depleted leaf water such as at dawn, photosynthetic rates are usually very low, requiring even longer closure periods.

Clearly, there are many difficulties with the approaches described above. The only remaining option is to achieve better analytical and experimental precision for measuring $\delta^{18}\text{O}_{\text{atm}}$. The question then is: how precisely would we have to measure $\delta^{18}\text{O}_{\text{atm}}$? For illustration: A hypothetical increase in the CO₂ mixing ratio by 100 ppm, from 300 to 400 ppm, constitutes a change of 33 % with respect to the original CO₂ inventory. If this change is achieved by adding CO₂ with an isotopic composition differing from that of the original CO₂ pool by 20 ‰, then the overall isotopic composition of that pool will change by about 5 ‰, well within the detection range (see section 2). In contrast, an increase in the O₂ mixing ratio of the same magnitude, 100 ppm, from 209500 to 209600 ppm, changes the original O₂ inventory by about 0.0005 %. If the isotopic composition of the added O₂ differs from that of the already existing O₂ pool by the same value of 20 ‰, then the overall $\delta^{18}\text{O}_{\text{atm}}$ of that pool will change by only about 10 permeg.

Uncertainties in changes of $\delta^{18}\text{O}_{\text{atm}}$ values are roughly 1.4 times those for single data points. Hence, to determine a 10 permeg change at the 5 permeg precision level would require $\delta^{18}\text{O}_{\text{atm}}$ values to be determined with 3.5 permeg precision. Of course, overall experimental precision would have to be increased appropriately to gain advantage from increased laboratory precision. To achieve 10 % relative error, i.e. 1 permeg uncertainty, would require 0.7 permeg precision of single measurements. At this precision level,

$\delta^{18}\text{O}_c$ would have an uncertainty of $\approx 2\%$. This would be sufficient for studying cycles of leaf water enrichment under natural conditions that might have amplitudes of 10 times that value, but it would still not allow to identify which leaf water compartments transfer their isotopic signature to CO_2 and O_2 , whether they are identical, or how large and variable their offsets are. While this could be examined in laboratory studies by, for example, supplying plants with isotopically very depleted water, measurements under field conditions might have to wait until the analytical precision has reached the sub-permeg level, i.e. about 1/100 of its currently best value.

On the other hand, analytical standard errors at the sub-permeg level could be achieved by repeating laboratory analyses of air samples. The standard error of measurements corresponds to the standard deviation divided by the square root of the number of measurements. Thus, the standard error decreases with increasing measurement repeats. For example, the single data point standard error of 0.7 permeg (as above) would require approximately 290 measurements at 12 permeg, 50 measurements at 5 permeg or 20 measurements at 3 permeg measurement standard deviation. This approach seems especially promising in the light of the automated mass spectrometric analysis procedures that are currently being developed (W. Brand, personal communication). In this case, measurements under field conditions might only have to be postponed until the analytical precision reaches about half to one quarter of its currently best value, which seems possible within the next few years. The measurements of $\delta^{18}\text{O}$ in O_2 presented might be useful to highlight a few problems and challenges such future studies might encounter.

Part II :

Canopy scale

integration of processes

7. Canopy scale integration of CO₂ exchange

Introduction

The main processes affecting the CO₂ mole fraction in canopy air are turbulent exchange with air from above the canopy, soil and foliage respiration and photosynthesis. Changes in CO₂ mole fraction of air within the canopy are accompanied by variations in its carbon and oxygen isotope composition. Respiration by foliage and soil increases the CO₂ mole fraction of canopy air while at the same time decreasing its carbon isotope composition, because the $\delta^{13}\text{C}$ signature of respired carbon reflects its substrate, mostly depleted plant and soil organic material. Soil respiration has the same effect on $\delta^{18}\text{O}$ of CO₂ if the soil water that it equilibrates with is depleted in ^{18}O with respect to the atmosphere, whereas the effect of nocturnal foliage respiration can be opposite if foliage water remains enriched at night. During the photosynthetic period, carbon assimilation by plants lowers the CO₂ mole fraction of canopy air while simultaneously enriching the remaining CO₂ in ^{13}C and, if transpiration from foliage has resulted in enriched $\delta^{18}\text{O}$ of water at the evaporating sites of foliage, also in ^{18}O .

In this section, the integrated canopy exchange of CO₂ and of $\delta^{13}\text{C}$ and $\delta^{18}\text{O}$ of CO₂ is estimated from the above listed component fluxes of gas exchange and their isotopic signatures. The predicted isotopic signatures of the separate fluxes utilised here have already been determined and discussed in sections 3 and 4. Net turbulent CO₂ fluxes and one-way turbulent fluxes of isotopic gas exchange are calculated from canopy exchange integrations, i.e. isotopic mass balances ("derived fluxes"). The derived net turbulent flux of CO₂ exchange is then compared to data from a nearby eddy covariance tower ("observed fluxes"). The goal of this section is firstly, to allow comparison of variations in $\delta^{18}\text{O}$ of O₂ in canopy air estimated in section 8, and secondly, to provide input fluxes for the partitioning of canopy gas exchange into component fluxes that will be presented in section 9.

Theory

Assuming there is no net horizontal advection of CO₂, temporal changes in the CO₂ mole fraction of well mixed canopy air (1 box model) can be calculated from a mass balance (equation 1 of Lloyd et al. (1996)):

$$M_i \frac{d}{dt} C_a = -F_n + R_s + R_f - A \quad (7.1)$$

where M_i (mol/m²) and C_a (μmol/mol) are moles of air per unit ground area and its CO₂ mole fraction within an air column of specified height from the soil surface. R_s , R_f and A (μmol/m²s) are rates of soil and foliage respiration and carbon assimilation, all with positive signs. F_n (μmol/m²s) is the net flux of CO₂ into or out of the canopy. The net flux is the difference between two one-way fluxes, $F_n = F_{io} - F_{oi}$, of turbulent gas exchange with air outside of the canopy, where F_{io} (in-out) denotes the flux of CO₂ leaving and F_{oi} (out-in) the flux entering the column so that positive F_n indicates a net turbulent flux directed out of the canopy.

Accordingly, temporal changes in δ¹³C and δ¹⁸O of CO₂ in canopy air can be calculated from isotopic mass balances (equation 10 of Lloyd et al. (1996)):

$$M_i C_a \frac{d}{dt} (\delta_i) = F_{oi} (\delta_o - \delta_i) + R_s (\delta_{Rs} - \delta_i) + R_f (\delta_{Rf} - \delta_i) + A \Delta \quad (7.2)$$

where δ_i and δ_o (‰) are carbon (δ¹³C_i, δ¹³C_o) and oxygen (δ¹⁸O_i, δ¹⁸O_o) isotopic compositions of CO₂ within the canopy and entering the canopy from above, respectively, δ_{Rs} and δ_{Rf} (‰) are the carbon (δ¹³C_{Rs}, δ¹³C_{Rf}) and oxygen (δ¹⁸O_{Rs}, δ¹⁸O_{Rf}) isotopic signatures of CO₂ produced by foliage and soil respiration, and Δ (‰) are the photosynthetic discriminations against ¹³C (¹³Δ) and ¹⁸O (¹⁸Δ), respectively. In the following, the separate components of equation 7.2 are referred to as isofluxes (μmol‰/m²s). In sections 7 and 9, all variables inside the canopy are denoted by the subscript i, with the exception of the CO₂ mole fraction denoted by C_a to distinguish it from the substomatal CO₂ mole fraction, C_i , as used in sections 2, 3, 4 and 9.

Additional observations

Eddy Covariance System

Fluxes of CO₂ and water vapour as well as canopy meteorological parameters were measured from a 15 m high instrument tower employed as part of the CarboEuroFlux project (description at www.bgc.jena.mpg.de/public/carboeur/sites/index_s.html). Thirty min average CO₂ and water vapour fluxes were determined from continuous above canopy measurements of CO₂, H₂O and wind velocity. The flux measurement system (Moncrieff et al. 1997) consisted of a three-dimensional sonic anemometer mounted at 15.2 m (Solent A1002R, Gill Instruments Ltd., Lymington, England) to measure the vertical wind component, a pumping unit to draw air at a flow rate of 6 L/min through 18 m of heated tubing (6 mm i.d. Dekabon 1300, Furon, Gembloux, Belgium), a fast-response closed-path infrared gas analyser (IRGA) for CO₂ and H₂O analysis (LI-6262, Li-Cor Inc., Lincoln, Nebraska), and a laptop using the EdiSol software (Moncrieff et al. 1995). A description of the instrumentation, calibration and corrections applied during processing of data can be found in Clement (in preparation).

Soil gas exchange

In addition to the soil chamber measurements described in section 2, soil CO₂ efflux rates were also measured with a portable soil chamber and CO₂ analyser setup, the coupled SRC-1 and EGM-1 (PP Systems, Hitchin, Hertfordshire, England). At 3 sites each in a 0.01 ha plot, 12 PVC collars (100 mm tall, 3 mm wall thickness, inserted 2 cm into the soil) were distributed over the distinct strata of the soil surface (furrows, flats and ridges). A customised adapter was used to connect the collars to the portable soil chamber. Air was then drawn from within the collars to a portable infrared gas analyser. CO₂ fluxes were calculated from gradients in chamber CO₂ mole fractions measured every 8 seconds over 2 minutes. The collars enclosed a surface area of $7.1 \times 10^{-3} \text{ m}^2$. A small, low speed fan ensured mixing of air within the chamber during the measurements. Soil CO₂ fluxes were calculated by software included with the IRGA. The system is described further by Jensen et al. (1996).

Data was collected with the portable soil chamber throughout the diurnal measurement cycle coinciding with the sampling intervals for the branch bags and soil chambers. Soil

temperature was measured concurrently between 1 and 5 cm depth in the soil profile using a pair of RTD (PT100, RS Components, UK). Half of the soil surface area was covered by ridges and 25 % each by flats and by furrows. Differences in rates of soil CO₂ fluxes were more marked between strata than across sites, with mean rates of $2.3 \pm 0.8 \mu\text{mol/m}^2\text{s}$ for ridges, $1.6 \pm 0.8 \mu\text{mol/m}^2\text{s}$ for flats, and $1.1 \pm 0.8 \mu\text{mol/m}^2\text{s}$ for furrows. Soil CO₂ flux rates were described using an Arrhenius function relationship with soil temperature as the independent variable (see equation 3.7). Respiration rates at 10 °C, R_{10} , determined from 128 measurements, were $2.6 \pm 0.2 \mu\text{mol/m}^2\text{s}$ for ridges, $2.0 \pm 0.15 \mu\text{mol/m}^2\text{s}$ for flats, and $0.94 \pm 0.24 \mu\text{mol/m}^2\text{s}$ for furrows. Figure 7.1 illustrates diurnal cycles of average soil temperatures (thick lines) that were constructed from sets of 12 measurements at each time step.

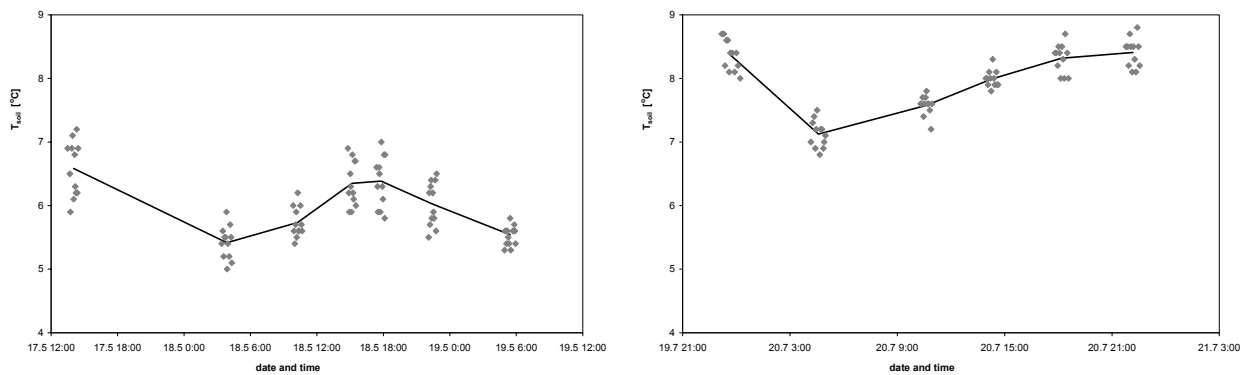


Figure 7.1: Diurnal cycles of soil temperature (°C) at a depth of 1 to 5 cm in the soil profile for May (left) and July (right) 2001. Thick lines indicate averages, grey diamonds indicate the separate measurements (sets of 12 at each time step).

7.1 Net ecosystem exchange of CO₂

The top panel of Figure 7.2 shows diurnal variations in the CO₂ mole fraction of canopy air for separate branch bags, over three days following sampling periods in May and July 2001. Data on CO₂ mole fractions obtained from flask samples of air from open branch bags are shown for comparison. The thick lines indicate values of CO₂ mole fractions used for subsequent calculations and isotope regressions, calculated from averages of all branch bags and smoothed over three time steps of 20 minutes each (also applied to all other average fluxes and discriminations referred to in Part 2).

In July, average night-time CO₂ mole fractions were higher (400 to 425 ppm) than in May (390 to 400 ppm). In both months, the nocturnal increase in CO₂ mole fraction was less marked during the second and stronger during the third night examined. Day-time values in July (340 to 350 ppm) were lower than in May (360 to 370 ppm). Thus, diurnal changes were more pronounced in July than in May. During the first half of the May sampling day and around noon on the July sampling day, occasional low CO₂ mole fractions were recorded by the IRGA that were in contrast with the flask data, whereas flask and IRGA data were in good agreement for all other times. Technical difficulties were encountered during branch bag measurements on the first half of the May sampling day (18.5). Therefore, average CO₂ mole fractions for all time steps until 11:00 were calculated using only data from the top3 and mid branch bags, and using only mid bag data between 4:40 and 5:40.

The bottom panel of Figure 7.2 presents rates of soil respiration (R_s) subsequently used in calculations of CO₂ and isotopic exchanges within canopy air. The plots also show values from soil chamber flask measurements (soil 1 and 2 obs). Soil respiration rates

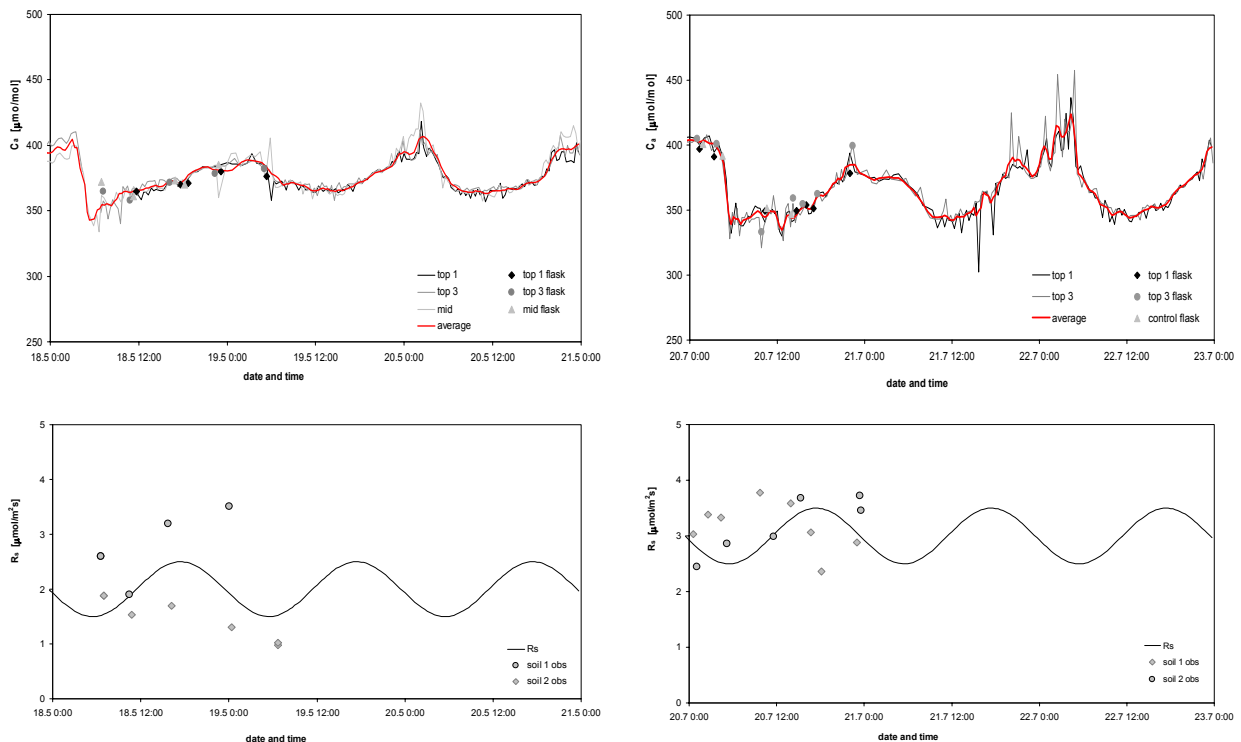


Figure 7.2: Diurnal changes over three days in May (left) and July (right) 2001. Top: CO₂ mole fraction of canopy air (C_a) for separate branch bags and averages. Bottom: CO₂ flux released in soil respiration.

have been assumed here to depend primarily on soil temperature. Hence, diurnal cycles of soil respiration were constructed from diurnal patterns of soil temperature (see Figure 7.1), using parameters (R_{10}) from regressions between respiration rates and soil temperatures. Because temperatures or respiration measurements were not available for soils over the full three day periods, time courses of respiration rates were assigned from a sinusoidal curve with minima shortly after dawn (5:20) and maxima in the late afternoon (17:20). The timing of diurnal phases as well as total peak to peak amplitudes were assumed to be the same in both months ($1 \mu\text{mol}/\text{m}^2/\text{s}$), but at a slightly higher level in July, ranging from night-time values of 2.5 to $3.5 \mu\text{mol}/\text{m}^2/\text{s}$ during the day, than in May (1.5 to $2.5 \mu\text{mol}/\text{m}^2/\text{s}$). The assigned rates were in the same order of magnitude as those obtained from flask data of soil chamber measurements.

Diurnal variations of daytime assimilation (A) and nocturnal respiration (R_f) rates of foliage are presented in Figure 7.3. Here, foliage respiration rates are displayed as negative fluxes. Mid-day maxima of assimilation rates were slightly lower in May (6 to $7 \mu\text{mol}/\text{m}^2/\text{s}$) than in July (7 to $8 \mu\text{mol}/\text{m}^2/\text{s}$). In both months, nocturnal respiration rates were between 0.5 and $1 \mu\text{mol}/\text{m}^2/\text{s}$, and similar for all branch bags. Averaging assimilation rates removed most scatter on time scales of one hour, but it should be noted that differences between bags were substantial at day-times. In both months, assimilation rates were generally slightly higher in the top1 than in the top3 branch bag. Even higher assimilation rates were measured in the mid bag in May, where a maximum assimilation rate of $12.5 \mu\text{mol}/\text{m}^2/\text{s}$ was observed at noon on the third day. Due to technical difficulties on the May sampling day, data from the top1 branch bag were excluded from calculation of average assimilation rates between 6:40 and 9:40.

Figure 7.4 shows fluxes of CO_2 exchange within a column of canopy air over three days starting with sampling periods in May and July 2001. Biological fluxes contributing to net ecosystem exchange of CO_2 in canopy air were photosynthesis and soil respiration during the day and foliage and soil respiration at night. Day-time dark respiration by foliage was included in net rates of assimilation. The average tree height, 10 m , was used as the height of the well mixed column of canopy air. The total canopy leaf area index was estimated to be $6 \text{ m}^2/\text{m}^2$. The canopy was assumed to consist of an upper and a lower layer, each containing 50% of the canopy leaf area. The upper half of the canopy leaf area was assigned average gas exchange rates obtained from the top and middle branch bags (see thick lines in Figure 7.3). Pooled data from measurements in

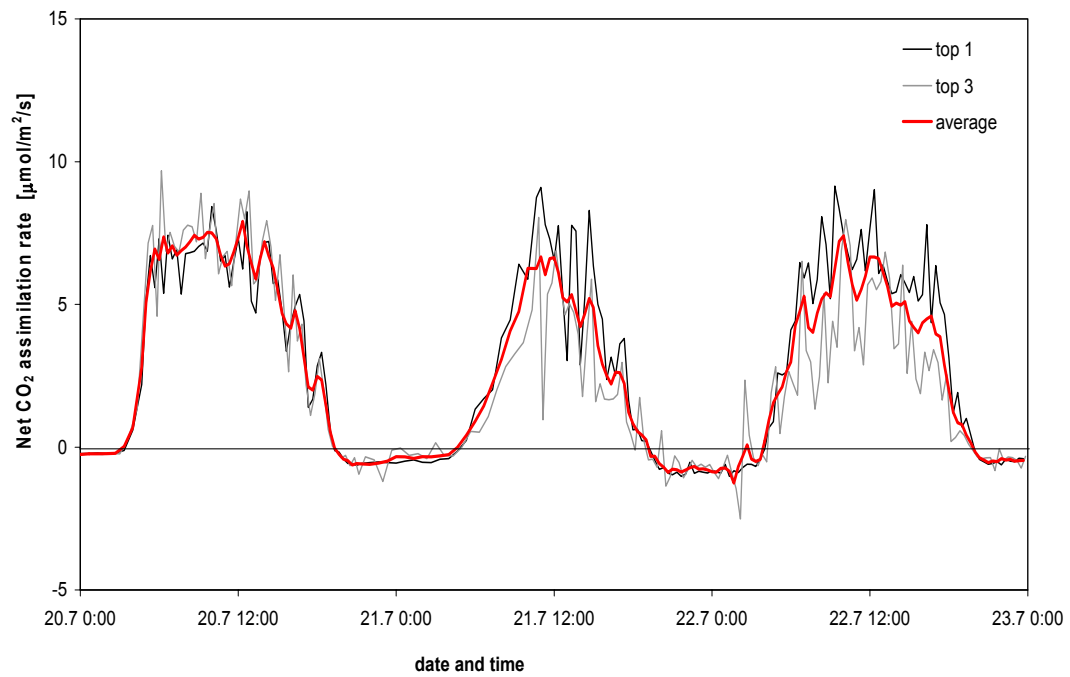
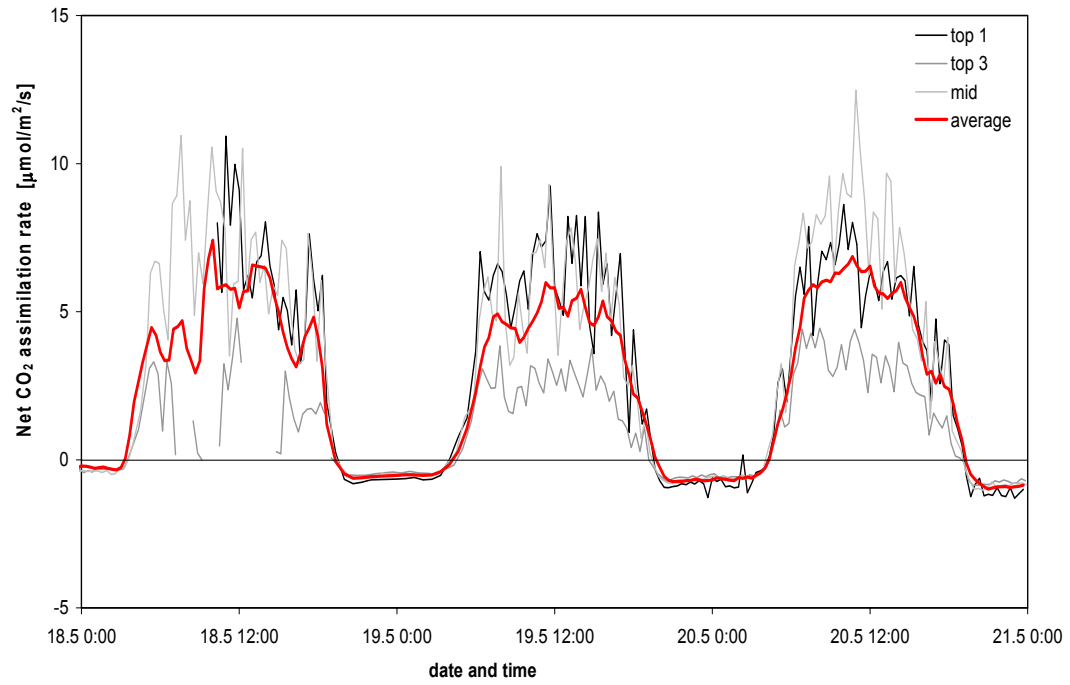


Figure 7.3: Rates of foliage daytime assimilation and nocturnal respiration of CO₂ from branch bag measurements, separate bags and averages, in May (top) and July (bottom) 2001.

July 2000 indicated that photosynthetic rates of branches lower in the canopy were $24 \pm 13\%$ of upper canopy rates. Accordingly, gas exchange rates in the lower half of the canopy were derived as a percentage of those in the upper half of the canopy. Foliage gas exchange rates were thus effectively obtained by scaling average top branch bag rates by a leaf area of approximately $4 \text{ m}^2/\text{m}^2$. Maximum rates of canopy photosynthesis on a ground area basis were 22 to 25 $\mu\text{mol}/\text{m}^2/\text{s}$ in May and 24 to 28 $\mu\text{mol}/\text{m}^2/\text{s}$ in July. Stem and branch respiration were neglected and root respiration is implicitly included in soil respiration. Net ecosystem exchange consisted of two fluxes, a storage flux of temporal changes in CO_2 inventory of canopy air and a net flux, F_n , of turbulent exchange with air outside of the canopy. The derived net turbulent exchange fluxes (F_n derived) were calculated from all other exchange components using the mass balance of equation 7.1. For comparison, the net fluxes of turbulent exchange obtained from continuous measurements over two days at a nearby eddy tower are also shown.

Day-time magnitudes and variations of derived net turbulent exchange fluxes were mainly determined by those of photosynthetic fluxes. In comparison, soil respiration fluxes were more uniform over time, and changes in CO_2 inventory of canopy air were neglectably small at most times except at dawn on the sampling days and during the third night in July. Resulting derived mid-day net turbulent exchange fluxes were generally smaller in May and on the second July day ($\approx 20 \mu\text{mol}/\text{m}^2/\text{s}$) than on the other two July days ($\approx 25 \mu\text{mol}/\text{m}^2/\text{s}$). Integrated daily rates (over 24 hours) of derived net turbulent exchange fluxes were -0.74, -0.57 and -0.64 $\text{mol}/\text{m}^2/\text{day}$ for the three days in May, and -0.84, -0.33 and -0.64 $\text{mol}/\text{m}^2/\text{day}$ for the three days in July, respectively.

The derived rates of net turbulent exchange of CO_2 were in reasonable agreement with those obtained from eddy flux measurements. In both months, net CO_2 fluxes from the eddy tower were smaller than those derived from the mass balance of integrated canopy exchanges. The shapes of derived and observed net exchange fluxes were in good agreement for the first day in May and the second day in July. However, the derived curve did not show the observed strong positive flux of CO_2 ($\approx 10 \mu\text{mol}/\text{m}^2/\text{s}$) leaving the canopy at dawn on the second day in May, and derived rates were two to four times as large as observed rates during the morning of the first July day. Total daily rates of net turbulent exchange from eddy flux data were -0.57 and -0.36 $\text{mol}/\text{m}^2/\text{day}$ on the first and second day in May, and -0.38 and -0.10 $\text{mol}/\text{m}^2/\text{day}$ on the first and second day in July, i.e. one third to half of the total daily rates derived from canopy integrations.

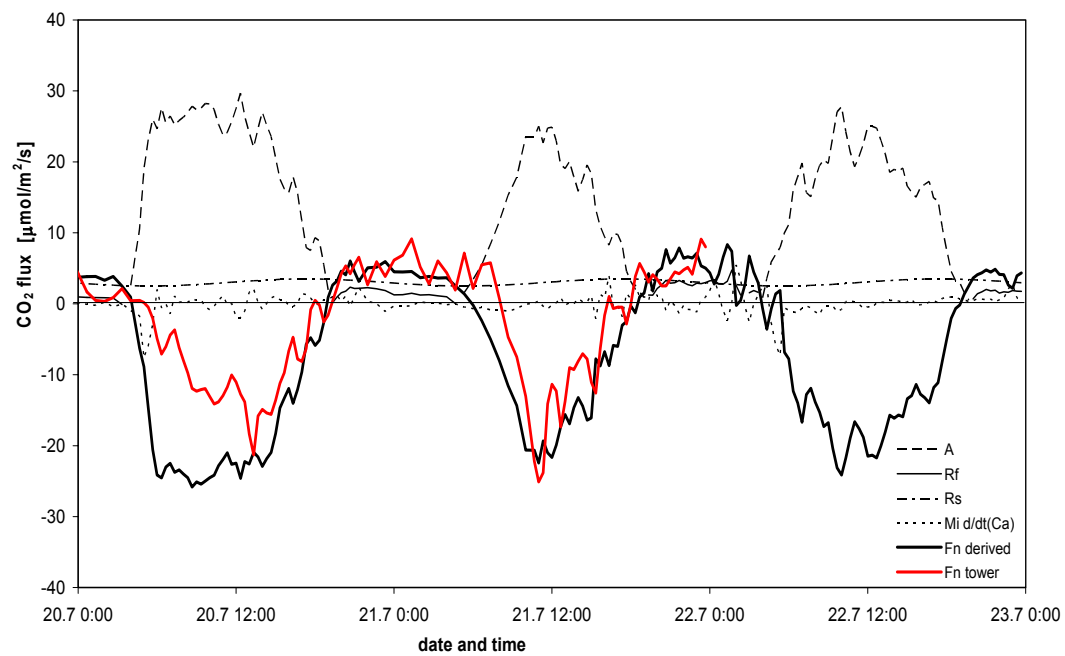
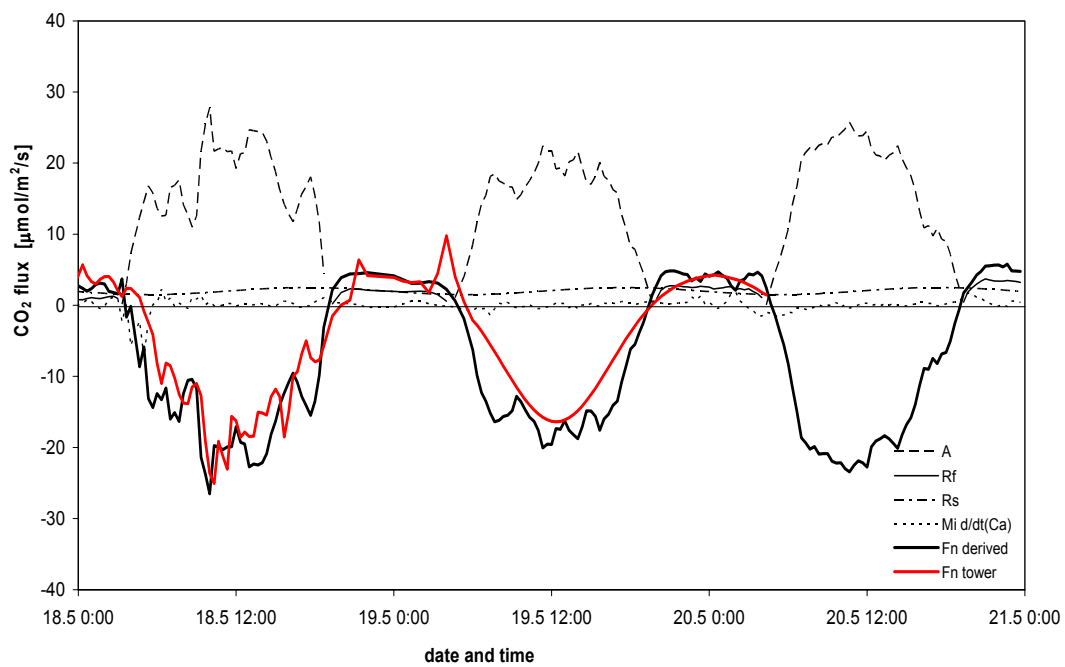


Figure 7.4: CO₂ fluxes contributing to net ecosystem exchange of canopy air in May (top panel) and July (bottom panel) 2001. Fluxes of turbulent exchange derived from mass balances for 3 days and obtained from measurements at a nearby eddy tower for 2 days.

7.2 $\delta^{13}\text{C}$ of canopy CO_2 exchange

The top panel of Figure 7.5 shows diurnal variations in the $\delta^{13}\text{C}$ composition of CO_2 in canopy air ($\delta^{13}\text{C}_i$) for separate branch bags over three days starting with sampling periods in May and July 2001. Continuous values were derived from a regression of isotopic composition versus mole fraction of CO_2 constructed from flask data obtained from open branch bags (correlation coefficients $R^2 > 0.9$). Flask measurements of $\delta^{13}\text{C}$ of CO_2 obtained from air samples of open branch bags are shown for comparison. Thick lines indicate again average $\delta^{13}\text{C}$ values calculated from all branch bags. Average $\delta^{13}\text{C}_i$ values at night were more depleted in July (-8.9 to -10.7 ‰) than in May (-8.8 to -9.6 ‰), and day-time values were more enriched in July (-6.5 to -6.8 ‰) than in May (-7.6 to -7.9 ‰). Diurnal changes were thus larger in July than in May. Flask and continuous data were in reasonably good agreement.

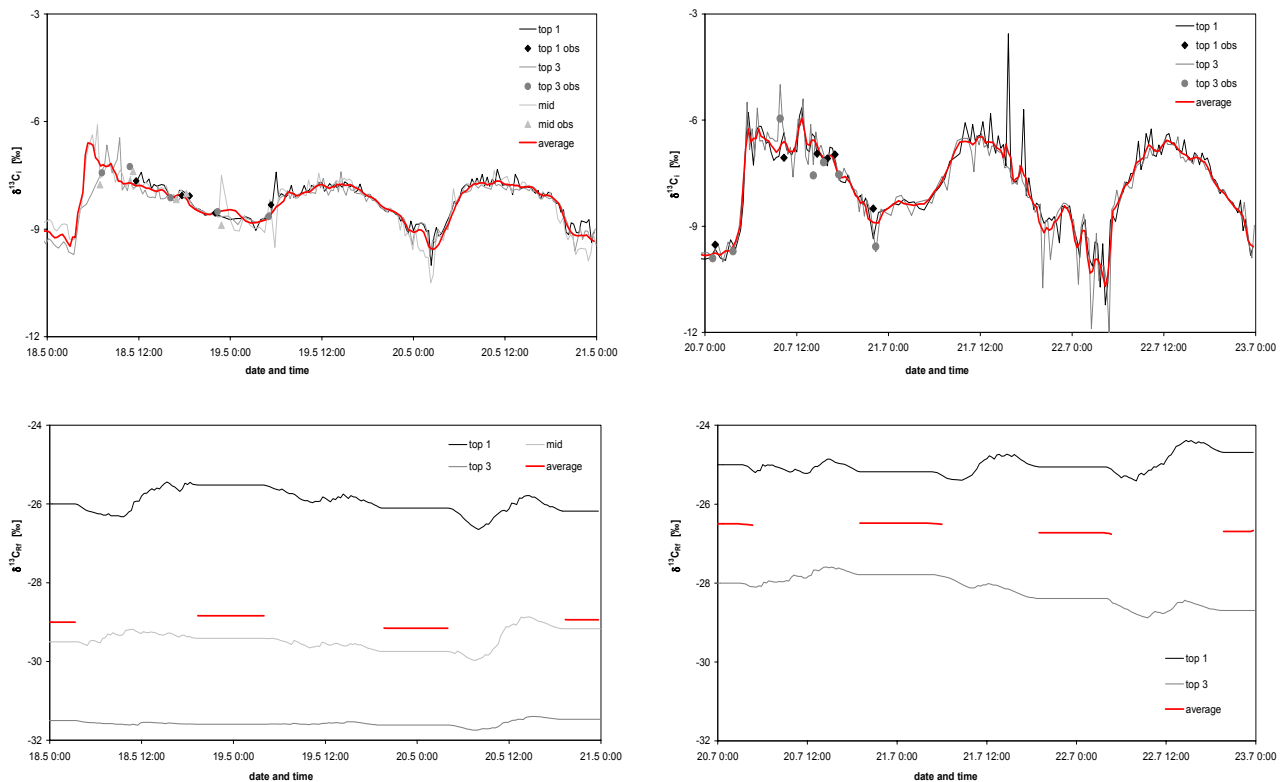


Figure 7.5: Diurnal changes over three days in May (left) and July (right) 2001. Top: $\delta^{13}\text{C}_i$ of CO_2 in canopy air. Bottom: $\delta^{13}\text{C}_{\text{RF}}$ of foliage respiration at night, both for separate branch bags and averages.

The lower panel of Figure 7.5 presents isotopic signatures of foliage respiration used for nocturnal respiration isofluxes, $\delta^{13}\text{C}_{\text{Rf}}$, for separate branch bags and for flux rate weighted averages over three days in May and July 2001. $\delta^{13}\text{C}_{\text{Rf}}$ values were calculated assuming a constant size of the soluble carbohydrate pool of 500 mmolC/m² in foliage,

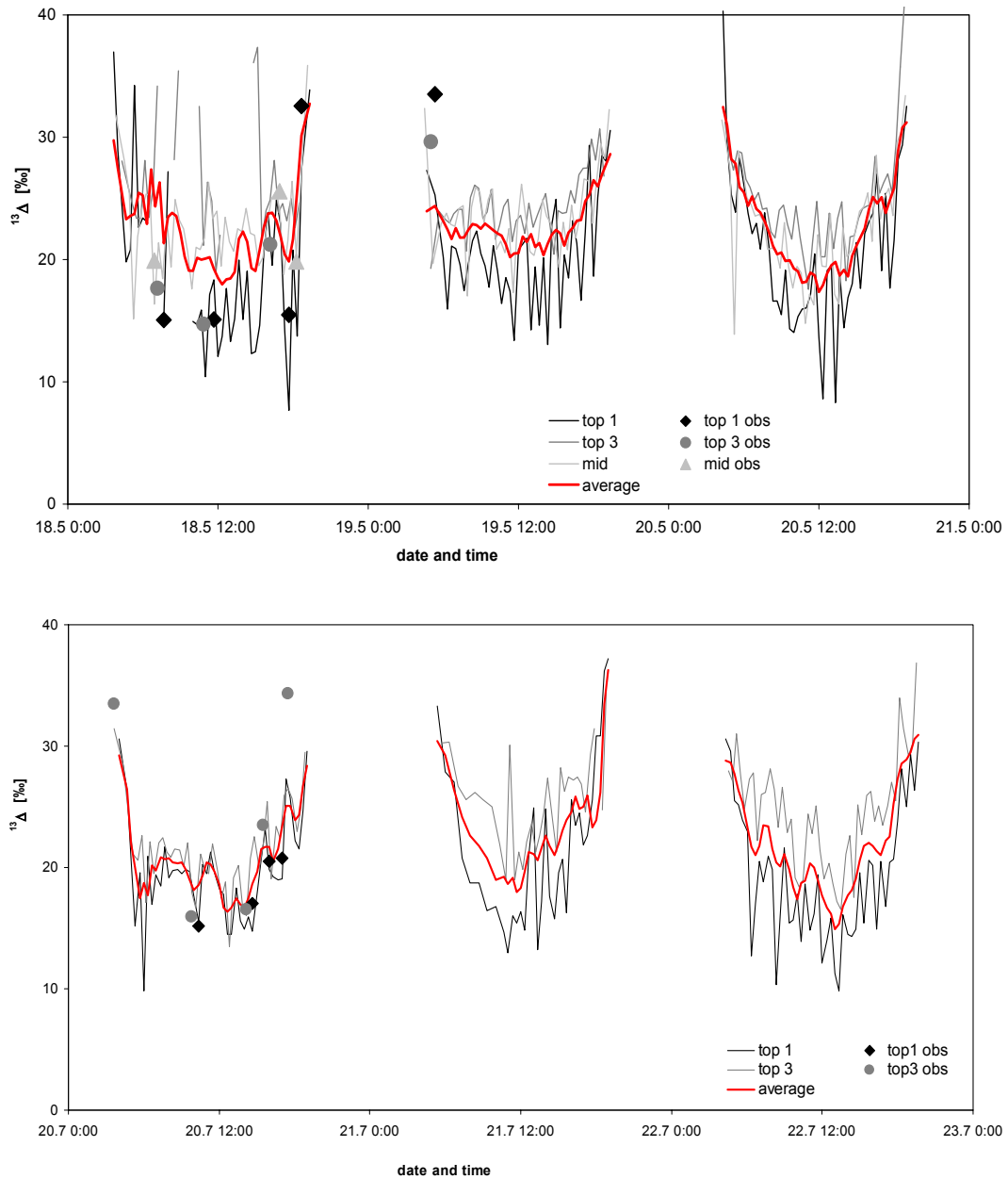


Figure 7.6: Diurnal cycle of discrimination for single branch bags and smoothed average over three days starting with sampling periods in May and July 2001.

equivalent to average turnover times of two days (same as solid lines in Figure 3.9). Calculations of $\delta^{13}\text{C}_{\text{Rf}}$ of dark respiration from foliage are detailed in section 3.2. Here, average values of $\delta^{13}\text{C}_{\text{Rf}}$ used for nocturnal foliage respiration were -29.0 ‰ in May and -26.3 ‰ in July, with only small variations between nights of 0.2 ‰ in May, 0.5 ‰ in July. The isotopic signature of soil respired CO_2 , $\delta^{13}\text{C}_{\text{Rs}}$, was taken as constant using average values from soil chamber measurements, -29.6 ‰ in May and -29.0 ‰ in July.

Diurnal cycles of ^{13}C discrimination (from the full formulation of equation 3.9), $^{13}\Delta$, are shown in Figure 7.6 for separate branch bags and averages over three days following sampling periods in May and July 2001. For comparison, observed values of $^{13}\Delta$ from flask measurements are also shown. Average values of ^{13}C discrimination had maxima of around 30 ‰ and higher at dawn and dusk on all days, and were lower during the rest of the day, 17 to 20 ‰ in May and 15 to 18 ‰ in July. These changes resulted in pronounced diurnal amplitudes of 10 to 15 ‰, except during the sampling day in May, when values varied by up to 12 ‰ within short time periods of one hour. Effects of concurrent photorespiration and day-time dark respiration on isotopic gas exchange during photosynthesis have been included in the $^{13}\Delta$ calculations. Theory and results of $^{13}\Delta$ calculations have already been detailed in section 3.1.

Isofluxes for ecosystem CO_2 exchange for a column of canopy air, $\delta^{13}\text{C}_{\text{flux}} \times \text{flux}$ (‰ $\mu\text{mol}/\text{m}^2/\text{s}$), combined from $\delta^{13}\text{C}$ signatures of fluxes as described above and flux rates as described in section 7.1, are presented in Figure 7.7 over three days following sampling periods in May and July 2001. Respiration fluxes and storage fluxes caused by temporal changes in $\delta^{13}\text{C}$ values of CO_2 in canopy air varied somewhat but were relatively small compared to mid-day photosynthetic isofluxes. Isofluxes of photosynthesis had positive signs as both isotopic signature ($^{13}\Delta$) and rates of assimilation have positive values. Contributions of concurrent photorespiration and day-time dark respiration were included in photosynthetic isofluxes via their influences on $^{13}\Delta$. Following equation 7.2, $(\delta^{13}\text{C}_o - \delta^{13}\text{C}_i)F_o$ was thus calculated from the mass balance of all other exchange components.

Maximum photosynthetic isofluxes were 500 to 550 ‰ $\mu\text{mol}/\text{m}^2/\text{s}$ in May, slightly less than in July with 500 to 600 ‰ $\mu\text{mol}/\text{m}^2/\text{s}$. Photosynthetic isofluxes primarily determined magnitudes and variations of one-way turbulent exchange isofluxes. Maximum isofluxes of one-way turbulent exchange were smaller in May (-430 to -470 ‰ $\mu\text{mol}/\text{m}^2/\text{s}$) than on

two of the July days (-450 to -560 ‰ $\mu\text{mol}/\text{m}^2/\text{s}$) but comparable to those on the second day in July (≈ -440 ‰ $\mu\text{mol}/\text{m}^2/\text{s}$). Daily integrated one-way turbulent isofluxes were also smallest on that day (-7.3 ‰ $\text{mol}/\text{m}^2/\text{day}$), only about half of those in May (-15.9, -13.0 and -13.7 ‰ $\text{mol}/\text{m}^2/\text{day}$) and the other two July days (-16.6 and -12.8 ‰ $\text{mol}/\text{m}^2/\text{day}$).

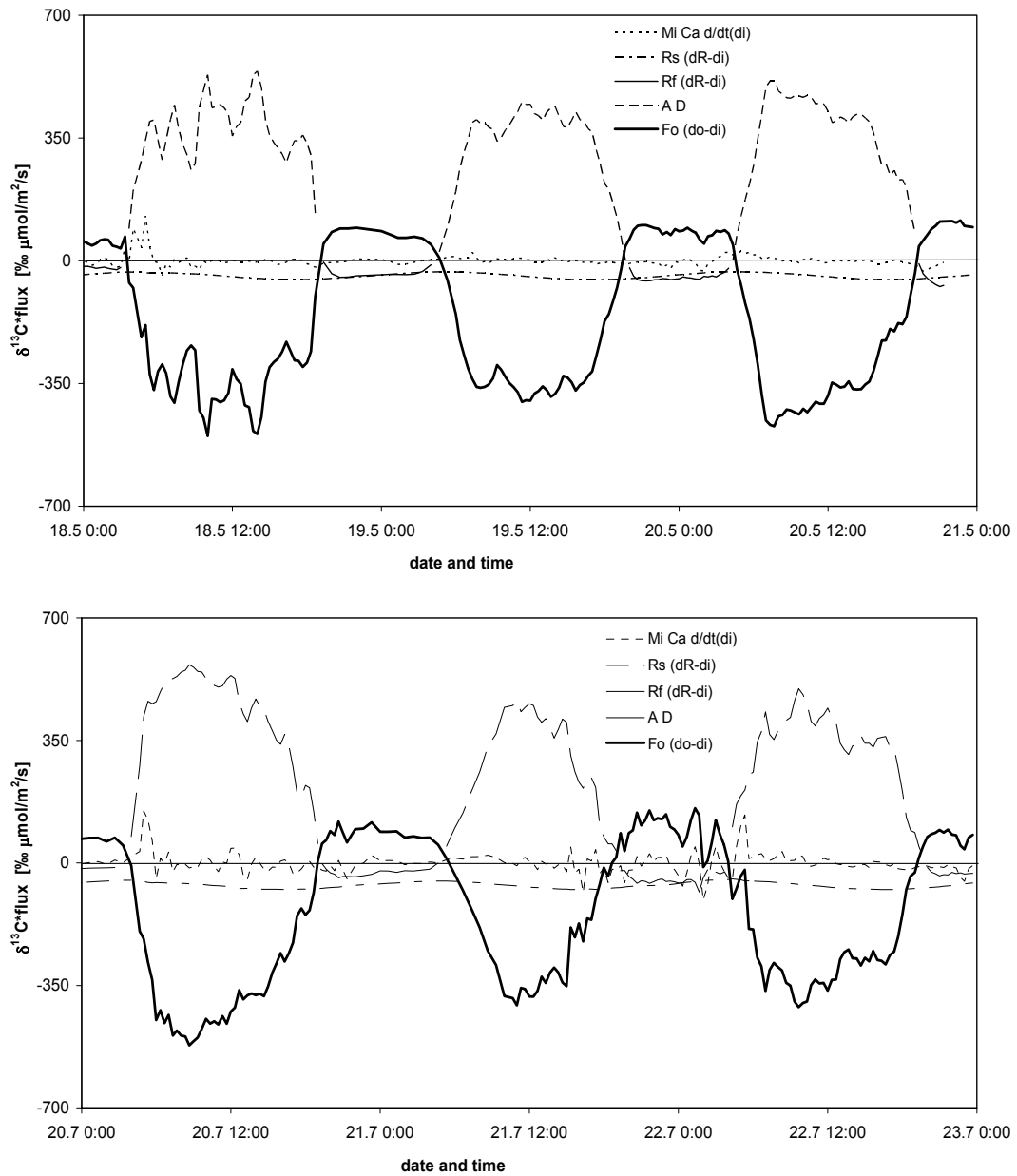


Figure 7.7: Diurnal cycles of isofluxes of $\delta^{13}\text{C}$ signatures of fluxes multiplied with CO_2 flux rates within canopy air in May and July 2001.

7.3 $\delta^{18}\text{O}$ of canopy CO_2 exchange

The top panel of Figure 7.8 presents diurnal changes in $\delta^{18}\text{O}$ of CO_2 in canopy air ($\delta^{18}\text{O}_i$) for separate branch bags over three days following sampling periods in May and July 2001. Flask measurements of $\delta^{18}\text{O}$ of CO_2 from air samples of open branch bags used to derive time courses of continuous values are also shown for comparison. Regressions of $\delta^{18}\text{O}_i$ versus the inverse of the CO_2 mole fraction from open branch bag flask data (R^2 of 0.91 in May, but only 0.53 in July) were not as reliable as those used to derive $\delta^{13}\text{C}_i$ values. This might reflect partly apparent enrichments in $\delta^{18}\text{O}_i$ of flask samples not correlated to changes in ^{18}O content of CO_2 but caused by some other unidentified compound (see section 4.2 for details). Average $\delta^{18}\text{O}_i$ values calculated from all branch bags are indicated by thick lines. In July, regressed $\delta^{18}\text{O}_i$ values were more enriched at night (0.3 to 0.8 ‰) and during the day (1.6 ‰) than in May (-0.3 to 0.2 ‰ and 1.0 ‰), with similar diurnal amplitudes of around 1 ‰ in both months.

Isotopic signatures assigned to soil respired CO_2 , $\delta^{18}\text{O}_{\text{RS}}$, for May and July are presented in the middle panel of Figure 7.8, including values from soil chamber measurements (soil 1 and soil 2) as described in section 4.2. The influence of atmospheric invasion was included in assigned $\delta^{18}\text{O}_{\text{RS}}$ values, leading to effective diurnal cycles of $\delta^{18}\text{O}_{\text{RS}}$ of soil respired CO_2 . Continuous data was derived assuming sinusoidal diurnal variations similar to those of CO_2 flux rates of soil respiration, with the same phasing. Diurnal amplitudes were larger in July, ranging from -22 to -14 ‰, and smaller but with similar minima in May, ranging from -22 to -17 ‰.

Isotopic signatures of nocturnal foliage respiration isofluxes, $\delta^{18}\text{O}_{\text{Rf}}$, are presented in the bottom panel of Figure 7.8 for separate branch bags and averages over three days in May and July 2001. $\delta^{18}\text{O}_{\text{Rf}}$ values were calculated assuming foliage respired CO_2 to have an isotopic signature in temperature dependent equilibrium with foliage water at the evaporating sites, $\delta^{18}\text{O}_{\text{E}}$, from the non steady state (NSS) formulation as described in section 4.1. Because $\delta^{18}\text{O}_{\text{E}}$ values were derived taking the influence of foliage transpiration into account, average values of $\delta^{18}\text{O}_{\text{Rf}}$ decreased throughout the night, with starting values determined by the degree of isotopic enrichment of foliage water during the day. $\delta^{18}\text{O}_{\text{Rf}}$ values were between 0.5 and 15 ‰ in May and -4 to 12 ‰ in July.

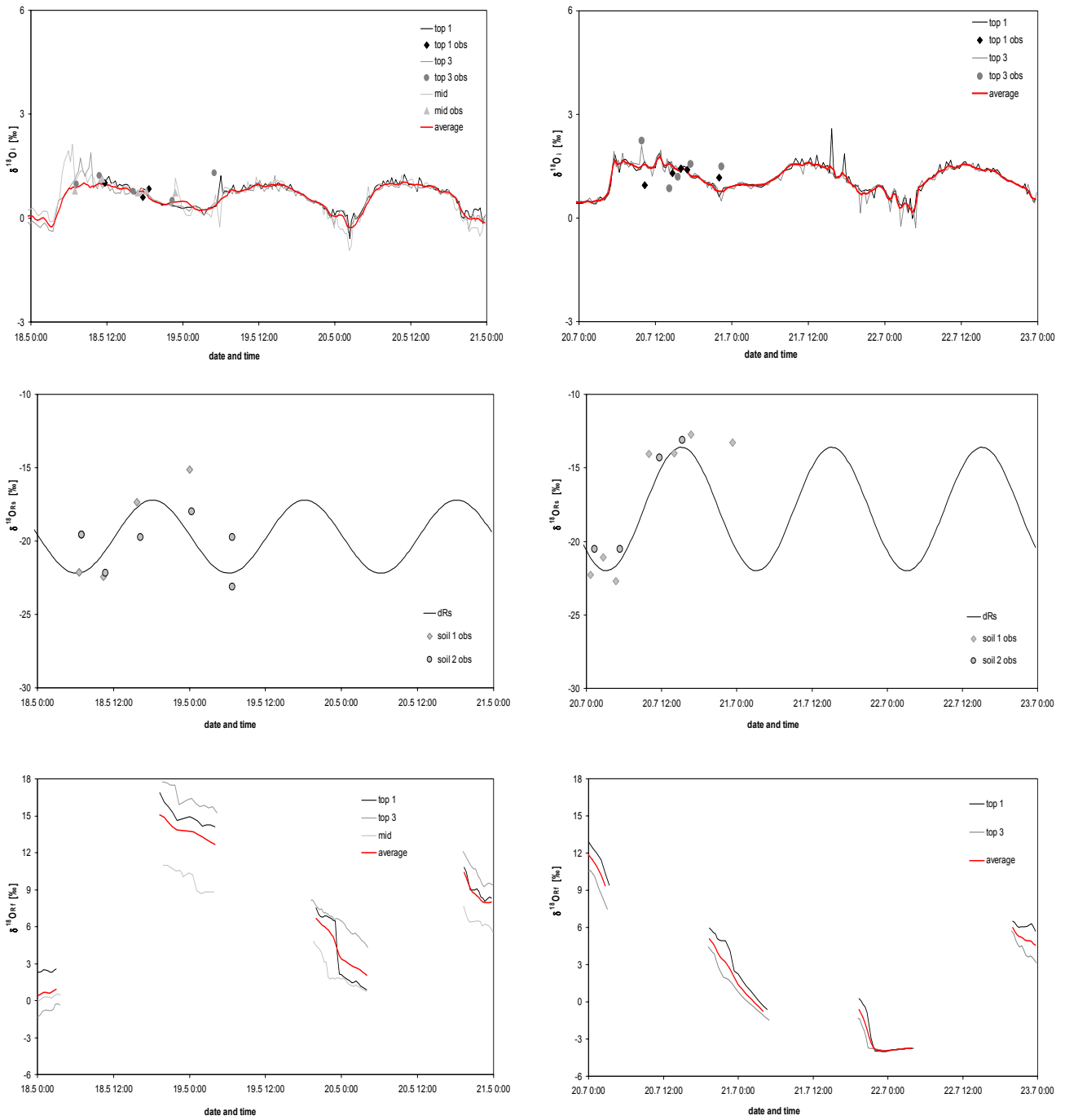


Figure 7.8: Diurnal changes over the course of three days following sampling campaigns in May (left) and July (right) 2001. Top: $\delta^{18}O_i$ of CO_2 in canopy air for separate branch bags and averages with some observations. Middle: $\delta^{18}O_{Rs}$ of soil respiration with some observations. Bottom: $\delta^{18}O_{Rf}$ of foliage respiration at night for separate branch bags and averages.

Figure 7.9 presents diurnal cycles of ^{18}O discrimination (from NSS formulation), $^{18}\Delta$, for separate branch bags and averages over three days in May and July 2001. $^{18}\Delta$ values from flask measurements are also shown for comparison. Average values of ^{18}O discrimination showed pronounced diurnal cycles, with extreme dawn and dusk values of 90 to 120 ‰ in May and -60 to -100 ‰ or 60 to 130 ‰ in July. During the rest of the day, $^{18}\Delta$ generally ranged from 25 to 35 ‰ in May, fluctuating by 20 ‰ on the sampling day, whereas $^{18}\Delta$ was gradually increasing from 10 to 30 ‰ on the first day, between -20 and 10 ‰ during the second day and steeply increasing from -10 to 40 ‰ over the course of the third day in July. Theory and results of $^{18}\Delta$ calculations have already been detailed in section 4.1.

Figure 7.10 shows derived oxygen isofluxes, $\delta^{18}\text{O}_{\text{flux}} \times \text{flux}$ (‰ $\mu\text{mol}/\text{m}^2/\text{s}$), over three days following sampling periods in May and July 2001. Analogous to $\delta^{13}\text{C}$, isofluxes of $\delta^{18}\text{O}$ have been derived from combined $\delta^{18}\text{O}$ signatures of fluxes as described above and flux rates as described in section 7.1. Isofluxes of soil respiration had negative signs because of negative $\delta^{18}\text{O}$ signatures of soil water transferred to $\delta^{18}\text{O}_{\text{Rs}}$ values of soil respired CO_2 . Isofluxes of nocturnal foliage respiration had positive or negative signs depending on whether foliage water was more or less enriched in ^{18}O than ambient CO_2 . Storage fluxes from changes in $\delta^{18}\text{O}_i$ of CO_2 in canopy air were around zero. Oxygen isofluxes of photosynthesis had mostly positive signs as enrichment through transpiration resulted in mostly positive isotopic signatures of foliage water, and hence $^{18}\Delta$. Negative photosynthetic isofluxes were determined in the mornings of the second and third day in July. Thus, $(\delta^{18}\text{O}_o - \delta^{18}\text{O}_i)F_o$ was calculated from all other exchange components using the mass balance of equation 7.2. Magnitudes and variations of one-way turbulent exchange isofluxes were mainly determined by diurnal patterns of photosynthetic isofluxes.

Maximum photosynthetic isofluxes were around 1000 ‰ $\mu\text{mol}/\text{m}^2/\text{s}$ in May, and only around 600 ‰ $\mu\text{mol}/\text{m}^2/\text{s}$ in July. Maximum isofluxes of one-way turbulent exchange were much larger in May (-700 to -900 ‰ $\mu\text{mol}/\text{m}^2/\text{s}$) than in July (-200 to -500 ‰ $\mu\text{mol}/\text{m}^2/\text{s}$). Daily integrated derived one-way turbulent isofluxes (over 24 hours) were much higher in May (-29.0, -29.1 and -27.2 ‰ $\text{mol}/\text{m}^2/\text{day}$) than on the first and third day in July (-18.2 and -8.8 ‰ $\text{mol}/\text{m}^2/\text{day}$) and smallest on the second July day (-2.2 ‰ $\text{mol}/\text{m}^2/\text{day}$).

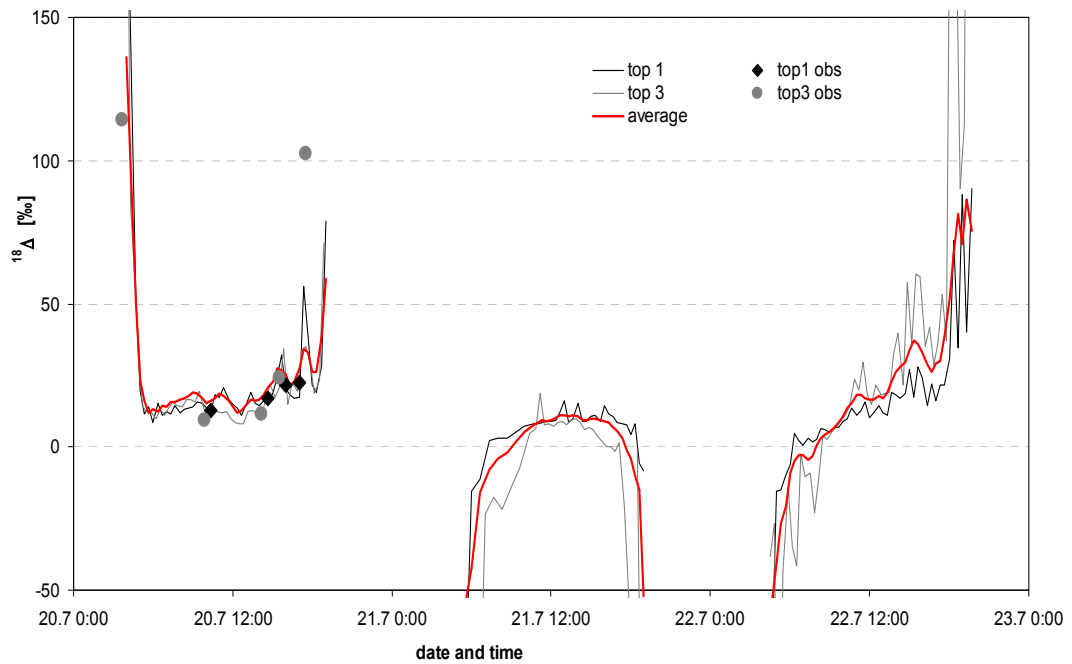
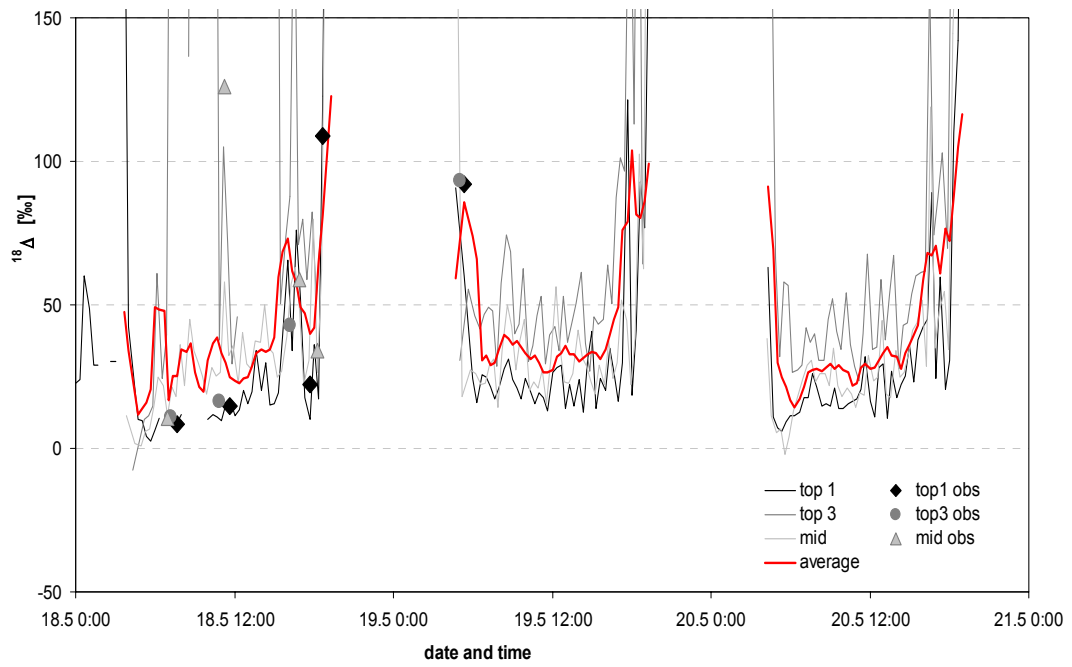


Figure 7.9: Diurnal cycles of ^{18}O discrimination for separate branch bags and averages over three days starting with sampling periods in May and July 2001.

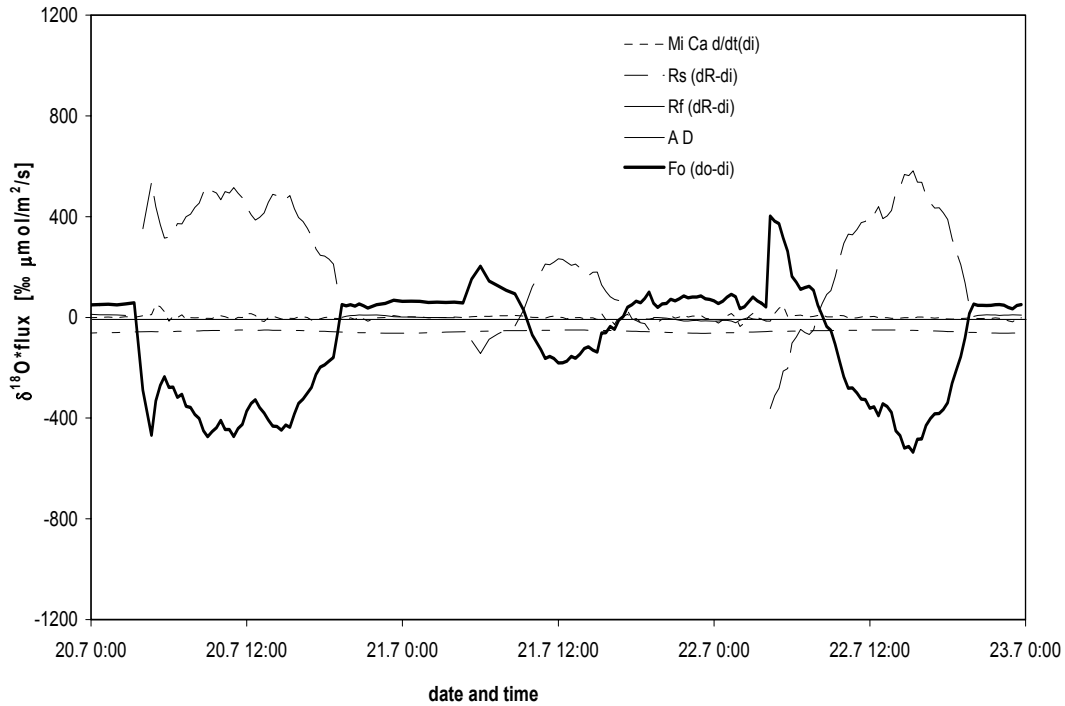
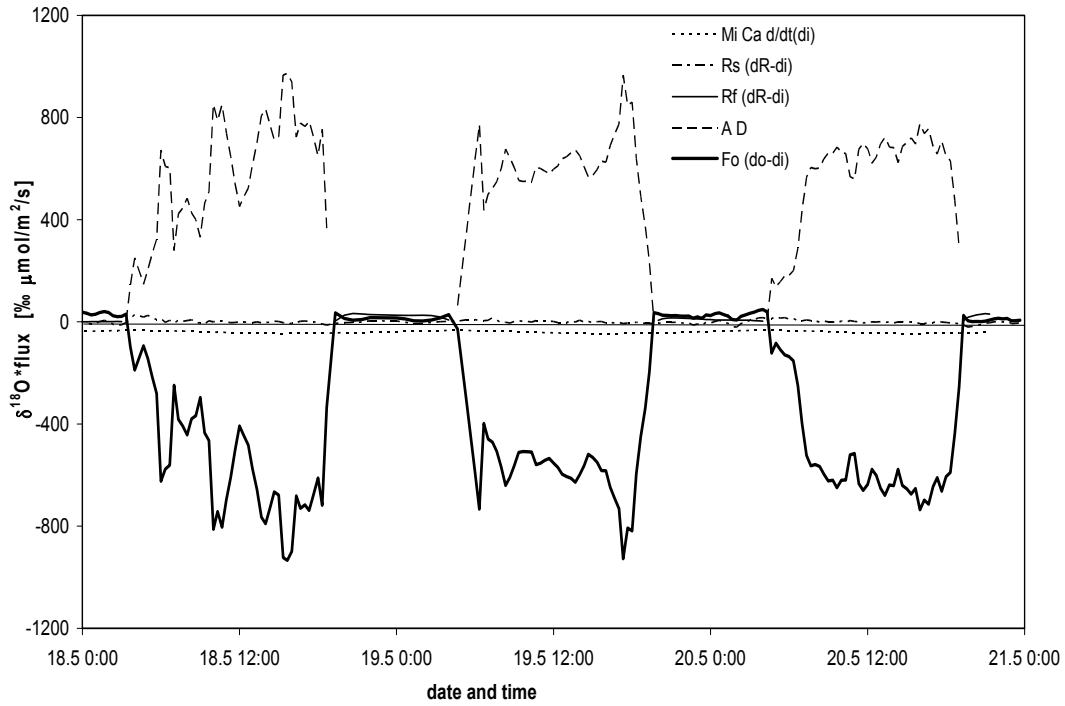


Figure 7.10: Diurnal changes in isofluxes ($\delta^{18}\text{O}_{\text{flux}} \times \text{CO}_2$ flux rates) of ecosystem CO₂ exchange over the course of three days following sampling campaigns in May and July 2001.

Discussion

Diurnal changes of assimilation and respiration fluxes of CO₂ scaled to the canopy level resulted in predicted diurnal variations in net ecosystem exchange of CO₂ comparable to results from previous studies using chamber or eddy flux methods. Peak rates of photosynthesis (22 - 28 μmol/m²/s) and respiration (4 - 6 μmol/m²/s) were in the same range as those observed in another Sitka spruce plantation in Scotland, 10 - 25 μmol/m²/s and up to 7 μmol/m²/s, respectively (Beverland et al. 1996). The daily variability of assimilation and net exchange fluxes were also similar to those reported for a pine forest in central Siberia although their overall magnitudes were smaller (Lloyd et al. 2001, Lloyd et al. 2002).

Derived fluxes of net turbulent CO₂ exchange showed similar diurnal patterns but were generally stronger than fluxes calculated from eddy covariance data obtained from a nearby tower. The general overestimation of net exchange fluxes in canopy integrations could have been caused by an overestimation of the canopy leaf area. Another factor limiting the accuracy of derived net exchange rates is the scaling of photosynthetic fluxes, i.e. the proportions of the canopy leaf area assigned to the upper and lower canopy layers. Here, no distinction was made between sun and shade layers of the canopy. The main reason for this was that all branch bags situated within the upper canopy layer (top and middle bags) had similar maximum and daily integrated assimilation rates although their environmental conditions were somewhat different on average (more direct light and lower relative humidity at the top of the canopy vs. more diffuse light and higher relative humidity just below the canopy top). However, employing a more refined light regime model to calculate assimilation rates in different parts of the canopy would certainly improve the accuracy of predictions of net exchange fluxes.

Discrepancies in the magnitude, shape and timing between derived and observed curves are probably mostly due to the fact that eddy flux measurements determine fluxes averaged over the footprint area of the tower (approximately 1 km²), whereas canopy integrations were calculated from localised branch bag measurements. Furthermore, potential influences of CO₂ advection could not be assessed with the 1 box model approach employed here. Also, the actual canopy height is unlikely to be the height of the well mixed air column during the day because of turbulent mixing of canopy air into the convective boundary layer. Additional offsets could arise from

differences in productivity, water or nutrient availability or penetration of sunlight at the two sites, as well as from errors in storage term calculations due to lack of vertical information on CO₂ mole fractions in canopy air. Errors in storage fluxes might have been particularly large at night and dawn as gradients in the CO₂ mole fraction of canopy air were neglected by extrapolating point measurements of the CO₂ mole fraction to the entire column. In conclusion, net turbulent fluxes of CO₂ exchange derived from eddy data might not be representative for the local canopy CO₂ exchange calculated from integrations of gas exchange processes that were measured separately.

CO₂ fluxes, and thus the component isofluxes and the derived one-way turbulent isofluxes of ecosystem carbon isotopic exchange were about four times as large as those calculated for a boreal forest in Siberia, more comparable to those calculated for an Amazonian rain forest (Lloyd et al. 1996). Oxygen isofluxes of ecosystem exchange had similar magnitudes but very different overall diurnal patterns than those predicted for several boreal forest ecosystems in central Canada. This is largely due to differences in photosynthetic isofluxes, mostly because diurnal variability of C_i/C_a was not taken into account in the Canadian study (Flanagan et al. 1997).

Carbon isofluxes were less variable between different days and the two months than oxygen isofluxes, that had peak isofluxes about twice as large in May than in July. Also, diurnal cycles of oxygen isofluxes were more different in shape and had larger fluctuations than carbon isofluxes on all days. For example, oxygen isofluxes of turbulent exchange were negative at day-times in May and on the first July day, whereas they were positive in the morning and overall much smaller on the other two days in July. An example for the simultaneous use of both turbulent isofluxes in ecosystem studies will be given in section 9.

8. $\delta^{18}\text{O}$ of canopy O_2 exchange

Introduction

Analogous to the isotopic exchange of CO_2 described in sections 7.2 and 7.3, changes in the O_2 mixing ratio of air within the canopy are accompanied by variations in its oxygen isotope composition. Plant and soil respiration lower the O_2 mixing ratio of canopy air while at the same time discriminating against ^{18}O (Schleser 1979, Guy et al. 1989), thereby increasing its oxygen isotope composition. Photosynthesis releases O_2 into canopy air with an isotopic composition identical to that at the sites of its production (Stevens et al. 1975, Guy et al. 1993). This results in a decrease in the $\delta^{18}\text{O}$ of O_2 in canopy air if the enrichment in $\delta^{18}\text{O}$ of foliage water is below that of ambient O_2 , 23.8 ‰ (Kroopnick and Craig 1972, Horibe et al. 1973).

The expected concurrent changes in the O_2 mixing ratio and the $\delta^{18}\text{O}$ of O_2 due to photosynthetic and respiratory gas exchange during the closure periods of branch bags and soil chambers have already been described in section 6. Here, the integrated canopy exchange of O_2 and its $\delta^{18}\text{O}$ composition are estimated from gross O_2 fluxes and their $\delta^{18}\text{O}$ signatures predicted from theory, over the same three day period in July already described in the previous chapter. The purpose of this simulation is to estimate the magnitude of the ecosystem Dole-Morita effect and the diurnal variations of $\delta^{18}\text{O}$ of O_2 in canopy air. Once the required analytical precision (see section 6) will be available for observations of concurrent fluctuations in the mixing ratio and the $\delta^{18}\text{O}$ of O_2 in canopy air, such observations may provide further constraints on ecosystem functioning.

Theory

Assuming constant ratios of O_2 : CO_2 exchange for photosynthesis and respiration and absence of net horizontal advection, temporal changes of O_2 mixing ratios in canopy air can be calculated from a mass balance equivalent to that of CO_2 (equation 7.1):

$$M_i \frac{d}{dt} O_a = -F_{nx} - R_{sx} - R_{fx} + A_x \quad (8.1)$$

where M_i (mol/m²) and O_a (μmol/mol) are mol of air per unit ground area and O₂ mixing ratios within a column of canopy air defined as for CO₂ in section 7. A_x , R_{fx} and R_{sx} (μmol/m²s) are the rates of O₂ evolution during photosynthesis and O₂ uptake during respiration by foliage and soil with the respective O₂ : CO₂ exchange ratios ($A_x = S_f A$, $R_{fx} = S_f R_f$, $R_{sx} = S_s R_s$). F_{nx} (μmol/m²s) is the net flux of O₂ into or out of the canopy, with an exchange ratio of S_n ($F_{nx} = -S_n F_n$). Here, all stoichiometric ratios are positive. Again, F_{nx} is the difference between two one-way fluxes, $F_{nx} = F_{iox} - F_{oix}$, of O₂ leaving (F_{iox}) and entering (F_{oix}) the column, where positive F_{nx} indicates a net O₂ flux leaving the canopy.

Temporal changes in $\delta^{18}\text{O}$ of O₂ in canopy air can be estimated from an isotopic mass balance approach similar to that for CO₂ isotopes (see sections 7.2 and 7.3):

$$M_i O_a \frac{d}{dt} (\delta^{18} O_{ix}) = (\delta^{18} O_{ox} - \delta^{18} O_{ix}) F_{oix} + (\delta^{18} O_c - \delta^{18} O_{ix}) H + R_{px} b_p + R_{dx} b_d + R_{sx} b_s \quad (8.2)$$

where $\delta^{18}\text{O}_{ix}$, $\delta^{18}\text{O}_{ox}$ and $\delta^{18}\text{O}_c$ (‰) are isotopic compositions of O₂ within the canopy, entering the canopy from outside and chloroplast water, respectively. b_d and b_p are discrimination factors of O₂ uptake by autotrophic and by photorespiration. b_s is discrimination by combined root respiration and microbial decomposition in soils. Note also that fractionation during O₂ diffusion into the soil might additionally impact the effective discrimination factor of soil respiration (Aggarwal and Dillon 1998, Angert et al. 2001). Discrimination during concurrent photo- and dark respiration needs to be weighted by the respective oxygen uptake rates. This in turn has to be taken into account in the gross rate of photosynthetic O₂ evolution, H , which can be expressed following Farquhar and von Caemmerer (1982) as:

$$H = A_x \frac{C_c + 2\Gamma^*}{C_c - \Gamma^*} + R_{dx} \quad (8.3)$$

$$R_{px} = \frac{3A_x\Gamma^*}{C_c - \Gamma^*} \quad (8.4)$$

where R_{px} and R_{dx} are the rates of O₂ uptake during photorespiration and day-time dark respiration ($R_{dx} = S_f R_d$), with the stoichiometric ratio of R_{dx} (and implicitly of R_{px}) assumed equal to that of A_x (see equations 3.4 and 3.10 for definition of Γ^* and C_c).

Ecosystem exchange of O₂

Figure 8.1 shows diurnal variations of O₂ fluxes ($\mu\text{mol}/\text{m}^2/\text{s}$) that contribute to oxygen exchange within the canopy over three days following the sampling period in July 2001. The stoichiometric O₂ : CO₂ exchange ratios were assigned values as observed from canopy air and branch bag measurements reported in section 5. O₂ fluxes of photosynthesis and respiration were calculated from the respective CO₂ fluxes assuming stoichiometric O₂ : CO₂ exchange ratios of 1.2 for photosynthesis and foliage respiration and 1.1 for soil respiration. Temporal changes in the O₂ mixing ratio, $d/dt(O_a)$, were calculated as inverse of changes in the CO₂ mixing ratio, $d/dt(C_a)$, with an O₂ : CO₂ exchange ratio of 1.0 assumed for canopy air, estimated from open sample measurements. F_{nx} was calculated as a residual from the mass balance (equation 8.1).

Because they are stoichiometrically linked, derived diurnal patterns of O₂ exchange were very similar to those of CO₂ exchange. During the day, F_{nx} fluxes had maxima at $\approx 30 \mu\text{mol}/\text{m}^2/\text{s}$, while nocturnal F_{nx} fluxes were in the order of 5 to 10 $\mu\text{mol}/\text{m}^2/\text{s}$. The net turbulent fluxes of O₂ out of the canopy were 3 to 10 $\mu\text{mol}/\text{m}^2/\text{s}$ lower than the photosynthetic O₂ production within the canopy. Most of the variability in this difference

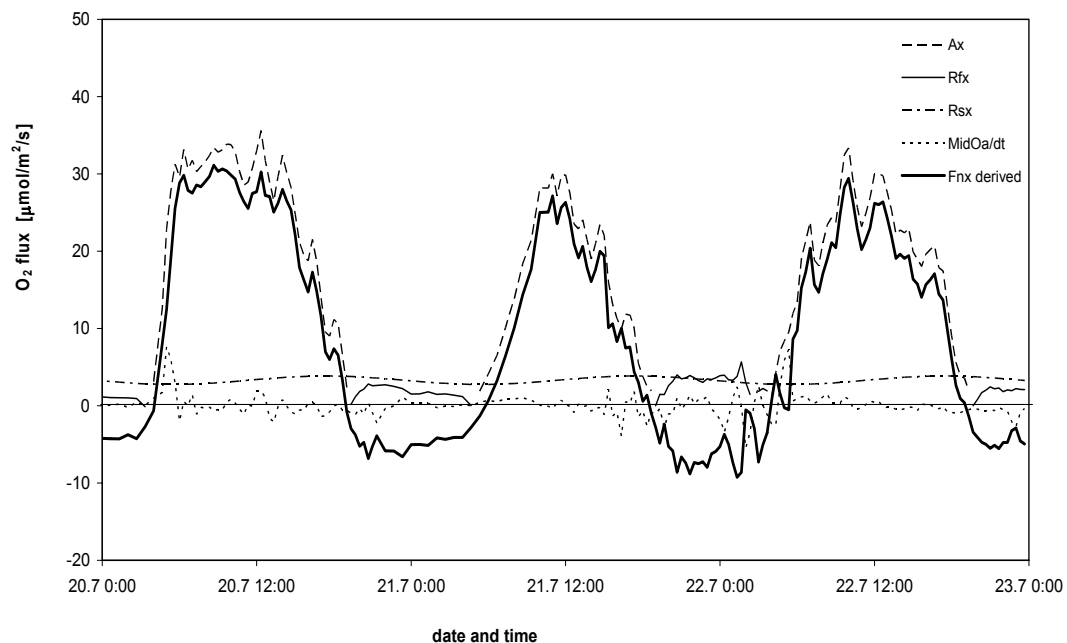


Figure 8.1: O₂ fluxes contributing to ecosystem O₂ exchange of canopy air over three days in July 2001.

is caused by fluctuations in the O_2 inventory of canopy air. Similar to CO_2 fluxes, total daily F_{nx} (integrated over 24 hours) was largest on the first, the sampling day ($1.0 \text{ mol/m}^2/\text{day}$), smallest on the second ($0.4 \text{ mol/m}^2/\text{day}$) and larger again on the third day ($0.8 \text{ mol/m}^2/\text{day}$). In contrast to CO_2 fluxes, the net turbulent flux F_{nx} had positive values during the day, i.e. net O_2 fluxes were directed outwards from the canopy air column. The predicted stoichiometric ratio of net turbulent exchange fluxes was derived from the ratio of $-F_{nx}$ to F_n . It was close to 1.2 during the day and around 1.15 at night.

Figure 8.2 illustrates how the concurrent temporal variations of O_2 and CO_2 mixing ratios in canopy air could form a hysteresis curve over the full diurnal cycle, for two days in July 2001. The stoichiometric $O_2 : CO_2$ exchange ratios applied were 1.2 for photosynthesis and foliage respiration and 1.15 for soil respiration. Here, F_{nx} was also assigned a constant $O_2 : CO_2$ exchange ratio. Thus, the net turbulent O_2 exchange flux was calculated with a stoichiometric ratio of 1.22 from the net turbulent CO_2 exchange flux. The storage flux, $M_d/dt(O_a)$, was then calculated as residual flux from the mass balance (equation 8.1). Temporal changes in the O_2 mixing ratio, $d/dt(O_a)$, were subsequently calculated from this residual flux, i.e. from the changes in canopy storage.

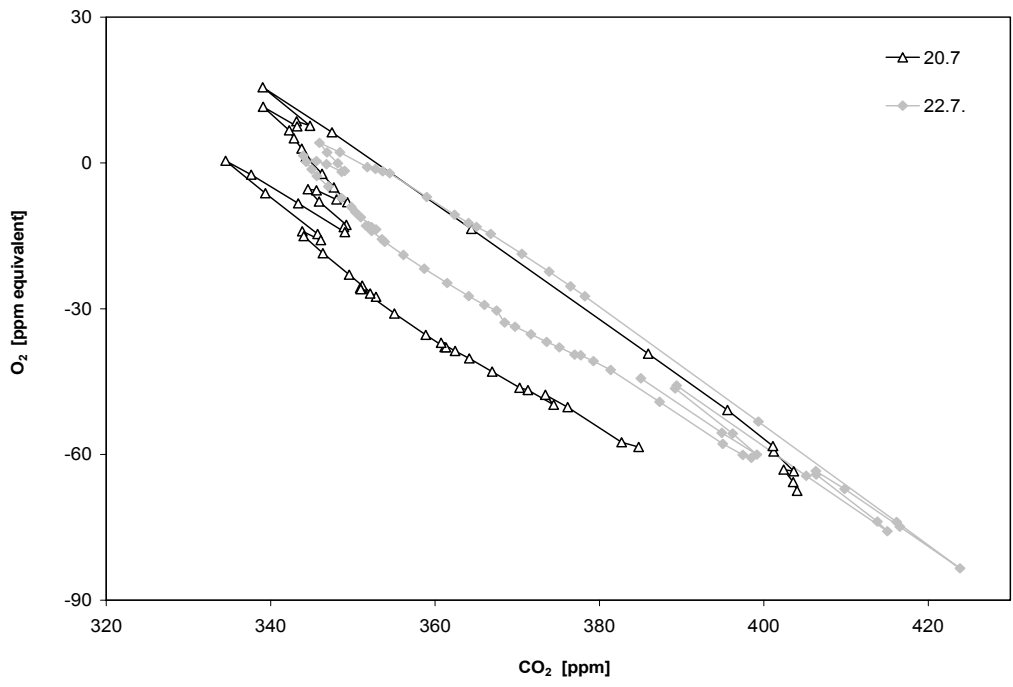


Figure 8.2: Hysteresis curves of O_2 vs. CO_2 mixing ratios over 24 h in canopy air for two days in July 2001.

The hysteresis loops of O₂ : CO₂ mixing ratios over time are caused by differences in the phasing of canopy O₂ fluxes with different stoichiometric ratios. The O₂ : CO₂ mixing ratios move anticlockwise along the hysteresis loops. The spread of the loops is only about half as wide on 22. July as on 20. July, although the stoichiometric ratios of the fluxes are the same. A geometric mean regression over all values of the diurnal cycle yields O₂ : CO₂ exchange ratios of 1.17 ± 0.06 on 20. July and 1.09 ± 0.03 on 22. July. These ratios correspond to the stoichiometric ratios of integrated canopy exchange that might result from observations of O₂ and CO₂ mixing ratios in canopy air as described in section 5 (see Figure 5.5). Note that on the second day, the integrated ratio is lower than the stoichiometric ratios of all separate gas exchange fluxes contributing to this ratio. This supports the interpretation of such a phenomenon observed during field measurements as reflecting a hysteresis loop (see section 5).

$\delta^{18}\text{O}$ of canopy O₂ exchange

Diurnal variations in the isotopic composition of O₂ in canopy air, $\delta^{18}\text{O}_{\text{ix}}$ (see Figure 8.6), were predicted from a regression of $\delta^{18}\text{O}$ values versus $\delta(\text{O}_2/\text{N}_2)$ ratios from open branch bag samples (slope of -2×10^{-5} ‰ between $(\delta^{18}\text{O}_{\text{ix}} - \delta^{18}\text{O}_{\text{atm}})$ and $(\delta(\text{O}_2/\text{N}_2) - \delta(\text{O}_2/\text{N}_2)_{\text{mean}})$ with $\delta^{18}\text{O}_{\text{atm}} = 23.8$ ‰). For the three days following the sampling period in July 2001, typical day-time values were around -2 permeg, whereas night-time values were mostly between 2 and 4 permeg. Here, all $\delta^{18}\text{O}$ values of O₂ in air are again reported as offsets from 23.8 ‰ in permeg.

The discrimination factor of O₂ uptake during dark respiration of foliage and roots, b_d , was taken as 20.2 ‰ (Guy et al. 1989). The discrimination factor of O₂ uptake during photorespiration, b_p , was taken as 21.7 ‰ (Guy et al. 1993), consisting of 2/3 from fractionation by RuBP oxygenase (21.3 ‰) and to 1/3 from fractionation by glycolate oxidase (22.7 ‰). Soil respiration was assumed to consist of 70 % microbial (≈ 18 ‰, Schleser 1979) and 30 % root components, with a discrimination factor of combined soil O₂ uptake, b_s , of 18.7 ‰, neglecting fractionation during O₂ diffusion into the soil.

Figure 8.3 shows diurnal cycles of $\delta^{18}\text{O}_E$ of foliage water at the sites of evaporation (in isotopic steady state (ISS) and non steady state (NSS) versions, see section 4.1) for separate branch bags and averages over three days starting with the sampling period in

July 2001. $\delta^{18}\text{O}_E$ of evaporating site water was used as approximation of $\delta^{18}\text{O}_c$, the isotopic composition of chloroplast water, in equation 8.2. Average maximum values occurred at around 14:00 and were highest on the third day (13 ‰) and intermediate on the first day (7 ‰). By contrast, $\delta^{18}\text{O}$ of foliage water was substantially depleted throughout most of the second day, rising above 0 ‰ only between 11:00 and 14:00, with maximum values of 1 ‰. Mid-day maxima of the non steady state formulation were lower than those assuming steady state by 8 ‰ on the first day, but only by 2 to 3 ‰ on the other days.

Also shown in Figure 8.3 is the isotopic composition of ambient O_2 in canopy air, $\delta^{18}\text{O}_{ix} \approx 23.8$ ‰. Changes in $\delta^{18}\text{O}_{ix}$, on the permeg scale, were too small to be visible. The difference between $\delta^{18}\text{O}$ of foliage water and that of ambient O_2 , $\delta^{18}\text{O}_c - \delta^{18}\text{O}_{ix}$, constitutes the isotopic signal mixed into the O_2 inventory of canopy air by gross photosynthesis. As can be seen from the plot, this difference was largest when $\delta^{18}\text{O}$ of foliage water was most depleted, for example at early morning and some late evening times and also on the whole second day. Lowering of mid-day maxima by taking non

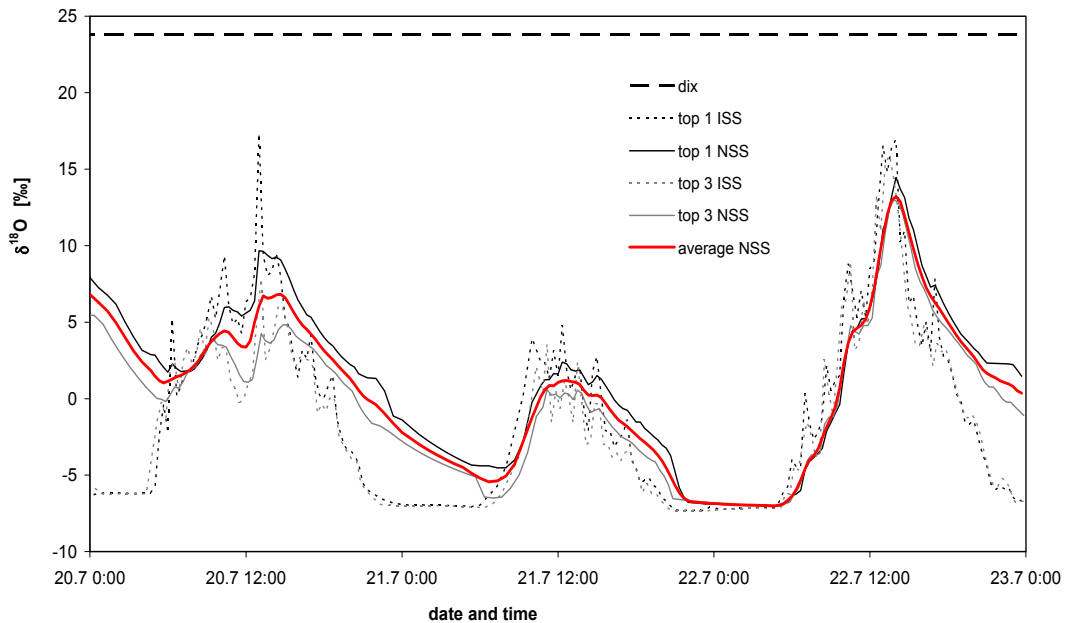


Figure 8.3: Diurnal cycle of $\delta^{18}\text{O}$ of water at the evaporating sites of foliage for single branch bags and smoothed average over three days starting with sampling period in July 2001.

steady state effects into account also contributed to larger differences. Magnitudes of $(\delta^{18}\text{O}_c - \delta^{18}\text{O}_{ix})$ varied between minima of 10 ‰ at noon on the third day to maxima of 29 ‰ at dawn and dusk on the second day.

In analogy to CO_2 , isofluxes of O_2 exchange within the column of canopy air, $\delta^{18}\text{O}_{\text{flux}} \times \text{O}_2$ flux ($\text{‰}\mu\text{mol}/\text{m}^2/\text{s}$), are presented in Figure 8.4 over three days in July 2001. Contributions from inventory changes were surprisingly large despite small variations in $\delta^{18}\text{O}_{ix}$ on the permeg scale, because isotopic variations were amplified by large sizes of the O_2 inventory (21 ‰). The resulting inventory fluxes (up to $\pm 50 \text{‰}\mu\text{mol}/\text{m}^2/\text{s}$) were in the same order of magnitude as contributions from soil respiration (50 to 70 $\text{‰}\mu\text{mol}/\text{m}^2/\text{s}$) and from foliage respiration (10 to 120 $\text{‰}\mu\text{mol}/\text{m}^2/\text{s}$). The gross photosynthetic isoflux on the second day was not significantly different from that on the other two days even though O_2 flux rates were substantially smaller ($> 50 \%$). This is because the isotopic signal of the photosynthetic O_2 flux was much larger, with differences between $\delta^{18}\text{O}_c$ and $\delta^{18}\text{O}_{ix}$ two to three times as large as on the other days.

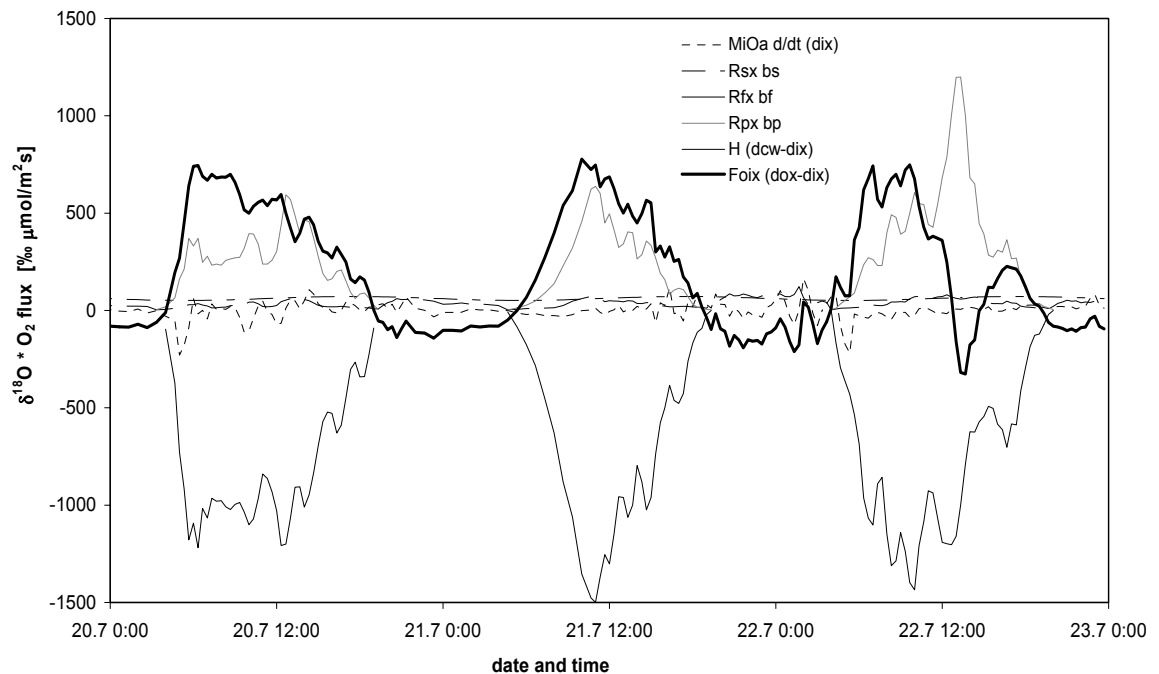


Figure 8.4: Diurnal changes in isofluxes ($\delta^{18}\text{O} \times \text{O}_2$ flux rates) of ecosystem O_2 exchange over the course of three days following sampling campaign in July 2001.

Also of note is the large impact of photorespiration on isotopic exchange of O₂ in canopy air. At most times, the isoflux of photorespiration (400 to 1200 ‰μmol/m²/s) was in the same order of magnitude as the isoflux of gross one-way turbulent exchange with air outside of the canopy (600 to 700 ‰μmol/m²/s). Expressed differently, contributions from photorespiration reduced the impact of gross photosynthesis on gross turbulent exchange fluxes by about a factor of two. At noon on the third day, the gross turbulent exchange isoflux even changed direction, falling from 360 to -330 ‰μmol/m²/s within one hour, due to an exceptionally high photorespiratory isoflux. At the same time, the turbulent exchange isoflux also reached its highest negative value, as it was usually not more than half of that (around -100 ‰μmol/m²/s) during the night.

Figure 8.5 presents $\delta^{18}\text{O}_{\text{canopy}}$, the isotopic composition of ambient O₂ that would result from combined canopy exchange if the biological fluxes were the sole determinants of the isotopic composition of O₂. Calculations were based on respiratory discrimination weighted by O₂ uptake rates of respiration and $\delta^{18}\text{O}_c$, the isotopic composition of foliage water, weighted by gross photosynthetic rates of O₂ release. On all three days, the same general patterns in $\delta^{18}\text{O}_{\text{canopy}}$ variations were found, consisting of a gradual increase over the course of the day, with afternoon values 5 to 8 ‰ higher than in the morning, interrupted by noon maxima 4 to 10 ‰ higher than afternoon and 10 to 20 ‰

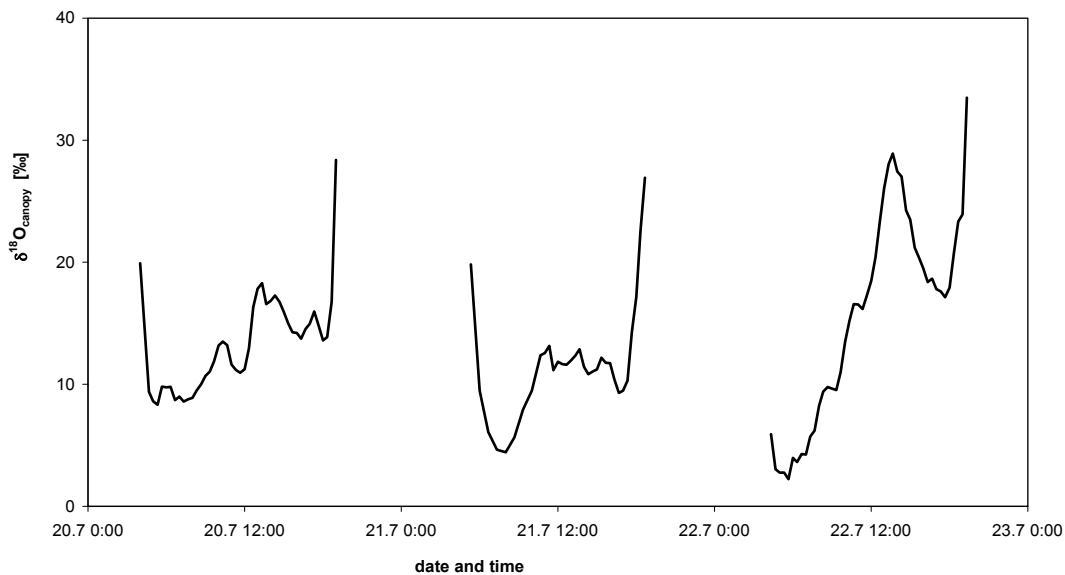


Figure 8.5: Diurnal variations in resulting $\delta^{18}\text{O}_{\text{canopy}}$ of integrated biological canopy O₂ exchange fluxes, over the course of three days in July 2001.

higher than morning values. Another conspicuous feature were abrupt dawn decreases and dusk increases by 10 to 18 ‰ over time periods of about one hour, except at dawn on the third day. Maximum noon values were highest on the third (29 ‰) and much lower on the first (18 ‰) and second day (13 ‰).

$\delta^{18}\text{O}_{\text{canopy}}$ is not comparable to an ecosystem version of the Dole-Morita effect. An "instantaneous magnitude" of the Dole-Morita effect would only result if isotopic fluxes were at steady state, i.e. of equal magnitude at each time step, or of equal daily integrated magnitude for determination of a daily integrated Dole-Morita effect. In the ecosystem studied here, for example, instantaneous and daily integrated rates of (depleted) photosynthetic fluxes were far higher than those of (enriching) respiration, dominating ecosystem gas exchange. If rates of release are not balanced by uptake rates, an isotopic steady state approach such as required for calculating the Dole-Morita effect cannot be applied. Here, isofluxes of canopy O_2 exchanges were integrated but O_2 fluxes were not required to be equal at each time step. Thus, $\delta^{18}\text{O}_{\text{canopy}}$ can be more appropriately described as a "transient magnitude" of the Dole-Morita effect on a short time scale. This can be seen from overall values of $\delta^{18}\text{O}_{\text{canopy}}$. As they were mainly determined by isotopic signatures of photosynthesis, $\delta^{18}\text{O}_{\text{canopy}}$ values (13.6, 13.8 and 18.8 ‰) were much lower than the isotopic composition of ambient O_2 (23.8 ‰).

Daily integrated magnitudes of a steady-state Dole-Morita effect were obtained by scaling of fluxes so that respiration rates were equal to rates of photosynthesis, resulting in magnitudes of 25.8, 21.6 and 26.9 ‰, within the range expected for terrestrial contributions to the global Dole-Morita effect (Bender et al. 1994). Assuming the isotopic composition of foliage water at the evaporating sites ($\delta^{18}\text{O}_E$) to be at isotopic steady state (ISS) increases the calculated Dole-Morita effect by more than 1 ‰. Applied at the global scale, it would mean that taking into account non steady state effects on the enrichment of foliage water at the evaporating sites might lower estimates of the terrestrial Dole-Morita effect by as much as 1 ‰.

Variations in isotopic signatures of CO_2 and O_2 in canopy air

Changes in $\delta^{18}\text{O}$ signatures of O_2 and CO_2 in canopy air are coupled via their dependence on the $\delta^{18}\text{O}$ of water at the evaporating sites of foliage. Thus, simultaneous isotopic measurements of CO_2 and O_2 in canopy air may be useful in determining the

$\delta^{18}\text{O}$ signatures of photosynthetic fluxes and theoretically also in constraining rates of gross ecosystem exchange of CO_2 and O_2 . However, contemporary variations in $\delta^{18}\text{O}$ of atmospheric O_2 have not been observed under natural conditions yet because measurement uncertainties are large compared to signals (see section 5). In the following simplistic approach, an effective air volume is estimated into which the biological component fluxes of photosynthesis and respiration have to be mixed to achieve variations in $\delta^{13}\text{C}$ and $\delta^{18}\text{O}$ of CO_2 in canopy air in qualitative agreement with those predicted from regressions of observed data (see section 7). Based on this estimated effective air volume, expected variations in $\delta^{18}\text{O}$ of O_2 in canopy air are then derived using the same mixing assumption for biological fluxes applied to CO_2 isotopes.

Figure 8.6 presents variations in the isotopic compositions of CO_2 and O_2 in canopy air over three days in July 2001. The dashed lines show values from regressions of isotopic compositions versus mixing ratios (see Figures 7.5 and 7.8). Solid lines illustrate the expected diurnal changes in isotopic compositions of canopy O_2 and CO_2 from mixing of isofluxes of photosynthesis and respiration into constant air volumes within hypothetical columns of 10 m and 30 m height, where 10 m corresponds to the actual mean canopy height. These air volumes were assumed to contain CO_2 and O_2 with background values of -8.0‰ for $\delta^{13}\text{C}_i$ and 1.0‰ for $\delta^{18}\text{O}_i$ of CO_2 , and of 23.8‰ for $\delta^{18}\text{O}_{ix}$ of CO_2 .

The top panel of Figure 8.6 shows variations in $\delta^{13}\text{C}_i$ of CO_2 in canopy air. Average amplitudes of diurnal variations in $\delta^{13}\text{C}_i$ from regressions (2 to 3 ‰) were in good agreement with those from mixing with a 30 m air column (2 ‰) but much smaller than from mixing with a 10 m column (5 to 6 ‰). Night-time $\delta^{13}\text{C}_i$ values were mostly $\approx -9\text{‰}$, with regressed and calculated $\delta^{13}\text{C}_i$ values within 1 ‰ of each other, except in the third night, when mixing values did not decrease to the minimum regressed $\delta^{13}\text{C}_i$ (-10.7‰). $\delta^{13}\text{C}_i$ enrichments during the photosynthetic period calculated assuming a 30 m column agreed well with regressed values (to within 0.3 ‰), whereas those calculated assuming a 10 m column were 2 to 3 ‰ more enriched than values derived from regressions.

The middle panel presents variations in $\delta^{18}\text{O}_i$ of canopy CO_2 . Diurnal variations in $\delta^{18}\text{O}_i$ from mixing with a 10 m column were up to 10 ‰ larger than those from regressions ($\approx 1\text{‰}$). Variations in $\delta^{18}\text{O}_i$ from mixing with a 30 m column were again in better agreement but still higher (2 to 3 ‰) than those from regressions. Dawn and dusk values were -3 to 10‰ depleted or enriched compared to regressions, but less strongly in the 30 m

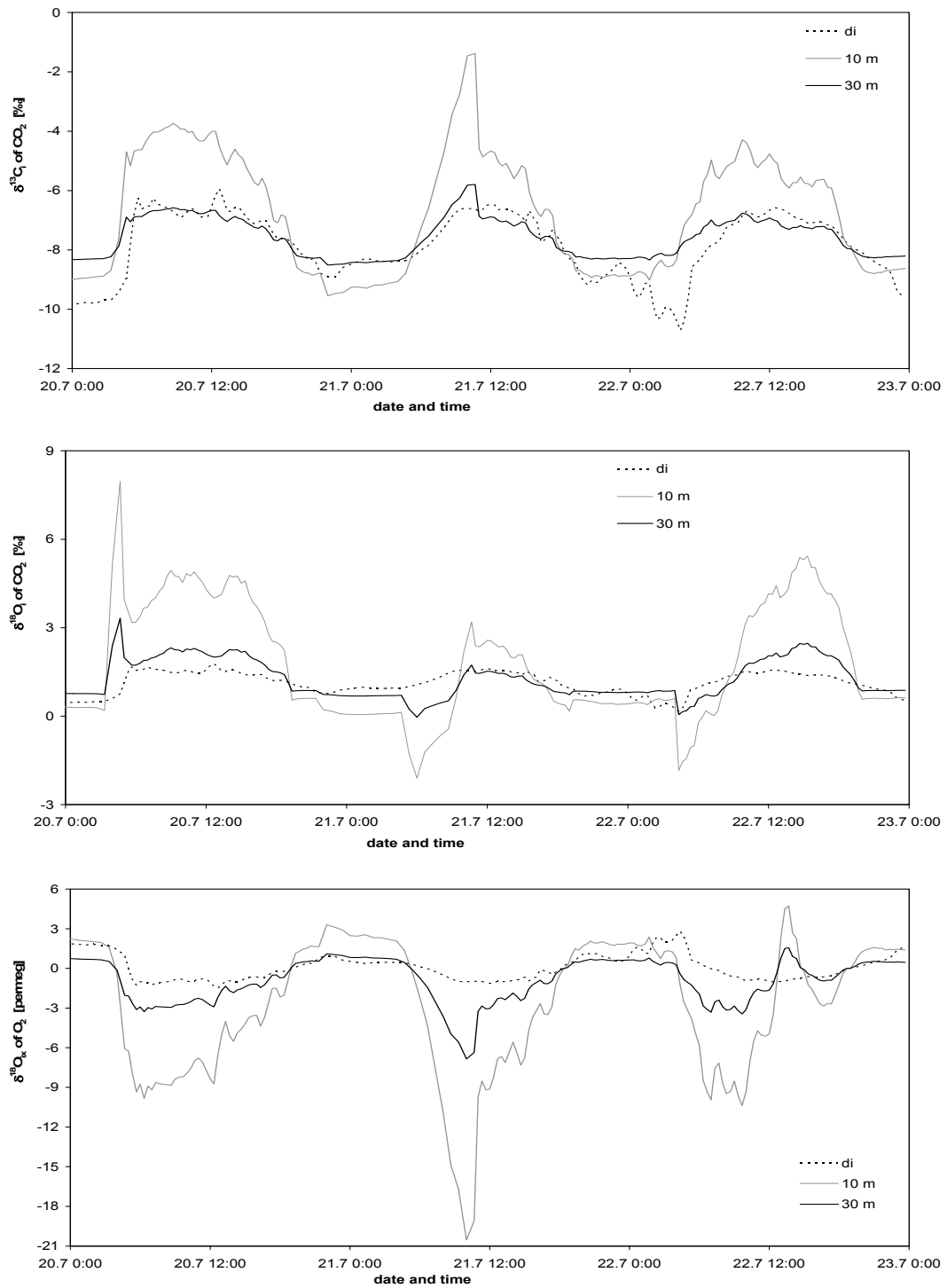


Figure 8.6: $\delta^{13}\text{C}_i$ and $\delta^{18}\text{O}_i$ of CO_2 and $\delta^{18}\text{O}_{ix}$ of O_2 in canopy air from regressions (di) and from mixing of photosynthetic and respiratory fluxes within a constant air volume based on columns of 10 m and 30 m height, over three days in July 2001.

mixing scenario. At night, regressed and calculated $\delta^{18}\text{O}_i$ values were mostly between 0 and 1 ‰. During the day, calculated values from mixing with a 30 m column were similar to regressions on the second day (≈ 1 ‰) and up to 1 ‰ higher on the other two days.

The bottom panel of Figure 8.6 illustrates expected variations in $\delta^{18}\text{O}_{ix}$ of O_2 in canopy air. These variations are expressed as offsets from 23.8 ‰ in units of permeg. As was the case for CO_2 isotopes, assuming a mixing height of 10 m resulted in much larger variations in $\delta^{18}\text{O}_{ix}$ than assuming a 30 m column. Changes of $\delta^{18}\text{O}_{ix}$ in the 30 m mixing version were similar in magnitude to $\delta^{18}\text{O}_{ix}$ from the regression, but not the same in details. Whereas mixing values derived with a 30 m column were close to regressed values at night (1 permeg), they were 2 to 3 permeg lower during the day. They were 3 permeg higher at 13:20 on the third day, when photorespiration had its largest impact on isotopic exchange of canopy O_2 .

Temporal variations of isotopic compositions of CO_2 in canopy air derived assuming a column height of 30 m yielded better agreement with regressed values than with the actual average canopy column height of 10 m. Of course, the canopy height is not an effective mixing height at most times of the day, as canopy fluxes are mixed into a much larger volume by turbulent exchange (Lloyd et al. 1996). The most conspicuous features of variations in $\delta^{18}\text{O}$ of CO_2 , rapid fluctuations at dawn and dusk, were not observed for $\delta^{13}\text{C}$. Such discrepancies might highlight problems with deriving $\delta^{18}\text{O}$ values of CO_2 from regressions. They might also indicate overestimation of ^{18}O discrimination at such times.

The good qualitative agreement between mixed and regressed values for both $\delta^{13}\text{C}$ and $\delta^{18}\text{O}$ of CO_2 indicates that a simple mixing scenario based on a 30 m air column might yield reasonable estimates for the magnitude of variations in $\delta^{18}\text{O}$ of O_2 in canopy air. If these estimates are realistic, then the largest night to day variations can be expected to be on the order of 4 to 8 permeg. Thus, expected changes in $\delta^{18}\text{O}$ of O_2 in canopy air would be comparable to those for branch bag measurements presented in section 5. As discussed in section 5, detection of such small gradients (and their variations) would require reductions in the experimental uncertainties as well as substantial improvements of the analytical precision (currently 12 permeg), while repeating the laboratory analyses would decrease the standard errors of the resulting data and help to improve the identification and interpretation of patterns in the $\delta^{18}\text{O}$ of O_2 in canopy air.

9. Application of canopy scale integration: Partitioning net ecosystem exchange of CO₂

Introduction

The mole fraction and carbon and oxygen isotopic signature of CO₂ in canopy air constitute independent tracers of canopy gas exchange. Measurements of their concurrent fluctuations may thus provide additional information that can be combined with measurements of net ecosystem exchange of CO₂, for example from eddy covariance systems. The goal of the partitioning methods is to utilise that information to constrain the rates of photosynthesis and respiration, i.e. the component fluxes of net ecosystem exchange.

Two different approaches to this have been developed. Both methods construct a mass balance for the CO₂ mole fraction in canopy air from the fluxes of assimilation, respiration and net turbulent exchange of CO₂. Both methods also construct a corresponding mass balance for the isotopic composition of CO₂ in canopy air. These isotopic mass balances rely on observations of the isotopic signature of ecosystem respiration. They are also based on the relationships between photosynthetic discrimination and the ratio of substomatal to ambient CO₂ mole fraction, C_i/C_a , and between C_i/C_a and stomatal conductance to CO₂. The two methods differ, however, in the formulation of the isotopic mass balance. The isofluxes of turbulent exchange (equivalent to the derived isofluxes in section 7) refer to the one-way turbulent exchange of CO₂ for the "one-way isoflux approach" (Lloyd et al. 1996), whereas they refer to the net turbulent exchange of CO₂ for the "net isoflux approach" (Bowling et al. 2001).

Here, another approach has been developed based on that of Lloyd et al. (1996). This method ("dual discrimination approach") takes advantage of the simultaneous availability of $\delta^{13}\text{C}$ and $\delta^{18}\text{O}$ signatures of CO₂ in canopy air. The goal of this section was to test the reliability of the different partitioning methods in estimating assimilation rates from net ecosystem exchange measured by an eddy covariance system and in retrieving the original assimilation rate used as input flux for integrated canopy exchange of $\delta^{13}\text{C}$ and $\delta^{18}\text{O}$ of CO₂ (see section 7). The July dataset was chosen for the testing of partitioning approaches because it had less variability of fluxes and isofluxes

on short time scales (≈ 1 hour) than the May dataset. The solutions of the partitioning equations can be constructed in a similar way for the different approaches. A more detailed description of the partitioning of net ecosystem exchange using the net isoflux approach is given as an example in the first part of this section (Theory).

Net isoflux approach

Theory

The net isoflux approach (Bowling et al. 2001) aims to calculate the rates of assimilation and respiration from measurements of net ecosystem exchange ("partitioning"). The partitioning approach is based on the mass balance equation for the mole fraction of CO₂ in canopy air (Lloyd et al. 1996):

$$M_i \frac{dC_a}{dt} + F_n = R_s - A \quad (9.1)$$

where M_i is the number of moles of air within a column of specified height per unit ground area (mol/m²) and C_a is the CO₂ mole fraction of canopy air ($\mu\text{mol/mol}$). A , R_s and F_n are the rates of assimilation, soil respiration and net turbulent exchange of CO₂ ($\mu\text{mol/m}^2/\text{s}$). Here, A had a positive sign (different from the sign convention of Bowling et al. 2001). Values of M_i , C_a and F_n can be obtained from measurements. Equation 9.1 thus contains two unknowns: the rates of soil respiration, R_s , and of assimilation, A .

To reduce the number of unknown variables, an isotopic mass balance is constructed by multiplying all components of the above mass balance by their respective $\delta^{13}\text{C}$ signatures (Bowling et al. 2001):

$$M_i \frac{d(C_a \delta^{13}C_i)}{dt} + \delta^{13}C_n F_n = \delta^{13}C_{R_s} R_s + ({}^{13}\Delta - \delta^{13}C_i) A \quad (9.2)$$

where ${}^{13}\Delta$ is the photosynthetic ${}^{13}\text{C}$ discrimination, and $\delta^{13}C_i$, $\delta^{13}C_{R_s}$ and $\delta^{13}C_n$ are the isotopic signatures of CO₂ in canopy air and released by soil respiration, and the isotopic composition of the eddy isoflux (see Bowling et al. 2001). Values of $\delta^{13}C_i$, $\delta^{13}C_{R_s}$ and $\delta^{13}C_n$ can be obtained from measurements.

To develop the partitioning equation, the two mass balance equations are combined by multiplying equation 9.1 by $\delta^{13}\text{C}_{R_s}$ and subtracting the result from equation 9.2, yielding:

$$M_i \left(C_a \frac{d\delta_i^{13}}{dt} + (\delta_i^{13} - \delta^{13}_{R_s}) \frac{dC_a}{dt} \right) + (2mC_a + n - \delta^{13}_{R_s}) F_n = ({}^{13}\Delta + \delta^{13}_{R_s} - \delta^{13}_i) A \quad (9.3)$$

The combined equation does not contain the respiration rate, R_s , any longer, but it still contains two unknowns: the photosynthetic ^{13}C discrimination, ${}^{13}\Delta$, and the net assimilation rate, A . If the value of ${}^{13}\Delta$ could be measured, then equation 9.3 could be solved for the assimilation rate. However, the magnitude of ${}^{13}\Delta$ discrimination cannot be determined directly. Instead, the relationship between ^{13}C discrimination, ${}^{13}\Delta$, and the ratio of substomatal to ambient CO_2 mole fraction, C_i/C_a , as well as that between C_i/C_a and stomatal conductance to CO_2 , g_c , can be utilised. For example, in the simple version, ${}^{13}\Delta$ is substituted by C_i/C_a from equation 3.1 (${}^{13}\Delta = a + (b - a) C_i/C_a$), and C_i/C_a is in turn substituted by the stomatal conductance to CO_2 , g_c , from equation 2.6 ($A = g_c (C_a - C_i)$). Because g_c also depends on the assimilation rate, the substitutions result in a quadratic equation for A . The partitioned net rate of CO_2 assimilation can then be calculated from the solution of this quadratic equation (see Appendix 2). Because the relationship between the substomatal CO_2 mole fraction, C_i , and stomatal conductance, g_c , is used to solve the partitioning equations for the assimilation rate, the net isoflux approach relies on canopy integrated values of stomatal conductance to CO_2 .

Two different formulations of partitioning equations were used: a "simple" alternative version where only stomatal conductance was considered in the derivation of partitioning solutions and a "full" version that also included mesophyll conductance. For the full version, a value of $q = 0.09$ was used to approximate the offset between substomatal and chloroplast CO_2 mole fraction ($C_i - C_c = qC_a$, see Lloyd et al. 1996). This also applies to the other approaches. Simple and full versions of the derivation of partitioning solutions for the net isoflux approach are detailed in Appendix 2.

Results

The $\delta^{13}\text{C}$ signature of net turbulent exchange, $\delta^{13}\text{C}_n = 2mC_a + n$ (see Bowling et al. 2001, equation 16), was derived from a regression of $\delta^{13}\text{C}_i$ values versus CO_2 mole fraction

(C_a) from air samples collected in open branch bags during the day. The parameters from a regression of the form $\delta^{13}C_i = mC_a + n$, obtained from 13 samples, were $m = -0.054$ and $n = 12.04$ ($R^2 = 0.96$). Because the goal was to derive rates of assimilation, only day-time fluxes were considered so that foliage respiration, R_f , could be omitted from the equations. For the same reason, $\delta^{13}C_{R_s}$ of soil respiration was used instead of $\delta^{13}C_R$ of integrated ecosystem respiration for the isotopic composition of respiratory contributions during the day. However, the difference between the two was small (-28.8 ‰ for ecosystem and -29.0 ‰ for soil respiration). Storage CO_2 fluxes and isofluxes were calculated in the same way as for canopy scale integrations described in section 7. Fluxes of net turbulent CO_2 exchange were either derived from canopy integrations (mass balances) or obtained from eddy covariance measurements (both detailed in section 7, see Figure 7.4).

Assimilation rates derived from partitioning (A_p) using the net isoflux approach are shown in Figure 9.1. Also shown are the original assimilation rates (A) used as input into canopy scale integration of CO_2 exchange (see Figure 7.3). Thin lines indicate partitioned assimilation rates from the simple version, considering only the impact of stomatal conductance on ^{13}C discrimination (equation P.11). Thick lines indicate partitioned rates from the full version, also including the impact of mesophyll conductance on ^{13}C discrimination (equation P.8).

The top panel of Figure 9.1 presents partitioned assimilation rates calculated from derived fluxes. Rates from the simple partitioning of derived fluxes were 5 to 15 $\mu\text{mol}/\text{m}^2/\text{s}$ higher than original rates, while rates from the full partitioning formulation were higher or lower than original rates by 2 to 5 $\mu\text{mol}/\text{m}^2/\text{s}$. Partitioned assimilation rates could be calculated for early morning and late evening times but results were up to 10 times higher than original rates, even for the full version.

The bottom panel of Figure 9.1 presents rates of assimilation obtained from partitioning of eddy fluxes, supplied from eddy covariance measurements at the nearby tower. With the simple formulation, partitioned assimilation rates from eddy fluxes were 8 to 40 $\mu\text{mol}/\text{m}^2/\text{s}$ higher than input rates. With the full version, partitioned rates were 4 to 26 $\mu\text{mol}/\text{m}^2/\text{s}$ higher than input assimilation rates. Even with the full formulation, the assimilation rates derived from partitioning of eddy fluxes were 50 to 100 % higher than input assimilation rates.

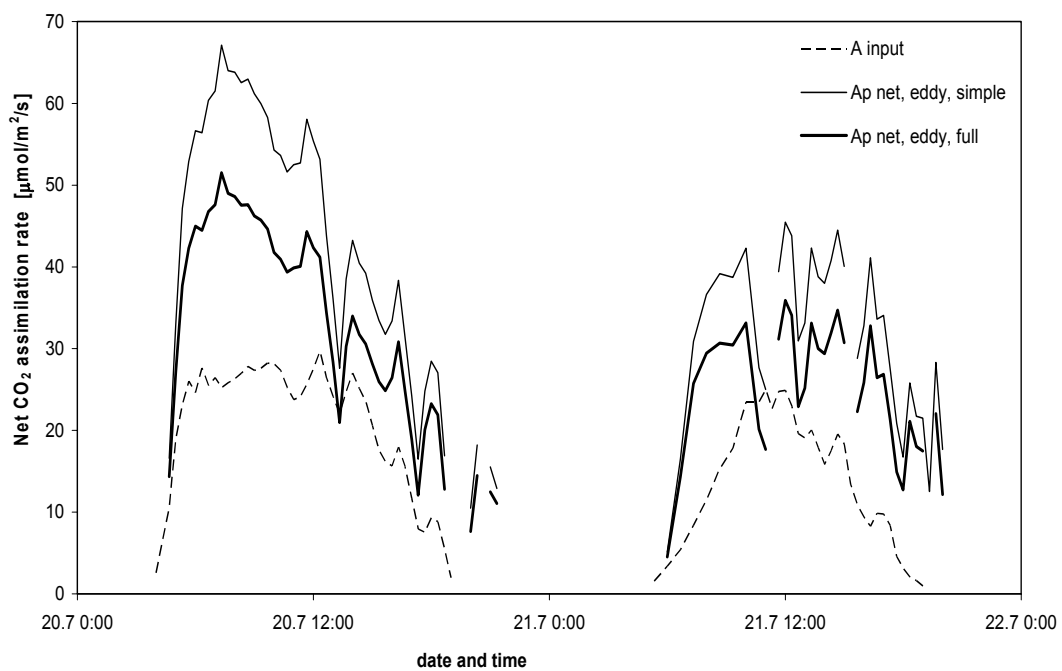
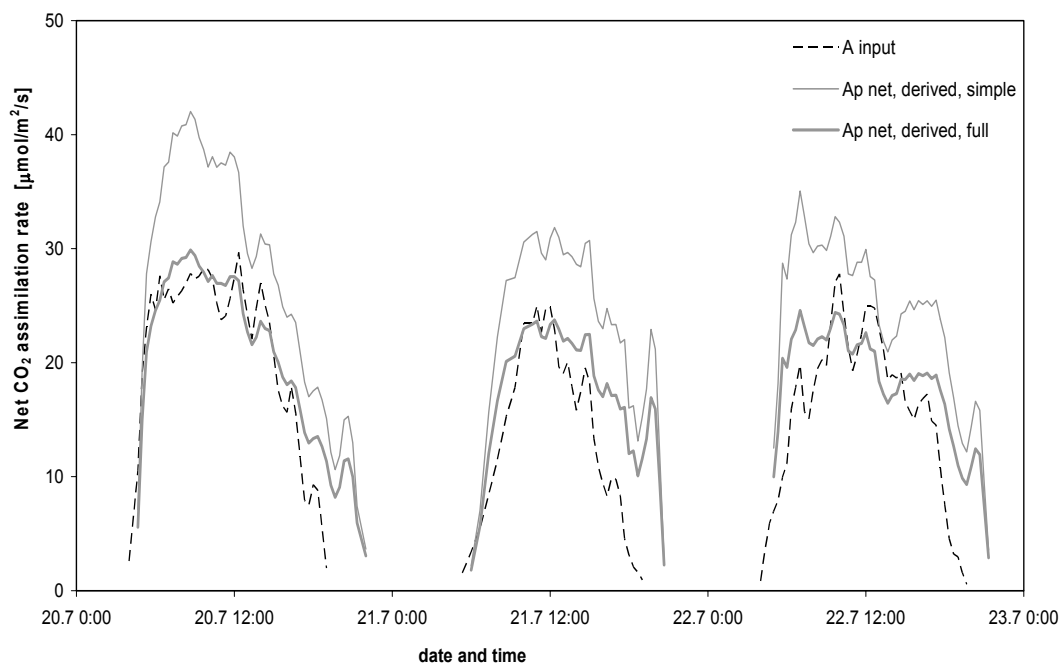


Figure 9.1: Net assimilation rate (A_p) of canopy foliage from partitioning of net CO_2 exchange with the net isoflux approach using simple and full formulations, for July 2001. Top: from derived isofluxes of net turbulent exchange. Bottom: from eddy fluxes of net turbulent exchange and regressed isotopic compositions.

One-way isoflux approach

Theory

The one-way isoflux approach is based on the mass balance equations for CO₂ mole fractions and $\delta^{13}\text{C}$ of CO₂ in canopy air from Lloyd et al. (1996) introduced in section 7 (see equation 7.1 and 7.2):

$$M_i \frac{dC_a}{dt} + F_n = R_s - A \quad (9.1)$$

$$M_i C_a \frac{d\delta^{13}C_i}{dt} - F_{oi} (\delta^{13}C_o - \delta^{13}C_i) = (\delta^{13}C_{Rs} - \delta^{13}C_i) R_s + {}^{13}\Delta A \quad (9.4)$$

The mass balance equation for the CO₂ mole fraction is the same for net and one-way isoflux approaches (equation 9.1), but the isotopic mass balance equations of the two approaches differ. This is due to the different formulations of turbulent exchange isofluxes between the ecosystem and the boundary layer (compare equations 9.2 and 9.4). For the net isoflux approach, the net CO₂ flux of turbulent exchange carries the isotopic signature of CO₂ leaving the canopy, whereas for the one-way isoflux approach, the one-way CO₂ flux of turbulent exchange is scaled by the difference between isotopic signatures of air within and outside of the canopy.

Definitions and units of all variables used in the following are the same as for the net isoflux approach and can also be found in section 7. The partitioning equation for the one-way isoflux approach is determined by combining the two mass balance equations in the same way as described for the net isoflux approach. The one-way isoflux approach also relies on canopy integrated values of stomatal conductance, where ${}^{13}\Delta$ is in the simple version substituted by C_i/C_a (equation 3.1), and C_i/C_a in turn by the stomatal conductance to CO₂ (equation 2.6). The combined expression with substitutions yields again a quadratic equation that can be solved for A . However, the one-way isoflux approach requires estimates of the isotopic composition of air outside the canopy, $\delta^{13}C_o$, which were not available from measurements in this study. The procedure employed here to simulate such measurements is described in the following.

Procedure

In analogy to the net isoflux approach, a "simple" alternative formulation (only stomatal conductance) and a full formulation (also mesophyll conductance) were applied. Simple and full versions of partitioning solutions for the one-way isoflux approach are derived in Appendix 2. Because day-time fluxes were considered, foliage respiration, R_f , was again omitted, and $\delta^{13}C_{Rs}$ of soil respiration (-29.0 ‰) was used for the isotopic composition of respiratory contributions during the day. Storage fluxes and isofluxes were calculated as for the net isoflux approach. Net turbulent exchange fluxes were derived from canopy integrations or obtained from eddy covariance data (see Figure 7.4).

One-way fluxes of turbulent exchange leaving the forest (F_{io}) were estimated from an empirical relationship (Lloyd et al. 1997, equation 1):

$$F_{io} \propto \frac{\rho_a \sigma_w C_a}{2} \quad (9.5)$$

where ρ_a is the molar density of air (mol/m^3) and σ_w is the standard deviation of the vertical wind speed (m/s). A value of 0.74 was inferred for the slope of this relationship. One-way turbulent exchange fluxes entering the forest (F_{oi}) were calculated as differences between F_{io} and F_n , the net turbulent exchange ($F_{oi} = F_{io} - F_n$, see Lloyd et al. 1996). From the ratio of the two one-way fluxes, the ratio of CO_2 mole fractions outside and within the canopy was estimated ($F_{oi}/F_{io} \approx C_o/C_a$, see Lloyd et al. 1996). This ratio was used to obtain C_o , the CO_2 mole fraction in the air above the forest (convective boundary layer during the day). In addition, the derived one-way isofluxes, $F_{oi}(\delta^{13}C_o - \delta^{13}C_i)$, calculated from canopy integrations of isotopic exchange (see equation 9.4), were divided by one-way fluxes of turbulent CO_2 exchange entering the forest, F_{oi} , to obtain estimates for $(\delta^{13}C_o - \delta^{13}C_i)$. The latter is the isotopic signature of the one-way flux of CO_2 entering the forest, i.e. the difference in isotopic composition of CO_2 above and within the canopy. This difference was then added to $\delta^{13}C_i$ to estimate $\delta^{13}C_o$.

The calculations described above were used to gain estimates of mole fractions and $\delta^{13}C_o$ signatures of CO_2 in the boundary layer above the forest. During a field campaign, establishing these variables could be achieved by collecting air samples in the convective boundary layer during the day, for example using sampling systems mounted

on aircraft. Mole fractions and isotopic signatures of CO₂ obtained from such air samples would most likely be used to construct a regression between $\delta^{13}\text{C}_o$ and $1/C_o$ for CO₂ in the boundary layer, assuming mixing of air from the canopy with a constant background of tropospheric air. The parameters inferred from such a regression could then be applied to CO₂ mole fraction data from above the forest, for example obtained from sampling inlets at the top of towers if these are 10 to 20 m higher than the canopy. From this, continuous values for $\delta^{13}\text{C}_o$ of CO₂ in the boundary layer could be derived.

Here, to "simulate" such a procedure, the same method of obtaining continuous data from a regression between $\delta^{13}\text{C}_o$ and $1/C_o$ was applied. Values for these two variables were estimated as described above. Regression were constructed for day-times and night-times separately ($R^2 = 0.99$). $\delta^{13}\text{C}_o$ values obtained from the day-time regression were combined with $\delta^{13}\text{C}_i$ values again to calculate the difference in isotopic compositions, $(\delta^{13}\text{C}_o - \delta^{13}\text{C}_i)$, i.e. the isotopic signature of the CO₂ flux of one-way turbulent exchange. Finally, the (simulated) "eddy" one-way turbulent isoflux, $F_{oi}(\delta^{13}\text{C}_o - \delta^{13}\text{C}_i)$, was determined from the observed eddy one-way turbulent exchange flux, F_{oi} ,

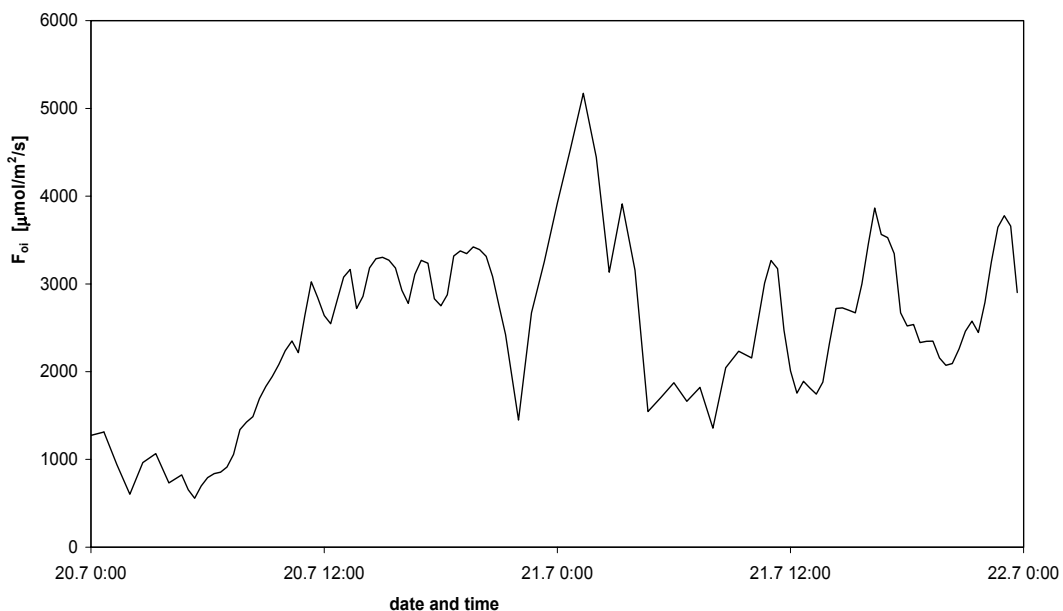


Figure 9.2: One-way fluxes of turbulent CO₂ exchange entering the canopy from above from eddy covariance data in July 2001.

and the isotopic difference, ($\delta^{13}\text{C}_o - \delta^{13}\text{C}_i$), determined from the regressed isotopic compositions. In principle, the experiment simulated here should correspond to the situation encountered and the procedure followed during actual field measurements.

Results

Figure 9.2 presents F_{oi} , one-way turbulent exchange fluxes of CO_2 entering the forest obtained from eddy covariance measurements over two days in July 2001. One-way turbulent exchange fluxes were increasing from 1000 to 3000 $\mu\text{mol}/\text{m}^2/\text{s}$ over the course of the first day and varying between 2000 and 3000 $\mu\text{mol}/\text{m}^2/\text{s}$ during the second day, with a maximum of 5000 $\mu\text{mol}/\text{m}^2/\text{s}$ shortly after midnight on the second day, during a period characterised by strong wind.

Figure 9.3 illustrates calculated differences between isotopic compositions of CO_2 outside and within the canopy, ($\delta^{13}\text{C}_o - \delta^{13}\text{C}_i$), over two days in July 2001. As detailed above, these differences were estimated from derived one-way isofluxes and eddy data

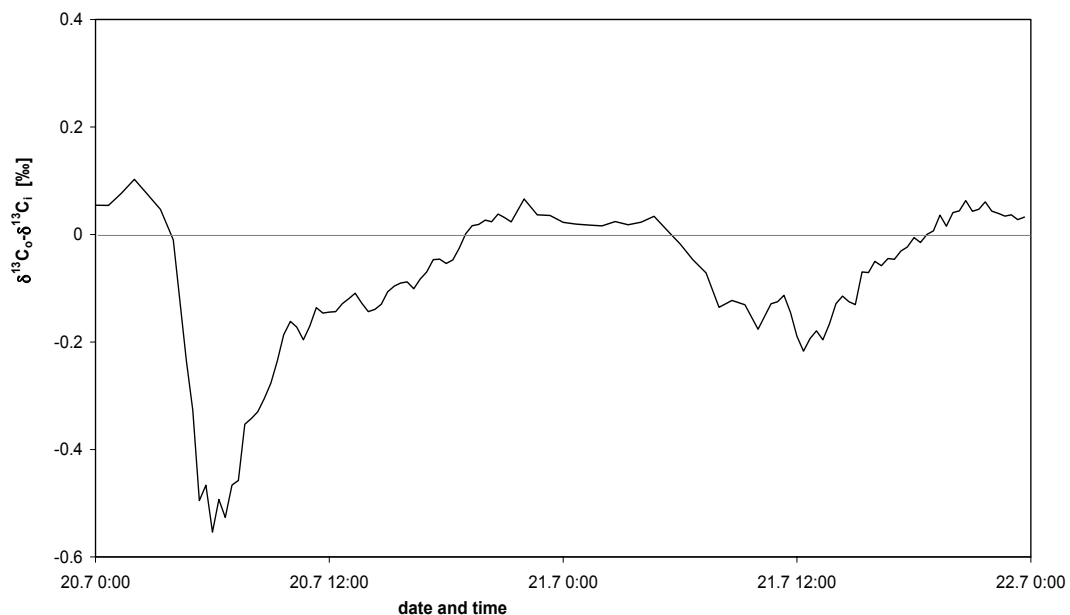


Figure 9.3: Differences in isotopic composition ($\delta^{13}\text{C}_o - \delta^{13}\text{C}_i$) between CO_2 above and within the canopy on two days in July 2001, calculated from eddy covariance data and derived isofluxes.

of one-way CO₂ fluxes of turbulent exchange. During the day, $\delta^{13}\text{C}_i$ enrichment caused by photosynthetic activity resulted in negative differences, i.e. $\delta^{13}\text{C}_i$ was higher than $\delta^{13}\text{C}_o$. At night, release of depleted CO₂ from nocturnal soil and foliage respiration resulted in positive differences, i.e. $\delta^{13}\text{C}_i$ was depleted with respect to $\delta^{13}\text{C}_o$. Differences were mostly between -0.2 and 0.1 ‰. The largest difference of ≈ -0.5 ‰ was inferred for the morning of the first day, when one-way turbulent fluxes were small. Sign changes from positive to negative values were gradual, except at dawn on the first day.

Figure 9.4 presents assimilation rates from partitioning (A_p) using the one-way isoflux approach. The original assimilation rates (A) used as input into canopy scale integration of CO₂ exchange (see Figure 7.3) are also shown. As in Figure 9.1, the partitioned assimilation rates from the simple version (equation P.18, only stomatal conductance) are indicated by thin lines, partitioned rates from the full version (equation P.17, including mesophyll conductance) are indicated by thick lines.

Net CO₂ assimilation rates from partitioning of derived fluxes are presented in the top panel of Figure 9.4. Whereas simple partitioned assimilation rates were 5 to 10 $\mu\text{mol}/\text{m}^2/\text{s}$ higher than original rates during most of the day, partitioned rates using the full formulation were in excellent agreement with original rates of assimilation. However, assimilation rates could not be obtained from either version of the one-way isoflux partitioning approach at early morning and late evening times.

Assimilation rates inferred from partitioning of simulated one-way "eddy" fluxes are presented in the bottom panel of Figure 9.4. Partitioned assimilation rates were 5 to 10 $\mu\text{mol}/\text{m}^2/\text{s}$ higher than input rates with the simple formulation. With the full formulation, partitioned rates followed input rates with small variations of ± 2 to 5 $\mu\text{mol}/\text{m}^2/\text{s}$ during most of the day, except in the afternoon of the second day, when partitioned rates were up to 10 $\mu\text{mol}/\text{m}^2/\text{s}$ higher than input assimilation rates.

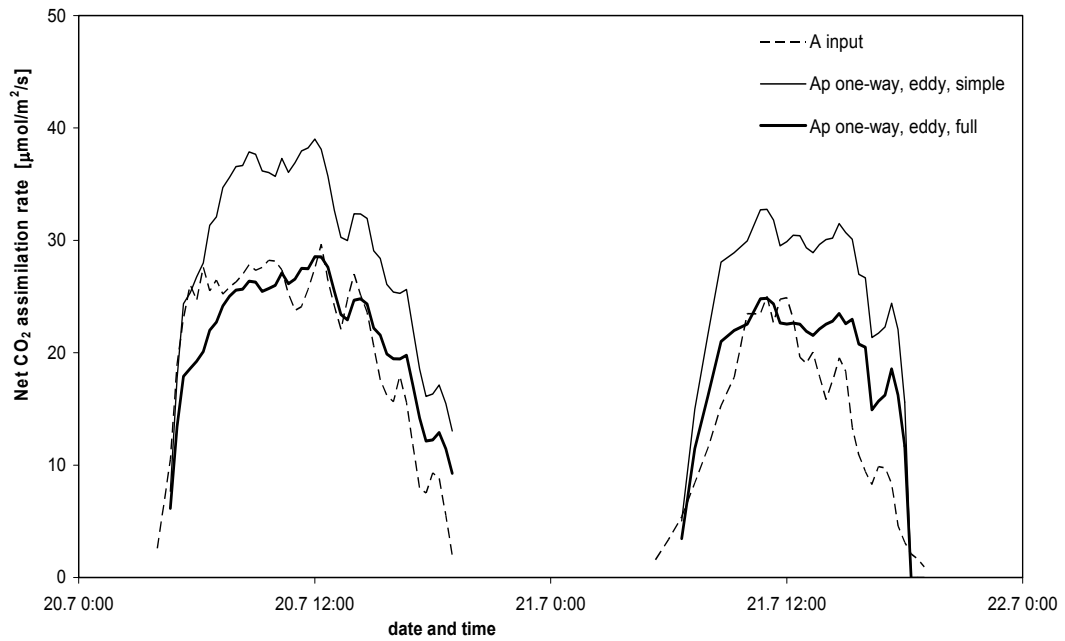
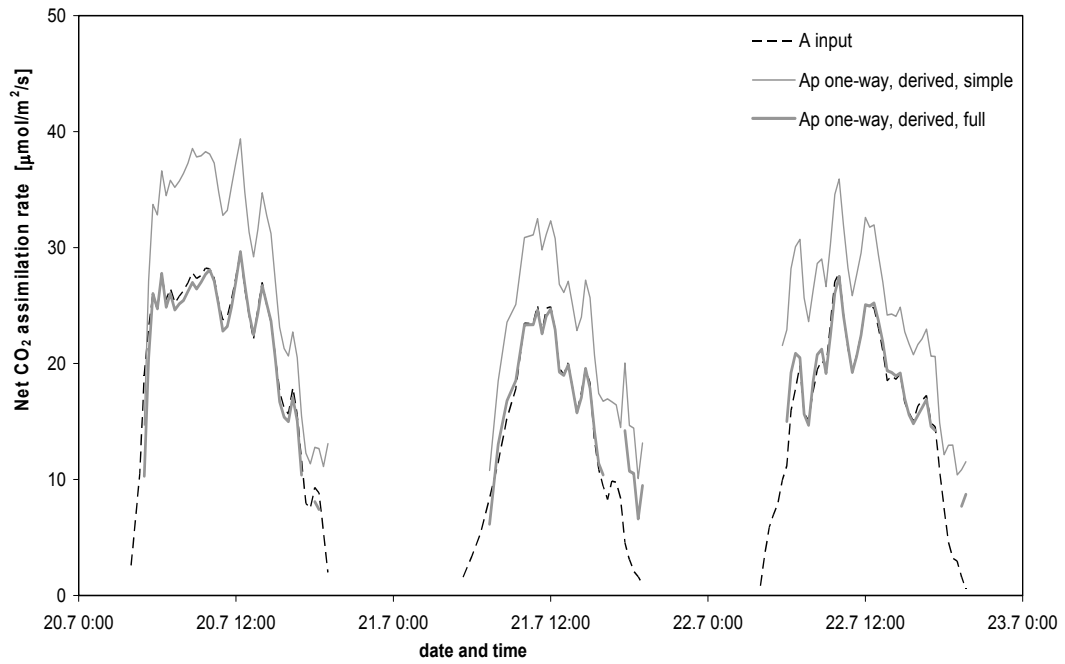


Figure 9.4: Net assimilation rate (A_p) of canopy foliage from partitioning of net CO₂ exchange with the one-way isoflux approach using simple and full formulations, for July 2001. Top: from derived isofluxes of one-way turbulent exchange. Bottom: from eddy fluxes of one-way turbulent exchange and regressed isotopic compositions.

Dual discrimination approach

Theory

The dual discrimination approach developed here is based on the same mass balance equations as the one-way isoflux approach (Lloyd et al. 1996, see equations 9.1 and 9.4 and section 7). In contrast to the one-way isoflux approach, however, the dual discrimination method makes use of the simultaneous availability of $\delta^{13}\text{C}$ and $\delta^{18}\text{O}$ data. Thus, it does not rely on canopy integrated values of stomatal conductance. The isotopic mass balance for $\delta^{18}\text{O}$ is equivalent to that for $\delta^{13}\text{C}$:

$$M_i C_a \frac{d\delta^{18}\text{O}_i}{dt} - F_{oi} (\delta^{18}\text{O}_o - \delta^{18}\text{O}_i) = (\delta^{18}\text{O}_{R_s} - \delta^{18}\text{O}_i) R_s + {}^{18}\Delta A \quad (9.6)$$

The two isotopic mass balances for $\delta^{13}\text{C}$ and $\delta^{18}\text{O}$ can be coupled because their photosynthetic discriminations, ${}^{13}\Delta$ and ${}^{18}\Delta$, both depend on C_i/C_a (or C_c/C_a). In the simple version, where discrimination values only depend on C_i/C_a (equivalent to those introduced for the two other approaches), ${}^{18}\Delta$ can be expressed as:

$${}^{18}\Delta = \bar{a} + (\delta^{18}\text{O}_c - \delta^{18}\text{O}_i) \frac{C_i}{C_a - C_i} \quad (9.7)$$

An expression for $C_i/(C_a - C_i)$ is then derived from equation 3.1 (${}^{13}\Delta = a + (b - a) C_i/C_a$) and substituted into equation 9.7. The resulting equation contains both ${}^{13}\Delta$ and ${}^{18}\Delta$ (equation P.29). These can be substituted by expressions derived from their respective mass balance equations, thus eliminating ${}^{13}\Delta$ and ${}^{18}\Delta$ in the partitioning solution (equation P.31). In this way, the three mass balances (one for the mole fraction, two for the isotopic signatures of CO_2) can be combined to derive a quadratic equation that can be solved for A . This requires the isotopic composition of foliage water at the evaporating sites (approximating $\delta^{18}\text{O}_c$) to be established.

Again, a "simple" alternative formulation (using C_i/C_a) and a full formulation (using C_i/C_a and C_c/C_a) of partitioning solutions were applied for the dual discrimination approach. Their derivations are described in Appendix 2. Foliage respiration, R_f , was again

omitted, and $\delta^{13}\text{C}_{\text{Rs}}$ of soil respiration (-29.0 ‰) was used for the isotopic composition of respiratory contributions during the day. Storage fluxes and isofluxes were calculated as for the other approaches. Net turbulent exchange fluxes were derived from canopy integrations or obtained from eddy covariance data (see Figure 7.4). The procedure to derive estimates for (simulated) one-way "eddy" isofluxes for $\delta^{13}\text{C}$, $F_{\text{oi}}(\delta^{13}\text{C}_\text{o} - \delta^{13}\text{C}_\text{i})$, has already been described in the one-way isoflux approach. This procedure was repeated here to yield estimates for a (simulated) one-way "eddy" isoflux for $\delta^{18}\text{O}$, $F_{\text{oi}}(\delta^{18}\text{O}_\text{o} - \delta^{18}\text{O}_\text{i})$. The one-way fluxes of turbulent exchange, F_{oi} , were the same as those used in the derivation for $\delta^{13}\text{C}$ (see Figure 9.2).

Results

The differences between oxygen isotopic composition of CO_2 outside and within the canopy, $(\delta^{18}\text{O}_\text{o} - \delta^{18}\text{O}_\text{i})$, are illustrated in Figure 9.5. The differences inferred for $\delta^{18}\text{O}$ closely matched those inferred for $\delta^{13}\text{C}$, with values between -0.1 and 0.1 ‰ at all times except in the morning of the first day, when it was -0.5 ‰. Again, differences were

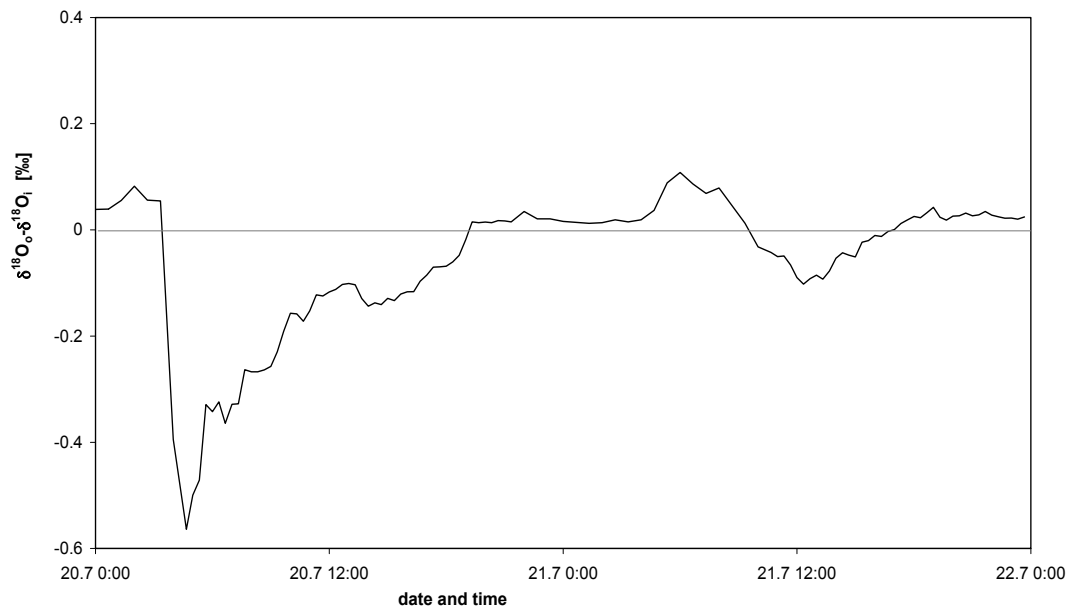


Figure 9.5: Differences in isotopic composition ($\delta^{18}\text{O}_\text{o} - \delta^{18}\text{O}_\text{i}$) between CO_2 above and within the canopy on two days in July 2001, calculated from eddy covariance data and derived isofluxes.

negative during the day, i.e. $\delta^{18}\text{O}_i$ was higher than $\delta^{18}\text{O}_o$, whereas $\delta^{18}\text{O}_i$ was lower than $\delta^{18}\text{O}_o$ at night, resulting in positive differences. A rapid change from positive to negative signs was inferred at dawn on the first day, while other changes were more gradual.

Partitioned assimilation rates (A_p) estimated from the dual discrimination approach are presented in Figure 9.6. Also shown are original assimilation rates (A) used as input into canopy scale integration of CO_2 exchange (see Figure 7.3). As in Figures 9.1 and 9.4, partitioned assimilation rates from the simple version (equation P.36) are indicated by thin lines, while thick lines indicate partitioned assimilation rates from the full version (equation P.33).

The top panel of Figure 9.6 presents net CO_2 assimilation rates partitioned from derived fluxes. On the first and third day, assimilation rates from simple partitioning were up to $15 \mu\text{mol}/\text{m}^2/\text{s}$ higher or up to $10 \mu\text{mol}/\text{m}^2/\text{s}$ lower than original rates, but in reasonable agreement on the second day and at most early morning and late evening times. Partitioned assimilation rates from the full version were in good agreement with original rates (to within $2 \mu\text{mol}/\text{m}^2/\text{s}$) on the second and third day, but higher or lower by 5 to $15 \mu\text{mol}/\text{m}^2/\text{s}$ sporadically on the first day. Assimilation rates could not be derived for some early morning and late evening times with the full version and around noon on the first and third day with the simple version.

The bottom panel of Figure 9.6 shows assimilation rates inferred from partitioning of simulated "eddy" fluxes. With the simple version, partitioned assimilation rates were 1 to $5 \mu\text{mol}/\text{m}^2/\text{s}$ higher or lower than input rates on the second day, whereas they could not be obtained throughout most of the first day. With the full version, partitioned assimilation rates on the first day were 2 to $10 \mu\text{mol}/\text{m}^2/\text{s}$ lower than input rates in the morning, $10 \mu\text{mol}/\text{m}^2/\text{s}$ higher at noon and within $1 \mu\text{mol}/\text{m}^2/\text{s}$ in the afternoon. On the second day, they were mostly between 2 and $10 \mu\text{mol}/\text{m}^2/\text{s}$ higher than input assimilation rates.

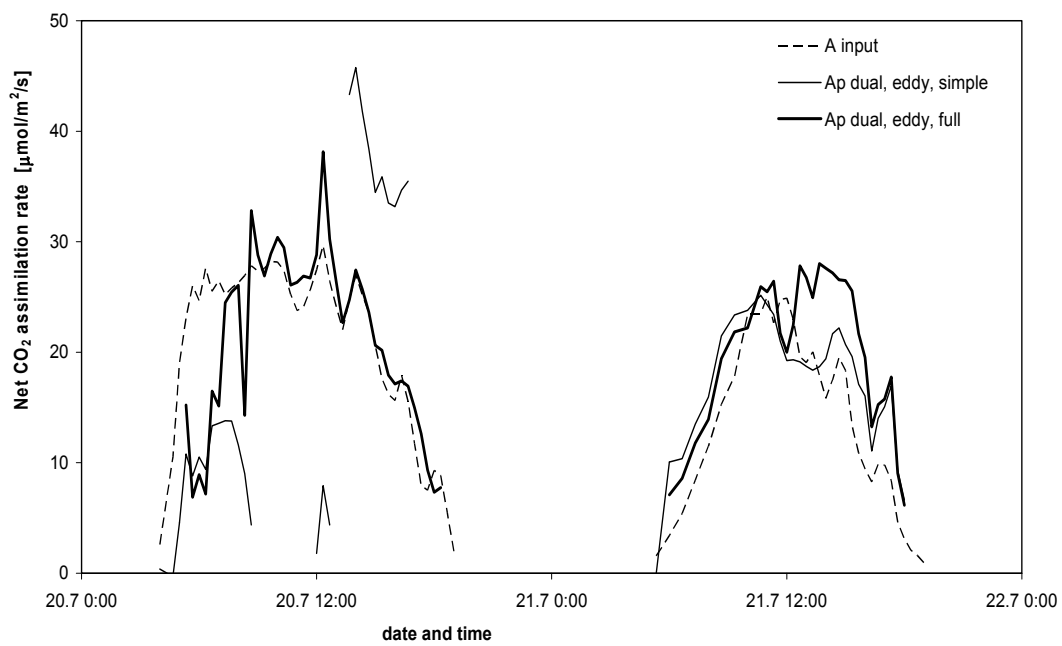
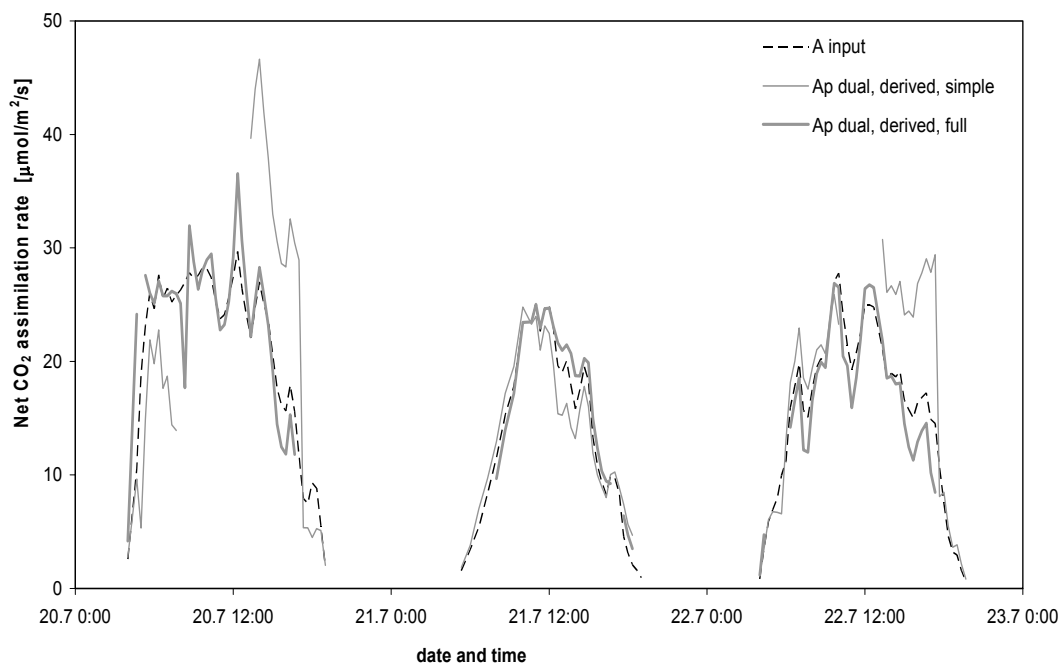


Figure 9.6: Net assimilation rate (A_p) of canopy foliage from partitioning of net CO_2 exchange with the dual discrimination approach using simple and full formulations, for July 2001. Top: from derived isofluxes of one-way turbulent exchange. Bottom: from eddy fluxes of one-way turbulent exchange and regressed isotopic compositions.

Comparison and Discussion

Assimilation rates obtained from the different partitioning approaches described above are presented in Figure 9.7 for partitioning of derived fluxes and in Figure 9.8 for partitioning of eddy fluxes. The partitioned rates are plotted versus the original rates of assimilation used as input variables in calculations of isofluxes. The top panel of each figure shows the relationship between partitioned and original rates for the simple alternative formulations, and the bottom panel shows the relationship for the full formulations, respectively.

The quantitative analysis could be applied more strictly to partitioned rates from derived fluxes, because these were calculated from integrated canopy exchange based on the same assimilation rates that were inferred from partitioning. Clearly, partitioned assimilation rates from derived fluxes were much closer to original rates when applying full approaches than from simple derivations. The average ratios of partitioned fluxes with respect to original (derived) assimilation fluxes for full and simple formulations are listed in Table 9.1 (two columns on the left). For average values, one-way isoflux and dual discrimination approaches achieved the overall best agreements between partitioned and original (input) assimilation rates. In addition, the one-way isoflux method also showed excellent agreement for instantaneous values of assimilation rates.

partitioning of:	derived fluxes		eddy fluxes	
	full	simple	full	simple
net isoflux	1.13	1.5	1.71	2.1
one-way isoflux	1.01	1.4	1.04	1.4
dual discrimination	1.01	1.2	1.14	1.2

Table 9.1: Average ratios of partitioned fluxes from the net isoflux, the one-way isoflux and the dual discrimination approach with respect to original (derived) fluxes (left columns) and with respect to input (eddy) fluxes (right columns), both for full and simple formulations, respectively. The calculations of average ratios were weighted by assimilation rates.

Partitioned rates from eddy covariance data were in reasonable agreement with input assimilation rates for the one-way isoflux approach on both days and the dual discrimination approach on the second day, whereas they were noticeably higher for the net isoflux approach. The average ratios of partitioned to input (eddy) assimilation fluxes for full and simple formulations are listed in Table 9.1 (two columns on the right). The one-way isoflux approach showed again the best agreement with respect to average as well as to instantaneous assimilation rates partitioned from eddy flux measurements.

On the other hand, partitioned rates from eddy covariance data cannot be compared strictly to input assimilation rates because eddy turbulent exchange fluxes reflect a different site, that of the eddy tower. The difference between the net and the two one-way isoflux approaches could be partly due to the fact that one-way isofluxes were derived from isotopic signatures that had been regressed using observed one-way CO₂ fluxes, so that the resulting one-way isofluxes were representative for the study site, whereas net isofluxes were representative for the site of the eddy tower. Although the two sites had virtually identical properties (plantation of uniform age), assimilation rates were different at the eddy tower site (see Figure 7.4), indicating that values of stomatal conductance, photosynthetic isotope discrimination and isotopic composition of canopy air would also most likely have been different at the eddy tower. However, despite these differences, the one-way approaches showed some agreement of partitioned assimilation rates with assimilation rates scaled from branch bag measurements.

At several times, assimilation rates could not be inferred through partitioning. This occurred when the subtraction of terms of similar magnitude resulted in negative numbers under the square root. This problem occurred more often at dawn and in the late evening, when all terms were small, especially in the dual discrimination approach.

The difference between full and simple derivations of partitioning equations was the same for all approaches described above, with mesophyll conductance taken into account in full but neglected in simple derivations, thereby causing discrepancies between assumed values of ¹³C discrimination, i.e. those used for partitioning, and actual values of ¹³C discrimination, i.e. those used in calculations of integrated δ¹³C of canopy CO₂ exchange, corresponding to more realistic values likely to be encountered under natural conditions. This caused offsets between assimilation rates from full and simple partitioning, and hence also between rates from simple partitioning and original

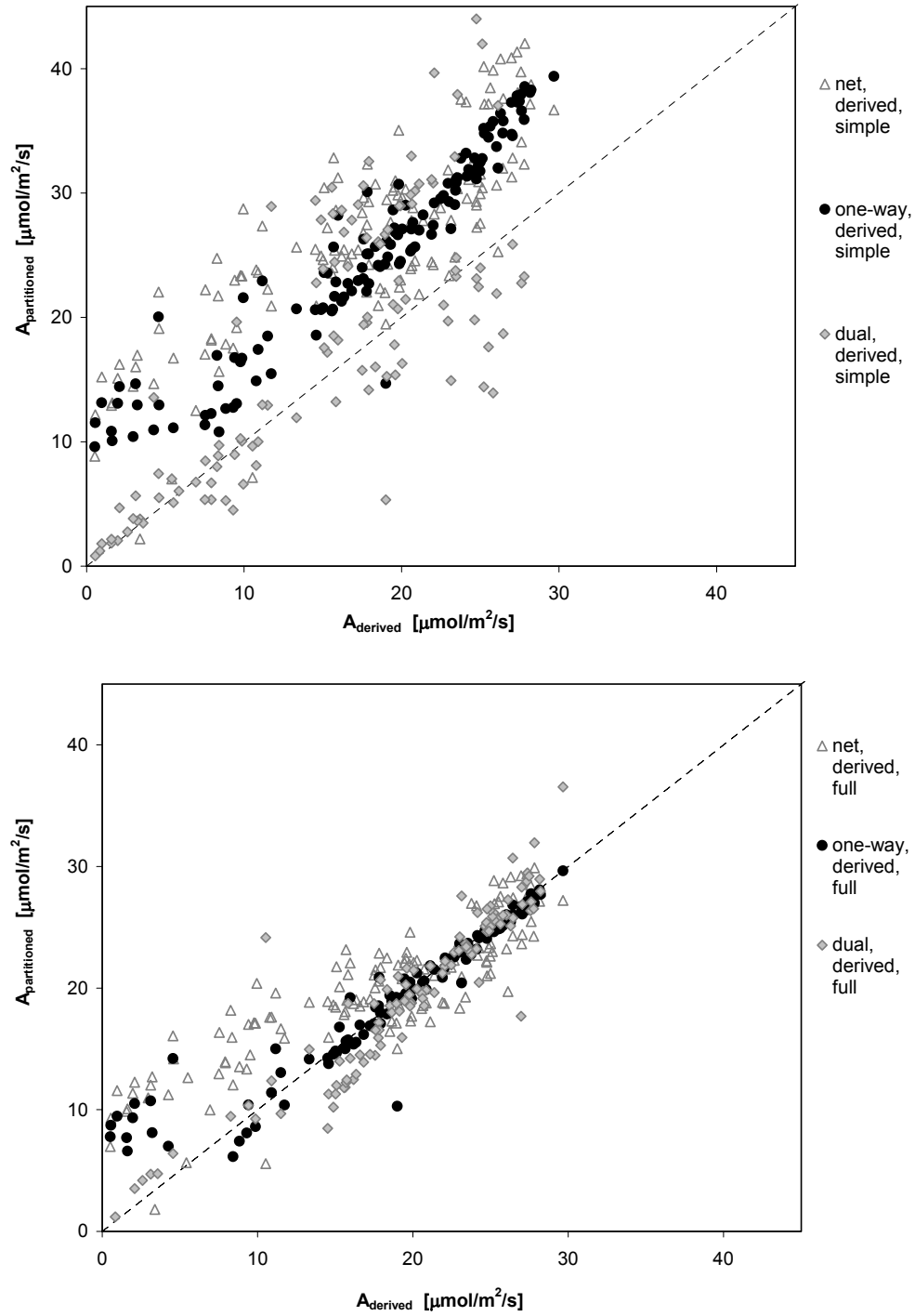


Figure 9.7: Net CO₂ assimilation rates (A_p) from partitioning of derived fluxes versus original derived flux rates (A) for July 2001. Top: simple, bottom: full formulations of net isoflux, one-way isoflux and dual discrimination approach.

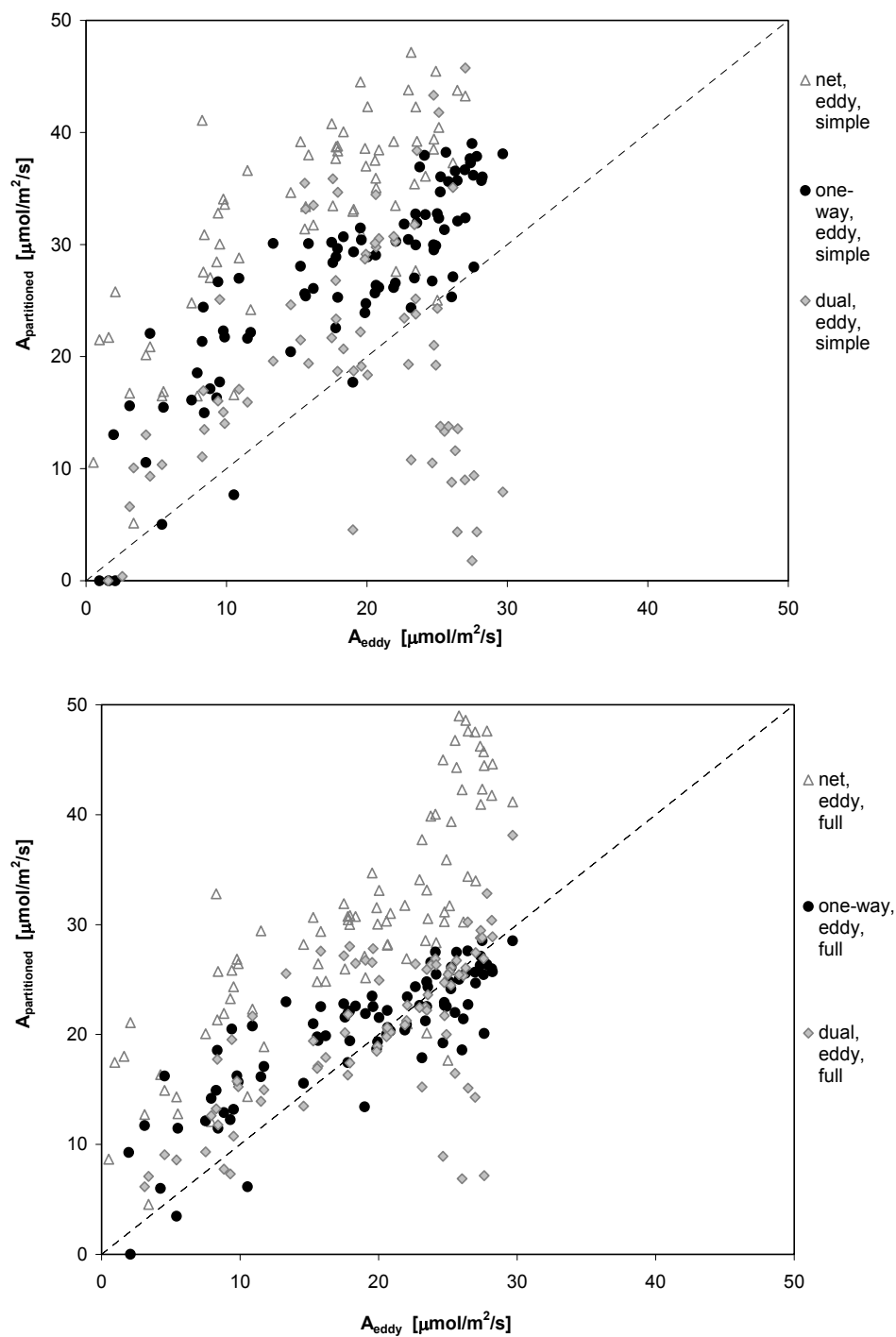


Figure 9.8: Net CO₂ assimilation rates (A_p) from partitioning of eddy fluxes versus original eddy flux rates (A) for July 2001. Top: simple, bottom: full formulations of net isoflux, one-way isoflux and dual discrimination approach.

rates of assimilation. By contrast, differences between original assimilation rates and those from full partitioning were mainly due to neglecting the effects of photo- and dark respiration on ^{13}C discrimination. This is especially obvious for the partitioning attempts using derived fluxes. For the net isoflux method, additional differences between original and partitioned rates were caused by using values obtained from a regression for $\delta^{13}\text{C}$ isofluxes of net turbulent exchange. This resulted in some variability of instantaneous values around mean levels, but average values obtained from this approach were in reasonably good agreement for the partitioning of derived fluxes.

For practical purposes, the main difference between the above described approaches lies in their required input parameters, i.e. the measurements required to solve partitioning equations. Both one-way and net isoflux approaches use total integrated values of ecosystem stomatal conductance, in turn necessitating accurate measurements of water vapour fluxes on the ecosystem scale. For the dual discrimination approach, $\delta^{18}\text{O}$ signatures of various ecosystem components need to be obtained. Although $\delta^{18}\text{O}$ signatures of CO_2 are routinely determined along with $\delta^{13}\text{C}$ signatures from flask samples of canopy air, sampling strategies would have to be adjusted to allow more extensive collections of solid and liquid samples for $\delta^{18}\text{O}$ analysis. Characterizing potentially highly variable $\delta^{18}\text{O}$ signatures of ecosystem exchange fluxes is clearly a disadvantage of the dual discrimination method. Its advantage is that combinations of independent tracers might contribute additional information not contained in other tracers.

Compared to that, the net isoflux method is much simpler to apply in the field. However, so far it has only yielded good results when some of the input values were averaged over longer time periods (Bowling et al. 2001), whereas its reliability for instantaneous observations has not been established yet. The one-way isoflux method also requires more measurements to be made, including determination of one-way gross fluxes of turbulent CO_2 exchange and differences in isotopic composition between CO_2 within and outside of the canopy. Especially the latter might be impractical for field studies. Nevertheless, the one-way isoflux approach should be applied and evaluated under field conditions as it showed overall best agreement with original input rates of assimilation when influences of mesophyll conductance on ^{13}C discrimination were taken into consideration.

10. Summary and Conclusions

This work combined a theoretical analysis of processes controlling the isotopic composition of CO₂ and O₂ and observations from a field study with the aim to better understand the mechanisms and coupling of isotopic gas exchange in terrestrial ecosystems. Measurements of photosynthetic discrimination against ¹³C and ¹⁸O during field campaigns in spring and summer 2001 form the experimental basis of this study. Diurnal variations in the isotopic composition of CO₂ in canopy air and the isotopic signatures of foliage and soil respiration were also investigated.

Branch bag measurements revealed pronounced diurnal cycles in photosynthetic discrimination against ¹³C and ¹⁸O, with highest values of ¹³Δ and ¹⁸Δ at dawn and dusk. Predictions of ¹³Δ and ¹⁸Δ were derived using parameters calculated from concurrent micro-climate, CO₂ and water flux measurements, following formulations derived from theoretical descriptions of isotope fractionation during photosynthesis (Farquhar and Lloyd 1993).

Predictions of ¹³C discrimination from the commonly applied simple equation underestimated diurnal variations and overestimated diurnal integrals of ¹³Δ. At dawn and dusk, the values found for net observed ¹³C discrimination could not be predicted from theory, even with the extended formulation (Farquhar et al. 1982). Dark respiration in the light was identified as an important component of isotopic gas exchange at these times. Existing theory was thus modified to include an "effective fractionation" factor during day-time dark respiration, expressing the difference between the (relatively) stable average isotopic composition of plant assimilate used as a substrate for dark respiration and the variable instantaneous values of photosynthetic discrimination. This effective fractionation was found to contribute substantially to the observed pronounced diurnal changes in ¹³C discrimination. Good agreement of predicted with observed ¹³Δ values was achieved by combining influences of photosynthesis on the isotopic composition of ambient CO₂ with those of concurrent dark respiration, photorespiration and mesophyll conductance. The high values of ¹³C discrimination observed at dawn and dusk emphasize the importance of accurate determination of C_c/C_a, whereas the lower values during the rest of the day highlight the need of reliable determination of mesophyll conductance. This is important with respect to numerical simulations

describing processes in natural environments, especially on smaller spatial resolution and shorter time scales.

Comparison of the $\delta^{13}\text{C}$ composition of plant and soil organic material with that of respired CO_2 did not indicate significant fractionation during foliage and soil respiration. However, the magnitude of respiratory fractionation might be species dependent and needs to be examined further.

The comparison of predicted values of $^{18}\Delta$ with observations was useful for evaluating different formulations of the ^{18}O enrichment of foliage water at evaporating sites, i.e. the ^{18}O signal that is transferred to atmospheric CO_2 . Discrepancies were found between observed $^{18}\Delta$ values and those predicted by the Craig and Gordon equation (Craig and Gordon 1965), which is based on the assumption of evaporating site water at an (instantaneous) isotopic steady state. These discrepancies showed limitations of the Craig and Gordon equation widely used in numerical models. In this study, an isotopic steady state was only observed during the early afternoon. Steady state predictions overestimated the enrichment of evaporating site water in the morning and underestimated it in the evening. Better agreement was achieved with the non steady state formulation of Dongmann et al. (1974) which accounts for a gradual approach towards the isotopic steady state for water at the evaporating sites of foliage under natural conditions. Because the time required to reach steady state depends mainly on the rate of transpiration, any deviations from predictions assuming steady state enrichment are likely to be more pronounced in species with low transpiration rates, such as conifers. High precision measurements of transpiration rates are an important prerequisite to estimate non steady state enrichment of evaporating site water, gradients in isotopic signature of water within foliage, C_s/C_a , and hence photosynthetic ^{18}O discrimination. Further measurements are needed to establish correlations between the isotopic composition of foliage water at the evaporating sites and in chloroplasts under field conditions. Accurate descriptions of the oxygen isotopic signatures that are transferred to ambient CO_2 during photosynthesis will enhance our ability to use the ^{18}O signal of atmospheric CO_2 as a tracer of carbon cycling.

The oxygen isotopic signature of CO_2 released during foliage respiration could not be determined in this study, because night-time measurements yielded apparent levels of leaf water enrichment that were unrealistically high. Interference from an unidentified mass 46 compound with mass spectrometric analyses of $\text{C}^{16}\text{O}^{18}\text{O}$ was suspected to be

the cause of the apparent ^{18}O enrichment. The search for this compound, present in air samples collected at night, did not yield satisfactory results, because none of the likely candidates displayed the required set of properties.

The oxygen isotopic composition of soil respired CO_2 was found to vary diurnally. This is in contrast to the $\delta^{18}\text{O}$ signature expected from a simple isotopic equilibration of CO_2 with soil water, assumed to have only minor diurnal variations in isotopic composition. The existence of diurnal cycles could be explained by a concurrent flux of atmospheric invasion of CO_2 entering and leaving the soil with intermittent equilibration with soil water. While this invasion flux was estimated to be approximately constant over time, the soil respiration flux varied following diurnal changes in soil temperature. When the diurnally variable ratio of these two fluxes was taken into consideration, predicted oxygen isotopic signatures of soil respired CO_2 were in good agreement with measurements.

Stoichiometric ratios of O_2 : CO_2 exchange were obtained from measurements of photosynthetic, respiratory and integrated canopy gas exchange. Photosynthesis and foliage respiration were found to have a stoichiometric ratio of 1.1 to 1.2. This is within limits of oxidative ratios based on composition of average foliage material. Stoichiometric ratios of integrated canopy gas exchange were virtually indistinguishable from 1.0. The offset between this ratio and the stoichiometric ratios of photosynthetic or respiratory gas exchange could arise from incomplete sampling of a hysteresis-type relationship between the concentrations of O_2 and CO_2 in canopy air. This might also indicate that measurements of concurrent changes of O_2 and CO_2 mole fractions in canopy air are not the appropriate method to determine the stoichiometric ratio of the ecosystem gas exchange.

Attempts to measure changes in the isotopic signature of O_2 during canopy gas exchange processes showed that experimental uncertainties are currently too large to allow determination of isotopic signatures of O_2 fluxes. The analytical precision required to resolve changes in the isotopic composition of O_2 in canopy air and during chamber experiments was derived from estimates of the expected magnitude of signals.

The integration of assimilation and respiration fluxes scaled to the canopy level yielded magnitudes and diurnal variations in net ecosystem exchange of CO_2 that were in reasonable agreement with data obtained from the nearby eddy covariance tower.

Combining the CO₂ fluxes with their respective isotopic signatures predicted from theory and evaluated with observations (see Part I) provided estimates of component isofluxes of ecosystem isotopic exchange. One-way isofluxes of turbulent exchange were derived from mass balances of all other isofluxes. The isofluxes of one-way turbulent exchange were similar for the different days and the two months of sampling with respect to carbon isotopic composition but substantially different between days and months with respect to oxygen isotopic composition. Thus, simultaneous measurements of both isofluxes might add information not contained in the individual signals.

Finally, the reliability of different partitioning methods to estimate assimilation rates from canopy fluxes of turbulent CO₂ exchange was evaluated. Three formulations of partitioning equations were compared: the net isoflux approach (Bowling et al. 2001), the one-way isoflux approach (Lloyd et al. 1996) and the dual discrimination approach (this study). For solving the partitioning equations, the first two methods rely on canopy integrated values of stomatal conductance whereas the latter takes advantage of the coupling of carbon and oxygen isotopic discrimination during photosynthesis. The different methods were applied to turbulent fluxes from eddy measurements as well as to residual turbulent fluxes from canopy scale integrations. The one-way isoflux and dual discrimination approaches achieved the overall best agreement of partitioned with original rates of assimilation. The dual discrimination approach was, however, less reliable due to numerical instabilities. For residual fluxes, the net isoflux approach agreed well on average but poorly at specific times over the diurnal cycle. For eddy fluxes, the net isoflux approach overestimated input assimilation rates by up to 100 %. The partitioning study revealed that of the less well known parameters, mesophyll conductance appeared to be crucial for reliable partitioning of ecosystem CO₂ exchange. If the influence of fractionation during CO₂ transfer in foliage mesophyll on ¹³C discrimination was neglected, partitioned rates were up to 50 % higher than original rates.

In conclusion, stable isotopes are important tools for investigating the gas exchange at the ecosystem, leaf and cell level with an emphasis on process understanding. For example, when carbon is cycled through plants from uptake by foliage to release by roots, its $\delta^{13}\text{C}$ signatures provides a natural labelling that can be used to estimate the speed of this cycling. Variations in stable isotope signatures are linked to environmental parameters such as temperature and relative humidity. This provides the basis for the interpretation of isotopic paleorecords such as tree rings and fossil plant samples.

The stable isotopes of CO₂ (and O₂) are also valuable tools in integrations of carbon exchange at the global level. For example, the simultaneous simulation of mole fraction and isotopic composition of atmospheric CO₂ requires theoretical descriptions of the underlying processes and isotope fractionations. How well these are represented in the models can be examined by comparing the model results to field data.

Furthermore, including stable isotopes in field studies might even help to identify problems with experimental methods. For example, if measurements of environmental variables yield very low values of stomatal conductance then this could be caused by low transpiration rates due to closed stomata or it could point to a problem with one of the measurements (water vapour mole fraction, temperature and relative humidity). Additional isotopic analyses have helped in such a case to identify unreliable water vapour data as the problem and to confirm that the plants did indeed transpire.

In summary, this work has shown that a multi-tracer approach, making use of simultaneous availability of independent information on concentration and isotopic composition of CO₂ and O₂, has considerable potential to gain a better understanding of carbon exchange on the ecosystem scale. This knowledge can be applied to models and measurements of the carbon cycle on regional and global scales.

11. References

- Aggarwal PK and Dillon MA (1998) Stable isotope composition of molecular oxygen in soil gas and groundwater: A potentially robust tracer for diffusion and oxygen consumption processes. *Geochimica Et Cosmochimica Acta* 62: 577-584.
- Angert A and Luz B (2001) Fractionation of oxygen isotopes by root respiration: Implications for the isotopic composition of atmospheric O₂. *Geochimica Et Cosmochimica Acta* 65: 1695-1701.
- Apel EC, Riemer DD, Hills A, Baugh W, Orlando J, Faloon I, Tan D, Brune W, Lamb B, Westberg H, Carroll MA, Thornberry T and Geron CD (2002) Measurement and interpretation of isoprene fluxes and isoprene, methacrolein, and methyl vinyl ketone mixing ratios at the PROPHET site during the 1998 Intensive. *Journal of Geophysical Research* 107: 4019-4034.
- Arneth A, Kelliher FM, McSeveny TM and Byers JN (1998) Fluxes of carbon and water in a *Pinus radiata* forest subject to soil water deficit. *Australian Journal of Plant Physiology* 25: 557-570.
- Atkin OK, Evans JR, Ball MC, Lambers H and Pons TL (2000) Leaf respiration of snow gum in the light and dark. Interactions between temperature and irradiance. *Plant Physiology* 122: 915-923.
- Barbour MM, Andrews TJ and Farquhar GD (2001) Correlations between oxygen isotope ratios of wood constituents of *Quercus* and *Pinus* samples from around the world. *Australian Journal of Plant Physiology* 28: 335-348.
- Barton C (1997) Effects of elevated atmospheric carbon dioxide concentration on growth and physiology of Sitka spruce (*Picea sitchensis* (Bong.) Carr.). Thesis, University of Edinburgh, Edinburgh, UK.
- Beerling DJ, Lake JA, Berner RA, Hickey LJ, Taylor DW and Royer DL (2002) Carbon isotope evidence implying high O₂/CO₂ ratios in the Permo-Carboniferous atmosphere. *Geochimica Et Cosmochimica Acta* 66: 3757-3767.
- Bender M, Sowers T and Labeyrie L (1994) The Dole effect and its variations during the last 130,000 years as measured in the Vostok ice core. *Global Biogeochemical Cycles* 8: 363-376.
- Berry JA (1988) Studies of mechanisms affecting the fractionation of carbon isotopes in photosynthesis. In: Rundell PW, Ehleringer JR and Nagy KA (Eds), *Stable Isotopes in Ecological Research*. Springer, New York, pp. 82-94.
- Berry JA (1992) Biosphere, atmosphere, ocean interactions: A plant physiologist's

- perspective. In: Falcowski PG and Woodhead AD (Eds), Primary Productivity and biogeochemical cycles in the sea. Plenum Press, New York, pp. 441-454.
- Beverland IJ, Milne R, Boissard C, Oneill DH, Moncrieff JB and Hewitt CN (1996) Measurement of carbon dioxide and hydrocarbon fluxes from a Sitka Spruce forest using micrometeorological techniques. *Journal of Geophysical Research* 101: 22807-22815.
- Bird MI, Santruckova H, Lloyd J and M. VE (2001) The global soil organic carbon pool. In: Schulze E, Heimann M, Harrison S, Holland E, Lloyd J, Prentice IC and Schimel D (Eds), *Global Biogeochemical Cycles in the Climate System*. Academic Press, San Diego, pp. 185-199.
- Bloom AJ, Caldwell RM, Finazzo J, Warner RL and Weissbart J (1989) Oxygen and carbon dioxide fluxes from Barley shoots depend on nitrate assimilation. *Plant Physiology* 91: 352-356.
- Bousquet P, Ciais P, Peylin P, Ramonet M and Monfray P (1999) Inverse modeling of annual atmospheric CO₂ sources and sinks 1. Method and control inversion. *Journal of Geophysical Research* 104: 26161-26178.
- Bowling DR, Tans PP and Monson RK (2001) Partitioning net ecosystem carbon exchange with isotopic fluxes of CO₂. *Global Change Biology* 7: 127-145.
- Breninkmeijer CAM, Kraft P and Mook WG (1983) Oxygen isotope fractionation between CO₂ and H₂O. *Isotope Geoscience* 1: 181-190.
- Brooks A and Farquhar GD (1985) Effect of temperature on the CO₂/O₂ specificity of Ribulose-1,5-bisphosphate carboxylase oxygenase and the rate of respiration in the light - Estimates from gas-exchange measurements on spinach. *Planta* 165: 397-406.
- Buchmann N, Brooks JR and Ehleringer JR (2002) Predicting daytime carbon isotope ratios of atmospheric CO₂ within forest canopies. *Functional Ecology* 16: 49-57.
- Buchmann N, Kao WY and Ehleringer J (1997) Influence of stand structure on carbon-13 of vegetation, soils, and canopy air within deciduous and evergreen forests in Utah, United States. *Oecologia* 110: 109-119.
- Buhay WM, Edwards TWD and Aravena R (1996) Evaluating kinetic fractionation factors used for ecologic and paleoclimatic reconstructions from oxygen and hydrogen isotope ratios in plant water and cellulose. *Geochimica Et Cosmochimica Acta* 60: 2209-2218.
- Cerling TE, Solomon DK, Quade J and Bowman JR (1991) On the isotopic composition of carbon in soil carbon dioxide. *Geochimica Et Cosmochimica Acta* 55: 3403-3405.

- Cernusak LA, Pate JS and Farquhar GD (2002) Diurnal variation in the stable isotope composition of water and dry matter in fruiting *Lupinus angustifolius* under field conditions. *Plant Cell and Environment* 25: 893-907.
- Ciais P, Denning AS, Tans PP, Berry JA, Randall DA, Collatz GJ, Sellers PJ, White JWC, Trolier M, Meijer HAJ, Francey RJ, Monfray P and Heimann M (1997a) A three-dimensional synthesis study of $\delta^{18}\text{O}$ in atmospheric CO_2 . 1. Surface fluxes. *Journal of Geophysical Research* 102: 5857-5872.
- Ciais P, Tans PP, Denning AS, Francey RJ, Trolier M, Meijer HAJ, White JWC, Berry JA, Randall DA, Collatz GJ, Sellers PJ, Monfray P and Heimann M (1997b) A three-dimensional synthesis study of $\delta^{18}\text{O}$ in atmospheric CO_2 . 2. Simulations with the TM2 transport model. *Journal of Geophysical Research* 102: 5873-5883.
- Clement R (2003) Thesis, in preparation, University of Edinburgh, Edinburgh.
- Craig H (1953) The geochemistry of the stable carbon isotopes. *Geochimica Et Cosmochimica Acta* 3: 53-92.
- Craig H and Gordon L (1965) Deuterium and oxygen-18 variation in the ocean and marine atmosphere, *Stable Isotopes in Oceanography Studies of Paleotemperature*, Laboratory of Geology and Nuclear Science, Pisa, pp. 9-130.
- Dawson TE, Mambelli S, Plamboeck AH, Templer PH and Tu KP (2002) Stable isotopes in plant ecology, *Reviews in Advance*, *Annual Review of Ecology and Systematics*, pp. 507-559.
- Dole M (1935) The relative atomic weight of oxygen in water and in air. *Journal of the American Chemical Society* 57: 2731.
- Dole M, Hawkings RC and Barker HA (1947) Bacterial fractionation of oxygen isotopes. *Journal of the American Chemical Society* 69: 226-228.
- Dole M and Jenks G (1944) Isotopic composition of photosynthetic oxygen. *Science* 100: 409.
- Dole M, Lane GA, Rudd DP and Zaukelies DA (1954) Isotopic composition of atmospheric oxygen and nitrogen. *Geochimica Et Cosmochimica Acta* 6: 65-78.
- Dongmann G, Nürnberg HW, Förstel H and Wagener K (1974) Enrichment of H_2^{18}O in leaves of transpiring plants. *Radiation and Environmental Biophysics* 11: 41-52.
- Duranceau M, Ghashghaie J, Badeck F, Deleens E and Cornic G (1999) $\delta^{13}\text{C}$ of CO_2 respired in the dark in relation to $\delta^{13}\text{C}$ of leaf carbohydrates in *Phaseolus vulgaris* L under progressive drought. *Plant Cell and Environment* 22: 515-523.
- Duranceau M, Ghashghaie J and Brugnoli E (2001) Carbon isotope discrimination during photosynthesis and dark respiration in intact leaves of *Nicotiana sylvestris*: comparisons between wild type and mitochondrial mutant plants.

- Australian Journal of Plant Physiology 28: 65-71.
- Ekblad A and Högberg P (2001) Natural abundance of ^{13}C in CO_2 respired from forest soils reveals speed of link between tree photosynthesis and root respiration. *Oecologia* 127: 305-308.
- Evans JR, Sharkey TD, Berry JA and Farquhar GD (1986) Carbon isotope discrimination measured concurrently with gas-exchange to investigate CO_2 diffusion in leaves of higher plants. *Australian Journal of Plant Physiology* 13: 281-292.
- Evans JR and Von Caemmerer S (1996) Carbon dioxide diffusion inside leaves. *Plant Physiology* 110: 339-346.
- Farquhar GD (1983) On the nature of carbon isotope discrimination in C_4 species. *Australian Journal of Plant Physiology* 10: 205-226.
- Farquhar GD and Lloyd J (1993) Carbon and oxygen isotope effects in the exchange of carbon dioxide between terrestrial plants and the atmosphere. In: Ehleringer JR, Hall AE and Farquhar GD (Eds), *Stable Isotopes and Plant Carbon-Water Relations*. Academic Press, NY, pp. 47-70.
- Farquhar GD, Lloyd J, Taylor JA, Flanagan LB, Syvertsen JP, Hubick KT, Wong SC and Ehleringer JR (1993) Vegetation effects on the isotope composition of oxygen in atmospheric CO_2 . *Nature* 363: 439-443.
- Farquhar GD, O'Leary MH and Berry JA (1982) On the relationship between carbon isotope discrimination and the inter-cellular carbon dioxide concentration in leaves. *Australian Journal of Plant Physiology* 9: 121-137.
- Farquhar GD and Richards RA (1984) Isotopic composition of plant carbon correlates with water-use efficiency of wheat genotypes. *Australian Journal of Plant Physiology* 11: 539-552.
- Farquhar GD and Von Caemmerer S (1982) Modelling of photosynthetic response to environmental conditions. In: Lange OL, Nobel PS, Osmond CB and Ziegler H (Eds), *Encyclopedia of Plant Physiology*. Springer Verlag, Berlin, pp. 549-598.
- Flanagan LB, Brooks JR, Varney GT, Berry SC and Ehleringer JR (1996) Carbon isotope discrimination during photosynthesis and the isotope ratio of respired CO_2 in boreal forest ecosystems. *Global Biogeochemical Cycles* 10: 629-640.
- Flanagan LB, Brooks JR, Varney GT and Ehleringer JR (1997) Discrimination against $\text{C}^{18}\text{O}^{16}\text{O}$ during photosynthesis and the oxygen isotope ratio of respired CO_2 in boreal forest ecosystems. *Global Biogeochemical Cycles* 11: 83-98.
- Flanagan LB, Kubien DS and Ehleringer JR (1999) Spatial and temporal variation in the carbon and oxygen stable isotope ratio of respired CO_2 in a boreal forest

- ecosystem. *Tellus Series B* 51: 367-384.
- Francey RJ, Gifford RM, Sharkey TD and Weir B (1985) Physiological influences on carbon isotope discrimination in Huon Pine (*Lagarostrobos-Franklinii*). *Oecologia* 66: 211-218.
- Francey RJ and Tans PP (1987) Latitudinal variation in ^{18}O of atmospheric CO_2 . *Nature* 327: 495-497.
- Francey RJ, Tans PP, Allison CE, Enting IG, White JWC and Trolrier M (1995) Changes in oceanic and terrestrial carbon uptake since 1982. *Nature* 373: 326-330.
- Friedman I and O'Neil JR (1977) Compilation of stable isotope fractionation factors of geochemical interest. U.S. Geological Survey Professional Paper 440-KK, Data of Geochemistry, Sixth Edition: Chapter KK, KK1-KK12.
- Fung I, Field CB, Berry JA, Thompson MV, Randerson JT, Malmstrom CM, Vitousek PM, Collatz GJ, Sellers PJ, Randall DA, Denning AS, Badeck F and John J (1997) Carbon 13 exchanges between the atmosphere and biosphere. *Global Biogeochemical Cycles* 11: 507-533.
- Geron C, Rasmussen R, Arnts RR and Guenther A (2000) A review and synthesis of monoterpene speciation from forests in the United States. *Atmospheric Environment* 34: 1761-1781.
- Ghashghaie J, Duranceau M, Badeck FW, Cornic G, Adeline MT and Deleens E (2001) $\delta^{13}\text{C}$ of CO_2 respired in the dark in relation to $\delta^{13}\text{C}$ of leaf metabolites: comparison between *Nicotiana sylvestris* and *Helianthus annuus* under drought. *Plant Cell and Environment* 24: 505-515.
- Gillon JS (1997) Carbon isotope discrimination interactions between respiration, leaf conductance and photosynthetic capacity. Thesis, University of Newcastle-upon-Tyne, Newcastle-upon-Tyne, 185 pp.
- Gillon JS and Yakir D (2000) Internal conductance to CO_2 diffusion and $(\text{COO})\text{-}^{18}\text{O}$ discrimination in C_3 leaves. *Plant Physiology* 123: 201-213.
- Glasius M, Boel C, Bruun N, Easa LM, Hornung P, Klausen HS, Klitgaard KC, Lindeskov C, Moller CK, Nissen H, Petersen APF, Kleefeld S, Boaretto E, Hansen TS, Heinemeier J and Lohse C (2001) Relative contribution of biogenic and anthropogenic sources to formic and acetic acids in the atmospheric boundary layer. *Journal of Geophysical Research* 106: 7415-7426.
- Glasius M, Wessel S, Christensen CS, Jacobsen JK, Jorgensen HE, Klitgaard KC, Petersen L, Rasmussen JK, Hansen TS, Lohse C, Boaretto E and Heinemeier J (2000) Sources to formic acid studied by carbon isotopic analysis and air mass characterization. *Atmospheric Environment* 34: 2471-2479.

- Goodman HS and Francey RJ (1988) $^{13}\text{C}/^{12}\text{C}$ and $^{18}\text{O}/^{16}\text{O}$ in baseline CO_2 . In: Forgan BW and Fraser PJ (Eds), Baseline Atmospheric Program (Australia). CSIRO, Canberra, Australia, pp. 54-58.
- Goulden ML, Munger JW, Fan S, Daube BC and Wofsy SC (1996) Measurements of carbon sequestration by long-term eddy covariance: methods and a critical evaluation of accuracy. *Global Change Biology* 2: 169-182.
- Grace J, Malcolm DC and Bradbury IK (1975) Effect of wind and humidity on leaf diffusive resistance in Sitka spruce seedlings. *Journal of Applied Ecology* 12: 931-940.
- Griffiths H, Borland AM, Gillon JS, Harwood KG, Maxwell K and Wilson JM (1999) Stable isotopes reveal exchanges between soil, plants and the atmosphere. In: Press MC, Scholes JD and Barker MG (Eds), *Advances in Physiological Plant Ecology*. Blackwell Science, Oxford, pp. 415-441.
- Guy RD, Berry JA, Fogel ML and Hoering TC (1989) Differential fractionation of oxygen isotopes by cyanide-resistant and cyanide-sensitive respiration in plants. *Planta* 177: 483-491.
- Guy RD, Fogel ML and Berry JA (1993) Photosynthetic fractionation of the stable isotopes of oxygen and carbon. *Plant Physiology* 101: 37-47.
- Hargreaves PR, Leidi A, Grubb HJ, Howe MT and Mugglestone MA (2000) Local and seasonal variations in atmospheric nitrogen dioxide levels at Rothamsted, UK, and relationships with meteorological conditions. *Atmospheric Environment* 34: 843-853.
- Harwood KG, Gillon JS, Griffiths H and Broadmeadow MSJ (1998) Diurnal variation of $\delta^{13}\text{CO}_2$, $\delta\text{C}^{18}\text{O}^{16}\text{O}$ and evaporative site enrichment of $\delta\text{H}_2^{18}\text{O}$ in *Piper aduncum* under field conditions in Trinidad. *Plant Cell and Environment* 21: 269-283.
- Harwood KG, Gillon JS, Roberts A and Griffiths H (1999) Determinants of isotopic coupling of CO_2 and water vapour within a *Quercus petraea* forest canopy. *Oecologia* 119: 109-119.
- Heimann M (2001) The cycle of atmospheric molecular oxygen and its isotopes. In: Schulze E, Heimann M, Harrison S, Holland E, Lloyd J, Prentice IC and Schimel D (Eds), *Global biogeochemical cycles in the climate system*. Academic Press, San Diego, pp. 235-244.
- Heimann M, Keeling CD and Tucker CJ (1989) A three-dimensional model of atmospheric CO_2 transport based on observed winds: 3. Seasonal cycle and synoptic time scale variations. In: Peterson DH (Ed), *Aspects of Climate Variability in the Pacific and the Western Americas*, AGU Monograph 55.

- American Geophysical Union, Washington, pp. 277-303.
- Helmig D, Klinger LF, Guenther A, Vierling L, Geron C and Zimmerman P (1999) Biogenic volatile organic compound emissions (BVOCs) I. Identifications from three continental sites in the US. *Chemosphere* 38: 2163-2187.
- Hesterberg R and Siegenthaler U (1991) Production and stable isotopic composition of CO₂ in a soil near Bern, Switzerland. *Tellus Series B* 43: 197-205.
- Horibe Y, Shigehar.K and Takakuwa Y (1973) Isotope separation factor of carbon dioxide water system and isotopic composition of atmospheric oxygen. *Journal of Geophysical Research* 78: 2625-2629.
- IPCC (2001) *Climate Change 2001: The Scientific Basis*. Contribution of Working Group I to the Third Assessment Report of the Intergovernmental Panel on Climate Change. Cambridge University Press, Cambridge, UK and New York, USA.
- Jensen LS, Mueller T, Tate KR, Ross DJ, Magid J and Nielsen NE (1996) Soil surface CO₂ flux as an index of soil respiration in situ: a comparison of two chamber methods. *Soil Biology and Biogeochemistry* 28: 1297-1306.
- Kaplan JO, Prentice IC and Buchmann N (2001) The stable carbon isotope composition of the terrestrial biosphere, In: *Geophysical Applications of Vegetation Modeling*. Thesis, Lund University, Lund, pp. 89-109.
- Katul GG, Ellsworth DS and Lai CT (2000) Modelling assimilation and intercellular CO₂ from measured conductance: a synthesis of approaches. *Plant Cell and Environment* 23: 1313-1328.
- Keeling CD (1961) The concentration and isotopic abundance of carbon dioxide in rural and marine air. *Geochimica et Cosmochimica Acta* 24: 277-298.
- Keeling CD, Piper SC and Heimann M (1989) A three-dimensional model of atmospheric CO₂ transport based on observed winds: 4. Mean annual gradients and interannual variations. In: Peterson DH (Ed), *Aspects of Climate Variability in the Pacific and the Western Americas*, AGU Monograph 55. American Geophysical Union, Washington, pp. 305-363.
- Keeling RF (1988a) Development of an interferometric oxygen analyzer for precise measurements of the atmospheric O₂ mole fraction. Thesis, Harvard University, Cambridge, Massachusetts, USA, 179 pp.
- Keeling RF (1988b) Measuring correlations between atmospheric oxygen and carbon dioxide mole fractions: A preliminary study in urban air. *Journal of Atmospheric Chemistry* 7: 153-176.
- Keeling RF, Najjar RP, Bender ML and Tans PP (1993) What atmospheric oxygen measurements can tell us about the global carbon cycle. *Global Biogeochemical*

Cycles 7: 37-67.

- Keeling RF and Shertz SR (1992) Seasonal and interannual variations in atmospheric oxygen and implications for the global carbon cycle. *Nature* 358: 723-727.
- Kesselmeier J (2001) Exchange of short-chain oxygenated volatile organic compounds (VOCs) between plants and the atmosphere: A compilation of field and laboratory studies. *Journal of Atmospheric Chemistry* 39: 219-233.
- Kroopnick P and Craig H (1972) Atmospheric oxygen - Isotopic composition and solubility fractionation. *Science* 175: 54.
- Lamb B, Grosjean D, Pun B and Seigneur C (1999) Review of the emissions, atmospheric chemistry, and gas/particle partition of biogenic volatile organic compounds and reaction products, Atmospheric and Environmental Research, Inc., Atlanta.
- Lane GA and Dole M (1956) Fractionation of oxygen isotopes during respiration. *Science* 123: 574-576.
- Lin GH and Ehleringer JR (1997) Carbon isotopic fractionation does not occur during dark respiration in C₃ and C₄. *Plant Physiology* 114: 391-394.
- Lloyd J and Farquhar GD (1994) ¹³C Discrimination During CO₂ Assimilation By the Terrestrial Biosphere. *Oecologia* 99: 201-215.
- Lloyd J, Francey RJ, Mollicone D, Raupach MR, Sogachev A, Arneth A, Byers JN, Kelliher FM, Rebmann C, Valentini R, Wong SC, Bauer G and Schulze ED (2001) Vertical profiles, boundary layer budgets, and regional flux estimates for CO₂ and its ¹³C/¹²C ratio and for water vapor above a forest/bog mosaic in central Siberia. *Global Biogeochemical Cycles* 15: 267-284.
- Lloyd J, Kruijt B, Hollinger DY, Grace J, Francey RJ, Wong SC, Kelliher FM, Miranda AC, Farquhar GD, Gash JHC, Vygodskaya NN, Wright IR, Miranda HS and Schulze ED (1996) Vegetation effects on the isotopic composition of atmospheric CO₂ at local and regional scales: Theoretical aspects and a comparison between rain forest in amazonia and a boreal forest in Siberia. *Australian Journal of Plant Physiology* 23: 371-399.
- Lloyd J, Kruijt B, Hollinger DY, Grace J, Francey RJ, Wong SC, Kelliher FM, Miranda AC, Farquhar GD, Gash JHC, Vygodskaya NN, Wright IR, Miranda HS and Schulze ED (1997) An alternative interpretation of the appropriateness and correct means for the evaluation of CO₂ recycling indices - Response. *Australian Journal of Plant Physiology* 24: 399-405.
- Lloyd J, Shibistova O, Zolotoukhine D, Kolle O, Arneth A, Wirth C, Styles J, Tchebakova N and Schulze E (2002) Seasonal and annual variations in the photosynthetic

- productivity and carbon balance of a central Siberian pine forest. *Tellus Euro Siberian Carbonflux Special Issue*, submitted.
- Lloyd J, Syvertsen JP, Kriedemann PE and Farquhar GD (1992) Low conductances for CO₂ diffusion from stomata to the sites of carboxylation in leaves of woody species. *Plant Cell and Environment* 15: 873-899.
- Majoube M (1971) Oxygen-18 and deuterium fractionation between water and steam. *Journal De Chimie Physique Et De Physico-Chimie Biologique* 68: 1423-&.
- Malaize B, Paillard D, Jouzel J and Raynaud D (1999) The Dole effect over the last two glacial-interglacial cycles. *Journal of Geophysical Research* 104: 14199-14208.
- Moncrieff JB, Massheder JM, deBruin H, Elbers J, Friborg T, Heusinkveld B, Kabat P, Scott S, Soegaard H and Verhoef A (1997) A system to measure surface fluxes of momentum, sensible heat, water vapour and carbon dioxide. *Journal of Hydrology* 189: 589-611.
- Mook WG (1986) ¹³C in atmospheric CO₂. *Netherlands Journal of Sea Research* 20: 211-223.
- Mook WG, Bommerson JC and Staverman WH (1974) Carbon isotope fractionation between dissolved bicarbonate and gaseous carbon-dioxide. *Earth and Planetary Science Letters* 22: 169-176.
- Morita N (1935) The increased density of air oxygen relative to water oxygen. *Journal of the Chemical Society of Japan* 56: 1291.
- Mortazavi B and Chanton JP (2002) Carbon isotopic discrimination and control of nighttime canopy δ¹⁸O-CO₂ in a pine forest in the southeastern United States. *Global Biogeochemical Cycles* 16: art. no.-1008.
- Neter J, Wasserman W and Kutner MH (1985) *Applied linear statistical models*, Irwin, Homewood, Illinois, 1127 pp.
- Ogee J, Peylin P, Ciais P, Bariac T, Brunet Y, Berbigier P, Roche C, Richard P, Bardoux G and Bonnefond J-M (2003) Partitioning net ecosystem carbon exchange into net assimilation and respiration using ¹³CO₂ measurements: a cost-effective sampling strategy, submitted.
- O'Leary MH (1981) Carbon isotope fractionation in plants. *Phytochemistry* 20: 553-567.
- O'Leary MH (1984) Measurement of the isotope fractionation associated with diffusion of carbon-dioxide in aqueous solution. *Journal of Physical Chemistry* 88: 823-825.
- O'Leary MH (1988) Carbon isotopes in photosynthesis. *Bioscience* 38: 328-336.
- O'Neill AL, Kupiec JA and Curran PJ (2002) Biochemical and reflectance variation throughout a Sitka spruce canopy. *Remote Sensing of Environment* 80: 134-142.

- Park R and Epstein S (1961) Metabolic fractionation of ^{13}C and ^{12}C in plants. *Plant Physiology* 36: 133-&.
- Pessaraki M (1997) Handbook of photosynthesis. II. Series. M. Dekker, New York.
- Peylin P, Ciais P, Denning AS, Tans PP, Berry JA and White JWC (1999) A 3-dimensional study of $\delta^{18}\text{O}$ in atmospheric CO_2 : Contribution of different land ecosystems. *Tellus Series B* 51: 642-667.
- Pio C, Alves C and Duarte A (2001) Organic components of aerosols in a forested area of central Greece. *Atmospheric Environment* 35: 389-401.
- Rakestraw NM, Rudd DP and Dole M (1951) Isotopic composition of oxygen in air dissolved in Pacific ocean water as a function of depth. *Journal of the American Chemical Society* 73: 2976-2976.
- Rayment MB and Jarvis PG (1999) Seasonal gas exchange of black spruce using an automatic branch bag system. *Canadian Journal of Forest Research* 29: 1528-1538.
- Rayment MB, Loustau D and Jarvis PG (2002) Photosynthesis and respiration of black spruce at three organizational scales: shoot, branch and canopy. *Tree Physiology* 22: 219-229.
- Rayner PJ, Enting IG, Francey RJ and Langenfelds R (1999) Reconstructing the recent carbon cycle from atmospheric CO_2 , $\delta^{13}\text{C}$ and O_2/N_2 observations. *Tellus Series B* 51: 213-232.
- Riley WJ, Still CJ, Torn MS and Berry JA (2002) A mechanistic model of H_2^{18}O and C^{18}OO fluxes between ecosystems and the atmosphere: Model description and sensitivity analyses. *Global Biogeochemical Cycles*.
- Roake WE and Dole M (1950) Oxygen isotope exchange in the electric discharge. *Journal of the American Chemical Society* 72: 36-40.
- Roeske CA and O'Leary MH (1984) Carbon isotope effects on the enzyme-catalyzed carboxylation of ribulose biphosphate. *Biochemistry* 23: 6275-6284.
- Rooney MA (1988) Short-term carbon isotope fractionation by plants. Thesis, University of Wisconsin, Madison.
- Ruben S, Randall M, Kamen M and Hyde JL (1941) Heavy oxygen (^{18}O) as tracer in the study of photosynthesis. *Journal of the American Chemical Society* 63: 877-879.
- Santruckova H, Bird MI and Lloyd J (2000) Microbial processes and carbon-isotope fractionation in tropical and temperate grassland soils. *Functional Ecology* 14: 108-114.
- Sauer F, Beck J, Schuster G and Moortgat GK (2001) Hydrogen peroxide, organic peroxides and organic acids in a forested area during FIELDVOC'94.

- Chemosphere-Global Change Science 3: 309-326.
- Schleser GH (1979) Oxygen isotope fractionation during respiration for different temperatures of *T. utilis* and *E. coli* K12. *Radiation and Environmental Biophysics* 17: 85-93.
- Scholze M, Kaplan JO, Knorr W and Heimann M (2003) Climate and interannual variability of the atmosphere-biosphere $^{13}\text{CO}_2$ flux. *Geophysical Research Letters*, in press.
- Seibt U (1997) Simulation der $^{18}\text{O}/^{16}\text{O}$ -Zusammensetzung von atmosphärischem Sauerstoff. Diploma Thesis, Universität Tübingen, Germany.
- Severinghaus JP (1995) Studies of the terrestrial O_2 and carbon cycles in sand dune gases and in Biosphere 2. Thesis, Columbia University, New York, 148 pp.
- Smith BN (1971) Carbon isotope ratios of respired CO_2 from castor bean, corn, peanut, pea, radish, squash, sunflower and wheat seedlings. *Plant and Cell Physiology* 12: 451-455.
- Smith BN and Turner BL (1975) Distribution of Kranz syndrome among Asteraceae. *American Journal of Botany* 62: 541-545.
- Sparks JP, Monson RK, Sparks KL and Lerdau M (2001) Leaf uptake of nitrogen dioxide (NO_2) in a tropical wet forest: Implications for tropospheric chemistry. *Oecologia* 127: 214-221.
- Stern L, Baisden WT and Amundson R (1999) Processes controlling the oxygen isotope ratio of soil CO_2 : Analytic and numerical modeling. *Geochimica Et Cosmochimica Acta* 63: 799-814.
- Stevens CLR, Schultz D, Vanbaalen C and Parker PL (1975) Oxygen isotope fractionation during photosynthesis in a blue-green and a green alga. *Plant Physiology* 56: 126-129.
- Street RA, Duckham SC and Hewitt CN (1996) Laboratory and field studies of biogenic volatile organic compound emissions from sitka spruce (*Picea sitchensis* Bong) in the United Kingdom. *Journal of Geophysical Research* 101: 22799-22806.
- Syvertsen JP, Lloyd J, McConchie C, Kriedemann PE and Farquhar GD (1995) On the relationship between leaf anatomy and CO_2 diffusion through the mesophyll of hypostomatous leaves. *Plant Cell and Environment* 18: 149-157.
- Tans PP (1980) On calculating the transfer of ^{13}C in reservoir models of the carbon cycle. *Tellus* 32: 464-469.
- Tans PP (1998) Oxygen isotopic equilibrium between carbon dioxide and water in soils. *Tellus Series B* 50: 163-178.
- von Caemmerer S and Farquhar GD (1981) Some relationships between the

- biochemistry of photosynthesis and the gas exchange of leaves. *Planta* 153: 376-387.
- Wainhouse D, Ashburner R, Ward E and Rose J (1998) The effect of variation in light and nitrogen on growth and defence in young Sitka Spruce. *Functional Ecology* 12: 561-572.
- Wang XF and Yakir D (2000) Using stable isotopes of water in evapotranspiration studies. *Hydrological Processes* 14: 1407-1421.
- Wang XF, Yakir D and Avishai M (1998) Non-climatic variations in the oxygen isotopic compositions of plants. *Global Change Biology* 4: 835-849.
- Werner RA and Brand WA (2001) Referencing strategies and techniques in stable isotope ratio analysis. *Rapid Communications in Mass Spectrometry* 15: 501-519.
- Werner RA, Bruch BA and Brand WA (1999) ConFlo III - An interface for high precision $\delta^{13}\text{C}$ and $\delta^{15}\text{N}$ analysis with an extended dynamic range. *Rapid Communications in Mass Spectrometry* 13: 1237-1241.
- Werner RA, Rothe M and Brand WA (2001) Extraction of CO_2 from air samples for isotopic analysis and limits to ultra high precision $\delta^{18}\text{O}$ determination in CO_2 gas. *Rapid Communications in Mass Spectrometry* 15: 2152-2167.
- Williams TG, Flanagan LB and Coleman JR (1996) Photosynthetic gas exchange and discrimination against $(\text{CO}_2)^{13}\text{C}$ and $(\text{COO})^{18}\text{O}^{16}\text{O}$ in tobacco plants modified by an antisense construct to have low chloroplastic carbonic anhydrase. *Plant Physiology* 112: 319-326.
- Wingate L (2003) The contribution of photosynthesis and respiration to the net ecosystem exchange of a Sitka spruce plantation. Thesis, submitted, University of Edinburgh, Edinburgh.
- Yakir D, Berry JA, Giles L and Osmond CB (1994) Isotopic heterogeneity of water in transpiring leaves - Identification of the component that controls the $\delta^{18}\text{O}$ of atmospheric O_2 and CO_2 . *Plant Cell and Environment* 17: 73-80.
- Yakir D and Wang XF (1996) Fluxes of CO_2 and water between terrestrial vegetation and the atmosphere estimated from isotope measurements. *Nature* 380: 515-517.

Appendix 1

Derivation of C_i/C_a from observed $^{13}\Delta$

An expression for C_i/C_a (equation 4.2) was derived from extended formulation of ^{13}C discrimination (equation 3.3, see Appendix 2 of Farquhar et al. 1982):

$$^{13}\Delta = a \frac{C_a - C_i}{C_a} + a_m \frac{C_i - C_c}{C_a} + b \frac{C_c}{C_a} - f \frac{\Gamma^*}{C_a} - e \frac{R_d}{kC_a} \quad (\text{A.1})$$

The equation is based on the assumption that isotopic signatures of respiratory substrates are the same as those of fresh plant assimilates (from assimilation weighted $^{13}\Delta$). This is likely to be the case for photorespiration on average as well as instantaneously, as it recycles freshly assimilated carbon with isotopic signature of (or close to) instantaneous $^{13}\Delta$. For mass balance reasons, it must also be true for dark respiration on average, with $\delta^{13}\text{C}_{\text{plant}} = \delta^{13}\text{C}_{\text{atm}} - ^{13}\Delta$, but not always for instantaneous observations.

The substrate of dark respiration has an isotopic composition of average assimilation weighted $^{13}\Delta$ (denoted by $\int^{13}\Delta$), whereas instantaneous $^{13}\Delta$ follows a pronounced diurnal cycle with values different from this average at most times. To take this into account, the above equation has to be modified. An effective fractionation factor, e^* , is defined expressing the difference between isotopic signals of dark respiration ($\delta^{13}\text{C}_{\text{res}} = \delta^{13}\text{C}_{\text{atm}} - \delta^{13}\text{C}_{\text{plant}}$) and photosynthesis ($^{13}\Delta$) at each time step according to:

$$e^* = \delta^{13}\text{C}_{\text{res}} - ^{13}\Delta = \delta^{13}\text{C}_{\text{atm}} - \delta^{13}\text{C}_{\text{plant}} - ^{13}\Delta \quad (\text{A.2})$$

Because $\delta^{13}\text{C}_{\text{plant}} = \delta^{13}\text{C}_{\text{atm}} - \int^{13}\Delta$, e^* is zero on average.

With this, equation A.1 is modified to:

$$^{13}\Delta = a + (a_m - a) \frac{C_i}{C_a} + (b - a_m) \frac{C_c}{C_a} - f \frac{\Gamma^*}{C_a} - (e + e^*) \frac{R_d}{kC_a} \quad (\text{A.3})$$

using $k = (A + R_d)/(C_i(1 - \Gamma^*/C_i))$ (from Appendix 2 of Farquhar et al. (1982)) gives:

$$^{13}\Delta = a + (a_m - a) \frac{C_i}{C_a} + (b - a_m) \frac{C_c}{C_a} - f \frac{\Gamma^*}{C_a} - (e + e^*) \frac{R_d}{A + R_d} \frac{C_i}{C_a} + (e + e^*) \frac{R_d}{A + R_d} \frac{\Gamma^*}{C_a} \quad (\text{A.4})$$

and substituting C_c from equation 3.10 ($A = g_w(C_i - C_c)$) yields:

$$^{13}\Delta = a + (b - a) \frac{C_i}{C_a} - (b - a_m) \frac{A}{g_w C_a} - f \frac{\Gamma^*}{C_a} - (e + e^*) \frac{R_d}{A + R_d} \frac{C_i}{C_a} + (e + e^*) \frac{R_d}{A + R_d} \frac{\Gamma^*}{C_a} \quad (\text{A.5})$$

By collecting like terms and rearranging, this can be solved for C_i/C_a :

$$\frac{C_i}{C_a} = \frac{^{13}\Delta - a + (b - a_m) \frac{A}{g_w C_a} + \left(f - (e + e^*) \frac{R_d}{A + R_d} \right) \frac{\Gamma^*}{C_a}}{b - a - (e + e^*) \frac{R_d}{A + R_d}} \quad (\text{A.6})$$

[Remark: Introduction of the term e^* would change equation B8 (and B9 etc) in Appendix 2 of Farquhar et al. (1982) from

$$R_d'/R_d = (1 - e/1000)(A'/A) \quad \text{to}$$

$$R_d'/R_d = (1 - (e + e^*)/1000)(A'/A)$$

$$\text{with } R_d'/R_d = (1 - e/1000)(l'/l) \quad \text{and} \quad l'/l = (1 - e^*/1000)(A'/A)$$

so that e^* , as difference between fresh assimilate (A'/A) and long term mean assimilate (l'/l), is an "effective fractionation" but zero on average.]

Appendix 2

Partitioning equations

Net isoflux approach

The net isoflux approach applies the CO₂ mass balance equation of Lloyd et al. (1996) but the isoflux of turbulent exchange is based on the net turbulent CO₂ exchange instead of on the one-way turbulent CO₂ exchange as in Lloyd et al. (1996). This results in a different formulation of non-biological fluxes in the isotopic mass balance for δ¹³C of CO₂ in canopy air (see equations 1 and 5 of Bowling et al. (2001)):

$$M_i \frac{dC_a}{dt} + F_n = R_s - A \quad (\text{P.1})$$

$$M_i \left(C_a \frac{d\delta_i^{13}}{dt} + \delta_i^{13} \frac{dC_a}{dt} \right) + (2mC_a + n)F_n = \delta^{13} R_s R_s + ({}^{13}\Delta - \delta_i^{13})A \quad (\text{P.2})$$

where $(2mC_a + n)$ is the isotopic composition of the net eddy isoflux (F_n) as in equation 16 of Bowling et al (2001). A and R have positive signs. R_f is omitted (see section 9). Subtracting equation P.1 multiplied by $\delta^{13}C_{R_s}$ from P.2 and rearranging:

$$M_i \left(C_a \frac{d\delta_i^{13}}{dt} + (\delta_i^{13} - \delta^{13} R_s) \frac{dC_a}{dt} \right) + (2mC_a + n - \delta^{13} R_s)F_n = ({}^{13}\Delta + \delta^{13} R_s - \delta_i^{13})A \quad (\text{P.3})$$

Combining equation 3.9 (simplified by neglecting contributions from photo- and day-time dark respiration):

$${}^{13}\Delta = a \frac{C_a - C_i}{C_a} + a_m \frac{C_i - C_c}{C_a} + b \frac{C_c}{C_a} \quad (\text{P.4})$$

with stomatal and mesophyll conductances from equations 3.10 ($A = g_w (C_i - C_c)$) and simple version of equation 2.6 ($A = g_c (C_a - C_i)$) yields:

$${}^{13}\Delta = b + \frac{(a-b)g_w + (a_m - b)g_c}{g_w g_c C_a} A \quad (\text{P.5})$$

Substituting $^{13}\Delta$ from P.5 into P3 and solving for A results in a quadratic equation for A :

$$0 = \frac{(a-b)g_w + (a_m - b)g_c}{g_w g_c C_a} A^2 + (b + \delta^{13}_{Rs} - \delta^{13}_i)A - F_{NIA} \quad (\text{P.6})$$

with the following abbreviation:

$$F_{NIA} = M_i \left(C_a \frac{d\delta_i^{13}}{dt} + (\delta_i^{13} - \delta^{13}_{Rs}) \frac{dC_a}{dt} \right) + (2mC_a + n - \delta^{13}_{Rs})F_n \quad (\text{P.7})$$

with two possible solutions, where only one gives realistic results for A :

$$A_{1/2} = \frac{-(b + \delta^{13}_{Rs} - \delta^{13}_i) \pm \sqrt{(b + \delta^{13}_{Rs} - \delta^{13}_i)^2 + 4F_{NIA} \frac{(a-b)g_w + (a_m - b)g_c}{g_w g_c C_a}}}{2 \frac{(a-b)g_w + (a_m - b)g_c}{g_w g_c C_a}} \quad (\text{P.8})$$

For the simple alternative derivation, replacing equation P.4 with the simplest (and most commonly used) version (see equation 3.1):

$$^{13}\Delta = a \frac{C_a - C_i}{C_a} + b \frac{C_i}{C_a} \quad (\text{P.9})$$

would change equation P.5 to:

$$^{13}\Delta = b + \frac{(a-b)}{g_c C_a} A \quad (\text{P.10})$$

In this case, the resulting possible solutions would be:

$$A_{1/2} = \left(-(b + \delta^{13}_{Rs} - \delta^{13}_i) \pm \sqrt{(b + \delta^{13}_{Rs} - \delta^{13}_i)^2 + 4F_{NIA} \frac{(a-b)}{g_c C_a}} \right) \cdot \left(2 \frac{(a-b)}{g_c C_a} \right)^{-1} \quad (\text{P.11})$$

(Note that equation A5 of Bowling et al. (2001) contains a typographical error so that it is not a solution for the quadratic equation for A given in their appendix).

One-way isoflux approach

Starting with mass balance equations for CO₂ mole fraction and δ¹³C of CO₂ in canopy air (from Lloyd et al. (1996), see equation 7.1 and 7.2, omitting R_f):

$$M_i \frac{dC_a}{dt} + F_n = R_s - A \quad (\text{P.12})$$

$$M_i C_a \frac{d\delta_i^{13}}{dt} - F_{oi} (\delta_o^{13} - \delta_i^{13}) = (\delta_{Rs}^{13} - \delta_i^{13}) R_s + {}^{13}\Delta A \quad (\text{P.13})$$

The difference between the net isoflux approach and the one-way isoflux approach can be seen by comparing equations P.2 and P.13. Multiplying P.12 by (δ¹³C_{Rs} - δ¹³C_i) and subtracting the result from P.13:

$$M_i C_a \frac{d\delta_i^{13}}{dt} - (\delta_o^{13} - \delta_i^{13}) F_{oi} - (\delta_{Rs}^{13} - \delta_i^{13}) \left(M_i \frac{dC_a}{dt} + F_n \right) = ({}^{13}\Delta + \delta_{Rs}^{13} - \delta_i^{13}) A \quad (\text{P.14})$$

Again, substituting ¹³Δ from P.5 into P.14 and solving for A results in a quadratic equation for A:

$$0 = \frac{(a-b)g_w + (a_m - b)g_c}{g_w g_c C_a} A^2 + (b + \delta_{Rs}^{13} - \delta_i^{13}) A - F_{OIA} \quad (\text{P.15})$$

where:

$$F_{OIA} = M_i C_a \frac{d\delta_i^{13}}{dt} - (\delta_o^{13} - \delta_i^{13}) F_{oi} - (\delta_{Rs}^{13} - \delta_i^{13}) \left(M_i \frac{dC_a}{dt} + F_n \right) \quad (\text{P.16})$$

with two possible solutions, where (usually) only one gives realistic results for A:

$$A_{1/2} = \frac{-(b + \delta_{Rs}^{13} - \delta_i^{13}) \pm \sqrt{(b + \delta_{Rs}^{13} - \delta_i^{13})^2 + 4F_{OIA} \frac{(a-b)g_w + (a_m - b)g_c}{g_w g_c C_a}}}{2 \frac{(a-b)g_w + (a_m - b)g_c}{g_w g_c C_a}} \quad (\text{P.17})$$

In the simple alternative derivation, as above, substituting $^{13}\Delta$ from equation P.10 instead of P.5 into P.14 yields different solutions:

$$A_{1/2} = \left(-\left(b + \delta^{13}_{Rs} - \delta^{13}_i \right) \pm \sqrt{\left(b + \delta^{13}_{Rs} - \delta^{13}_i \right)^2 + 4F_{OIA} \frac{(a-b)}{g_c C_a}} \right) \cdot \left(2 \frac{(a-b)}{g_c C_a} \right)^{-1} \quad (\text{P.18})$$

Dual discrimination approach

This approach is based on simultaneously solving mass balances for mole fraction, $\delta^{13}\text{C}$ and $\delta^{18}\text{O}$ of CO_2 in canopy air (also from Lloyd et al. (1996), see above):

$$M_i \frac{dC_a}{dt} + F_n = R_s - A \quad (\text{P.19})$$

$$M_i C_a \frac{d\delta_i^{13}}{dt} - F_{oi} (\delta_o^{13} - \delta_i^{13}) = (\delta^{13}_{Rs} - \delta_i^{13}) R_s + ^{13}\Delta A \quad (\text{P.20})$$

$$M_i C_a \frac{d\delta_i^{18}}{dt} - F_{oi} (\delta_o^{18} - \delta_i^{18}) = (\delta^{18}_{Rs} - \delta_i^{18}) R_s + ^{18}\Delta A \quad (\text{P.21})$$

Multiplying 9.19 by $(\delta^{13}\text{C}_{Rs} - \delta^{13}\text{C}_i)$ and $(\delta^{18}\text{O}_{Rs} - \delta^{18}\text{O}_i)$ and subtracting the results from 9.20 and 9.21, respectively, yields:

$$F_{13} = (^{13}\Delta + \delta^{13}_{Rs} - \delta^{13}_i) A \quad (\text{P.22})$$

$$F_{18} = (^{18}\Delta + \delta^{18}_{Rs} - \delta^{18}_i) A \quad (\text{P.23})$$

with the following abbreviations to improve readability:

$$F_{13} = M_i C_a \frac{d\delta_i^{13}}{dt} - (\delta_o^{13} - \delta_i^{13}) F_{oi} - (\delta^{13}_{Rs} - \delta_i^{13}) \left(M_i \frac{dC_a}{dt} + F_n \right) \quad (\text{P.24})$$

$$F_{18} = M_i C_a \frac{d\delta_i^{18}}{dt} - (\delta_o^{18} - \delta_i^{18}) F_{oi} - (\delta^{18}_{Rs} - \delta_i^{18}) \left(M_i \frac{dC_a}{dt} + F_n \right) \quad (\text{P.25})$$

As was seen in section 4.1, $^{18}\Delta$ can be estimated (using equation 4.1) from:

$${}^{18}\Delta = \bar{a} + (\delta_{cw}^{18} - \delta_i^{18}) \frac{C_c}{C_a - C_c} \quad (\text{P.26})$$

$C_c/(C_a - C_c)$ can be derived from equation P.4:

$$\frac{C_c}{C_a - C_c} = \frac{{}^{13}\Delta - a + q(a - a_m)}{b - {}^{13}\Delta - q(a - a_m)} \quad (\text{P.27})$$

where q approximates the offset between C_c and C_i (see Lloyd et al. 1996):

$$C_i - C_c = qC_a \quad (\text{P.28})$$

Now, substituting $C_c/(C_a - C_c)$ from equation P.27 into P.26 yields for ${}^{18}\Delta$:

$${}^{18}\Delta = \bar{a} + (\delta_{cw}^{18} - \delta_i^{18}) \frac{{}^{13}\Delta - a + q(a - a_m)}{b - {}^{13}\Delta - q(a - a_m)} \quad (\text{P.29})$$

and substituting ${}^{13}\Delta$ obtained from P.22 into P.29 gives:

$${}^{18}\Delta = \bar{a} + (\delta_{cw}^{18} - \delta_i^{18}) \frac{\frac{F_{13}}{A} - (\delta_{Rs}^{13} - \delta_i^{13}) - a + q(a - a_m)}{b - \frac{F_{13}}{A} + (\delta_{Rs}^{13} - \delta_i^{13}) - q(a - a_m)} \quad (\text{P.30})$$

This can then be combined with equation P.23 to:

$$\frac{F_{18}}{A} - (\delta_{cw}^{18} - \delta_i^{18}) = \bar{a} + (\delta_{cw}^{18} - \delta_i^{18}) \frac{\frac{F_{13}}{A} - (\delta_{Rs}^{13} - \delta_i^{13}) - a + q(a - a_m)}{b - \frac{F_{13}}{A} + (\delta_{Rs}^{13} - \delta_i^{13}) - q(a - a_m)} \quad (\text{P.31})$$

which, upon multiplication with A^2 and rearrangement, yields a quadratic equation in A : (P.32)

$$0 = [(\delta_{cw}^{18} - \delta_i^{18})(\delta_{Rs}^{13} - \delta_i^{13} + a - q(a - a_m)) - (\delta_{cw}^{18} - \delta_i^{18} + \bar{a})(\delta_{Rs}^{13} - \delta_i^{13} + b - q(a - a_m))]A^2$$

$$\dots + [(\delta_{Rs}^{13} - \delta_i^{13} + b - q(a - a_m))F_{18} + (\delta_{cw}^{18} - \delta_i^{18} + \bar{a})F_{13}]A - F_{18}F_{13}$$

where possible solutions are given by:

$$A_{1/2} = \frac{-b_q \pm \sqrt{b_q^2 + 4a_q F_{18} F_{13}}}{2a_q} \quad (\text{P.33})$$

with further abbreviations to improve readability:

$$a_q = \left[(\delta_{cw}^{18} - \delta_i^{18}) (\delta_{Rs}^{13} - \delta_i^{13} + a - q(a - a_m)) - (\delta_{Rs}^{18} - \delta_i^{18} + \bar{a}) (\delta_{Rs}^{13} - \delta_i^{13} + b - q(a - a_m)) \right] \quad (\text{P.34})$$

$$b_q = \left[(\delta_{Rs}^{13} - \delta_i^{13} + b - q(a - a_m)) F_{18} + (\delta_{Rs}^{18} - \delta_{cw}^{18} + \bar{a}) F_{13} \right] \quad (\text{P.35})$$

For the simple alternative version, $C_c/(C_a - C_c)$ is replaced with $C_i/(C_a - C_i)$ in equation P.26. Then, $C_i/(C_a - C_i)$ derived from $^{13}\Delta$ in equation P.9 is substituted into equation P.26. The resulting expression for $^{18}\Delta$ is used instead of P.29 in the subsequent rearrangements. This yields again a quadratic equation in A with possible solutions:

$$A_{1/2} = \frac{-b_p \pm \sqrt{b_p^2 + 4a_p F_{18} F_{13}}}{2a_p} \quad (\text{P.36})$$

where:

$$a_p = \left[(\delta_{cw}^{18} - \delta_i^{18}) (\delta_{Rs}^{13} - \delta_i^{13} + a) - (\delta_{Rs}^{18} - \delta_i^{18} + \bar{a}) (\delta_{Rs}^{13} - \delta_i^{13} + b) \right] \quad (\text{P.37})$$

$$b_p = \left[(\delta_{Rs}^{13} - \delta_i^{13} + b) F_{18} + (\delta_{Rs}^{18} - \delta_{cw}^{18} + \bar{a}) F_{13} \right] \quad (\text{P.38})$$

Acknowledgements

First of all, I thank Hans Bemme and Siegfried Neubauer, my inspiring geography teachers. Without them, I would not write this now.

It has been a challenge and a pleasure to work at three different institutes during my time as a PhD student. The people I have met have shaped my life in many ways.

To begin with, I thank my supervisor Martin Heimann for taking me on as a PhD student at the MPI for Meteorology in Hamburg and for giving me the chance to work at these different places. Thank you, Martin, for letting me develop and pursue my own research agenda and for supporting me even outside of your own field of scientific interests. Thank you also for convincing me to come to Jena despite my hesitations which turned out to be a fortunate decision indeed.

I liked being with Patrick Heimbach, Bernadette Walter and the other members of Martin's group. Maike and Julia were great company aboard Caledonia II.

Thanks to the support by Martin Heimann and Klaus Hasselmann, I spent a year at the Scripps Institution of Oceanography in La Jolla. There, Jeff Severinghaus taught me mass spectrometry. Thank you, Jeff, for showing me how to be careful and thorough in experimental design and laboratory work and for reminding me to do the math.

I wish to thank Derek Mastroianni, Andrew Manning and Julianna Fessenden for help and discussions. I also thank Julianna for a pleasant week in the lab in Utah. Andrew helped, among other things, with assembling flasks in the middle of the night. When I emailed Derek about a rapidly disintegrating desiccant he replied that he had, just in case, prepared cold traps at once to be sent off at my notice.

I enjoyed my time with Helen and Kim, having lunch or trying to learn surfing.

For their help in Harvard Forest, I thank Bill Munger, John Budney, Alfram Bright and Cassandra Horii.

I first met Lisa Wingate, Jed Kaplan and Almut Arneth in the Stable Isotope Ecology course of Jim Ehleringer. Jed and Almut encouraged me to come to Jena. Meeting Lisa was a turning point in my career, but I did not know it.

Jon Lloyd was employed by Martin as my co-supervisor when I came to the MPI for Biogeochemistry in Jena. Jon taught me about all aspects of ecosystem research from

the planning of field experiments to the analysis and interpretation of data. Thank you, Jon, for demonstrating how to work in the field and how to sleep in a trough, and for finding encouraging or comforting words at the right time.

For their help in Griffin Forest I thank Jens Schmerler, Robert Clement, Sandra Patiño, Agyro Zerva and Francesco Ripullone. Thanks go to Jeff and to Suan Chin Wong for the loan of equipment.

Howard Griffiths, Nick Betson and Kate Maxwell helped with water analyses and hosted my stay in Cambridge, where I learnt to use lab equipment built from baked beans tins, plastic plant pots and styrofoam drinking cups.

It was a privilege and pleasure to work with Willi Brand. He answered tons of questions, or rather the questions I should have been asking. He trusted me with his precious machine – my mass spectrometric history with Jeff certainly was an advantage here. Thank you also, Willi, for suggesting to solve the problems Lisa and I had with the water measurements by heating up the branch bags to one hundred degrees. It made our day. Willi is the head of a truly extraordinary lab, and one reason for that must be his choice of people. I wish to thank the members of that lab, Michael Rothe, Armin Jordan, Roland Werner and Heike Geilmann for carrying out concentration and isotope analyses and for always being helpful and friendly. When I was rapidly approaching a pre-conference panic, Armin spent extra time in the lab running my last samples, saying "don't worry, we will definitely make it". Michael helped to prepare flasks for the Hainich campaign in record time despite being in urgent need of a holiday himself.

I thank Gerd Gleixner for answering questions about photosynthesis and other matters and for helping search for a mysterious molecule, and Nina Buchmann for isotopic discussions and significant help with statistics. Olaf Kolle, Karl Kübler and other members of the MPI-BGC helped with field work preparations. Michael Patecki helped in the Hainich during the flood of the century. Thanks go to Lina Mercado for discussions about photosynthesis, to Claudia Czimczik for revealing some of the intricacies of soils to me and to Corinne Le Quéré for polishing my talk in Sendai. I appreciated the numerous discussions with Jed Kaplan about isotopes and food (separately). Jed also managed to distill my scientific opinions and ideas through persistent questioning.

For many enjoyable lunches, barbeques, parties and evenings in Jena, I wish to thank Almut, Andrew, Antje, Eric, Jens, Jo, Karen, Pia, my housemates Corinne and David,

Patricia and Karl, Alison and Erik, Lina also for being a great flatmate, and especially Claudia, Oli, Helga and Jed.

Lisa Wingate has enriched my life during the past two and a half years. We regularly spend hours on the phone, discussing our data and encouraging one another. Thank you, Lisa, for having gone through this demanding, satisfying and frustrating experience with me, for your hospitality and generosity and for being a friend. I am looking forward to our next field campaign.

I thank my family, Hannelore, Volker and Beate, for making the bold and somewhat adventurous decision to leave a country together, for being there for me, and for not asking how much longer this work would take.

Thank you, Christian, for always being on my side.

